

1 **Interactions of Water with Mineral Dust Aerosol: Water Adsorption,**  
2 **Hygroscopicity, and Cloud Condensation and Ice Nucleation Activities**

3 M. J. Tang<sup>1</sup>, D. J. Cziczo<sup>2</sup>, V. H. Grassian<sup>1,\*</sup>

4 1 Department of Chemistry, University of Iowa, Iowa City, IA 52242, USA

5 2 Department of Earth, Atmospheric and Planetary Sciences and Civil and Environmental  
6 Engineering, Massachusetts Institute of Technology, Cambridge, MA 02139, USA

7

8 **Abstract:** Mineral dust aerosol is one of the major types of aerosol present in the troposphere. The  
9 molecular level interactions of water vapor with mineral dust are of global significance.  
10 Hygroscopicity, light scattering and absorption, heterogeneous reactivity and the ability to form  
11 clouds are all related to water-dust interactions. In this review article, experimental techniques to  
12 probe water interactions with dust and theoretical frameworks to understand these interactions are  
13 discussed. A comprehensive overview of laboratory studies of water adsorption, hygroscopicity,  
14 and cloud condensation nucleation and ice nucleation activity of fresh and atmospherically aged  
15 mineral dust particles is provided. Finally, we relate laboratory studies and theoretical simulations  
16 that provide fundamental insights into these processes on the molecular level with field  
17 measurements that illustrate the atmospheric significance of these processes. Overall, the details  
18 of water interactions with mineral dust are covered from multiple perspectives in this review article.

## 19 CONTENTS

20	1 Introduction.....	4
21	1.1 Significance of mineral dust aerosol in the atmosphere .....	4
22	1.2 Overview of the interaction of water with mineral dust aerosol: adsorption, hygroscopic	
23	growth, and cloud condensation and ice nucleation .....	8
24	2 An overview of sample preparation methods and experimental techniques.....	14
25	2.1 Methods used for sample preparation .....	16
26	2.2 Mineral dust particles supported on substrates .....	18
27	2.2.1 Mass measurements of adsorbed water as a function of water vapor pressure .....	18
28	2.2.2 FTIR measurements of water uptake .....	20
29	2.2.3 Surface analysis techniques used for water uptake measurements .....	21
30	2.3 Levitated single particle measurements .....	26
31	2.4 Aerosol measurements .....	27
32	2.4.1 Hygroscopic tandem differential mobility analyzer measurements.....	27
33	2.4.2 Optical properties.....	28
34	2.4.3 Cloud condensation nuclei activity .....	28
35	2.5 Discussion.....	30
36	3 Introduction of different theories.....	32
37	3.1 Theories and models used to describe sub-saturation conditions .....	33
38	3.1.1 Brunauer-Emmet-Teller adsorption isotherm model.....	33
39	3.1.2 Freundlich adsorption isotherm model .....	34
40	3.1.3 Frenkel-Halsey-Hill adsorption isotherm model .....	36
41	3.1.4 Hygroscopic growth theory.....	37
42	3.1.5 Discussion .....	38
43	3.2 Theories and models used to describe super-saturation conditions .....	39
44	3.2.1 $\kappa$ -Köhler activation theory .....	39
45	3.2.2 Frenkel-Halsey-Hill adsorption activation theory .....	41
46	3.2.3 Discussion .....	43
47	3.3 Suggested guidelines used for data comparison .....	44
48	4 Water adsorption properties, hygroscopicity, and CCN activity of fresh and aged mineral dust	
49	particles.....	46
50	4.1 Calcium carbonate .....	47
51	4.1.1 Fresh CaCO <sub>3</sub> particles.....	47
52	4.1.2 Effect of chemical aging .....	52
53	4.2 Arizona Test Dust .....	60
54	4.2.1 Fresh ATD particles.....	60

55	4.2.2 Effect of chemical aging .....	65
56	4.3 Illite .....	66
57	4.4 Kaolinite.....	69
58	4.5 Montmorillonite .....	73
59	4.6 Quartz.....	80
60	4.7 Metal oxides (TiO <sub>2</sub> , Al <sub>2</sub> O <sub>3</sub> , and Fe <sub>2</sub> O <sub>3</sub> ) .....	84
61	4.7.1 TiO <sub>2</sub> .....	84
62	4.7.2 Al <sub>2</sub> O <sub>3</sub> .....	85
63	4.7.3 Fe <sub>2</sub> O <sub>3</sub> .....	88
64	4.8 Authentic complex dust mixture.....	89
65	4.9 Theoretical studies on water adsorption on mineral dust surface .....	93
66	4.9.1 Calcium carbonate .....	93
67	4.9.2 Kaolinite.....	94
68	4.9.3 Montmorillonite .....	98
69	4.9.4 Quartz.....	98
70	4.10 Chemical aging modifies the interaction of water vapor with mineral dust particles:	
71	results from field measurements .....	99
72	4.11 Summary .....	106
73	4.11.1 Fresh dust particles .....	106
74	4.11.2 Aged dust particles.....	111
75	5 Effects of chemical aging on ice nucleation activity of mineral dust particles .....	111
76	5.1 Sulfate coating and exposure to SO <sub>2</sub> .....	115
77	5.1.1 Sulfate coating .....	120
78	5.1.2 Exposure to SO <sub>2</sub> .....	129
79	5.2 Organic coatings .....	130
80	5.3 Exposure to HNO <sub>3</sub> .....	135
81	5.4 Exposure to NH <sub>3</sub> .....	138
82	5.5 Exposure to O <sub>3</sub> .....	139
83	5.6 Summary .....	140
84	6 Concluding remarks and recommendations for future studies .....	141
85	Author information .....	145
86	Corresponding author.....	145
87	Notes .....	145
88	Biographies .....	146
89	Acknowledgement .....	147
90	References.....	147

91

## 92 **1 Introduction**

### 93 **1.1 Significance of mineral dust aerosol in the atmosphere**

94 Atmospheric aerosols are ubiquitous in the atmosphere and consist of solid and liquid particles  
95 that range in size from a few nanometers to tens of micrometers. In addition to their impacts on air  
96 quality, human health, and visibility,<sup>1,2</sup> these particles can alter the energy balance of the earth by  
97 scattering and absorbing solar and terrestrial radiation and by influencing the formation and  
98 properties of clouds.<sup>3,4</sup> The lack of a complete understanding of the role of aerosols (and thus  
99 clouds) on the climate system becomes a bottleneck for reliable and accurate projections of climate  
100 change.<sup>5</sup> Mineral dust aerosol is one of the main types of aerosol in the troposphere. Mineral dust  
101 particles are mainly emitted from arid and semi-arid regions (e.g., Saharan and Gobi Deserts),<sup>6,7</sup>  
102 with an annual flux of ~2000 Tg yr<sup>-1</sup>.<sup>8,9</sup> It is estimated that natural dust sources account for 75%  
103 of the emission and anthropogenic sources account for the other 25%.<sup>10</sup> One outstanding issue is  
104 the abundance of relatively bare mineral dust emitted from arid regions versus internally mixed  
105 “fertile soil dust” containing both mineral and organic components. Forster et al.<sup>11</sup> suggested the  
106 latter contributed 0-20% of the global mineral dust budget, while a more recent satellite-based  
107 study<sup>10</sup> coupled to land usage maps suggested ~25%. After being lifted into the troposphere,  
108 mineral dust particles have lifetimes of up to several days<sup>9</sup> and can be transported over thousands  
109 of kilometres.<sup>12-18</sup>

110 **Table 1.** Average emission fluxes and atmospheric loadings of different types of aerosol particles in the  
111 troposphere, as estimated by models participating in the aerosol model intercomparison initiative  
112 (AeroCom).<sup>8</sup>

aerosol type	emission (Tg yr <sup>-1</sup> )	atmospheric loading (Tg)
mineral dust	1840	19.2
sea spray	16600	7.52

sulfate	179	1.99
primary organic matter	96.6	1.7
black carbon	11.9	0.24

---

113

114 The average emission fluxes and atmospheric abundances of different types of tropospheric  
 115 aerosol particles, as estimated by models participating in the aerosol model intercomparison  
 116 initiative (AeroCom),<sup>8</sup> are provided in Table 1. While the emission of mineral dust is the second  
 117 largest in the troposphere, with sea spray being the largest, it is the most abundant type of aerosol  
 118 particle by mass with an estimated average atmospheric loading of 19.2 Tg,<sup>8</sup> as much of sea spray  
 119 particles have diameters larger than 10  $\mu\text{m}$  and thus are quickly removed from the atmosphere  
 120 through deposition.<sup>19</sup> A substantial fraction of mineral dust particles also have large diameters and  
 121 thus are quickly removed by dry deposition after they are entrained into the atmosphere.<sup>9</sup> Dust  
 122 emissions are closely linked to hydrological cycles, and climate variability can change dust  
 123 emissions, leading to further feedbacks on the climate system.<sup>10,20-28</sup>

124

125 Because of the overall loading and lifetime in the atmosphere, mineral dust can impact the Earth's  
 126 atmosphere and climate in a number of ways. Mineral dust particles can both scatter and absorb  
 127 solar and terrestrial radiations, thus having direct radiative effects.<sup>29-43</sup> <sup>44</sup>Optical scattering and  
 128 absorption by mineral dust particles can further change the photolysis rates and thus influence  
 129 photochemical cycles in the troposphere.<sup>45</sup> Mineral dust particles can also have indirect impact on  
 130 radiative forcing by acting as cloud condensation nuclei (CCN) to form liquid cloud droplets<sup>46-55</sup>  
 131 and ice nuclei (IN) to form ice clouds.<sup>56-73</sup> In fact, mineral dust particles may be the dominant IN  
 132 in the troposphere<sup>74,75</sup> and therefore have a significant impact on the Earth's radiative budget,<sup>76-79</sup>  
 133 precipitation, and the hydrological cycle.<sup>58,80-83</sup> Additionally, deposited mineral dust particles can  
 134 be a major contributor of several important elements, including Fe,<sup>84-87</sup> P,<sup>88-91</sup> and Cu,<sup>92,93</sup>

135 especially into open ocean waters<sup>88,94-97</sup> and the Amazon,<sup>98,99</sup> and therefore have strong effects on  
136 biogeochemical cycles and the Earth's climate system.<sup>100-103</sup>

137  
138 Mineral dust aerosol also influences air quality,<sup>104-106</sup> visibility,<sup>107</sup> and public health in dust-  
139 impacted regions.<sup>12,20,104,108-119</sup> For example, clear enhanced effects of particulate matter on  
140 respiratory and cerebrovascular diseases were observed during Saharan dust outbreaks in Roma,  
141 Italy.<sup>120</sup> A recent modeling study<sup>108</sup> estimated that the fraction of cardiopulmonary deaths caused  
142 by mineral dust aerosol is about 1.8% globally, and in countries most affected by dust storms it is  
143 up to 15-50%.

144  
145 The mineralogy of dust particles is very complex, showing large variation with their sources and  
146 atmospheric transport processes.<sup>121-130</sup> Different minerals can have very different physical and  
147 chemical properties, such as heterogeneous reactivity, refractive index, CCN and IN activity, and  
148 therefore have different impacts on atmospheric chemistry, cloud formation, and climate. For  
149 example, it has been shown that the kinetics of N<sub>2</sub>O<sub>5</sub> uptake onto mineral dust particles vary over  
150 almost two orders of magnitude for different minerals,<sup>131-139</sup> and the ice nucleation activity of  
151 different minerals can differ by several orders of magnitude.<sup>140,141</sup> It is also suggested that the iron  
152 solubility in dust particles is strongly dependent on the mineralogy.<sup>142-144</sup> Mineral dust particles in  
153 the troposphere consist of a variety of minerals that can be externally and internally mixed.<sup>145-149</sup>  
154 The emission fluxes and atmospheric abundance of the most abundant minerals, estimated by a  
155 recent modeling study,<sup>150</sup> are shown in Table 2.

156  
157 **Table 2.** Emission fluxes and atmospheric loadings of different mineral phases, estimated by a recent study  
158 <sup>150</sup> using the Community Atmosphere Model.

mineral	flux (Tg yr <sup>-1</sup> )	atmospheric loadings (Tg)
---------	-----------------------------	---------------------------

quartz	568.9	4.1
illite	370.1	4.2
montmorillonite	246.2	2.8
feldspar	205	1.4
kaolinite	192.3	2.2
calcite	145.1	1.3
hematite	24	0.2
gypsum	15.3	0.1

159

160 Less abundant minerals have not been included in most modeling studies; however, the impact of  
 161 a mineral in the troposphere is not necessarily proportional to its abundance. For example, the  
 162 mass fractions of TiO<sub>2</sub> in mineral dust particles are typically a few percents or less,<sup>32,151-153</sup> but its  
 163 semiconductor properties make it very important in heterogeneous photochemical reactions which  
 164 may play an important role in the formation or removal of reactive trace gases in the  
 165 troposphere.<sup>154-156</sup> Saharan dust particles only contain 0.09% phosphorus on average, though the  
 166 deposition of mineral dust particles from the Sahara desert is a major source of phosphorus for  
 167 oceans.<sup>97</sup> It has also been suggested that transition metals of trace amounts contained by mineral  
 168 dust particles (and probably also anthropogenic particles) may significantly enhance the  
 169 multiphase oxidation of SO<sub>2</sub>.<sup>157</sup> Furthermore, the complexity of mineral dust particles can be  
 170 significantly increased due to their transformations resulting from chemical processing during  
 171 transport.<sup>158-162</sup>

172

173 In addition, a few minerals with high refractive indexes (such as TiO<sub>2</sub> and Al<sub>2</sub>O<sub>3</sub>),<sup>138,139,163-165</sup> have  
 174 recently been proposed as alternative particles to be injected into the stratosphere to scatter more  
 175 solar radiation back into space, as a geoengineering method<sup>166</sup> to counteract global warming due  
 176 to increasing levels of greenhouse gases. For example, it is estimated that in order to achieve the

177 same scattering effect, the use of TiO<sub>2</sub> for stratospheric particle injection requires a factor of ~3  
178 less in mass than that of H<sub>2</sub>SO<sub>4</sub> aerosols which are present as a natural aerosol in the  
179 stratosphere.<sup>163</sup>

## 180 **1.2 Overview of the interaction of water with mineral dust aerosol: adsorption,** 181 **hygroscopic growth, and cloud condensation and ice nucleation**

182 Water is ubiquitous in the troposphere and can exist in the gas, liquid, and solid states. The amount  
183 of water vapor contained by air is usually described by relative humidity (RH), typically in %,  
184 which is defined as the ratio of its partial pressure to the saturated vapor pressure at the same  
185 temperature ( $T$ ) multiplied by 100, as shown in Eq. (1):

$$186 \quad RH = 100 \times \frac{P(\text{water})}{P_s(\text{water})} \quad (1),$$

187 where  $P(\text{water})$  is the partial pressure of water vapor and  $P_s(\text{water})$  is the saturated vapor pressure  
188 of water. Under sub-saturation conditions, i.e. RH is lower than 100%, some water vapor will  
189 partition onto/into mineral dust particles. The amount of water associated with particles, in  
190 equilibrium with water vapor in the gas phase, depends on RH,  $T$ , and the type of dust particles.  
191 The partitioning of water between the gas and particle phase, is called water adsorption in surface  
192 science and hygroscopicity in aerosol science. Hygroscopicity is in fact a general term which  
193 describes the ability to absorb or release water as a function of water activity and how a substance  
194 can attract and hold water molecules from the surrounding environment. In aerosol science, it  
195 usually refers to the change in diameter, volume, or mass of particles when exposed to water vapor.  
196 Different theories are used to describe water adsorption versus hygroscopicity which differ in  
197 fundamental underlying assumptions to describe water partitioning between gas and particle  
198 phases under sub-saturation conditions, as discussed in more detail in Section 3.

199

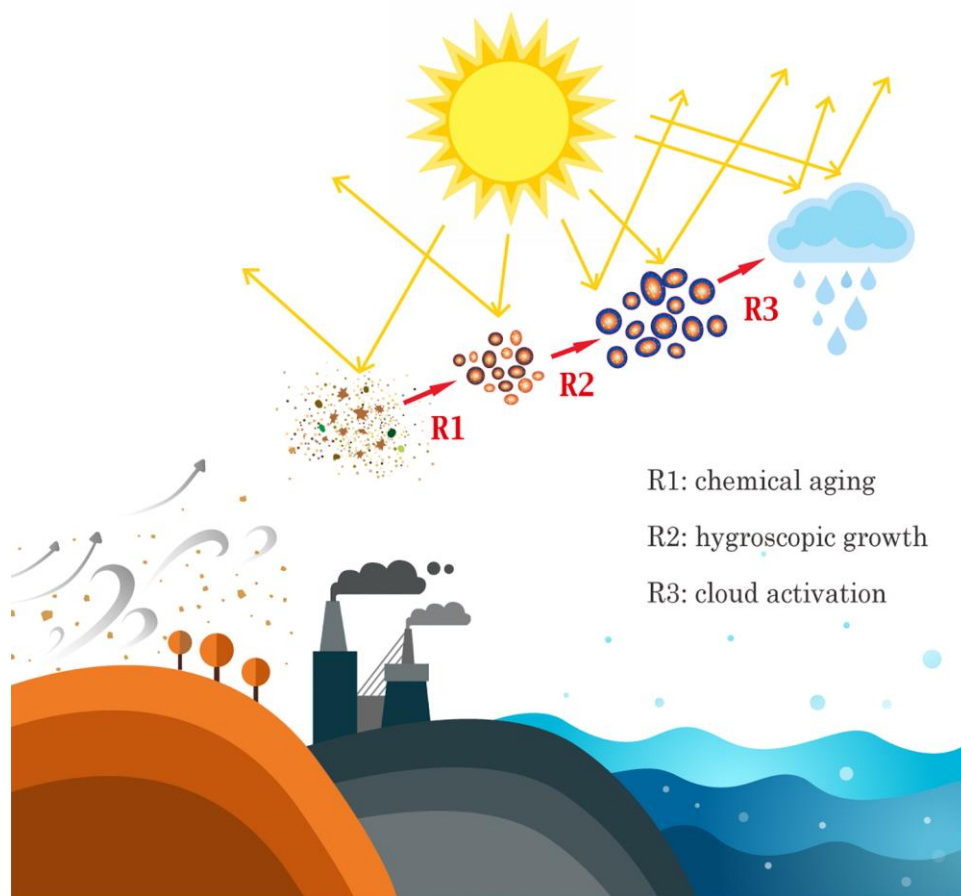


200 When RH is larger than 100%, i.e. under super-saturation conditions, dust aerosol particles can be  
201 activated to cloud droplets (a process called cloud condensation nucleation).<sup>167</sup> At a given super-  
202 saturation, the ability of a particle to be activated to a cloud droplet depends on the particles  
203 diameter<sup>168,169</sup> and also its CCN activity, which is determined by its chemical composition and  
204 mixing state.<sup>170</sup> When  $T$  is less than 273 K, mineral dust particles might be activated to form ice  
205 particles (ice nucleation) if the relative humidity to ice (RH<sub>i</sub>, defined as the ratio of the partial  
206 pressure of water vapor to the saturated pressure of ice at the same temperature) is larger than  
207 100%.<sup>167</sup> In this article RH and RH<sub>i</sub> are referred to relative humidity with respect to liquid water  
208 and ice, respectively.

209  
210 What makes water uptake properties of mineral dust more complicated is that, as well known,  
211 during transport mineral dust particles react with a wide range of trace gases in the  
212 troposphere.<sup>156,161,171-187</sup> These heterogeneous reactions involve gas-solid interactions. If mineral  
213 dust particles are activated to cloud droplets, multiphase reactions can occur in these aqueous cloud  
214 droplets.<sup>157,162,188-191</sup> Heterogeneous and multiphase reactions can directly and indirectly change  
215 the concentrations of several important trace gases,<sup>161,172,192-198</sup> such as NO<sub>x</sub>, O<sub>3</sub> and OH radicals,  
216 thus imposing significant impacts on tropospheric chemistry. Furthermore, these reactions also  
217 lead to a change in surface and sometimes even the bulk chemical composition of mineral dust  
218 particles,<sup>126,158,199-210</sup> thereby modifying their interactions with water, including surface  
219 adsorption,<sup>211,212</sup> hygroscopicity,<sup>213-215</sup> and cloud condensation nucleation<sup>216-218</sup> and ice nucleation  
220 activity.<sup>219-221</sup>

221  
222 The change in the interaction with water can in turn further influence the reactivity of mineral dust  
223 particles towards reactive trace gases. The change in composition and hygroscopicity of dust  
224 particles may influence both their refractive index<sup>222</sup> and optical diameters, and the change in

225 CCN and IN activity can results in the change in the probability of wet deposition,<sup>223,224</sup> thereby  
226 impacting their atmospheric lifetime.<sup>224</sup> In addition, heterogeneous chemistry can modify the  
227 solubility and/or bio-availability of elements within individual mineral dust particles.<sup>84,88,96,225</sup> The  
228 complex interactions of mineral dust particles with reactive trace gases and water, and their  
229 impacts on cloud formation, are depicted in Figure 1.



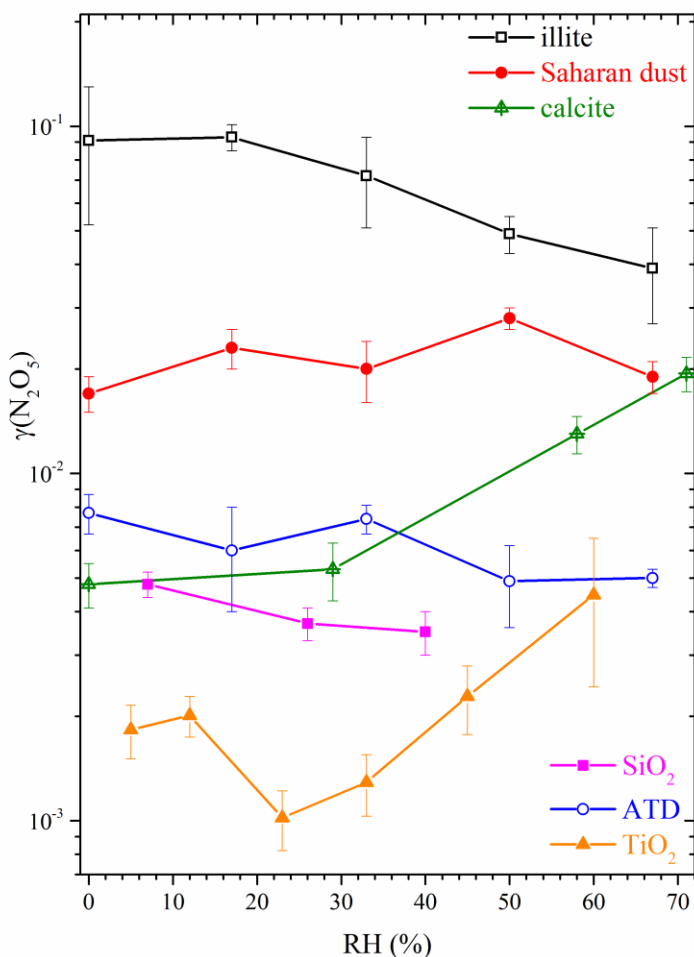
230

231

232 **Figure 1.** A schematic diagram of the interactions of mineral dust aerosol particles with reactive trace gases  
233 and water and their impacts on cloud formation and radiative balance. R1) chemical transformation/aging  
234 of mineral dust aerosol particles due to reactions with reactive trace gases; R2) enhanced hygroscopic  
235 growth of aged mineral dust aerosol particles; and R3) activation of mineral dust particles to cloud droplets  
236 and ice particles.

237

238 It is important to note that heterogeneous chemistry and photochemistry of mineral dust particles  
239 in the atmosphere have been summarized in several comprehensive review papers.<sup>161,171,172</sup> It has  
240 been widely recognized that water adsorbed by mineral dust plays a central role in determining the  
241 heterogeneous reactivity and photoreactivity towards reactive trace gases in the  
242 atmosphere.<sup>137,199,226-228</sup> In particular, a recent review paper<sup>229</sup> described in detail how surface  
243 adsorbed water can play a myriad of roles in the surface chemistry and can either enhance or  
244 suppress the reactivity of mineral dust particles towards reactive trace gases. For example, Figure  
245 2 shows the dependence of the uptake coefficient of  $\text{N}_2\text{O}_5$ ,  $\gamma(\text{N}_2\text{O}_5)$ , on RH (and thus surface  
246 adsorbed water) for different mineral dust particles. Even for the same trace gas, the influence of  
247 RH on the uptake kinetics can be very different for different minerals, highlighting the importance  
248 of accurate determination of water adsorption as a function of RH for a variety of different minerals  
249 that make up dust in the atmosphere. Adsorbed water can also change the reaction products and  
250 the partitioning of reaction products among different phases.<sup>229</sup>



251  
 252 **Figure 2.** Dependence of  $\gamma(\text{N}_2\text{O}_5)$  on RH for different mineral dust particles. Sources of data: illite,<sup>137</sup>  
 253 Saharan dust,<sup>136</sup> calcite,<sup>135</sup> SiO<sub>2</sub>,<sup>139</sup> Arizona Test Dust (ATD),<sup>137</sup> and TiO<sub>2</sub>.<sup>138</sup>

254  
 255 However, the interactions of mineral dust particles with water vapor at temperatures higher than  
 256 that for ice nucleation has hitherto not been reviewed in the context of atmospheric chemistry and  
 257 climate, despite that in the last two decades a large number of studies have been published by both  
 258 the surface science and aerosol science communities. We note that a recent review paper has  
 259 discussed the multi-faceted roles of surface adsorbed water in heterogeneous reactions of mineral  
 260 dust particles.<sup>229</sup> Therefore, in this article, we undertake a comprehensive review of the interactions  
 261 of water with mineral dust particles. Following the Introduction section, we summarize and discuss  
 262 experimental techniques used to study water adsorption properties, hygroscopicity, and CCN

263 activity of mineral dust particles (Section 2). In Section 3, we introduce and discuss theories used  
264 in this review to describe water adsorption in surface science and hygroscopicity and CCN activity  
265 in aerosol science, and we also describe guidelines used to compare experimental data reported in  
266 these previous studies. Following this, laboratory studies of water adsorption properties,  
267 hygroscopicity, and CCN activity of different mineral dust particles are reviewed in Section 4, in  
268 which the effects of chemical aging processes on water interaction are also discussed. We focus  
269 on mineral particles and surfaces which are of direct relevance for atmospheric chemistry and  
270 microphysics of aerosols and clouds. Therefore, water adsorption on single crystal surfaces,<sup>230-236</sup>  
271 although relevant, is not discussed in too much detail in this review. In this section, we also discuss  
272 some theoretical studies to illustrate how these studies can provide insight into the fundamental  
273 mechanisms of water adsorption on mineral surface on the molecular and sub-molecular levels. In  
274 addition, at the end of this section we also summarize results from field measurements which  
275 provide evidence that the hygroscopicity of mineral dust particles can be significantly modified  
276 due to heterogeneous reactions and cloud processing. Although ice nucleation activity of mineral  
277 dust particles has been reviewed in a few excellent recent papers,<sup>140,237-239</sup> these papers are mainly  
278 focused on fresh mineral dust particles and only one review article<sup>238</sup> has briefly summarized ice  
279 nucleation activity of aged mineral dust particles. Increasing number of laboratory studies suggest  
280 that chemical aging processes can significantly change the ice nucleation activity of mineral dust  
281 particles. Thus in Section 5, recent work on the effects of chemical aging on the ice nucleation  
282 activity of dust particles is reviewed. Finally, in Section 6 we outline several key questions from a  
283 physical chemistry view which preclude us from a better understanding of the interactions of  
284 mineral dust aerosol particles with water vapor (including water adsorption, hygroscopicity, and  
285 CCN and IN activities), and discuss how these challenges can be addressed through future research.

## 286 **2 An overview of sample preparation methods and experimental techniques**

287 Experimental techniques which have been used to investigate water adsorption properties,  
288 hygroscopicity, and CCN activity of mineral dust particles are briefly summarized here. Instead of  
289 providing a comprehensive discussion of each techniques, we introduce the basic principles and  
290 key features, and refer interested readers to the relevant literature for further details. These  
291 techniques can be classified into three groups which are discussed in Sections 2.2-2.4, according  
292 to the way particles under investigation exist: 1) particle ensembles or single particles deposited  
293 on a substrate; 2) levitated single particles; and 3) an ensemble of particles as an aerosol. A quick  
294 overview of these techniques is provided in Table 3 along with their key measurement features. A  
295 variety of sample preparation methods have been used in previous studies, and it has been  
296 suggested that experimental results may vary with sample preparation methods. Therefore, we first  
297 briefly discuss the effects of different particle preparation/generation methods in Section 2.1. In  
298 this review paper, we focus on techniques which have been used to quantitatively determine the  
299 amount of water adsorbed by mineral dust particles of direct atmospheric relevance. In addition,  
300 there have been a large number of studies on water adsorption on single crystals of minerals, for  
301 example,  $\text{CaCO}_3$ ,<sup>211</sup>  $\alpha\text{-Al}_2\text{O}_3$ ,<sup>230,240</sup>  $\text{TiO}_2$ ,<sup>231,232,241</sup>, and  $\alpha\text{-Fe}_2\text{O}_3$ .<sup>242</sup> Although surfaces of these  
302 single crystals may not completely resemble the complexity of mineral dust particles in the  
303 troposphere, studies using well-defined single crystal surfaces can provide a wealth of fundamental  
304 information and insights into water adsorption mechanisms and intermolecular interactions  
305 between water molecules and water molecules with surface atoms. Techniques used to study the  
306 ice nucleation activity have been discussed recently<sup>140,238,239</sup> and thus are not covered here.

307  
308 Note that one shortcoming of many laboratory studies is that overly simplistic dust samples, when  
309 compared to the complex internal mixtures found in the atmosphere,<sup>243,244</sup> <sup>158</sup> are often utilized.  
310 For example, atmospheric mineral dust is often associate with surface coatings due to

311 heterogeneous reactions with reactive trace gases,<sup>158,161,202,245</sup> but laboratory studies most often  
 312 consider unprocessed particles which may be only representative of mineral dust particles freshly  
 313 emitted into the troposphere.

314

315 **Table 3.** Summary of representative literature on different experimental techniques which have been used  
 316 to measure water adsorption, hygroscopicity, and CCN activity of mineral dust particles.

techniques	references	main features
QCM	Navea et al., 2010 <sup>246</sup>	Change in particle mass at different RH is quantified by the frequency change of the quartz crystal.
TGA	Gustafsson et al., 2005 <sup>247</sup>	Change in particle mass at different RH is directly measured.
PSA	Ma et al., 2010 <sup>248</sup>	Change in partial pressure of water vapor due to surface adsorption is measured.
ATR-FTIR	Schuttlefield et al., 2007 <sup>249</sup>	IR absorption of surface adsorbed water is measured and can be
transmission FTIR	Goodman et al., 2001 <sup>250</sup>	converted to the amount of adsorbed water.
DRIFTS	Gustafsson et al., 2005 <sup>247</sup>	
AP-XPS	Ketteler et al., 2007 <sup>241</sup>	Chemically specific and quantitative measurements of water and other species adsorbed on the surface can be achieved.
EDB	Pope et al., 2010 <sup>251</sup>	Relative change in mass of a single particle at different RH is determined from the change of the DC voltage used to balance the gravitational force.
optical levitation	Tong et al., 2011 <sup>252</sup>	Particle size change of a single particle at different RH is determined by light scattering.
H-TDMA	Herich et al., 2009 <sup>49</sup>	Mobility diameter change at different RH is measured.
aerosol extinction	optical Attwood and Greenslade, 2011 <sup>253</sup>	Change in aerosol optical extinction properties at different RH is measured, e.g., using an AE-CRD.
aerosol scattering	optical Li-Jones et al., 1998 <sup>254</sup>	Change in aerosol optical scattering properties at different RH is measured, e.g., using a nephelometer.

aerosol adsorption	optical	Utry et al., 2015 <sup>255</sup>	Change in aerosol optical scattering properties at different RH is measured, e.g., using a photoacoustic absorption spectrometer.
CCNc		Sullivan et al., 2010 <sup>256</sup>	Concentrations of aerosol particles activated to cloud droplets at a certain super-saturation are measured.

317 QCM: quartz crystal microbalance. TGA: thermogravimetric analyser. PSA: physisorption analyser. ATR-  
318 FTIR: attenuated total reflection Fourier transform infrared spectroscopy. DRIFTS: diffuse reflectance  
319 Fourier transform spectroscopy. AP-XPS: atmospheric pressure X-Ray photoelectron spectroscopy. EDB:  
320 electrodynamic balance. H-TDMA: hygroscopicity tandem differential mobility analyser. CCNc: cloud  
321 condensation nuclei counter.

## 322 **2.1 Methods used for sample preparation**

323 There are two common methods used to generate mineral dust aerosols: i) wet generation: aerosol  
324 particles were generated by atomizing the suspension of mineral dust powders in water,<sup>139,256,257</sup>  
325 ii) dry generation: mineral dust particles are directly dispersed and entrained into the air, typically  
326 by using a high-speed air jet.<sup>136,258-260</sup> Commercial instruments, such as rotating brusher generators  
327 <sup>134,136</sup> and fluidized beds,<sup>220,261</sup> are also available for dry generation of dust aerosol particles.  
328 Recent studies have shown that mineral dust particles generated by these two methods can have  
329 distinctive hygroscopicity and CCN activities,<sup>49,217,262,263</sup> with wet-generated aerosol particles  
330 having higher hygroscopicity and CCN activities. The change of hygroscopicity and CCN  
331 activities of dust particles after wet-generation can be due to a couple of reasons: 1) soluble  
332 impurities contained by the dust particles are enriched in generated aerosol particles by wet-  
333 generation, and 2) some components contained by dust particles may undergo chemical reaction  
334 in the water suspension. For example, Sullivan et al.<sup>256</sup> suggest that the formation of  $\text{Ca}(\text{HCO}_3)_2$ ,  
335 due to the reaction of  $\text{CaCO}_3$  with  $\text{H}_2\text{O}$  and  $\text{CO}_2$ , causes wet-generated  $\text{CaCO}_3$  particles to have  
336 higher CCN activity than dry-generated  $\text{CaCO}_3$ . This conclusion is further supported by Zhao et  
337 al.,<sup>264</sup> who have demonstrated that  $\text{Ca}(\text{HCO}_3)_2$  particles are more hygroscopic than  $\text{CaCO}_3$



338 particles. We expect that similar phenomena may occur for clay mineral but less likely for  
339 relatively inert minerals such as SiO<sub>2</sub>.

340

341 Compared to wet generation, dry generation produces dust aerosol particles which may better  
342 resemble the composition and thus the hygroscopicity of original powders used to generate those  
343 aerosol particles. On the other hand, dust aerosol particles can be activated to cloud droplets and  
344 undergo cloud processing several times during their residence in the troposphere,<sup>48,162,223,265-267</sup> and  
345 dust aerosol particles produced by wet generation might better resemble the properties of dust  
346 particles which were activated cloud droplets. Thus, to summarize, dry and wet generation  
347 methods have been shown to produce aerosol particles with different hygroscopicity and CCN  
348 activity. Nevertheless, currently it is not clear which method may generate aerosol particles which  
349 better resemble dust particles in the troposphere. This is because nascent dust or cloud activated  
350 dust may be very different and therefore may best described by dry generation and wet generation  
351 techniques, respectively.

352

353 To investigate water adsorption on mineral dust particles deposited on a substrate, typically a slurry  
354 of dust particles in water is deposited on the supporting substrate, leading to the formation of a  
355 relatively uniform dry film after the evaporation of water.<sup>268</sup> Alternatively, other solvents, such as  
356 methanol or ethanol, can be used instead of water.<sup>196</sup> In some studies<sup>269,270</sup> dry powders of dust  
357 were also directly placed on a substrate, without using any solvents. Whether a solvent is used  
358 during deposition of dust particles on a substrate may influence the measured water adsorption and  
359 hygroscopicity of dust particles; however, to date this has not been systematically examined.

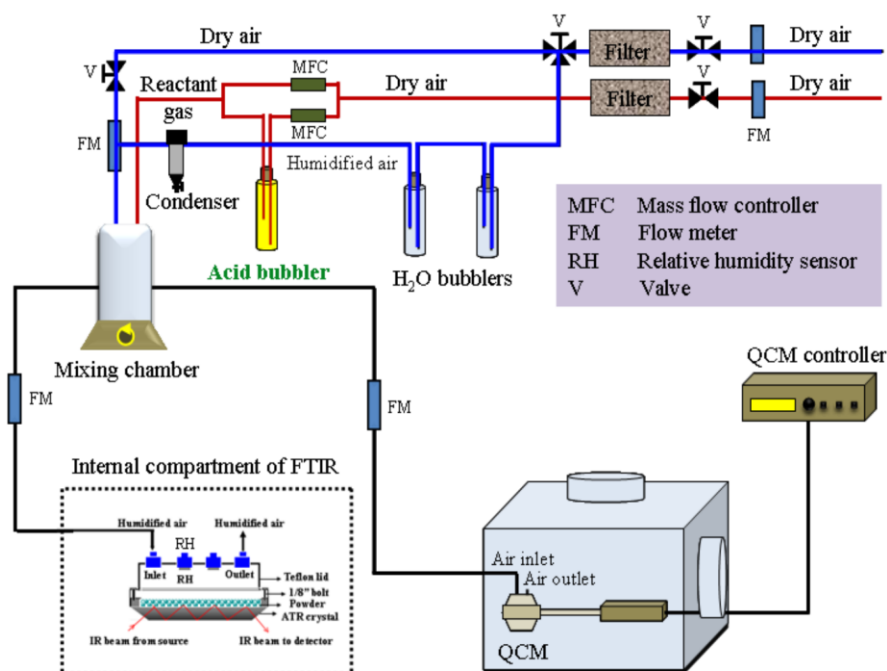
## 360 2.2 Mineral dust particles supported on substrates

### 361 2.2.1 Mass measurements of adsorbed water as a function of water vapor pressure

362 The mass of a particle ensemble can be measured at different RH (in %) to investigate the amount  
363 of adsorbed water by using several techniques. For examples, in a quartz crystal microbalance  
364 (QCM) experiment, the measured frequency of the quartz crystal reflects the mass of particles  
365 loaded on it.<sup>249,271</sup> The frequency change,  $\Delta f$  (Hz), is directly related to the change in mass,  $\Delta m$ ,  
366 according to the Sauerbrey equation:<sup>246,249,272</sup>

$$367 \Delta f = -C_f \Delta m \quad (2),$$

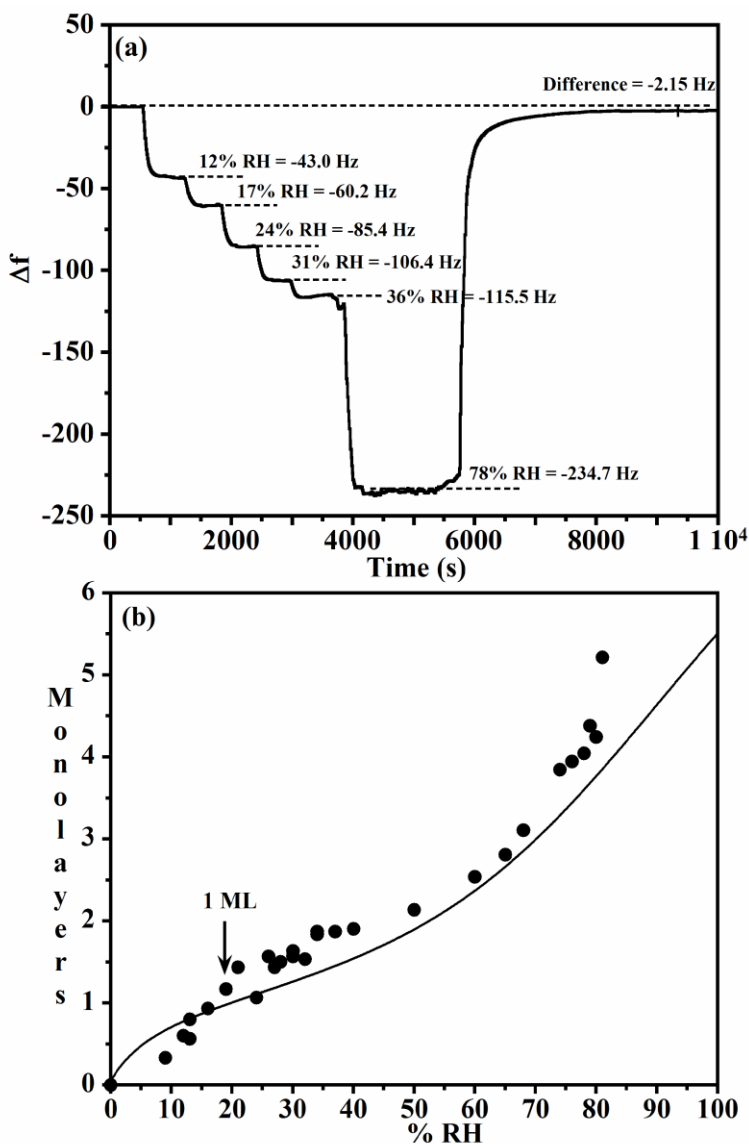
368 where  $C_f$  is the constant sensitivity factor for the specific QCM and can be experimentally  
369 calibrated. Usually a slurry of dust particles in water (or other solvents, e.g., methanol) was sprayed  
370 onto the quartz crystal and then dried to form a thin film on the quartz crystal.<sup>246,273</sup>



371  
372 **Figure 3.** A schematic diagram of ATR-FTIR spectroscopy and quartz crystal microbalance (QCM).  
373 Although these measurements are integrated in time and the gas phases above the samples are at the same  
374 relative humidity, it should be noted that the ATR-FTIR cell and the QCM cell both have separate thin film  
375 samples. Reprinted with permission from ref 274. Copyright 2012 American Chemical Society.

376

377 A schematic diagram of a typical QCM set-up,<sup>274</sup> is shown in Figure 3. The change in frequency  
378 of the quartz crystal (and thus the change in particle mass) measured at different RH, can be used  
379 to determine the amount of adsorbed water. Figure 4 shows the frequency change of a QCM (upper  
380 panel) and water adsorption isotherm (lower panel) for SiO<sub>2</sub> particles.<sup>273</sup>



381  
382 **Figure 4.** Water adsorption on SiO<sub>2</sub> at different RH as measured by QCM. (a) Change in frequency of the  
383 quartz crystal at different RH; (b) the number of adsorbed water layers on the surface at different RH, and  
384 the curve is the modified three-parameter BET fit reported by Goodman et al.<sup>250</sup> Reprinted with permission  
385 from ref 273. Copyright 2007 Society for Applied Spectroscopy.

386

387 Thermogravimetric analysers can also be used to investigate water adsorption on mineral dust  
388 particles. For example, a Mettlet-Toledo TGA/SDTA851e thermogravimetric analyzer (Mettler-  
389 Toledo, USA) with a mass measurement accuracy of  $\pm 1 \mu\text{g}$ , was used to measure the amount of  
390 water adsorbed on  $\text{CaCO}_3$  and Arizona Test Dust particles.<sup>247</sup>

391

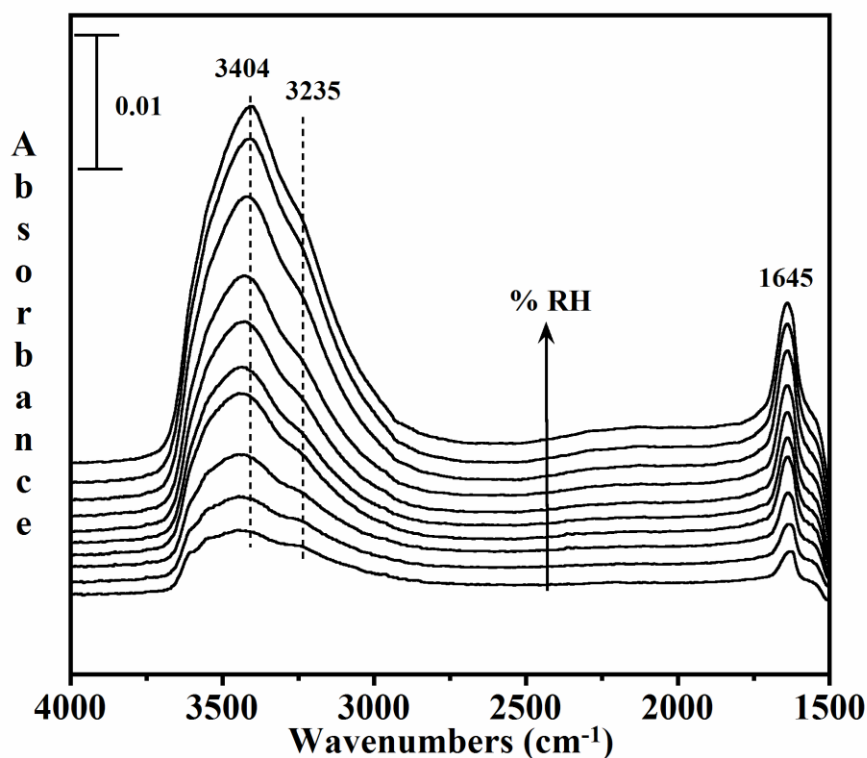
392 In addition, the amount of surface adsorbed water can also be quantified by measuring the change  
393 of water vapor pressure in the gas phase due to adsorption onto the surface, using a physisorption  
394 analyser (PSA).<sup>212,248</sup> The change in partial pressure of water vapor due to adsorption on mineral  
395 dust particles can be measured to determine the water adsorption isotherm, in a similar way to the  
396 BET surface area measurement using  $\text{N}_2$ . For example, a commercial physisorption analyser,  
397 AUTOSORB (Quantachrome, USA), was modified and used to investigate the hygroscopicity of  
398 fresh and aged  $\text{Al}_2\text{O}_3$  and  $\text{CaCO}_3$  particles.<sup>212,248</sup>

399

400 These experimental techniques provide direct quantification of water adsorbed by mineral dust  
401 particles. Water may also adsorb on the apparatus wall and cause artifacts, and this effect can be  
402 subtracted by blank experiments in which no particles are used.

### 403 **2.2.2 FTIR measurements of water uptake**

404 Water adsorbed on mineral dust surface at different RH can be monitored by Fourier transform  
405 infrared spectroscopy (FTIR), including transmission FTIR,<sup>250</sup> diffuse reflectance Fourier  
406 transform spectroscopy (DRIFTS),<sup>247</sup> and attenuated total reflection Fourier transform infrared  
407 spectroscopy (ATR-FTIR).<sup>273</sup> As shown in Figure 5, surface adsorbed water has two distinctive  
408 IR absorption peaks in the region extending from  $1500$  to  $4000 \text{ cm}^{-1}$ , one near  $3400 \text{ cm}^{-1}$  due to  
409 the O-H stretching mode and the other near  $1645 \text{ cm}^{-1}$  due to  $\text{H}_2\text{O}$  bending mode.<sup>250,273,275</sup>



410  
 411 **Figure 5.** ATR-FTIR spectra following the water uptake on 19.2 mg of SiO<sub>2</sub> at different RHs (5, 8, 13, 20,  
 412 27, 37, 47, 66, 74, and 78%). Reprinted with permission from ref 273. Copyright 2007 Society for Applied  
 413 Spectroscopy.

414  
 415 Since surface hydroxyl groups can also contribute to the O-H stretching mode, it is better to use  
 416 the H<sub>2</sub>O bending mode to analyze molecularly adsorbed water on the surface. The integrated IR  
 417 absorption can be used to quantify the amount of surface-adsorbed water, using a modified  
 418 Lambert-Beer law and assuming that the IR absorption cross section of surface-adsorbed water is  
 419 equal to that of liquid water.<sup>211,240</sup>

### 420 **2.2.3 Surface analysis techniques used for water uptake measurements**

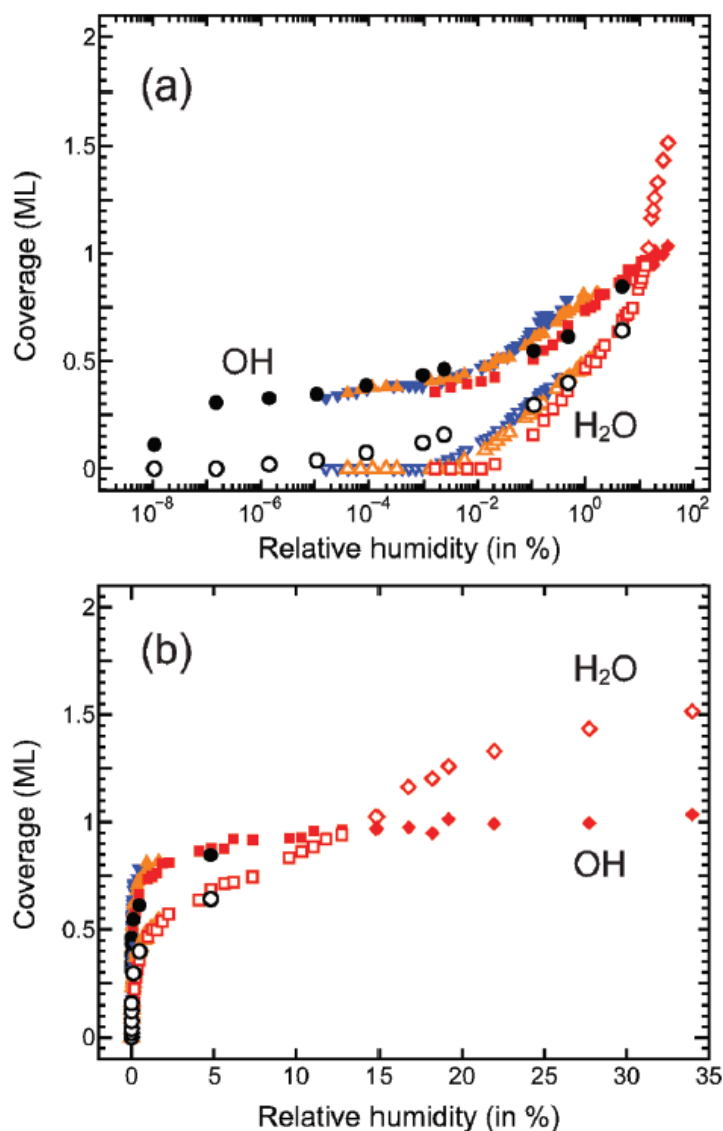
421 Surface techniques can be very valuable in studying water adsorption and hygroscopicity of  
 422 mineral dust particle. Some surface techniques are able to provide information on both chemical  
 423 composition and morphology of the surface under investigation, though absolute quantification of

424 the amount of water associated with the surface may be non-trivial. Here we provide several  
425 examples to demonstrate how different surface techniques can be used to understand water  
426 adsorption and hygroscopicity of fresh and aged mineral dust particles. In addition to the  
427 techniques mentioned in this section, there are many other surface techniques which have been  
428 used to study water adsorption on single crystals including scanning probe techniques such as  
429 scanning tunneling microscopy (STM).<sup>232,276-278</sup>

430  
431 The transformation of solid  $\text{CaCO}_3$  particles to aqueous droplets, due to the reaction with  $\text{HNO}_3$ ,  
432 has been observed in the laboratory for the first time by Krueger et al.,<sup>279</sup> using Scanning Electron  
433 Microscopy (SEM) and Energy Dispersive X-ray analysis (EDX). Two years later the atmospheric  
434 significance of this finding was supported by a field study,<sup>245</sup> which showed that dust particles  
435 collected in Israel have been substantially processed in the atmosphere and could exist in aqueous  
436 state even at very low RH (9-11%). Transmission Electron Microscopy can also be used to monitor  
437 the morphology change of mineral dust particles. For example, using TEM, Matsuki et al.<sup>159</sup> found  
438 that some of the Asian dust particles collected in Beijing are spherical, due to internal mixing with  
439 nitrate and sulfate. Liu et al.<sup>215</sup> used a micro-Raman spectrometry to investigate the hygroscopicity  
440 of  $\text{CaCO}_3$  particles after exposure to  $\text{NO}_2$ . They<sup>215</sup> found that after the reaction, irregular  $\text{CaCO}_3$   
441 particles are converted to spherical droplets at 37% RH and the internally mixed  $\text{CaCO}_3/\text{Ca}(\text{NO}_3)_2$   
442 particles have the same phase transition properties as pure  $\text{Ca}(\text{NO}_3)_2$  particles.

443  
444 Traditionally, X-Ray photoelectron spectroscopy (XPS) is a technique applied to surfaces in ultra-  
445 high vacuum, limiting its application under atmospheric relevant conditions (i.e. with pressures  
446 close to 1 bar). Over the past decade, advances in atmospheric pressure XPS (AP-XPS) makes it a  
447 very promising method to investigate the interaction of gases, including water vapor, with mineral  
448 dust particles, because of its chemically specific and quantitative nature.<sup>280-284</sup> Using this technique,

449 Ketteler et al.<sup>241</sup> measured the amounts of adsorbed water and surface OH groups on TiO<sub>2</sub>(110)  
450 surface over a very large RH range, from  $<1 \times 10^{-4}$  to almost 100%. In addition, they<sup>241</sup> found that  
451 AP-XPS can also differentiate the oxygen species (lattice O, OH, and H<sub>2</sub>O) on the surface by their  
452 difference in O1s binding energies, providing very useful information on mechanisms of water  
453 adsorption on the mineral surface. In another study,<sup>242</sup> the coverages of surface-adsorbed water  
454 and OH groups on single crystal  $\alpha$ -Fe<sub>2</sub>O<sub>3</sub>(0001) surface were measured as a function of RH, as  
455 shown in Figure 6. Though AP-XPS has shown large potential to quantify the amount of adsorbed  
456 water and to explore the adsorption mechanisms on a molecular and/or atomic level, to our  
457 knowledge AP-XPS has not been used to investigate the interaction of water vapor with clay  
458 mineral or authentic dust particles.



459  
 460 **Figure 6.** Coverages of surface OH groups (filled symbols) and molecularly adsorbed H<sub>2</sub>O (open symbols)  
 461 on  $\alpha\text{-Fe}_2\text{O}_3(0001)$  surface as a function of RH. RH is plotted on a logarithmic scale in (a) and a linear scale  
 462 in (b). Measurements were carried out at different experimental conditions: black circles, varying  $P(\text{water})$   
 463 with a constant temperature of 295 K; blue triangles, varying temperature with a constant  $P(\text{water})$  of 0.02  
 464 Torr; orange triangles, varying temperature with a constant  $P(\text{water})$  of 0.1 Torr; red squares, varying  
 465 temperature with a constant  $P(\text{water})$  of 1 Torr; red diamonds,  $P(\text{water})$  in the range of 1.0-2.0 Torr and  
 466 temperature in the range of 277-280 K. Reprinted with permission from ref 242. Copyright 2010 American  
 467 Chemical Society.

468



469 Surface vibrational spectroscopy, such as sum frequency generation (SFG), is a nonlinear and  
470 interface-specific technique to investigate the structure and dynamics of the interface.<sup>285-287</sup> SFG  
471 has been widely used to study the liquid water-air interface under environmental conditions, and  
472 have contributed to the elucidation of environmental interfacial processes at the molecular  
473 level.<sup>234,288</sup> Several studies also utilized SFG to investigate water adsorption on minerals, including  
474 Al<sub>2</sub>O<sub>3</sub> and SiO<sub>2</sub>. For example, Ma et al.<sup>289</sup> suggested that at 35% RH,  $\alpha$ -Al<sub>2</sub>O<sub>3</sub>(0001) surface can  
475 be described as a H-bonding network formed by molecularly adsorbed water and surface hydroxyl  
476 groups H-bonded to the adsorbed water. A further study by Liu et al.<sup>290</sup> found that for SiO<sub>2</sub> at 54%  
477 RH, isolated silanol OH groups were in fact the major surface species and molecularly adsorbed  
478 water only covered a limited fraction of the surface. SFG can provide invaluable insights into the  
479 mechanisms of water adsorption on mineral dust particles, though absolute quantification of the  
480 adsorbed water is non-trivial.

481  
482 Many surface spectroscopic methods, such as FTIR, Raman, and SFG, as discussed above,  
483 typically provide the average information of the surface under investigation. Atomic force  
484 microscopy is a technique which can provide spatial resolution down to sub-nanometres under  
485 atmospheric relevant conditions.<sup>291-294</sup> If complemented with spectroscopic measurements, it could  
486 help elucidate the mechanisms of water adsorption on mineral dust surface.<sup>229</sup>

487  
488 Knudsen cell reactors are widely utilized to study the heterogeneous reactions of mineral dust  
489 particles with atmospheric reactive trace gases.<sup>151,184,295-297</sup> They have also been used to investigate  
490 the interaction of water vapor with mineral dust.<sup>298,299</sup> Because a Knudsen cell reactor is typically  
491 operated in the molecular flow regime (with a total pressure of less than 1 mTorr), the partial  
492 pressure of water vapor (and thus the RH) used in these experiments is very low. Therefore, these  
493 studies are less relevant for atmospheric chemistry and climate, though they can provide valuable

494 insights into the mechanisms of water adsorption on mineral dust. Molecular beam scattering  
495 techniques have been used to explore how gas molecules interact with surfaces of atmospheric  
496 chemistry interest,<sup>236,300-305</sup> and if applied to study mineral dust surface, can potentially help us  
497 understand the fundamental dynamics and kinetics of water adsorption.

### 498 **2.3 Levitated single particle measurements**

499 Levitation of single particles avoids potential effects due to interaction of different particles and  
500 those due to contact with the substrate used to support particles. A few particle levitation  
501 techniques, such as the electrodynamic balance (EDB) and optical levitation, have been widely  
502 used to study the hygroscopicity of aerosol particles.<sup>306</sup> Acoustic levitation is limited to particles  
503 with sizes of larger than 20  $\mu\text{m}$ , which are less relevant for atmospheric aerosols; therefore, this  
504 technique is not further described here.<sup>306</sup> In an EDB a combination of AC and DC electric fields  
505 is used to trap and levitate a charged particle,<sup>307</sup> with typical sizes of 5 to 50  $\mu\text{m}$ .<sup>306</sup> The mass of  
506 the particle is proportional to the balancing DC voltage, and the relative change of the particle  
507 mass at different RH, usually compared to that at 0% RH, is determined from the change of the  
508 DC voltage used to balance the gravitational force.<sup>251,307</sup> Though this technique seems to be a  
509 suitable technique to study the hygroscopic growth of mineral dust particles, to our knowledge it  
510 has not been applied to mineral dust particles yet.

511  
512 Optical levitation methods, e.g., optical tweezers, can routinely trap and levitate aqueous (and thus  
513 spherical) particles of 1-10  $\mu\text{m}$ ,<sup>252,306,308-310</sup> limiting their applications to mineral dust particles.  
514 However, recent advances show that spherical and quasi-spherical solid particles can also be  
515 trapped for many hours.<sup>139,252,311</sup> The size of a particle which is optically levitated can be estimated  
516 from the measured intensity of scattered light as a function of scattering angle, i.e. the phase  
517 function. Very accurate size measurements have been achieved by using optical tweezers. For  
518 example, a precision of better than 1 nm for measuring the diameter of micrometer sized droplets

519 has been reported, with simultaneous measurements of complex refractive indexes.<sup>312,313</sup> However,  
520 most of the sizing techniques based on light scattering are strictly applicable to spherical particles  
521 and thus may not be suitable for mineral dust particles which are typically non-spherical.

522  
523 An advantage of these levitation techniques is that, in addition to online measurements of particle  
524 mass/size, several non-intrusive techniques, such as Raman spectroscopy<sup>139,314</sup> and fluorescence  
525 spectroscopy,<sup>315</sup> can be used to measure the particle composition change simultaneously.  
526 Therefore, these techniques have a large potential to investigate the change of both chemical  
527 composition and hygroscopicity of single mineral dust particles due to heterogeneous reactions as  
528 a function of time.

## 529 **2.4 Aerosol measurements**

### 530 **2.4.1 Hygroscopic tandem differential mobility analyzer measurements**

531 Hygroscopicity-tandem differential mobility analyzers (H-TMDA) have been widely used to  
532 investigate the hygroscopicity of aerosol particles. Comprehensive discussions of this technique  
533 have been provided elsewhere,<sup>316-319</sup> and only a brief description is given here. In a typical H-  
534 TDMA set-up, a dry aerosol flow is passed through a bipolar charger and then into the first  
535 differential mobility analyzer (DMA) which is used to produce a quasi-monodisperse aerosol flow  
536 based on mobility diameters. These size-selected particles are then humidified to a certain RH and  
537 then enter the second DMA coupled to a condensation nuclei counter (CPC) to measure the size  
538 distribution of the humidified aerosol particles. The change in aerosol particle diameters before  
539 and after humidification can be used to derive the hygroscopic growth factors.

540  
541 H-TDMA has been widely used to measure the hygroscopicity of mineral dust aerosol  
542 particles.<sup>49,247,260,320</sup> However, there are a few issues related to its application to mineral dust  
543 particles: 1) dust particles are non-spherical in general, and thus it is non-trivial to interpret the

544 H-TDMA measurements; 2) the hygroscopicity of dust particles is relatively low, and the mobility  
545 diameter change before and after humidification may not be significant; and 3) restructuring of  
546 clay minerals may occur during humidification/dehumidification. Very recently Ardon-Dryer et  
547 al.<sup>321</sup> used several different techniques to measure the size distribution of size-selected mineral  
548 dust aerosol particles using a DMA, and concluded that mobility size selection using a DMA  
549 usually does not yield mineral dust particles with desired physical sizes. Similar findings were also  
550 reported by Veghte and Freedman.<sup>322</sup>

#### 551 **2.4.2 Optical properties**

552 Water adsorption by mineral dust aerosol particles may lead to change in their size (and probably  
553 also refractive indices), thus modifying the optical properties. The change in optical properties of  
554 aerosol particles, in principle, can then be used to derive their hygroscopicity.<sup>323</sup> A variety of in-situ  
555 instruments are readily available to measure aerosol optical extinction,<sup>324,325</sup> scattering,<sup>254,326-328</sup>  
556 and absorption.<sup>255,329</sup> For example, light extinction properties at 532 nm were measured at different  
557 RH using a Cavity Ring-Down spectroscopy, to investigate the hygroscopicity of several clay and  
558 clay/salt aerosol particles.<sup>253</sup> However, it is non-trivial to convert change in optical diameter at  
559 different RH to hygroscopicity for mineral dust aerosol particles, again due to the non-sphericity  
560 of dust particles.

#### 561 **2.4.3 Cloud condensation nuclei activity**

562 Under super-saturation (i.e. RH larger than 100%) aerosol particles can be activated to cloud  
563 droplets, and the number concentration of activated particles at a given super-saturation can be  
564 measured by using cloud condensation nuclei counters (CCNc). If such an instrument is coupled  
565 to a CPC in parallel, the activation fraction, defined as the ratio of the concentration of activated  
566 particles to the total particle number concentration, can then be determined. The most widely used  
567 cloud condensation nuclei counters are commercialized by Droplet Measurement Technologies  
568 (Boulder, CO, USA), based on the original design by Roberts and Nenes.<sup>330</sup>

569

570 Details on the principle, operation, and calibration of this instrument are provided elsewhere.<sup>330-</sup>

571 <sup>333</sup> A typical schematic diagram of the experimental set-up used by Kumar et al.<sup>262</sup> to measure the

572 CCN activity of aerosol particles is shown in Figure 7. A dry aerosol flow is delivered through an

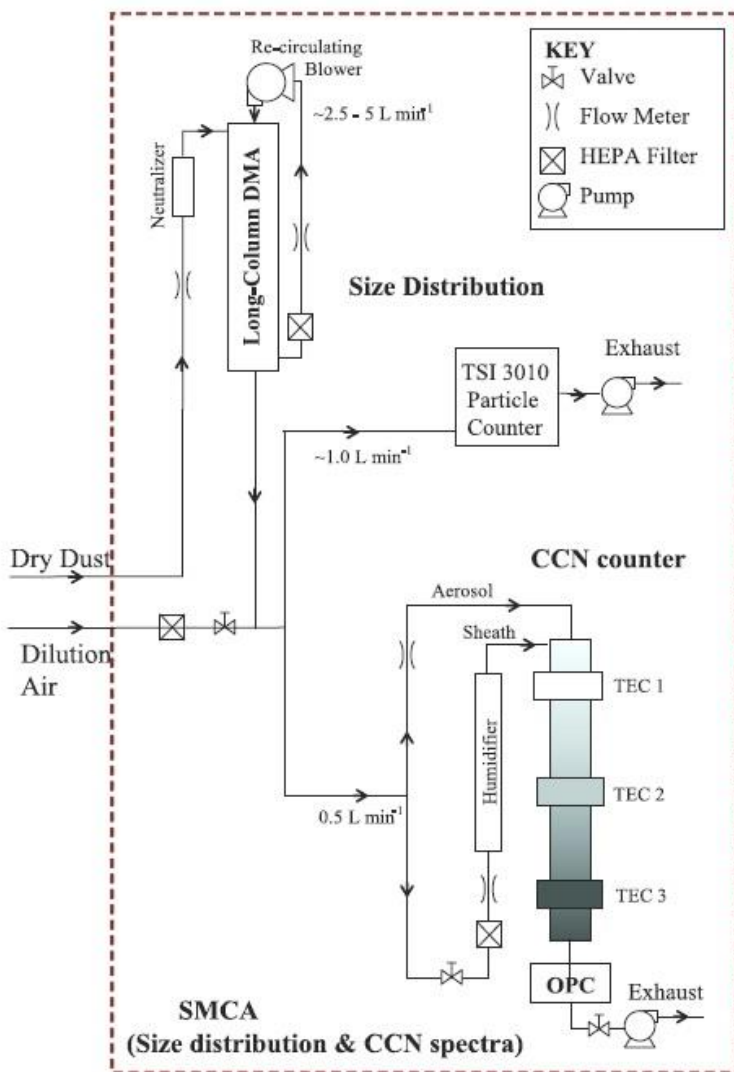
573 aerosol neutralizer and then into a DMA to produce a quasi-monodisperse aerosol particles. After

574 that, the aerosol flow is split: one flow is delivered into a CPC to measure the total particle number

575 concentration, and the other flow is delivered into a CCNc to measure the concentration of particles

576 activated to cloud droplets under a given super-saturation ratio (SS).

577



578

579 **Figure 7.** A schematic diagram of an experimental set-up used to determine the CCN activity of (mineral  
580 dust) aerosol particles. Reprinted with permission from ref 262. Copyright 2011 Copernicus Publications.

581  
582 There are usually two modes to operate a CCN counter: i) measuring the activation fraction as a  
583 function of super-saturation ratio for a given dry particle diameter to determine the critical super-  
584 saturation under which 50% of the aerosol particles are activated; ii) measuring the activation  
585 fraction as a function of the dry particle diameter under a given super-saturation to determine the  
586 critical dry diameter at which 50% of the aerosol particle are activated. This information can then  
587 be used to derive the cloud condensation nucleation activity of aerosol particles. This technique  
588 has been widely used to measure the cloud condensation nucleation activities of fresh and aged  
589 mineral dust particles,<sup>46,49,256,257,259,262</sup> significantly improving our understanding of the role of dust  
590 particles in the formation of clouds in the troposphere. Different theories used to describe the CCN  
591 activity, and the relation between hygroscopic growth under sub-saturation conditions and CCN  
592 activity under super-saturation conditions, are further discussed in more detail in Section 3.

## 593 **2.5 Discussion**

594 As summarized in this section, a wide range of techniques, based on different measurement  
595 principles, have been developed to study water adsorption, hygroscopicity, and CCN activity of  
596 mineral dust particles. Experimental techniques used to investigate the hygroscopic growth of  
597 mineral dust aerosol particles are based on measurements of changes in diameter at different RH.  
598 For examples, H-TDMA measures the change in mobility diameter and AE-CRD measures the  
599 change in optical extinction properties which can then be related to particle size using Mie theory  
600 which assumes particles are spherical. Since mineral dust particles are typically non-spherical, it  
601 is non-trivial to quantify the absolute amount of water associated with aerosol particles at a given  
602 RH, though they can provide other important information, such as the dependence of particle  
603 mobility and optical properties on RH. Aerosol particle mass analyzers (usually referred to as APM

604 or PMA) have been widely used to classify aerosol particles based on their mass.<sup>334-338</sup> In principle,  
605 two APM and one CPC can be combined to measure changes in the aerosol particle mass as a  
606 function as RH, in a similar way as a H-TDMA system is constructed. In brief, dry dust aerosol  
607 particles with the same mass is selected by the first APM; after that, the aerosol flow will be  
608 humidified to a given RH, and the mass distribution of the humidified dust aerosol particles will  
609 be measured by the second APM coupled to a CPC. This instrument has promising potential to  
610 quantitatively determine the mass change of mineral dust particles as a function of RH.

611  
612 Diameter changes of single particles trapped by optical levitation techniques at different RH are  
613 usually determined by light scattering. The non-sphericity of mineral dust particles can render the  
614 data interpretation difficult. Relative mass changes of single particles levitated in an EDB can be  
615 directly measured, regardless of the particle shape. EDB has been used to determine the amount  
616 of water adsorbed by pollen particles which are also non-spherical,<sup>339</sup> and therefore can also be  
617 used to study water adsorption by mineral dust particles. Nevertheless, it is still unclear if the EDB  
618 is sensitive enough to detect small mass changes of dust particle due to water adsorption.

619  
620 FTIR based techniques have been widely used to monitor adsorbed water by mineral dust particles  
621 supported on substrates.<sup>250,268,269</sup> Although in principle adsorbed water can be quantified by its IR  
622 absorption bands, this types of analysis typically requires several assumptions which may  
623 introduce uncertainties in quantification.<sup>249</sup> In this aspect, techniques which can directly quantify  
624 changes in dust particle mass<sup>247,249,271</sup> or water vapor pressure,<sup>212,248</sup> due to the interaction of water  
625 vapor with mineral dust, show their advantages. For techniques which use particles supported on  
626 substrates, particles are usually not size-selected and therefore it is difficult to investigate the size  
627 dependence of the amount of water associated with particles (for the same mass of dry materials,  
628 surface adsorption theories indicate that the amount of adsorbed water increases with decreasing

629 particle diameter while the hygroscopic growth theory implies that it is size-independent, as  
630 discussed in detail in Section 3). Many surface science techniques, though they may not  
631 quantitatively measure adsorbed water, can nevertheless provide valuable information about  
632 chemical composition, morphology, and adsorption mechanisms on the fundamental level, with  
633 some examples given in Section 2.2.3.

634  
635 For CCN activity measurements, it is critical to accurately determine the dry particle diameters.  
636 Typically a DMA is used to classify aerosol particles based on their mobility. The mobility  
637 diameter is not necessarily equivalent to the geometrical diameter for dust particles, due to their  
638 non-sphericity. This has also been supported by experimental work,<sup>321,322</sup> showing that mobility  
639 size selection using a DMA usually does not generate mineral dust particles with desired physical  
640 sizes. Additionally, after passing through the aerosol neutralizer, dry-generated dust aerosol  
641 particles may consist of a substantial fraction of multiply charged particles which in fact have larger  
642 diameters and can be activated to cloud droplets at lower supersaturation, compared to single  
643 charged particles. Both factors can lead to biases in the reported CCN activity,<sup>259</sup> and therefore  
644 charge and shape corrections should be applied in determining the CCN activity of mineral dust  
645 particles.

### 646 **3 Introduction of different theories**

647 Several different theories have been developed to describe the partitioning of water between the  
648 gas phase and mineral dust particles under both sub- and super-saturation conditions with respect  
649 to liquid water. Most widely used theories are introduced in this section. These theories can be  
650 generally classified to two groups, with one originating from surface science and surface chemistry  
651 and the other one developed for atmospheric aerosol science.



### 652 **3.1 Theories and models used to describe sub-saturation conditions**

653 Several different models are available to describe the amount of the adsorbate adsorbed at different  
654 partial pressures.<sup>340-342</sup> In this review, water is the adsorbate and its partial pressure is expressed as  
655 RH instead, and mineral dust particles (or their surfaces) are the adsorbents. Among adsorption  
656 models, the Langmuir adsorption isotherm model<sup>341-343</sup> is the first and probably the most widely  
657 used adsorption theory, but its application is limited to adsorption below one monolayer. Therefore,  
658 it is not suitable to describe water adsorption on mineral dust particles at high RH and thus no  
659 further discussion on the Langmuir adsorption isotherm is provided here.

#### 660 **3.1.1 Brunauer-Emmett-Teller adsorption isotherm model**

661 The Brunauer-Emmett-Teller (BET) adsorption isotherm<sup>341,342,344</sup> can be used to describe water  
662 adsorption for mineral dust particles.<sup>250</sup>

$$663 \theta = \frac{c \cdot RH}{(1 - RH)(1 - RH + c \cdot RH)} \quad (3),$$

664 where  $\theta$  is the surface coverage of adsorbed water, and  $c$  is a constant related to the enthalpy of  
665 desorption,  $\Delta_{des}H^0$  (kJ K<sup>-1</sup>):

$$666 c = \exp[(\Delta_{des}H^0 - \Delta_{vap}H^0)/RT] \quad (4),$$

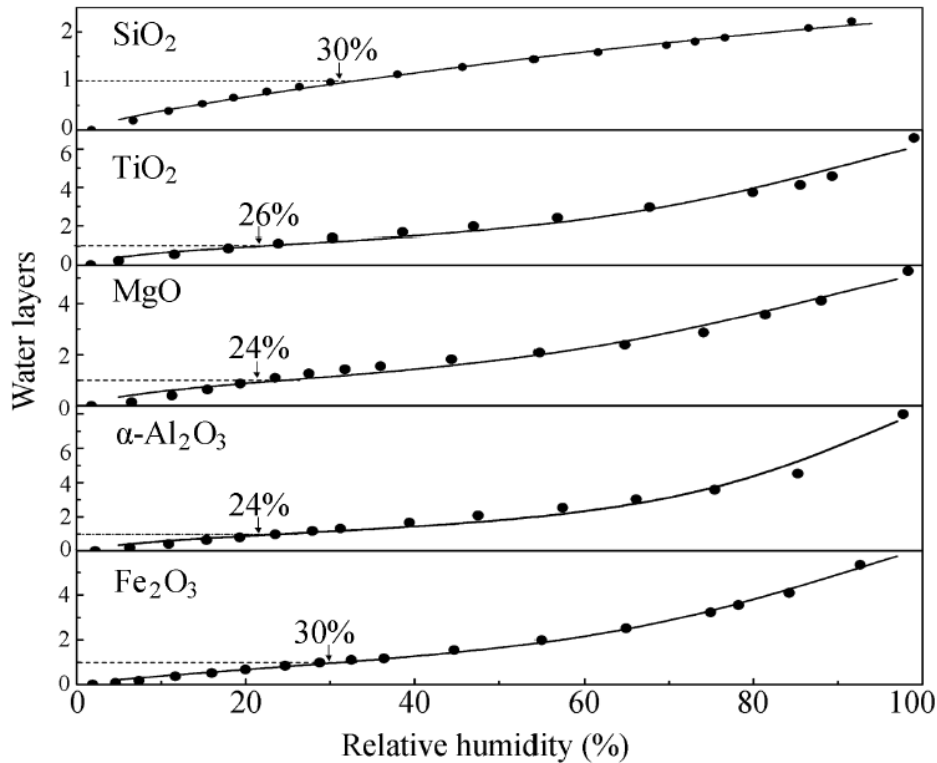
667 where  $R$  is the gas constant (8.314 J mol<sup>-1</sup> K<sup>-1</sup>),  $T$  is the temperature (K), and  $\Delta_{vap}H^0$  is the standard  
668 enthalpy of water evaporation (kJ K<sup>-1</sup>). For the adsorption of water on mineral dust,  $c$  is usually  
669 found to be  $>1$ , suggesting that  $\Delta_{des}H^0$  is larger than  $\Delta_{vap}H^0$ .<sup>250</sup>

670

671 It has been found that in many cases that the BET equation, Eq. (3), may overestimate the surface  
672 coverage of adsorbed water ( $\theta$ ) at high RH. Therefore, by introducing the third parameter,  $n$ , a  
673 modified three-parameter BET equation has been proposed to describe the water adsorption on  
674 mineral particles:<sup>345</sup>

$$675 \theta = \frac{c \cdot RH}{(1 - RH)} \cdot \frac{1 - (n+1) \cdot RH^n + n \cdot RH^{n+1}}{1 + (c-1) \cdot RH - c \cdot RH^{n+1}} \quad (5).$$

676 Goodman et al.<sup>250</sup> found that the three-parameter BET equation could fit fairly well the water  
 677 adsorption on several different mineral dust particles for RH ranging from ~0% to >90%. They<sup>250</sup>  
 678 also described in details how to derive  $c$  and  $n$  from experimentally measured  $\theta$  as a function of  
 679 RH, using Eq. (5). Ma et al.<sup>269</sup> also suggested that the three-parameter BET equations can fit well  
 680 water adsorption on five different oxides which they investigated, as shown in Figure 8.



681  
 682 **Figure 8.** Water adsorption on SiO<sub>2</sub>, TiO<sub>2</sub>, MgO, α-Al<sub>2</sub>O<sub>3</sub>, and Fe<sub>2</sub>O<sub>3</sub> as a function of RH at 30 °C. Circles  
 683 represent experimental data and curves represent corresponding fitted three-parameter BET isotherms.  
 684 Relative humidities under which a monolayer of adsorbed water is formed are given in the figure for each  
 685 minerals. Reprinted with permission from ref 269. Copyright 2011 Elsevier.

### 686 3.1.2 Freundlich adsorption isotherm model

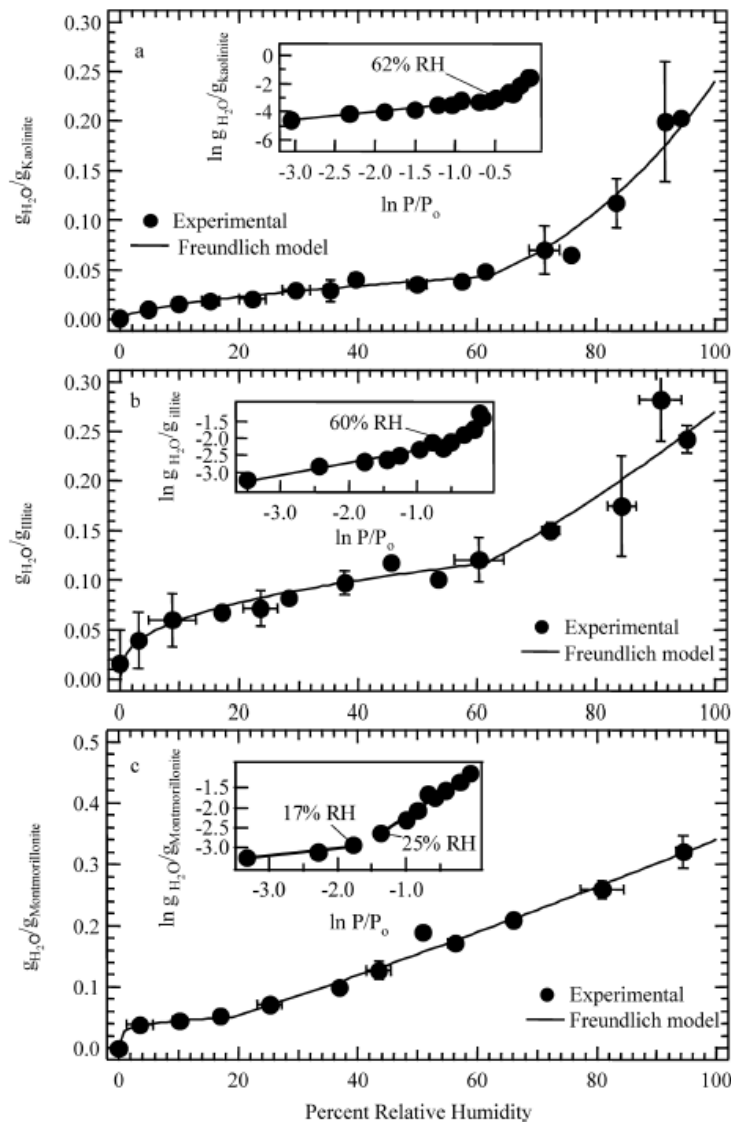
687 The Freundlich adsorption isotherm expresses the mass ratio of the adsorbed water to the dry  
 688 mineral dust particles as a function of partial pressure or RH:<sup>346,347</sup>

689 
$$\frac{m(\text{water})}{m(\text{mineral})} = A_F \cdot {}^{B_F}\sqrt{RH} \quad (6),$$

690 where  $m(\text{water})$  and  $m(\text{mineral})$  are the mass of adsorbed water and dry mineral dust particles, and  
 691  $A_F$  and  $B_F$  are the empirical Freundlich constants which represent the adsorption capacity and  
 692 strength, respectively.<sup>268</sup> Eq. (6) can be rearranged to

$$693 \ln \frac{m(\text{water})}{m(\text{mineral})} = \ln A_F + \frac{\ln(RH)}{B_F} \quad (7),$$

694 Therefore, simple linear regression of the natural logarithm of the mass ratio (of adsorbed water  
 695 to dry dust particles) versus the natural logarithm of RH can be used to derive  $A_F$  and  $B_F$ .



696  
 697 **Figure 9.** Measured and modeled water adsorption (represented by the mass ratio of adsorbed water to dry  
 698 mineral) at 298 K as a function of RH on (a) kaolinite, (b) illite, and (c) montmorillonite. The insets

699 represent the data fitted to the linear form of the Freundlich adsorption isotherm, i.e. Eq. (7). Reprinted with  
700 permission from ref 268. Copyright 2011 American Chemical Society.

701  
702 Hatch et al.<sup>268</sup> measured water adsorption on illite, kaolinite, and montmorillorite particles, and  
703 fitted these experimental results using the Freundlich adsorption isotherm, as shown in Figure 9.  
704 It was suggested that compared to the two-parameter BET adsorption isotherm, the Freundlich  
705 adsorption isotherm can better describe water adsorption by these three clay minerals they  
706 investigated.<sup>268</sup>

### 707 **3.1.3 Frenkel-Halsey-Hill adsorption isotherm model**

708 The Frenkel-Halsey-Hill (FHH) isotherm uses a two-parameter equation to describe RH as a  
709 function of surface coverage of adsorbed water,  $\theta$ :

$$710 \quad RH = \exp(-A_{FHH} \cdot \theta^{-B_{FHH}}) \quad (8),$$

711 where  $A_{FHH}$  and  $B_{FHH}$  are empirical parameters.<sup>341,348</sup>  $A_{FHH}$  describes interactions between the  
712 surface and first adsorbed water layer and interactions between adjacent adsorbed water molecules.  
713 Therefore, it governs the overall extent of water coverage, and higher  $A_{FHH}$  values suggest that  
714 more water may be adsorbed.  $B_{FHH}$  describes interactions between the surface and subsequent  
715 adsorbed water layers. Smaller  $B_{FHH}$  values mean that attractive forces function over a longer  
716 distance from the particle surface. As a result,  $B_{FHH}$  significantly influences the shape of the  
717 adsorption isotherm, especially at high RH. Consequently, CCN activation described by the FHH  
718 activation theory is predominantly determined by the magnitude of  $B_{FHH}$ ,<sup>47,52</sup> and this will be  
719 further discussed in Section 3.2.2.

720  
721 Eq. (8) can be rearranged to

$$722 \quad \ln[-\ln(RH)] = \ln A_{FHH} - B_{FHH} \cdot \ln(\theta) \quad (9).$$

723 As shown in Eq. (9),  $A_{FHH}$  and  $B_{FHH}$  can be derived from linear regression of  $\ln[-\ln(RH)]$  versus  
 724  $\ln(\theta)$ . We can also describe the surface coverage of adsorbed water as a function of RH by  
 725 rearranging Eq. (9):

$$726 \quad \theta = B_{FHH} \sqrt{\frac{A_{FHH}}{-\ln(RH)}} \quad (10).$$

### 727 3.1.4 Hygroscopic growth theory

728 The change of the diameter of a particle at elevated RH due to adsorption of water, called  
 729 hygroscopic growth in aerosol science, can be described by the single hygroscopicity parameter,  
 730  $\kappa$ .<sup>169</sup>

$$731 \quad RH = \frac{GF^3 - 1}{GF^3 - (1 - \kappa)} \exp\left(\frac{A_{Kelvin}}{D_d \cdot GF}\right) \quad (11),$$

$$732 \quad A_{Kelvin} = \frac{4\sigma M_w}{RT\rho_w} \quad (12),$$

733 where GF is the growth factor, defined as the ratio of the diameter of a particle at a given RH to  
 734 that of the dry particle ( $D_d$ ).<sup>169</sup> The second term in the right part of Eq. (11),  $\exp(A_{Kelvin}/D_d \cdot GF)$ , is  
 735 due to the Kelvin effect, referring to the increase of vapor pressure on a curved surface of the  
 736 particle, relative to that for a flat surface.  $A_{Kelvin}$  is a constant which describes the Kelvin effect,  
 737 depending on the surface tension ( $\sigma$ ), density ( $\rho_w$ ) and molar mass ( $M_w$ ) of water, and temperature.  
 738  $A_{Kelvin}$  is equal to  $2.1 \times 10^{-9}$  m for a surface tension of  $0.072$  J m<sup>-2</sup> (pure water) and temperature of  
 739  $298.15$  K.<sup>217</sup>

740

741 The Kelvin effect becomes negligible for large particles, and in this case Eq. (11) can be simplified  
 742 to

$$743 \quad RH = \frac{GF^3 - 1}{GF^3 - (1 - \kappa)} \quad (13).$$

744 Eq. (13) can then be rearranged to express GF as a function of RH:

$$745 \quad GF = \sqrt[3]{1 + \kappa \cdot \frac{RH}{1 - RH}} \quad (14).$$

746 Calculations show that the difference between calculated GF at 90% using Eq. (11) (i.e. taking  
747 into account the Kelvin effect) and that using Eq. (14) (i.e. neglecting the Kelvin effect) is  
748 negligible for particles with dry diameters larger than 100 nm. As a result, in this review for  
749 simplicity, Eq. (14) is used to calculate hygroscopic growth factors and thus also amounts of  
750 adsorbed water at different RH for mineral dust particles.

751 The surface coverage,  $\theta$ , can be expressed as the change of particle diameters:<sup>47,349</sup>

$$752 \quad \theta = \frac{D-D_d}{2D_w} = \frac{GF-1}{2} \cdot \frac{D_d}{D_w} \quad (15).$$

753 where  $D_d$  and  $D$  are the diameters of the dry particle and the wet particle.  $D_w$  is the average diameter  
754 of a water molecule adsorbed on the particle surface.  $D_w$  is sometimes assumed to be 0.275  
755 nm,<sup>47,349</sup> meaning that a water molecule adsorbed on mineral dust surface occupies an area of  
756  $5.9 \times 10^{-16}$  cm<sup>2</sup>. Al-Abadleh et al.<sup>211</sup> assumes that the hydroxylated CaCO<sub>3</sub> surface can  
757 accommodate  $1 \times 10^{15}$  water molecules per cm<sup>2</sup>, i.e. a water molecule adsorbed on the surface  
758 occupies an area of  $1 \times 10^{-15}$  cm<sup>2</sup> (or 0.1 nm<sup>2</sup>), corresponding to  $D_w$  of 0.36 nm. In this paper, the  
759 diameter of one water molecule adsorbed on a mineral dust particle is always assumed to be  
760 0.36 nm.

### 761 **3.1.5 Discussion**

762 There is a fundamental difference between adsorption theories originating from surface science  
763 and hygroscopicity theories used to describe the interaction of water vapor with mineral particles  
764 under sub-saturation conditions. All adsorption theories assume that at given RH and  $T$ , the amount  
765 of water adsorbed by mineral particles is proportional to the total surface area; therefore, for the  
766 same amount (mass or volume) of dry material, the amount of water adsorbed by mineral particles  
767 increase with decreasing average particle diameter. On the other hand, hygroscopicity theories  
768 assume that the amount of water is proportional to the volume of solute, and thus for the same  
769 amount of dry material, the amount of water associated with mineral dust is independent of particle

770 diameter, if the Kelvin effect is negligible. This difference can make direct comparison of some  
771 experimental measurements difficult, and this issue will be discussed further in Section 3.3.

## 772 **3.2 Theories and models used to describe super-saturation conditions**

### 773 **3.2.1 $\kappa$ -Köhler activation theory**

774 The saturation ratio of water vapor,  $S$ , in equilibrium with an aqueous droplet, can be describe by  
775 the Köhler theory,<sup>350</sup> which takes into account the effects of both water activity and surface  
776 curvature:

$$777 \quad S = a_w \cdot \exp\left(\frac{A_{\kappa}}{D}\right) \quad (16),$$

778 where  $a_w$  is the water activity, and  $D$  is the droplet diameter, and  $A_{\text{Kelvin}}$  is defined in Eq. (12). In  
779 fact the definition of  $S$  is the same as RH, as shown in Eq. (1). However, to keep consistent with  
780 conventional terminology,  $S$  is used for super-saturation conditions and RH is used for sub-  
781 saturation conditions. The single hygroscopicity parameter,  $\kappa$ , links water activity ( $a_w$ ), the volume  
782 of the dry particle ( $V_s$ ), and the volume of water ( $V_w$ ):<sup>169,351</sup>

$$783 \quad \frac{1}{a_w} = 1 + \kappa \frac{V_s}{V_w} \quad (17),$$

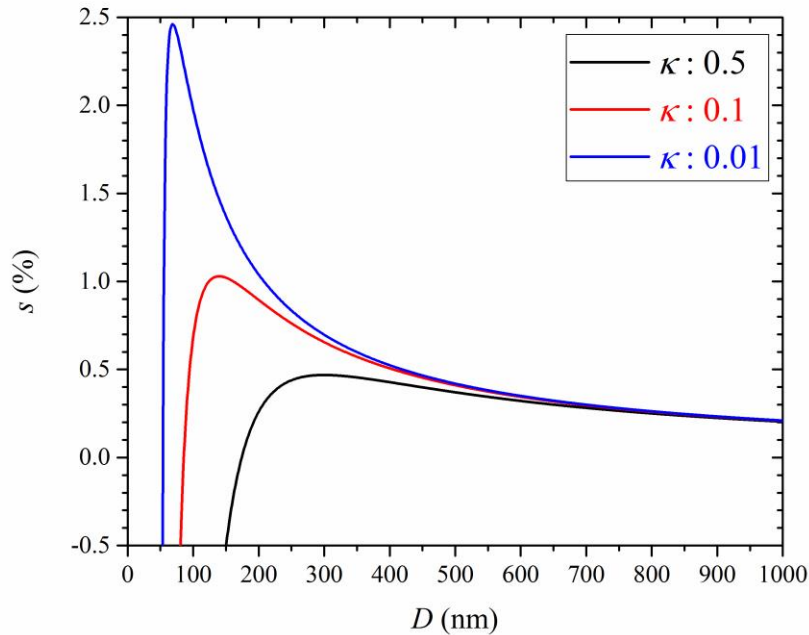
784 As shown by Petters and Kreidenweis (2007),<sup>169</sup> inserting Eq. (17) into Eq. (16) and converting  
785 volumes to corresponding diameters can yield the “ $\kappa$ -Köhler theory” equation:

$$786 \quad S(D) = \frac{D^3 - D_d^3}{D^3 - (1 - \kappa) \cdot D_d^3} \cdot \exp\left(\frac{A_{\kappa}}{D}\right) \quad (18).$$

787

788 The critical saturation for a dry particle,  $S_c$ , is defined as the saturation above which the particle is  
789 activated to a cloud droplet. The critical super-saturation,  $s_c$ , which is equal to  $S_c - 1$ , is more widely  
790 used in describing cloud condensation nucleation. For a particle with given dry diameter and  
791 hygroscopicity,  $S_c$  (and thus  $s_c$ ) can be calculated from the maximum of the  $\kappa$ -Köhler curve, i.e.  
792 Eq. (18). Three  $\kappa$ -Köhler curves, for particles with a dry diameter of 50 nm and different  
793 hygroscopicity, are plotted in Figure 10 as examples. The maxima of  $s$ , i.e.,  $s_c$ , are 0.47%, 1.03%,

794 and 2.46% for 50 nm particles with  $\kappa$  values of 0.5, 0.1, and 0.01, respectively. If the  
795 supersaturation ratio in the ambient air is larger than the  $s_c$  for a given particle, this particle will be  
796 activated to a cloud droplet.



797  
798 **Figure 10.** Calculated super-saturations as a function of the diameter of aqueous particles with a dry  
799 diameter of 50 nm and different hygroscopicity ( $\kappa$  is equal to 0.5, 0.1, and 0.01, respectively), using Eq.  
800 (18). Note that super-saturation ( $s$ ) instead of saturation ( $S$ ), is plotted.

801  
802 The same procedure can be applied to a wide range of  $D_d$  and  $\kappa$  to calculate corresponding  $s_c$ , and  
803 a look-up table for  $s_c$  as a function of  $D_d$  and  $\kappa$  can then be produced. The critical super-saturation,  
804  $s_c$ , for monodisperse aerosol particles with a dry diameter of  $D_d$ , or alternatively the critical  
805 diameter of polydisperse aerosol particles for a given super-saturation, can be measured using the  
806 procedure described in Section 2.3.3. Corresponding  $\kappa$  values can then be derived from  $s_c$  and  $D_d$ ,  
807 using the look-up table.



### 808 3.2.2 Frenkel-Halsey-Hill adsorption activation theory

809 The FHH adsorption activation theory<sup>349</sup> describes the activity of adsorbed water on the surface  
810 of insoluble particles:

$$811 a_w = \exp[-A_{FHH} \cdot \theta^{-B_{FHH}}] \quad (19),$$

812 where  $\theta$  is the surface coverage of water, and  $A_{FHH}$  and  $B_{FHH}$  are empirical parameters which are  
813 described in Eq. (8). Inserting Eq. (19) into Eq. (16) gives

$$814 S = \exp[-A_{FHH} \cdot \theta^{-B_{FHH}}] \cdot \exp\left(\frac{A_K}{D_d}\right) \quad (20).$$

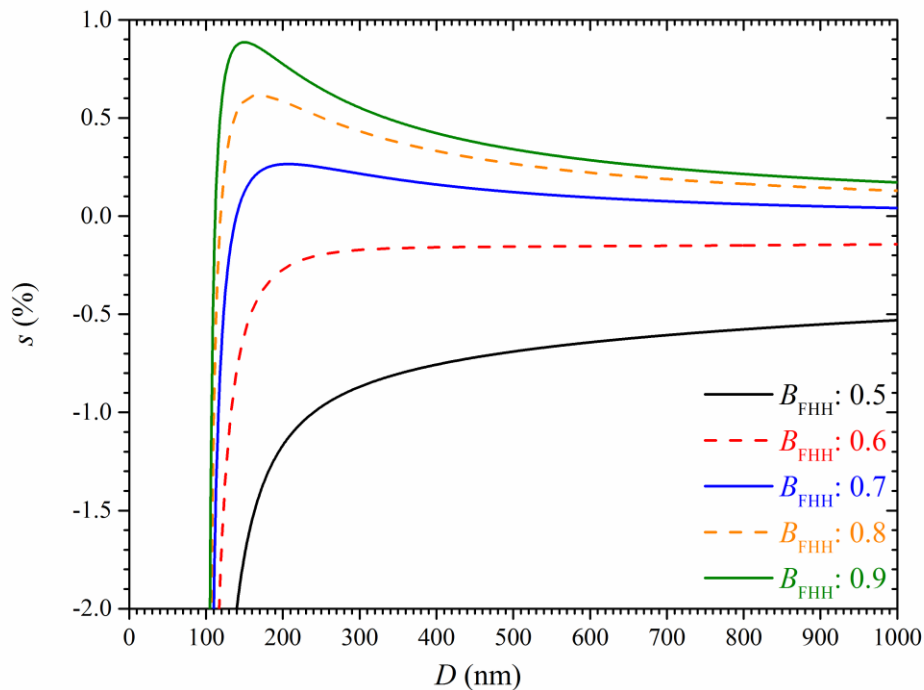
815  $A_{FHH}$  and  $B_{FHH}$  can be derived from the fit to the  $s_c$ - $D_d$  data, as detailed by Kumar et al.<sup>52</sup>

816

817  $A_{FHH}$  and  $B_{FHH}$  vary with different compounds. Typically,  $A_{FHH}$  ranges from 0.1 to 3.0, and  $B_{FHH}$   
818 ranges from 0.5 to 3.0.<sup>349</sup> If the dry diameter,  $A_{FHH}$  and  $B_{FHH}$  are known for a particle, the critical  
819 super-saturation can be calculated from the maximum of its FHH adsorption activation curve.  
820 Three FHH curves for  $B_{FHH}$  values of 0.7, 0.8, and 0.9 (all with an  $A_{FHH}$  value of 0.3) are shown in  
821 Figure 11, and have  $s_c$  values of ~0.26%, ~0.62%, and ~0.89%, respectively. If the supersaturation  
822 ratio in the ambient air is larger than the  $s_c$  for a given particle, this particle will be activated to a  
823 cloud droplet.

824

825 If  $B_{FHH}$  is small enough, the activation curve may never reach a maximum but instead asymptotes  
826 to a negative value,  $-s_\infty$ . Two FHH curves with  $B_{FHH}$  values of 0.5 and 0.6 (and  $A_{FHH}$  is 0.3 for both  
827 cases), are shown in Figure 11 for illustration. The asymptotic value of  $s$  at very large  $D_p$   
828 determines if this particle will be activated:<sup>47</sup> if it is smaller than 0, the particle can be  
829 spontaneously activated at RH less than 100%; otherwise, the particle will never be activated (i.e.  
830 always in stable equilibrium with the environment). However, such observations have not been  
831 reported yet, shedding doubt on its atmospheric relevance.



832

833 **Figure 11.** Calculated super-saturations as a function of the diameter of a wet particle, here for a dry  
 834 diameter of 100 nm, using Eq. (20).  $A_{\text{FHH}}$  is assumed to be 0.3, and  $B_{\text{FHH}}$  are assumed to be 0.5, 0.6, 0.7,  
 835 0.8, and 0.9, respectively. Note that super-saturation ( $s$ ) instead of saturation ( $S$ ), is plotted.

836

837 The two empirical FHH parameters,  $A_{\text{FHH}}$  and  $B_{\text{FHH}}$ , can be determined by measuring the surface  
 838 coverage ( $\theta$ ) of adsorbed water as a function of RH under sub-saturation conditions, as discussed  
 839 in Section 3.1.3. Alternatively, they can also be determined by measuring critical super-saturation  
 840 as a function of particle diameter under super-saturation conditions.<sup>262,263</sup>

841

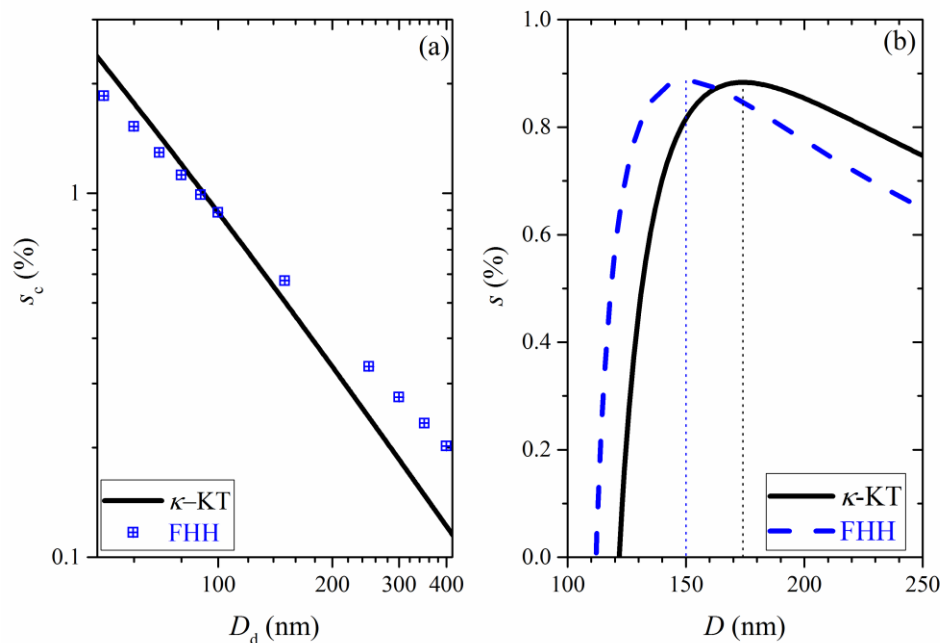
842 Activity of adsorbed water can also be described by other water adsorption isotherms (e.g., the  
 843 BET adsorption isotherm), and corresponding adsorption activation theories, analogous to Eq. (20),  
 844 can be subsequently derived. For example, the BET adsorption activation theory has been  
 845 developed and applied to describe cloud activation of black carbon particles.<sup>352</sup> To our knowledge,  
 846 this theory has not been used to describe cloud activation of mineral dust particles, and therefore  
 847 it is not discussed further in this review.

### 848 3.2.3 Discussion

849 It has been shown that both  $\kappa$ -Köhler and FHH theories are superior to the original Köhler theory,  
850 at the expense of increased complexity, since they can account for the hygroscopic content of  
851 mineral dust.<sup>47,52,217</sup> Differences do exist between these two methods. As noted by Kumar et al,<sup>47,52</sup>  
852 using FHH theory changes the maximum super-saturations and cloud droplet number with respect  
853 to aerosol variations, compared to the  $\kappa$ -Köhler theory. This is because when compared to the  $\kappa$ -  
854 Köhler theory, the FHH activation theory requires less water uptake to reach a critical diameter.  
855 This is further illustrated by Figure 12, displaying the  $\kappa$ -Köhler and FHH activation curves for a  
856 particles with a dry diameter of 100 nm. Both theories suggest that the particle will be activated at  
857 a super-saturation of  $\sim 0.88\%$ . However, the predicted wet particle diameters when super-saturation  
858 is equal to  $s_c$  are different, with 150 nm predicted by the FHH activation theory and 174 nm  
859 predicted by the  $\kappa$ -Köhler theory. As a result, compared to the  $\kappa$ -Köhler theory, the FHH activation  
860 theory requires less water uptake for the particle to be activated.

861

862 In addition, the two theories suggest different dependence of  $s_c$  on  $D_d$ , as shown in Figure 12. Both  
863 theories suggest that a particle with a dry diameter of 100 nm has the same  $s_c$ . Compared to the  $\kappa$ -  
864 Köhler theory, the FHH activation theory predicts that particles with  $D_d < 100$  nm will be activated  
865 at smaller  $s_c$  while they have larger  $s_c$  for  $D_d > 100$  nm.



866

867 **Figure 12.** Comparison of  $\kappa$ -Köhler ( $\kappa = 0.014$ ) and FHH ( $A_{\text{FHH}} = 0.3$ ,  $B_{\text{FHH}} = 0.9$ ) activation theories.

868 Values of  $\kappa$ ,  $A_{\text{FHH}}$ , and  $B_{\text{FHH}}$  are chosen in such a way that both theories predict that a particle with a dry

869 diameter ( $D_d$ ) of 100 nm will have a  $s_c$  of  $\sim 0.88\%$ . (a) Predicted  $s_c$  as a function of  $D_d$  by  $\kappa$ -Köhler (solid

870 black curve) and FHH (blue squares) activation theories. (b) Calculated activation curves for a particle with

871 a dry diameter of 100 nm by  $\kappa$ -Köhler (solid black curve) and FHH (dashed blue curve) activation theories.

872

873 A recent study suggests that the  $\kappa$ -Köhler activation theory provides a better fit to laboratory data

874 with slightly less complexity of calculation.<sup>259</sup> Nevertheless, it still remains under debate which

875 theory can better describe the activation of cloud droplets by mineral dust particles.

### 876 3.3 Suggested guidelines used for data comparison

877 The amounts of water adsorbed or condensed on mineral dust particles are reported in different

878 ways. The following guidelines are used to compare available data for each type of mineral

879 particles:

880

881 i) Under super-saturation conditions the single hygroscopic parameter,  $\kappa$ , is usually reported. Using  
882 Eq. (14), reported  $\kappa$  values can be converted to the hygroscopic growth factors, which are directly  
883 measured by H-TDMA under sub-saturation conditions.

884

885 ii) The change in particle diameters due to hygroscopic growth, calculated from measured  $\kappa$  values  
886 or directly measured by H-TDMA, can be converted to the surface coverage ( $\theta$ ) of adsorbed water,  
887 using Eq. (15). Usage of Eq. (15) requires the knowledge of dry particle diameter. In this review,  
888 three different dry particle diameters, i.e. 500, 1000, and 2000 nm, are used when we convert  
889 hygroscopic growth factors to surface coverages,  $\theta$ , using Eq. (15). The dry particle diameter ( $D_d$ )  
890 and the hygroscopic growth factor at a given RH can be used to calculate the wet particle diameter  
891 ( $D$ ) at this RH, and the number of monolayers (i.e. surface coverage) of adsorbed water is  
892 approximately equal to  $(D_d - D)/D_w$ , where  $D_w$  is the average diameter of the adsorbed water  
893 molecules. We choose these three diameters because they may reasonably represent the size range  
894 of tropospheric dust particles after long range transport. According to Eq. (15), the calculated  $\theta$  is  
895 proportional to the dry particle diameter used in the calculation. Therefore, large uncertainties may  
896 occur when converting hygroscopic growth factors to  $\theta$ , making data comparison difficult. For  
897 example, for the same hygroscopic growth factor, the calculated  $\theta$  using a dry particle diameter of  
898 1000 nm will be twice as large as that using a dry particle diameter of 500 nm. In some CCN  
899 activity measurements the two FHH parameters (instead of  $\kappa$  values) are reported,<sup>262,263</sup> in this case,  
900 the surface coverage of adsorbed water at different RH can be directly calculated using Eq. (10).

901

902 iii) If the mass ratio of adsorbed water to dry mineral particle is reported, the surface coverage ( $\theta$ )  
903 of adsorbed water can then be calculated by

904 
$$\theta = \frac{m(\text{water})}{m(\text{mineral})} \cdot \frac{N_A \cdot A(\text{water})}{M(\text{water}) \cdot A_{BET}} \quad (21),$$

905 where  $m(\text{water})$  and  $m(\text{mineral})$  are the masses (g) of adsorbed water and dry mineral,  $M_m(\text{water})$   
906 is the molar mass of water ( $\text{g mol}^{-1}$ ),  $N_A$  is the Avogadro constant ( $6.02 \times 10^{23} \text{ mol}^{-1}$ ),  $A(\text{water})$  is  
907 the average surface area of one adsorbed water molecule ( $1 \times 10^{-15} \text{ cm}^2$ ), and  $A_{\text{BET}}$  is the BET area  
908 ( $\text{cm}^2 \text{ g}^{-1}$ ) of the mineral.

909

910 It should be emphasized that large uncertainties may occur when we convert reported data in other  
911 units to  $\theta$ . The largest uncertainties may come from i) converting hygroscopic growth factors,  
912 either directly measured by using H-TDMA or calculated from  $\kappa$  values determined by CCN  
913 activity measurements, to surface coverages of adsorbed water, and ii) the nonsphericity (and  
914 probably also porosity) of mineral particles. In this review it is always assumed that the mass-,  
915 volume-, and surface area-equivalent diameters are equal to mobility diameters. However, this is  
916 a clear oversimplification and will inherently yield some uncertainty for mineral dust particles  
917 which are typically non-spherical.<sup>353</sup>

#### 918 **4 Water adsorption properties, hygroscopicity, and CCN activity of fresh and** 919 **aged mineral dust particles**

920 In this section, the interaction of water vapor with different components of mineral dust particles  
921 under both sub-saturation and super-saturation conditions are reviewed. Mineral dust particles  
922 covered in this section include calcium carbonate ( $\text{CaCO}_3$ , usually in the form of calcite), Arizona  
923 Test Dust, illite, kaolinite, montmorillonite, quartz, several metal oxides ( $\text{TiO}_2$ ,  $\text{Al}_2\text{O}_3$ , and  $\text{Fe}_2\text{O}_3$ ),  
924 and authentic desert dust samples. Laboratory studies on the effects of atmospheric aging through  
925 heterogeneous processes are also reviewed. We also discuss some theoretical studies on water  
926 adsorption on mineral dust surfaces. After that, we summarize some field measurements that have  
927 provided evidence that chemical transformation in the atmosphere could change the interaction of  
928 mineral dust particles with water vapor. A brief summary is then provided to conclude this section.

929 **4.1 Calcium carbonate**

930 With respect to the interaction with water vapor, calcium carbonate (CaCO<sub>3</sub>), usually in the form  
931 of calcite, is the most widely investigated component of mineral dust particles. We first review the  
932 interactions of water vapor with fresh CaCO<sub>3</sub>, and then discuss the effects of chemical aging on  
933 these interactions.

934 **4.1.1 Fresh CaCO<sub>3</sub> particles**

935 As shown in Table 4, the interaction of fresh CaCO<sub>3</sub> particles with water vapor has been  
936 investigated under both sub-saturation and super-saturation conditions by a number of studies.

937

938 **Table 4.** Water adsorption, hygroscopicity, and CCN activity of fresh CaCO<sub>3</sub> particles: summary of  
939 previous studies.

references	techniques	aerosol generation method
Al-Hosney et al., 2005 <sup>354</sup>	ATR-FTIR	not applicable
Gustafsson et al., 2005 <sup>247</sup>	DRIFTS, TGA, and H-TDMA	wet generation
Gibson et al., 2006 <sup>355</sup>	H-TDMA and CCNc	wet generation
Gibson et al., 2007 <sup>257</sup>	CCNc	wet generation
Schuttlefield, 2008 <sup>356</sup>	QCM	not applicable
Hatch et al., 2008 <sup>216</sup>	QCM and CCNc	wet generation
Sullivan et al., 2010 <sup>256</sup>	CCNc	wet and dry generation
Zhao et al., 2010 <sup>264</sup>	H-TDMA and CCNc	see text for details
Kumar et al., 2011 <sup>262</sup>	CCNc	dry generation
Kumar et al., 2011 <sup>263</sup>	CCNc	wet generation
Gierlus et al., 2012 <sup>218</sup>	CCNc	wet generation
Ma et al., 2012 <sup>212</sup>	PSA	not applicable
Tang et al., 2015 <sup>357</sup>	CCNc	dry generation

940

941 Al-Hosney et al.<sup>354</sup> investigated water adsorption on CaCO<sub>3</sub> particles at different RH, using ATR-  
942 FTIR, and observed that the bending (ca. 1646 cm<sup>-1</sup>) and stretching (3000-3700 cm<sup>-1</sup>) modes of  
943 adsorbed water both increase with RH. However, absolute amounts of adsorbed water was not  
944 reported.<sup>354</sup> DRIFTS was used by Gustafsson et al.<sup>247</sup> to study the water adsorption on CaCO<sub>3</sub>  
945 particles (BET surface area: 17.8 m<sup>2</sup> g<sup>-1</sup>), and they found that 1 and 4.5 monolayers of adsorbed  
946 water is formed at ~55% and 80% RH, respectively. The same study<sup>247</sup> also measured the  
947 hygroscopic growth of wet-generated CaCO<sub>3</sub> particles at different RH using a H-TDMA, and  
948 suggested that the relative change of mobility diameters can be described by the following equation:

949 
$$\frac{D}{D_0} = (1 - RH)^{-0.073} \quad (22).$$

950 It should be noted that CaCO<sub>3</sub> aerosol particles used by Gustafsson et al.<sup>247</sup> are polydisperse, with  
951 a first mode at 40 nm and a second mode at 250 nm. Gibson et al.<sup>355</sup> also used a H-TDMA to  
952 measure the hygroscopic growth of 100 nm wet-generated CaCO<sub>3</sub> particles, and found that the  
953 hygroscopic growth factor can be described by an average value of 1.00±0.02 over the entire RH  
954 range (0-85%), i.e. the hygroscopic growth of CaCO<sub>3</sub> particles is not significant within the  
955 experimental uncertainties.

956  
957 Ma et al.<sup>212</sup> measured the amount of water adsorbed on CaCO<sub>3</sub> (BET area: 0.6 m<sup>2</sup> g<sup>-1</sup>) at 278 K  
958 using a physisorption analyser. They<sup>212</sup> reported that there is one monolayer of adsorbed water  
959 formed on the surface at 52% RH, increasing to ~2 layers at 90% RH and ~7 layers at 95% RH.  
960 Hatch et al.<sup>216</sup> showed that the mass of adsorbed water on CaCO<sub>3</sub> particles (BET surface area: 10.1  
961 m<sup>2</sup> g<sup>-1</sup>) is equal to ~8% of the mass of dry CaCO<sub>3</sub> particles at 78% RH, corresponding to  
962 approximately 3 monolayers of water. The amount of water adsorbed on CaCO<sub>3</sub> particles at  
963 different RH was also measured by Schuttlefield et al.,<sup>356</sup> using a QCM.

964



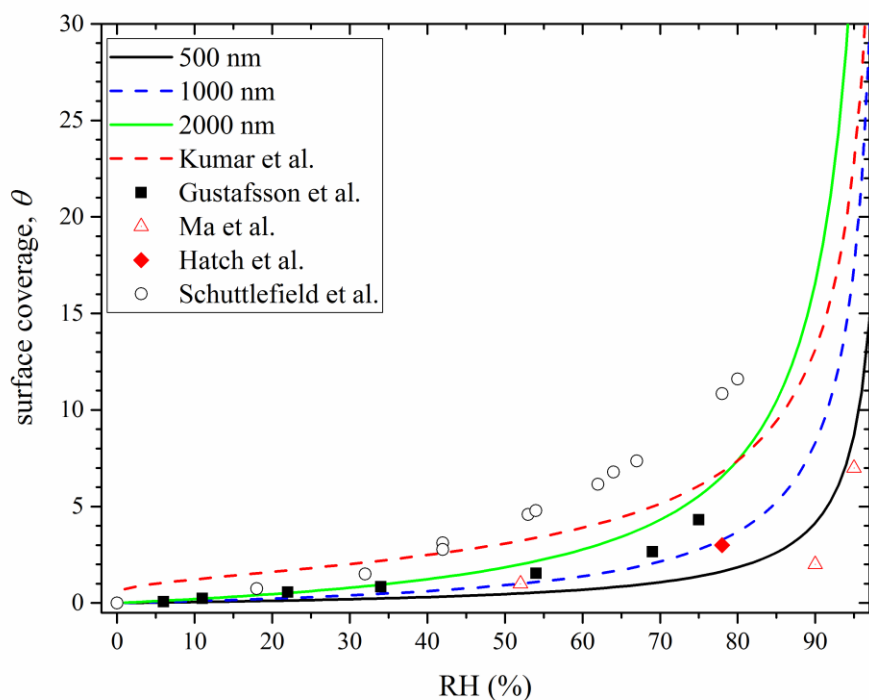
965 Wet-generated  $\text{CaCO}_3$  particles were reported to have  $\kappa$  values of  $\sim 0.043$  by Gibson et al.,<sup>355</sup>  
966  $0.0110 \pm 0.0015$  by Gibson et al.,<sup>257</sup>  $\sim 0.005$  by Hatch et al.,<sup>216</sup> and  $0.0070 \pm 0.0017$  by Gierlus et  
967 al.<sup>218</sup> from CCN activity measurements. The CCN activity of dry generated  $\text{CaCO}_3$  particles was  
968 studied by Sullivan et al.<sup>217</sup> and Tang et al.,<sup>357</sup> with reported  $\kappa$  values of  $0.0008$ - $0.0018$ <sup>217</sup> and  
969  $0.001$ - $0.003$ .<sup>357</sup> Zhao et al.<sup>264</sup> developed a novel method to produce dry  $\text{CaCO}_3$  particles, by  
970 transforming  $\text{Ca}(\text{HCO}_3)_2$  aerosol particles to  $\text{CaCO}_3$  particles via thermal decomposition in a tube  
971 furnace. They reported a mobility diameter growth factor of  $1.01$  at  $95\%$  RH (corresponding to  $\kappa$   
972 values of  $0.0016 \pm 0.004$ ) using a H-TDMA and  $\kappa$  values of  $0.0019 \pm 0.0007$  using a CCNc.<sup>264</sup>  
973 Kumar et al.<sup>262</sup> also investigated the CCN activity of dry-generated  $\text{CaCO}_3$  aerosol particles, and  
974 they suggested the activation of  $\text{CaCO}_3$  particles can be better described by the FHH activation  
975 theory, with  $A_{\text{FHH}}$  of  $3.00 \pm 0.04$  and  $B_{\text{FHH}}$  of  $1.30 \pm 0.03$ .

976

977 As summarized above, the CCN activities of  $\text{CaCO}_3$  aerosol particles were measured by several  
978 previous studies. For dry generated  $\text{CaCO}_3$  particles, different studies reported very similar CCN  
979 activities, with measured  $\kappa$  values of  $\sim 0.002$ .<sup>256,264,357</sup> The CCN activity of wet generated  $\text{CaCO}_3$   
980 aerosol particles is significantly higher.<sup>216,218,257,355</sup> The difference in the measured CCN activities  
981 of dry and wet generated  $\text{CaCO}_3$  particles has been investigated,<sup>256,262,263</sup> and it has been concluded  
982 that wet generation of  $\text{CaCO}_3$  aerosol particles will lead to higher CCN activities.

983

984 Using the data comparison guideline discussed in Section 3.3, a  $\kappa$  value of  $0.002$  means that the  
985 hygroscopic growth factors are  $1.003$ ,  $1.006$ , and  $1.013$  at RH of  $80\%$ ,  $90\%$ , and  $95\%$ . This shows  
986 excellent agreement with H-TDMA measured hygroscopic growth factors reported by the two  
987 previous studies ( $1.00 \pm 0.01$  for RH  $< 85\%$ <sup>355</sup> and  $1.01$  at  $95\%$  RH<sup>264</sup>).



988  
 989 **Figure 13.** Comparison of measured surface coverages ( $\theta$ ) of adsorbed water on  $\text{CaCO}_3$  particles reported  
 990 by previous studies. Squares: Gustafsson et al.;<sup>247</sup> diamonds: Hatch et al.;<sup>216</sup> circles: Schuttlefield et al.;<sup>356</sup>  
 991 triangles: Ma et al.;<sup>212</sup> dashed red curve: calculated using the two FHH parameters reported by Kumar et  
 992 al.<sup>262</sup> In addition, an average  $\kappa$  values of 0.002 is used to calculate  $\theta$  using Eq. (14-15) with assumed dry  
 993 particle diameters of 500 (solid black curve), 1000 (dashed green curve), and 2000 nm (solid green curve).  
 994  
 995 Surface coverages of adsorbed water, measured by the four previous studies using particles  
 996 deposited on some substrates,<sup>212,216,247,356</sup> are plotted in Figure 13 for comparison. Reasonably  
 997 good agreement is found between these four different studies, as shown in Figure 13. However,  
 998 discrepancies do also occur. For example, Gustafsson et al.<sup>247</sup> and Schuttlefield et al.<sup>356</sup> suggested  
 999 that 4.5 and ~12 monolayers, respectively, of adsorbed water are formed at 80% RH, while Ma et  
 1000 al.<sup>212</sup> found that only ~2 monolayers of adsorbed water are formed at ~90% RH. Surface coverages  
 1001 of adsorbed water can be calculated using the two FHH parameters reported by Kumar et al.<sup>262</sup> As  
 1002 shown by the dashed red curve in Figure 13, the calculated  $\theta$  fall into the range of those measured  
 1003 using particles deposited on substrates. We further calculate  $\theta$  using an average  $\kappa$  value of 0.002

1004 for CaCO<sub>3</sub>, with assumed dry particle diameters of 500, 1000, and 2000 nm, respectively. The  
1005 calculated  $\theta$  are within the same order of magnitude as those directly measured. Considering  
1006 measurement uncertainties and more importantly, uncertainties related to assumptions used in  
1007 converting reported  $\kappa$  values into surface coverage (as discussed in Section 3.3), these studies show  
1008 reasonably good agreement.

1009  
1010 There are also a few studies which may not be directly relevant for atmospheric interest but can  
1011 provide fundamental insight into the mechanisms of water adsorption on CaCO<sub>3</sub>. For example,  
1012 Neagle and Rochester<sup>358</sup> measured the mass of calcite samples at different temperatures and found  
1013 that a cumulative loss of particle mass by 5.2% when increasing temperature from 273 K to 873  
1014 K. Synchrotron X-ray reflectivity was used to measure the thickness of water adsorbed on single  
1015 crystal CaCO<sub>3</sub> surface (1014) at different RH by Bohr et al.,<sup>359</sup> and they found that the adsorbed  
1016 water was constant in thickness (1.55±0.1 nm) while RH was varied from <4% to 90%. The result  
1017 reported by Bohr et al.<sup>359</sup> appears to disagree with several other studies which suggest that the  
1018 amount of adsorbed water on CaCO<sub>3</sub> significantly increases with RH. The discrepancy may be due  
1019 to the fact that much less defect sites were present on the single crystals used by Bohr et al.<sup>359</sup>

1020  
1021 Most of the aforementioned studies on water adsorption by CaCO<sub>3</sub> used techniques which provide  
1022 information on the average ensemble for the surfaces under investigation, AFM can achieve spatial  
1023 resolution down to sub-nanometer. AFM has been widely used to study calcite surfaces in dry and  
1024 humid environments,<sup>292,360-362</sup> revealing that calcite surface is very dynamic and complex in the  
1025 presence of water vapor. More recently, alternating current AFM height images combined with  
1026 force measurements and phase imaging were used by Baltrusaitis and Grassian<sup>291</sup> to examine  
1027 surface structure and chemistry of calcite (1014) surface at 70% for a total period of ~ 3h and at  
1028 278 and 296 K. They<sup>291</sup> found that calcite surfaces under ambient conditions are complex and

1029 inhomogeneous in terms of surface composition and phases, containing regions with very different  
1030 water contents. Therefore, the heterogeneous reactivity of the surface will also be spatially  
1031 controlled and inhomogeneous,<sup>291</sup> though this complication has not been considered or understood.

#### 1032 **4.1.2 Effect of chemical aging**

1033 As summarized in Table 5, a number of previous laboratory studies have examined the change in  
1034 water adsorption, hygroscopicity, and CCN activity of CaCO<sub>3</sub> particles, using different  
1035 experimental techniques and methods to produce aged dust particles.

1036 **Table 5.** Laboratory studies on the effects of chemical aging processes on water adsorption, hygroscopicity, CCN activity of CaCO<sub>3</sub> particles:

1037 summary of previous studies

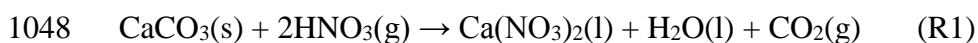
references	techniques	particle aging methods	major findings
Krueger et al., 2003 <sup>214</sup>	SEM-EDX	Particles deposited on supporting substrates were exposed to HNO <sub>3</sub> (g) at different RH.	Exposure to 26 ppbv HNO <sub>3</sub> at (41±1)% RH only for 1 hour will change irregular CaCO <sub>3</sub> particles to spherical aqueous droplets.
Al-Abadleh et al., 2003 <sup>363</sup>	FTIR	CaCO <sub>3</sub> single crystals were exposed to HNO <sub>3</sub> (g) at different RH.	CaCO <sub>3</sub> (104) and CaCO <sub>3</sub> (110) surfaces exposed to 100 mTorr HNO <sub>3</sub> at 23% RH have similar deliquescence relative humidities as amorphous Ca(NO <sub>3</sub> ) <sub>2</sub> particles.
Gibson et al., 2007 <sup>257</sup>	CCNc	Internally mixed CaCO <sub>3</sub> /Ca(NO <sub>3</sub> ) <sub>2</sub> aerosol particles were generated by atomizing CaCO <sub>3</sub> /Ca(NO <sub>3</sub> ) <sub>2</sub> /H <sub>2</sub> O mixture.	Internally mixed CaCO <sub>3</sub> /Ca(NO <sub>3</sub> ) <sub>2</sub> particles show much higher CCN activities than CaCO <sub>3</sub> particles, and the enhancement increases with the ratio of Ca(NO <sub>3</sub> ) <sub>2</sub> to CaCO <sub>3</sub> in the particles.
Hatch et al., 2008 <sup>216</sup>	QCM and CCNc	Aged CaCO <sub>3</sub> particles were generated by atomizing CaCO <sub>3</sub> /H <sub>2</sub> O mixtures containing humic acid sodium salt or fulvic acid.	CaCO <sub>3</sub> particles internally mixed with humic acid sodium salt and Suwannee River fulvic acid adsorb significantly larger amounts of water, compared to fresh CaCO <sub>3</sub> particles.
Liu et al., 2008 <sup>215</sup>	micro Raman spectrometry	CaCO <sub>3</sub> particles on supporting surface were exposed to NO <sub>2</sub> at different RH.	After exposure to 100 ppmv NO <sub>2</sub> for 50 min at 37% RH, CaCO <sub>3</sub> particles have much higher hygroscopicity compared to fresh particles, and they exhibit the same phase transition behavior as pure Ca(NO <sub>3</sub> ) <sub>2</sub> particles.
Sullivan et al., 2009 <sup>258</sup>	CCNc	Monodisperse CaCO <sub>3</sub> aerosol particles were exposed to gaseous HNO <sub>3</sub> in an aerosol flow tube at different RH.	Exposure to HNO <sub>3</sub> can increase the CCN activity of CaCO <sub>3</sub> particles from $\kappa = \sim 0.002$ to $\kappa = \sim 0.1$ very quickly. A comparison of different calcium-containing minerals shows a range of CCN activities.

Gierlus et al., 2012 <sup>218</sup>	CCNc	Internally mixed CaCO <sub>3</sub> particles were generated by atomizing CaCO <sub>3</sub> /H <sub>2</sub> C <sub>2</sub> O <sub>4</sub> /H <sub>2</sub> O mixture.	Internally mixed CaCO <sub>3</sub> /CaC <sub>2</sub> O <sub>4</sub> particles only have slightly higher CCN activity, compared to fresh CaCO <sub>3</sub> particles.
Ma et al., 2012 <sup>212</sup>	PSA	CaCO <sub>3</sub> particles on supporting surface were exposed to gaseous CH <sub>3</sub> COOH at different RH.	Reaction with CH <sub>3</sub> COOH can significantly enhance the amount of water adsorbed by CaCO <sub>3</sub> particles.
Tang et al., 2015 <sup>357</sup>	CCNc	Monodisperse CaCO <sub>3</sub> aerosol particles were exposed to N <sub>2</sub> O <sub>5</sub> in an aerosol flow tube at 0% RH.	Exposure of CaCO <sub>3</sub> aerosol particles to N <sub>2</sub> O <sub>5</sub> (~550 to 15000 ppbv·s) at 0% RH increases their $\kappa$ values from 0.001-0.003 to 0.02-0.04.

1038

1039

1040 Phase transformation of solid dust particles to liquid droplets, i.e. significant change in  
1041 hygroscopicity, due to heterogeneous chemistry, was first reported by Krueger et al.,<sup>214</sup> using  
1042 Scanning Electron Microscopy. It is found that exposure to 26 ppbv HNO<sub>3</sub> at (41±1)% RH only  
1043 for 1 hour will change irregular CaCO<sub>3</sub> particles to spherical aqueous droplets.<sup>214</sup> Similar phase  
1044 change of CaCO<sub>3</sub> particles was also observed at (17±1)% RH after exposed to HNO<sub>3</sub> of the same  
1045 concentration, though it only occurred after much longer exposure time.<sup>214</sup> Energy Dispersive X-  
1046 Ray (EDX) analysis reveals that the observed phase change of aged CaCO<sub>3</sub> particles is caused by  
1047 the formation of Ca(NO<sub>3</sub>)<sub>2</sub> (R1),<sup>199</sup> which has a much higher hygroscopicity than CaCO<sub>3</sub>.



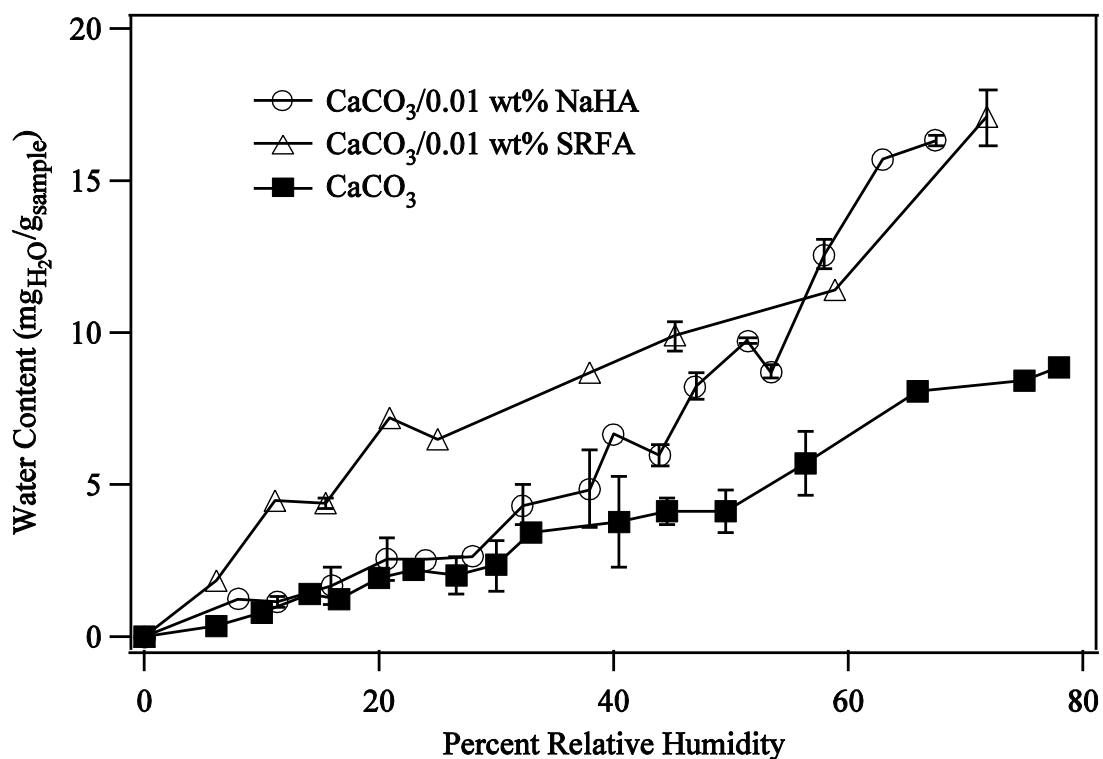
1049

1050 This innovative discovery has been supported by many following studies, which have provided  
1051 further insights and more quantitative results. For example, Al-Abadleh et al.<sup>211</sup> found that after  
1052 exposure to 100 mTorr HNO<sub>3</sub> at 23% RH and 295 K, the amount of adsorbed water by CaCO<sub>3</sub>  
1053 single crystals (104 and 110 surface planes) is significantly increased, due to the formation of  
1054 Ca(NO<sub>3</sub>)<sub>2</sub> on the surface. Aged CaCO<sub>3</sub>(104) and CaCO<sub>3</sub>(110) surfaces have deliquescence relative  
1055 humidities (DRH) of (9±2)% and (13±5)% at 295 K,<sup>211</sup> similar to that for amorphous Ca(NO<sub>3</sub>)<sub>2</sub>  
1056 particles.<sup>364</sup>

1057 In addition to HNO<sub>3</sub>, uptake of NO<sub>2</sub><sup>201,365</sup> and N<sub>2</sub>O<sub>5</sub><sup>131,136,139</sup> also lead to the formation of nitrate  
1058 on dust particles. Using micro-Raman spectrometry, Liu et al.<sup>215</sup> found that after exposure to 100  
1059 ppmv NO<sub>2</sub> for 50 min at 37% RH, fresh CaCO<sub>3</sub> particles were converted to internally mixed  
1060 CaCO<sub>3</sub>/Ca(NO<sub>3</sub>)<sub>2</sub> particles with much higher hygroscopicity. This study further showed those  
1061 internally mixed CaCO<sub>3</sub>/Ca(NO<sub>3</sub>)<sub>2</sub> particles, though still containing CaCO<sub>3</sub> inclusion, exhibit the  
1062 same phase transition behavior as pure Ca(NO<sub>3</sub>)<sub>2</sub> particles.<sup>215</sup>

1063

1064 Heterogeneous reactions of  $\text{CaCO}_3$  particles with other acidic trace gases, in addition to nitrogen  
1065 oxides, can also lead to the increase in hygroscopicity. For example, Hatch et al.<sup>216</sup> used a QCM  
1066 to measure the amount of water adsorbed on fresh  $\text{CaCO}_3$  and  $\text{CaCO}_3$  particles mixed with humic  
1067 acid sodium salt (NaHA) and Suwannee River fulvic acid (SRFA) at different RH. As shown in  
1068 Figure 14, compared to fresh  $\text{CaCO}_3$ , the amount of water is significantly increased for  $\text{CaCO}_3$   
1069 particles internally mixed with NaHA or SRFA.<sup>216</sup>



1070  
1071 **Figure 14.** Amounts of water adsorbed on fresh  $\text{CaCO}_3$  particles and  $\text{CaCO}_3$  mixed with humic acid sodium  
1072 salt (NaHA) and Suwannee River fulvic acid (SRFA) at different RH. Reprinted with permission from ref  
1073 216. Copyright 2008 Elsevier.

1074  
1075 Ma et al.<sup>212</sup> observed that at 90% RH, while fresh  $\text{CaCO}_3$  particles only contain 0.1% water,  
1076 internally mixed  $\text{CaCO}_3/\text{Ca}(\text{CH}_3\text{COO})_2$  particles formed in the reaction of  $\text{CaCO}_3$  with acetic acid  
1077 at 50% RH contains ~70% water. They found that these internally mixed  $\text{CaCO}_3/\text{Ca}(\text{CH}_3\text{COO})_2$   
1078 particles have almost the same DRH as pure  $\text{Ca}(\text{CH}_3\text{COO})_2$  particles.<sup>212</sup> Exposure to acetic acid at

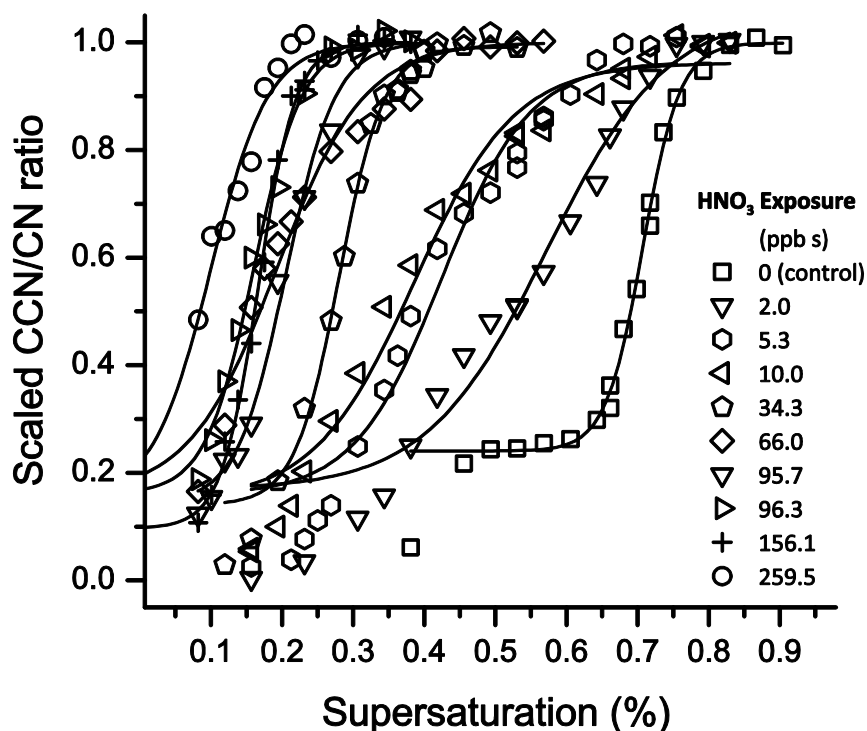


1079 0% RH also enhances the ability of  $\text{CaCO}_3$  to adsorb water, though the increase is smaller  
1080 compared to that at 50% RH.<sup>212</sup>

1081  
1082 As discussed previously, several studies suggest that the CCN activity of fresh  $\text{CaCO}_3$  particles is  
1083 very low, with  $\kappa$  values of  $<0.005$ .<sup>217,264,357</sup> Thermodynamic theories predict that the formation of  
1084 more hygroscopic materials through atmospheric aging processes on  $\text{CaCO}_3$  particles will increase  
1085 their CCN activities.<sup>366,367</sup> Indeed the CCN activities of several pure Ca-containing compounds  
1086 that could be formed in the atmospheric transformation of  $\text{CaCO}_3$  particles, are found to have  
1087 higher  $\kappa$  values. For example, the  $\kappa$  values are  $\sim 0.5$  for  $\text{Ca}(\text{NO}_3)_2$  and  $\text{CaCl}_2$ ,<sup>217,357</sup> similar to that  
1088 for  $(\text{NH}_4)_2\text{SO}_4$ , and 0.05 for  $\text{CaC}_2\text{O}_4$ .<sup>217</sup>

1089  
1090 The CCN activities of fresh  $\text{CaCO}_3$  and internally mixed particles, generated by atomization, have  
1091 been measured to mimic the effect of chemical aging on the CCN activities of  $\text{CaCO}_3$   
1092 particles.<sup>218,257</sup> For example, internally mixed  $\text{CaCO}_3/\text{Ca}(\text{NO}_3)_2$  particles show much higher CCN  
1093 activities than  $\text{CaCO}_3$  particles, and the enhancement of CCN activities increases with the mass  
1094 ratio of  $\text{Ca}(\text{NO}_3)_2$  to  $\text{CaCO}_3$  in the aqueous mixtures which were atomized to produce aerosol  
1095 particles.<sup>257</sup> On the other hand, another study<sup>218</sup> found that internally mixed  $\text{CaCO}_3/\text{CaC}_2\text{O}_4$   
1096 aerosol particles have  $\kappa$  values of  $0.0090 \pm 0.0019$ , only slightly higher than  $0.0070 \pm 0.0017$  for  
1097 fresh  $\text{CaCO}_3$  aerosol particles generated using a similar method. For a particle with a dry diameter  
1098 of 200 nm,  $\kappa$  values of 0.0070 and 0.0090 correspond to  $s_c$  of 0.442% and 0.402%, respectively.  
1099 The smaller enhancement in CCN activity of  $\text{CaCO}_3/\text{CaC}_2\text{O}_4$  particles, compared to fresh  $\text{CaCO}_3$   
1100 particles, may be explained by relative low CCN activity of  $\text{CaC}_2\text{O}_4$  particles, with  $\kappa$  values of  
1101  $\sim 0.05$ .<sup>217</sup> In addition, mixing humic acid sodium salt (NaHA) and fulvic acid can substantially  
1102 increase the CCN activities of  $\text{CaCO}_3$  particles and therefore reduce the critical super-saturation  
1103 required to activate these particles to cloud droplets.<sup>216</sup> It has been reported that for 235 nm

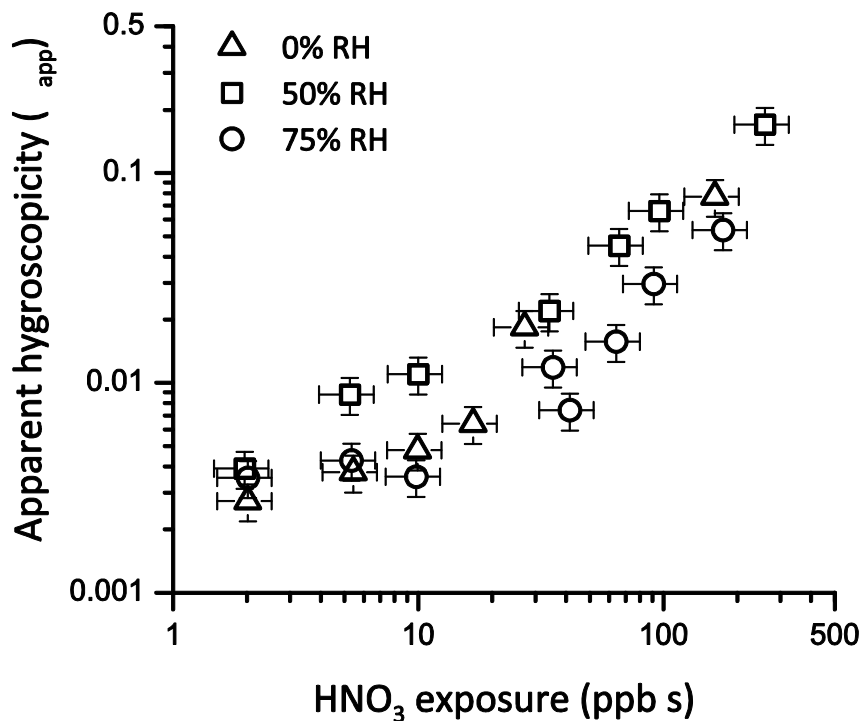
1104 particles, the critical super-saturation is 0.39% for fresh  $\text{CaCO}_3$ , 0.35% for  $\text{CaCO}_3$  mixed with 0.01  
 1105 wt.% NaHA, and 0.32% for  $\text{CaCO}_3$  mixed with 0.05 wt.% NaHA.<sup>216</sup> Similar but smaller effects  
 1106 have also been observed for  $\text{CaCO}_3$  particles mixed with fulvic acid.<sup>216</sup>  
 1107  
 1108 CCN activity of  $\text{CaCO}_3$  aerosol particles before and after exposure to reactive trace gases has been  
 1109 measured by a few studies to better mimic the effects of atmospheric aging processes. For  
 1110 examples, Sullivan et al.<sup>258</sup> exposed  $\text{CaCO}_3$  particles to  $\text{HNO}_3$  in the aerosol flow tube and then  
 1111 measured the CCN activities of reacted particles. In this study<sup>258</sup>  $\text{HNO}_3$  concentration, RH and  
 1112 exposure time were varied. As shown in Figure 15, they found<sup>258</sup> that the CCN activity of reacted  
 1113  $\text{CaCO}_3$  particles was significantly enhanced.



1114  
 1115 **Figure 15.** CCN activation curves of fresh and aged (exposure to  $\text{HNO}_3$  at 50% RH)  $\text{CaCO}_3$  aerosol  
 1116 particles with initial mobility diameters of 200 nm. Reprinted with permission from ref 258. Copyright  
 1117 2009 the PCCP Owner Societies.

1118

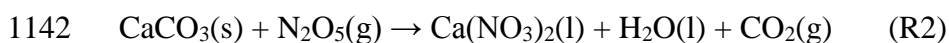
1119 It is clear that heterogeneous reactions can significantly change the CCN activity of  $\text{CaCO}_3$   
1120 particles. However, its relevance for cloud formation depends on how fast these changes occur in  
1121 the troposphere. This important question has just started to be explored. For example, Sullivan et  
1122 al.<sup>258</sup> investigated the CCN activity of aged particles as a function of  $\text{HNO}_3$  exposure, and  
1123 suggested that the  $\kappa$  values of  $\text{CaCO}_3$  particles increase with  $\text{HNO}_3$  exposure at three different RHs,  
1124 as shown in Figure 16. Interestingly no RH dependence is found, though the uptake of  $\text{HNO}_3$  by  
1125  $\text{CaCO}_3$  particles is enhanced at higher RH.<sup>199,227</sup> It is further concluded by Sullivan et al.<sup>258</sup> that  
1126 fresh  $\text{CaCO}_3$  particles will be rapidly converted to aged particles with  $\kappa$  values of  $>0.1$  within 4 h  
1127 for 10 pptv  $\text{HNO}_3$  and within 3 min for 1 ppbv  $\text{HNO}_3$ .  $\text{HNO}_3$  in the troposphere can reach up to  
1128 several ppbv,<sup>368-370</sup> suggesting that  $\text{CaCO}_3$  particles can be converted to hygroscopic particles soon  
1129 after they are emitted into the troposphere.



1130

1131 **Figure 16.** Measured CCN activities (represented by  $\kappa$  values) of aged  $\text{CaCO}_3$  particles (due to the reaction  
1132 with  $\text{HNO}_3$ ) as a function of nitric acid exposure at 0%, 50%, and 70% RH. Reprinted with permission from  
1133 ref 258. Copyright 2009 the PCCP Owner Societies.

1134  
1135  $\text{N}_2\text{O}_5$  concentrations up to several ppbv have been reported,<sup>371-374</sup> and its reaction with  $\text{CaCO}_3$  (R2)  
1136 could lead to the formation of nitrate in particles. In a very recent study, Tang et al.<sup>357</sup> found that  
1137 CCN activity of  $\text{CaCO}_3$  particles which had been exposed to  $\text{N}_2\text{O}_5$  at 0% RH in an aerosol flow  
1138 tube was enhanced, with  $\kappa$  increased from 0.001-0.003 to 0.02-0.04. It was also found that variation  
1139 of  $\text{N}_2\text{O}_5$  exposure from ~550 to 15000 ppbv-s did not lead to change in the CCN activity of aged  
1140  $\text{CaCO}_3$  particles,<sup>357</sup> probably because at 0% RH  $\text{CaCO}_3$  may be quickly saturated with respect to  
1141 reaction with  $\text{N}_2\text{O}_5$ .



## 1143 **4.2 Arizona Test Dust**

1144 Arizona Test Dust (ATD) is in fact one type of authentic dust samples. It is often used as a test  
1145 dust and a number of previous studies have investigated water adsorption, hygroscopicity and CCN  
1146 activity of both fresh and aged ATD, as listed in Table 6. Therefore, it is separately discussed here  
1147 in Section 4.2, instead of being included Section 4.8 together with other authentic dust samples.

### 1148 **4.2.1 Fresh ATD particles**

1149 Based on their DRIFTS measurement, Gustafsson et al.<sup>247</sup> suggested that ~2.5 and ~4 monolayers  
1150 of adsorbed water are formed on ATD particles at ~70% and ~80% RH, respectively, though the  
1151 BET surface area of their ATD samples was not clearly stated. Gustafsson et al.<sup>247</sup> also measured  
1152 the hygroscopic growth of wet-generated ATD aerosol particles which have the first mode at 56  
1153 nm and the second mode at 250 nm, and suggested that the hygroscopic growth factors of ATD  
1154 particles at different RH can be described by the following equation:

$$1155 \frac{D}{D_0} = (1 - RH)^{-0.036} \quad (23)$$

1156

1157 **Table 6.** Water adsorption, hygroscopicity, and CCN activity of fresh Arizona Test Dust (ATD) particles:  
1158 summary of previous studies.

references	techniques	aerosol generation method
Gustafsson et al., 2005 <sup>247</sup>	DRIFTS, TGA, and H-TDMA	wet generation
Vlasenko et al., 2005 <sup>260</sup>	H-TDMA	dry generation
Koehler et al., 2009 <sup>46</sup>	H-TDMA and CCNc	dry and wet generation
Herich et al., 2009 <sup>49</sup>	H-TDMA and CCNc	dry and wet generation
Navea et al., 2010 <sup>246</sup>	ATR-FTIR and QCM	not applicable
Sullivan et al., 2010 <sup>261</sup>	CCNc	dry generation
Sullivan et al., 2010 <sup>375</sup>	CCNc	dry generation
Kumar et al., 2011 <sup>262</sup>	CCNc	dry generation
Kumar et al., 2011 <sup>263</sup>	CCNc	wet generation
Yamashita et al., 2011 <sup>376</sup>	CCNc	dry generation
Garimella et al., 2014 <sup>259</sup>	CCNc	dry generation

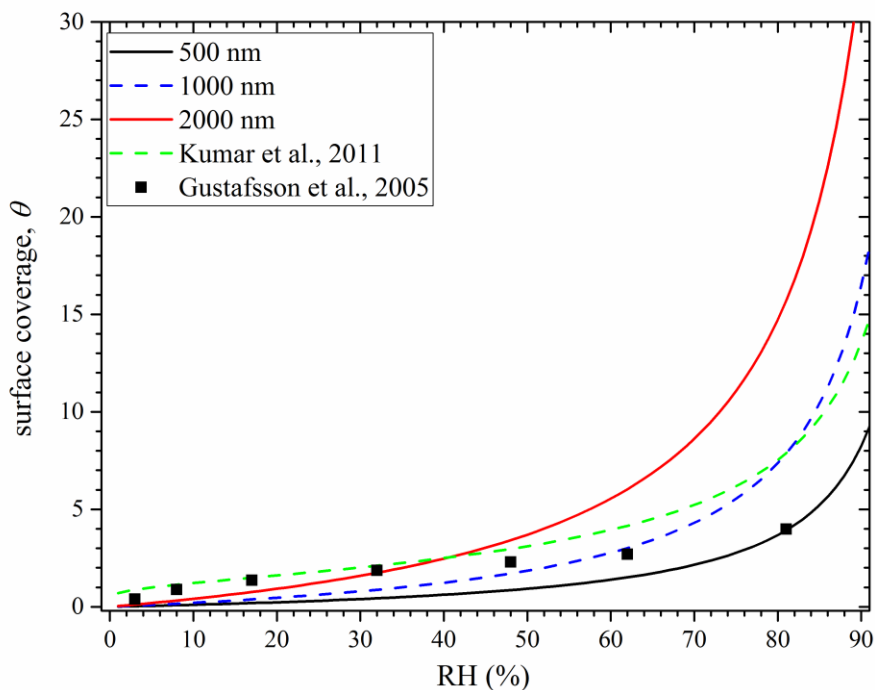
1159

1160 Navea et al.<sup>246</sup> investigated water adsorption on ATD particles using ATR-FTIR and QCM, and  
1161 reported the mass ratio of adsorbed water to dry particles from 0-70% RH. Vlasenko et al.<sup>260</sup> used  
1162 a H-TDMA to study the hygroscopic growth of ATD aerosol particles, and found that the  
1163 hygroscopic growth factors of monodisperse particles with mobility diameters of 55, 100, 250, and  
1164 400 nm are all <1.01 for RH up to 90%. Koehler et al.<sup>46</sup> measured the hygroscopic growth and  
1165 CCN activity of dry- and wet-generated ATD aerosol particles. The H-TDMA measurements show  
1166 both dry and wet generated ATD particles have a growth factor of 1.09 at 90% RH, corresponding  
1167 to a  $\kappa$  value of 0.03.<sup>46</sup> The CCN activity measurements suggest that while the dry generated ATD  
1168 particles have  $\kappa$  values of ~0.025, the CCN activity of wet generated ATD particles is much higher,  
1169 with  $\kappa$  values of 0.35.<sup>46</sup> This may indicate that compared to dry generation, wet generation can  
1170 lead to significant increase of CCN activities of mineral dust particles, as suggested by several

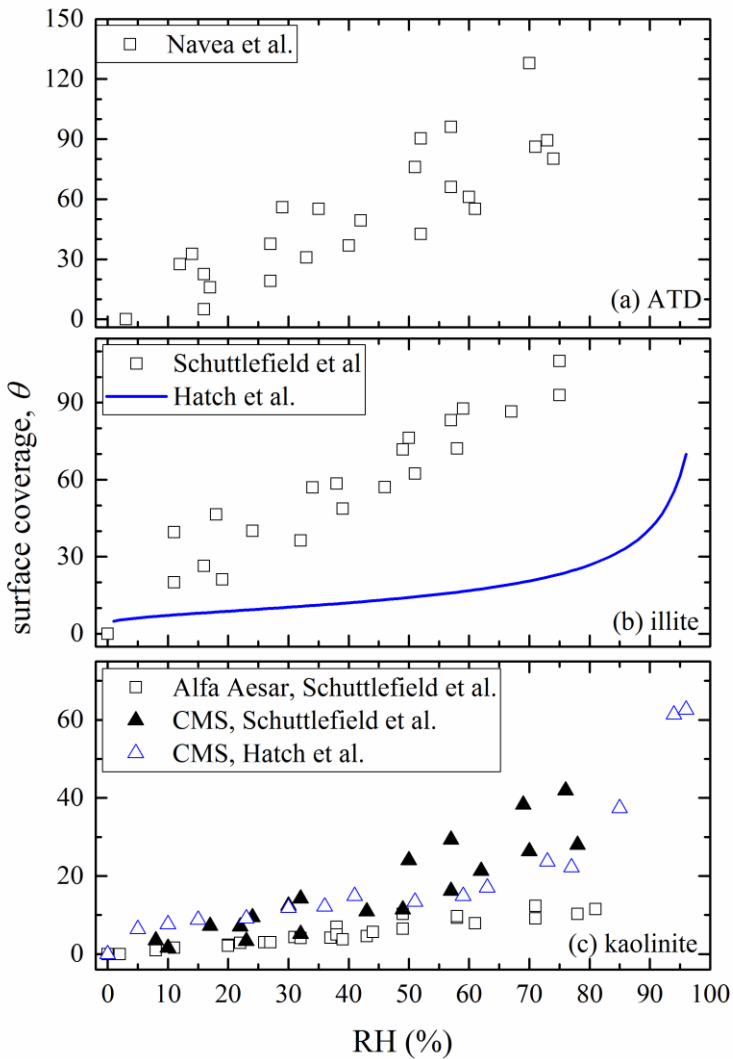
1171 other studies.<sup>49,256,263</sup> Therefore, the CCN activity of wet generated ATD particles reported by  
1172 Koehler et al.<sup>46</sup> is not included for further discussion.

1173

1174 The interaction of water vapor with dry and wet generated ATD particles was also studied by  
1175 Herich et al.<sup>49</sup> under both sub- and super-saturation conditions, using H-TDMA and CCNc,  
1176 respectively. They also found that wet-generated ATD particles show significantly higher CCN  
1177 activities, due to effects introduced by redistribution of soluble materials among the particles.<sup>49</sup>  
1178 The  $\kappa$  value derived from the CCN activity measurement is 0.003.<sup>49</sup> The  $\kappa$  value derived from H-  
1179 TDMA measurement appears to be slightly lower than that from CCN activity measurement;  
1180 however, the difference may not be significant due to the large uncertainty associated with the  
1181 measured growth factors.<sup>49</sup> The CCN activity of dry generated ATD particles was also investigated  
1182 by several other studies, with reported  $\kappa$  values being 0.0041,<sup>259</sup> 0.002,<sup>261</sup> 0.0042,<sup>375</sup> and 0.017,<sup>376</sup>  
1183 respectively. Kumar et al.<sup>262</sup> investigated the CCN activity of dry generated ATD aerosol particles  
1184 and interpreted their results using the FHH activation theory, with  $A_{\text{FHH}}$  of  $2.96 \pm 0.03$  and  $B_{\text{FHH}}$  of  
1185  $1.28 \pm 0.03$ . In another study, Kumar et al.<sup>263</sup> also investigated the CCN activity of wet-generated  
1186 ATD aerosol particles, and concluded that compared to dry generation, wet-generation will  
1187 significantly increase the CCN activity of ATD particles.



1188  
 1189 **Figure 17.** Comparison of measured and calculated surface coverages ( $\theta$ ) of adsorbed water on ATD  
 1190 particles. Black squares: measured by Gustafsson et al.,<sup>247</sup> solid black curve: calculated using an average  $\kappa$   
 1191 value of 0.004<sup>259,375</sup> and an assumed diameter of 500 nm; dashed blue curve: calculated using a  $\kappa$  value of  
 1192 0.004<sup>259,375</sup> and an assumed diameter of 1000 nm; solid red curve: calculated using a  $\kappa$  value of 0.004<sup>259,375</sup>  
 1193 and an assumed diameter of 2000 nm; dashed green curve: calculated using the two FHH parameters  
 1194 reported by Kumar et al.<sup>262</sup>  
 1195  
 1196 Surface coverages of adsorbed water on ATD particles reported by Gustafsson et al.<sup>247</sup> are plotted  
 1197 in Figure 17 together with those calculated using the two FHH parameters derived by Kumar et  
 1198 al.<sup>262</sup> from their CCN activity measurement. In addition, the surface coverages of adsorbed water  
 1199 are also calculated using an average  $\kappa$  value of 0.004<sup>259,375</sup> for particles with diameters of 500,  
 1200 1000, and 2000 nm, respectively. As shown in Figure 17, considering the experimental  
 1201 uncertainties and errors in extrapolating measurements done under super-saturation conditions to  
 1202 sub-saturation conditions, these studies show fairly good agreement, though some discrepancies  
 1203 also occur.



1204

1205 **Figure 18.** Surface coverage of adsorbed water on ATD (a), illite (b), and kaolinite (c), reported by Navea  
 1206 et al.,<sup>246</sup> Schuttlefield et al.,<sup>249</sup> and Hatch et al.<sup>268,348</sup> Alfa Aesar indicates that particles are provided by Alfa  
 1207 Aesar, and CMS indicates that particles are provided by Clay Mineral Society (CMS).

1208

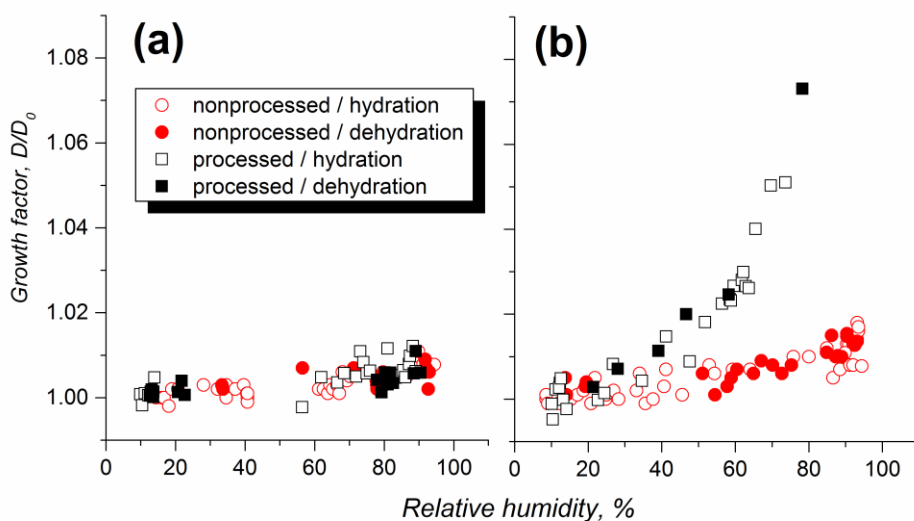
1209 The results reported by Navea et al.,<sup>246</sup> directly measured by using particles deposited a substrate,  
 1210 are shown in Figure 18a. Compared to those plotted in Figure 17, the surface coverages of adsorbed  
 1211 water measured by Navea et al.<sup>246</sup> are significantly higher. Navea et al.<sup>246</sup> deposited a water slurry  
 1212 of ATD particles on the quartz crystal surface in their QCM to form a dry dust film after the  
 1213 evaporation of water. When being mixed with water, clay minerals contained by ATD particles  
 1214 may undergo interaction with liquid water and therefore change their physicochemical properties,



1215 a phenomena known as swelling for some clay minerals.<sup>377</sup> This may begin to explain the relative  
1216 large difference between Navea et al.<sup>246</sup> and those shown in Figure 17. This may also be due to  
1217 possible chemical reactions of ATD particles (or some of their components) in the aqueous mixture,  
1218 leading to compositional changes. However, further studies are needed to explain and resolve this  
1219 discrepancy.

#### 1220 4.2.2 Effect of chemical aging

1221 The change of hygroscopicity of ATD particles due to heterogeneous reactions has been explored  
1222 by a few studies. For example, Vlasenko et al.<sup>213</sup> measured the hygroscopic growth of ATD  
1223 particles after being exposed to  $\text{HNO}_3$  ( $3 \times 10^{13}$  molecule  $\text{cm}^{-3}$ , i.e.  $\sim 1.2$  ppmv) for 3 min at different  
1224 RH in an aerosol flow tube. As shown in Figure 19, the change in hygroscopicity was negligible  
1225 for exposure at 30% RH; however, the hygroscopic growth factor at  $\sim 85\%$  RH increased from  
1226  $< 1.02$  to  $\sim 1.08$  after exposure to the same amount of  $\text{HNO}_3$  at 85% RH.<sup>213</sup>



1227  
1228 **Figure 19.** Hygroscopic growth of ATD particles with initial mobility diameters of 100 nm before (red  
1229 circles) and after (black squares) reaction with  $\text{HNO}_3$  of  $3 \times 10^{13}$  molecule  $\text{cm}^{-3}$  at RH of (a) 30% and (b)  
1230 85%. Reprinted with permission from ref 213. Copyright 2006 Copernicus Publications.

1231

1232 It is also found that exposure to  $\text{HNO}_3$ <sup>375</sup> and  $\text{H}_2\text{SO}_4$ <sup>261</sup> vapor could significantly increase the  
 1233 CCN activity of ATD aerosol particles. In another study, Keskinen et al.<sup>378</sup> suggested that  
 1234 secondary organic coatings which are formed from  $\alpha$ -pinene ozonolysis can also significantly  
 1235 enhance the CCN activity of ATD particles.

### 1236 4.3 Illite

1237 Illite is the most abundant clay in mineral dust particles,<sup>150</sup> and its interaction with water vapour  
 1238 has been investigated by several studies. Table 7 summarizes previous studies which have  
 1239 investigated water adsorption, hygroscopicity, and CCN activity of illite particles. The interaction  
 1240 of water vapor with illite particles was investigated by Schuttlefield et al.<sup>249</sup> using ATR-FTIR and  
 1241 QCM, and the amount of water adsorbed by illite was quantified at different RH. Hatch et al.<sup>268</sup>  
 1242 studied water adsorption on illite particles using ATF-FTIR. They found that the two-parameter  
 1243 BET adsorption isotherm failed to describe the experimental data at higher RH while the Feundlich  
 1244 adsorption model could fit the data over the entire RH range.<sup>268</sup> In a following study, Hatch et  
 1245 al.<sup>348</sup> also used the FHH adsorption isotherm to fit their data, with  $A_{\text{FFH}}$  and  $B_{\text{FFH}}$  equal to  $75 \pm 17$   
 1246 and  $1.77 \pm 0.11$ .

1247

1248 **Table 7.** Water adsorption, hygroscopicity, and CCN activity of fresh illite: summary of previous studies.

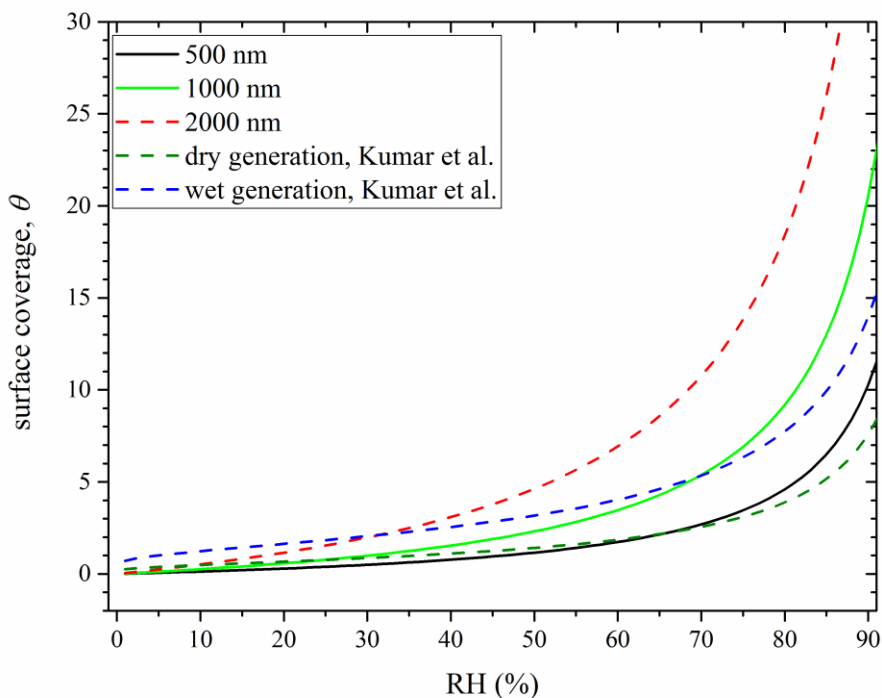
references	techniques (and aerosol generation method, if applicable)
Schuttlefield et al., 2007 <sup>249</sup>	ATR-FTIR and QCM
Herich et al., 2009 <sup>49</sup>	H-TDMA and CCNc (dry and wet generation)
Attwood and Greenslade, 2011 <sup>253</sup>	AE-CRD (wet generation)
Hatch et al., 2011 <sup>268</sup>	ATR-FTIR
Kumar et al., 2011 <sup>262</sup>	CCNc (dry generation)
Kumar et al., 2011 <sup>263</sup>	CCNc (wet generation)
Garimella et al., 2014 <sup>253</sup>	CCNc (dry generation)
Hatch et al., 2014 <sup>348</sup>	ATR-FTIR

1249

1250 Attwood and Greenslade<sup>253</sup> measured the optical extinction of wet-generated illite aerosol  
1251 particles at 532 nm and at different RH to study their hygroscopicity. The hygroscopic growth  
1252 factors were found to be 0.90, 0.93, and 1.06 at RH of 50%, 68%, and 90%, respectively.<sup>253</sup> It  
1253 should be pointed out that the hygroscopic growth reported by Attwood and Greenslade<sup>253</sup> is based  
1254 on the measured optical extinction coefficients. Hygroscopic growth factors smaller than 1, which  
1255 have also been reported for ATD particles using H-TDMA,<sup>46,260</sup> can be due to change in particle  
1256 morphology and even restructure of particles during humidification.<sup>46,253,260</sup> Since it is difficult to  
1257 convert change in optical extinction cross sections at different RH to the amount of adsorbed water,  
1258 the result reported by Attwood and Greenslade<sup>253</sup> is not included in further discussion.

1259

1260 Herich et al.<sup>49</sup> produced illite aerosol particles using both dry and wet generation methods, and  
1261 measured the hygroscopicity and CCN activity of generated illite aerosol particles using H-TDMA  
1262 and CCNc, respectively. They<sup>49</sup> found that wet-generated illite particles are more CCN active than  
1263 those generated by dry dispersion, and that the dry-generated illite particles has  $\kappa$  values of 0.002-  
1264 0.003. Kumar et al.<sup>262,263</sup> also investigated the CCN activity of dry- and wet-generated illite aerosol  
1265 particles, and suggested that the FHH activation theory could better describe CCN activation of  
1266 illite particles.  $A_{FHH}$  and  $B_{FHH}$  were reported to be  $1.02 \pm 0.38$  and  $1.12 \pm 0.04$  for dry-generated illite  
1267 particles,<sup>262</sup> and 3.00 and 1.27 for wet-generated illite particles.<sup>263</sup> Recently Garimella et al.<sup>259</sup> also  
1268 studied the CCN activity of dry-generated illite particles, and they suggested that the  $\kappa$ -Köhler  
1269 activation theory could adequately describe the CCN activation of illite particles, with an average  
1270  $\kappa$  value of 0.0072.



1271  
 1272 **Figure 20.** Comparison of calculated surface coverages ( $\theta$ ) of adsorbed water on illite particles. Surface  
 1273 coverages of adsorbed water are calculated using an average  $\kappa$  value of 0.005 and different dry particle  
 1274 diameters of 500 (solid black curve), 1000 (solid green curve), and 2000 nm (dashed red curve), and using  
 1275  $A_{FHH}$  and  $B_{FHH}$  for dry- (dashed olive curve) and wet-generated (dashed blue curve) illite aerosol particles  
 1276 reported by Kumar et al.<sup>262,263</sup>

1277  
 1278  $A_{FHH}$  and  $B_{FHH}$  parameters for dry- and wet-generated illite particles, derived by Kumar et al.<sup>262,263</sup>  
 1279 from their CCN activity measurements, are used to calculate surface coverages of adsorbed water  
 1280 under sub-saturation conditions.  $\kappa$  values for dry-generated illite aerosol particles were reported to  
 1281 be 0.002-0.003 by Herich et al.<sup>49</sup> and 0.0072 by Garimella et al.<sup>259</sup> An average  $\kappa$  value of 0.005 is  
 1282 then used here to calculate surface coverage of adsorbed water under sub-saturation conditions for  
 1283 particles with uniform diameters of 500, 1000, and 2000 nm. All the calculated results are shown  
 1284 in Figure 20, exhibiting relatively good agreement in general.

1286 Schuttlefield et al.<sup>249</sup> and Hatch et al.<sup>268,348</sup> experimentally measured water adsorption under sub-  
1287 saturation conditions on illite particles which were deposited on supporting substrates, and their  
1288 results are displayed in Figure 18b. Comparison of results shown in Figure 20 to those in Figure  
1289 18b suggests that surface coverages of adsorbed water reported by Schuttlefield et al.<sup>249</sup> and Hatch  
1290 et al.<sup>268,348</sup> are both significantly higher than those using aerosol particles, including those reported  
1291 by Kumar et al.<sup>263</sup> who generated aerosol particles by atomizing illite/water mixture. Therefore,  
1292 the difference between studies using particles deposited on substrates and those using aerosol  
1293 particles cannot be fully explained by the potential change in particle properties due to the  
1294 interaction of clay with liquid water during the sample preparation stage. Clay minerals are  
1295 inherently complex with variability between samples. Variability in clay minerals are due to  
1296 differences in metal cations present and potentially contamination with other clay components (e.g.  
1297 montmorillonite) can potentially cause the observed difference. Considering the abundance of illite  
1298 in tropospheric mineral dust particles, more studies are required to better understand its interaction  
1299 of water vapor.

#### 1300 **4.4 Kaolinite**

1301 Previous studies which reported water adsorption, hygroscopicity, and CCN activities of fresh  
1302 kaolinite are summarized in Table 8. ATR-FTIR and QCM were used by Schuttlefield et al.<sup>249</sup> to  
1303 investigate water adsorption on kaolinite particles at different RH. Two different kaolinite samples  
1304 were used,<sup>249</sup> with one purchased from Alfa Aesar and the other one provided by the Source Clay  
1305 Repository (Clay Mineral Society). Hatch et al.<sup>268</sup> also investigated water adsorption on Clay  
1306 Mineral Society kaolinite using ATR-FTIR, and suggested that the Freundlich adsorption isotherm  
1307 can better describe their experimental data, compared to the two-parameter BET adsorption  
1308 isotherm. Recently Hung et al.<sup>270</sup> used a physisorption analyser to study water adsorption on  
1309 kaolinite provided by Fluka.

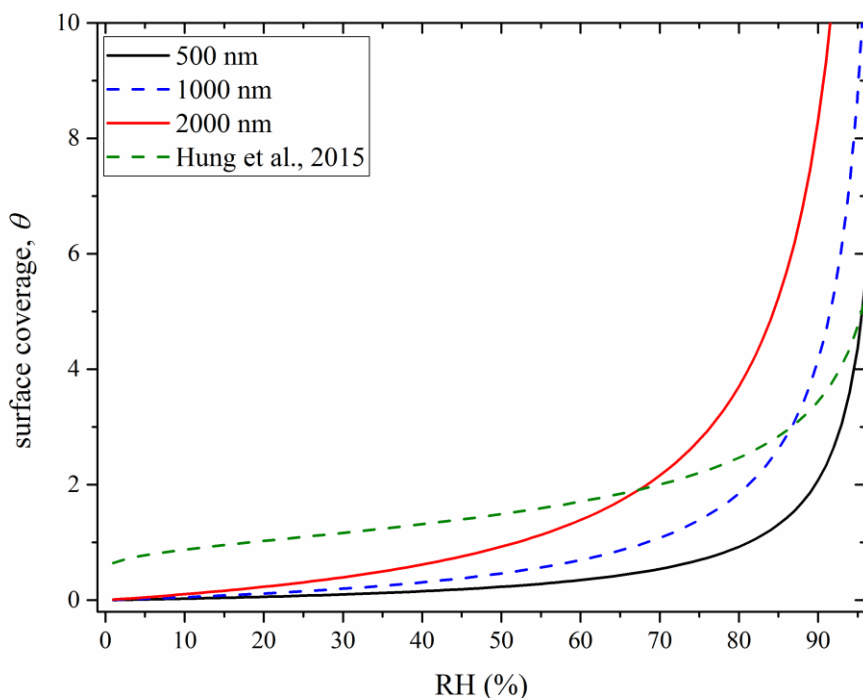
1310

1311 **Table 8.** Water adsorption, hygroscopicity, and CCN activity of fresh kaolinite: summary of previous  
 1312 studies.

references	techniques (and aerosol generation method, if applicable)
Schuttlefield et al., 2007 <sup>249</sup>	ATR-FTIR and QCM
Gibson et al., 2007 <sup>257</sup>	CCNc (wet generation)
Herich et al., 2009 <sup>49</sup>	H-TDMA and CCNc (dry and wet generation)
Hatch et al., 2011 <sup>268</sup>	ATR-FTIR
Attwood and Greenslade, 2011 <sup>253</sup>	AE-CRD (wet generation)
Kumar et al., 2011 <sup>263</sup>	CCNc (wet generation)
Hung et al., 2015 <sup>270</sup>	PSA

1313  
 1314 Optical extinction coefficients were measured at 532 nm using Cavity Ring-Down spectroscopy  
 1315 to determine the hygroscopic growth of Clay Mineral Society kaolinite particles at different RH.<sup>253</sup>  
 1316 The hygroscopic growth factors, relative to the diameter at <10% RH, were measured to be  
 1317  $0.90 \pm 0.08$ ,  $0.79 \pm 0.11$  and  $0.80 \pm 0.17$  at RH of 50%, 68%, and 90%, respectively.<sup>253</sup> Hygroscopic  
 1318 growth factors significantly smaller than 1 suggest that restructure of mineral dust particles may  
 1319 occur during humidification, and also make it difficult to derive the amount of adsorbed water  
 1320 from optical extinction measurements. It should be noted that potential restructure of dust particles  
 1321 can also affect H-TDMA measurements. For example, hygroscopic growth factors of ATD  
 1322 particles, as measured by H-TDMA, were reported to be slightly smaller than 1 at some RH.<sup>46,260</sup>  
 1323  
 1324 CCN activity of wet-generated Clay Mineral Society kaolinite aerosol particles were studied by  
 1325 Gibson et al.,<sup>257</sup> and the critical super-saturation was measured to be  $0.44 \pm 0.02$  for 200 nm dry  
 1326 particles, corresponding to a  $\kappa$  value of 0.0071. Herich et al.<sup>49</sup> used H-TDMA and CCNc to study  
 1327 the hygroscopicity and CCN activity of kaolinite particles, provided by Fluka and Clay Mineral  
 1328 Society. In the study by Herich et al.,<sup>49</sup> aerosol particles were produced by both dry and wet

1329 generation, and wet generation was found to increase the CCN activity of kaolinite particles. The  
1330 CCN activity of dry-generated kaolinite particles is quite low, with average  $\kappa$  values of  $\sim 0.001$ .<sup>49</sup>  
1331 By comparison, another study by Kumar et al.<sup>263</sup> found that wet-generated kaolinite aerosol  
1332 particles exhibited a  $\kappa$  values of 0.45 which is only slightly lower than that for ammonia sulfate,  
1333 highlighting that dry and wet generation methods can lead to considerable difference in the CCN  
1334 activities of resulting dust aerosol particles.



1335  
1336 **Figure 21.** Comparison of surface coverage ( $\theta$ ) of adsorbed water on kaolinite particles experimentally  
1337 measured by Hung et al.<sup>270</sup> (dashed olive curve) and those calculated using a  $\kappa$  value of 0.001 reported by  
1338 Herich et al.<sup>49</sup> and assumed particle diameters of 500 (solid black curve), 1000 (dashed blue curve), and  
1339 2000 nm (solid red curve).

1340  
1341 Surface coverages of adsorbed water on kaolinite particles experimentally by Hung et al.<sup>270</sup> are plotted in  
1342 Figure 21 together with those calculated using a  $\kappa$  value of 0.001 reported by Herich et al.<sup>49</sup> and assumed  
1343 particle diameters of 500, 1000, and 2000 nm. As shown in Figure 21, reasonably good agreement is found,

1344 considering the uncertainties (as discussed in Section 3.3) when using the  $\kappa$  value to calculate surface  
1345 coverages of adsorbed water.

1346

1347 Experimentally determined surface coverages of adsorbed water on kaolinite particles by Schuttlefield et  
1348 al.<sup>249</sup> and Hatch et al.<sup>268</sup> are shown in Figure 18c. Several conclusions can be drawn when comparing these  
1349 two studies.<sup>249,268</sup> First of all, Schuttlefield et al.<sup>249</sup> and Hatch et al.<sup>268</sup> used very similar techniques to  
1350 measure the amounts of water adsorbed by kaolinite particles from the same source (provided by Clay  
1351 Mineral Society), and their results agree quite well with each other, as shown in Figure 18c. Second,  
1352 Schuttlefield et al.<sup>249</sup> measured water adsorption on two different kaolinite samples, and significant  
1353 difference between these two samples was found. This may suggest the same type of dust particles from  
1354 different sources, because of variability within sources, could have very different ability to uptake water  
1355 vapor.

1356

1357 Surface coverages of adsorbed water on kaolinite particles measured by Schuttlefield et al.<sup>249</sup> and Hatch et  
1358 al.,<sup>268</sup> as shown in Figure 18c, are significantly higher than those (as shown Figure 21) directly measured  
1359 by Hung et al.<sup>270</sup> and those calculated using the  $\kappa$  value reported by Herich et al.<sup>49</sup> We note that Schuttlefield  
1360 et al.,<sup>249</sup> Hatch et al.<sup>268</sup>, and Hung et al.<sup>270</sup> all deposited kaolinite particles on supporting substrates. The  
1361 observed large discrepancy between the first two studies<sup>249,268</sup> and that by Hung et al.<sup>270</sup> is somehow  
1362 unexpected. A potential explanation is that the two studies by Schuttlefield et al.<sup>249</sup> and Hatch et al.<sup>268</sup> placed  
1363 particles onto the supporting substrates via depositing water slurry onto them, probably leading to swelling  
1364 and changes in the properties of kaolinite particles, while dry kaolinite powders were directly placed onto  
1365 the supporting substrate by Hung et al.<sup>270</sup>

1366

1367 Internally mixed kaolinite/ammonia sulfate particles, generated by atomizing kaolinite-ammonia  
1368 sulfate-water mixture, were found to have higher CCN activity compared to fresh kaolinite  
1369 particles.<sup>257</sup> The internally mixed kaolinite-ammonia sulfate particles have  $\kappa$  values of  $\sim 0.017$  and  
1370  $\sim 0.038$ , increasing with the mass ratio of ammonia sulfate to kaolinite in the aqueous mixtures



1371 which were atomized to produce aerosol particles.<sup>257</sup> Although this study<sup>257</sup> may not mimic actual  
 1372 atmospheric aging processes very well, it does suggest that the CCN activity of kaolinite particles  
 1373 can be substantially enhanced if being mixed more soluble compounds due to heterogeneous  
 1374 reactions and/or cloud processing.

#### 1375 **4.5 Montmorillonite**

1376 As summarized in Table 9, water adsorption, hygroscopicity, and CCN activity of montmorillonite  
 1377 particles have been investigated by several studies in the last 2-3 decades. For example, Hall and  
 1378 Astill<sup>379</sup> used a vacuum microbalance to measure the mass of montmorillonite particles at different  
 1379 RH (up to 70%) and at different temperature (25-75 °C). Four homoionic (Ca<sup>2+</sup>, Li<sup>+</sup>, Na<sup>+</sup>, and K<sup>+</sup>)  
 1380 exchanged forms of Clay Mineral Society montmorillonite (SWy-1) were studied.<sup>379</sup> Water  
 1381 adsorption by Na-exchanged montmorillonite was also investigated at different RH and 25 °C by  
 1382 Cases et al.,<sup>380</sup> using a microbalance. An environmental infrared microbalance was deployed by  
 1383 Xu et al.<sup>381</sup> to investigate water adsorption on Na-, Li-, Ca-, and Mg-exchanged forms of two  
 1384 montmorillonite samples (SWy-1 and SAz-1) provided by Clay mineral Society. Gas  
 1385 chromatography was used by Zent et al.<sup>382</sup> to study water uptake on Na-montmorillonite (Swy-1)  
 1386 at different RH and at 211 and 273 K.

1387  
 1388 **Table 9.** Water adsorption, hygroscopicity, and CCN activity of fresh montmorillonite: summary of  
 1389 previous studies.

references	techniques (and aerosol generation method, if applicable)
Hall and Astill, 1989 <sup>379</sup>	vacuum microbalance
Cases et al., 1992 <sup>380</sup>	microbalance
Xu et al., 2000 <sup>381</sup>	environmental infrared microbalance
Zent et al., 2001 <sup>382</sup>	gas chromatography
Frinak et al., 2005 <sup>383</sup>	Transmission FTIR

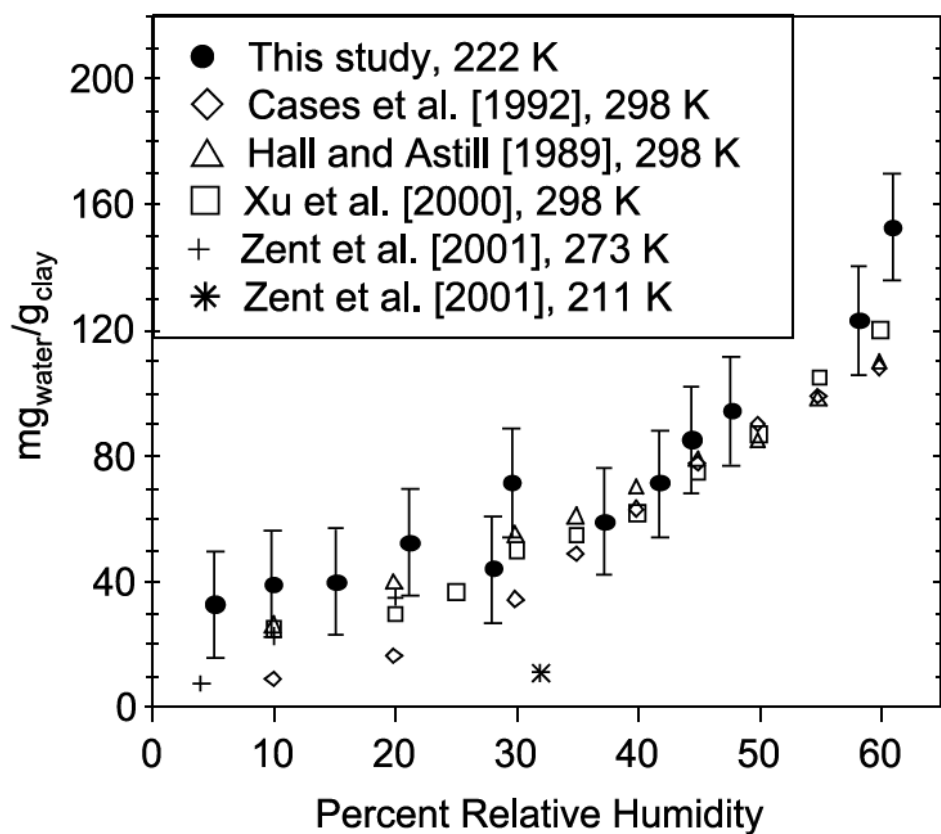
Schuttlefield et al., 2007 <sup>249</sup>	ATR-FTIR and QCM
Herich et al., 2009 <sup>49</sup>	H-TDMA and CCNc (dry and wet generation)
Attwood and Greenslade, 2011 <sup>253</sup>	AE-CRD (wet generation)
Hatch et al., 2011 <sup>268</sup>	ATR-FTIR
Kumar et al., 2011 <sup>262</sup>	CCNc (dry generation)
Kumar et al., 2011	CCNc (wet generation)
Hatch et al., 2014 <sup>348</sup>	ATR-FTIR
Garimella et al., 2014 <sup>259</sup>	CCNc (dry and wet generation)
Hung et al., 2015 <sup>270</sup>	PSA

1390

1391 More recently, Frinak et al.<sup>383</sup> used transmission FTIR to determine the amount of water adsorbed  
1392 on montmorillonite (SWy-2) provided by Clay Mineral Society as a function of temperature (212-  
1393 231 K) and RH. They found that water uptake by montmorillonite is almost as large as ammonia  
1394 sulfate.<sup>383</sup> It was further suggested by Frinak et al.<sup>383</sup> that though water adsorption on  
1395 montmorillonite depended strongly on RH, no strong dependence on temperature (212-231 K) was  
1396 observed.

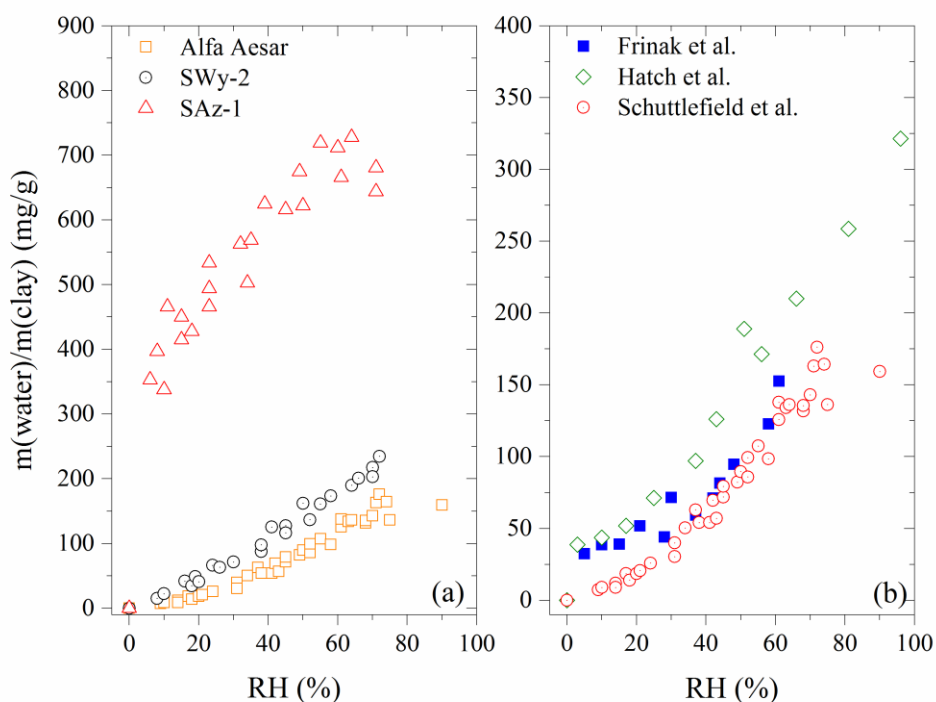
1397

1398 Frinak et al.<sup>383</sup> also compared their measurement to those reported in previous studies.<sup>379-382</sup> As  
1399 shown in Figure 22, except that reported by Zent et al.,<sup>382</sup> all the other studies in general show  
1400 good agreement. A close look reveals that the amount of adsorbed water measured by Cases et  
1401 al.<sup>380</sup> at RH<30% may be lower than those reported by Hall and Astill,<sup>379</sup> Xu et al.,<sup>381</sup> and Frinak  
1402 et al.<sup>383</sup>



1403  
 1404 **Figure 22.** Comparison of amounts of water adsorbed on SWy-2 (montmorillonite from Clay Mineral  
 1405 Society) measured by studies before 2006. Reprinted with permission from ref 383. Copyright 2005 John  
 1406 Wiley & Sons, Inc.

1407  
 1408 Water adsorption on three different montmorillonite samples (one from Alfa Aesar, the other two  
 1409 from Clay Mineral Society: SWy-2 and SAz-1) was investigated by Schuttlefield et al.<sup>249</sup> using  
 1410 ATR-FTIR and QCM. The amount of water adsorbed by montmorillonite was quantified at room  
 1411 temperature and at different RH, using QCM.<sup>249</sup> As shown in Figure 23a, montmorillonite particles  
 1412 from various sources exhibit different ability to adsorb water. At the same RH, the amount of water  
 1413 adsorbed by SAz-1 is much larger than those by the other two montmorillonite samples, and Alfa  
 1414 Aesar montmorillonite adsorbs the least amount of water.



1416

1417 **Figure 23.** (a) Water adsorption on three different montmorillonite samples as a function of RH, measured  
 1418 by Schuttlefield et al.<sup>249</sup> at room temperature. Squares: Alfa Aesar montmorillonite; circles: SWy-2 provided  
 1419 by Clay Mineral Society; triangles: SAz-1 provide by Clay Mineral Society. (b) Water adsorption on SWy-  
 1420 2 montmorillonite as a function of RH measured three different studies. Squares: measured by Frinak et  
 1421 al.<sup>383</sup> at 222 K; diamonds: measured by Hatch et al.<sup>268</sup> at room temperature; circles: measured by  
 1422 Schuttlefield et al.<sup>249</sup> at room temperature.

1423

1424 ATR-FTIR was used by Hatch et al.<sup>268</sup> to determine the amount of water adsorbed on Clay Mineral  
 1425 Society montmorillonite (SWy-2) particles at room temperature and at different RH, and the  
 1426 experimental result was fitted by the FHH adsorption isotherm with  $A_{FHH}$  and  $B_{FHH}$  equal to  $98 \pm 22$   
 1427 and  $1.79 \pm 0.11$ .<sup>348</sup> The mass ratios of adsorbed water to dry SWy-2, as a function of RH, measured  
 1428 by Frinak et al.<sup>383</sup> at 222 K and by Schuttlefield et al.,<sup>249</sup> and Hatch et al.<sup>268</sup> at room temperature,  
 1429 are plotted in Figure 23b for comparison. Results reported by studies<sup>379-382</sup> prior to Frinak et al.<sup>383</sup>  
 1430 are already shown in Figure 22, and therefore they are not included in Figure 23b. Considering the  
 1431 experimental uncertainties, all the three studies show very good agreement, even though Frinak et

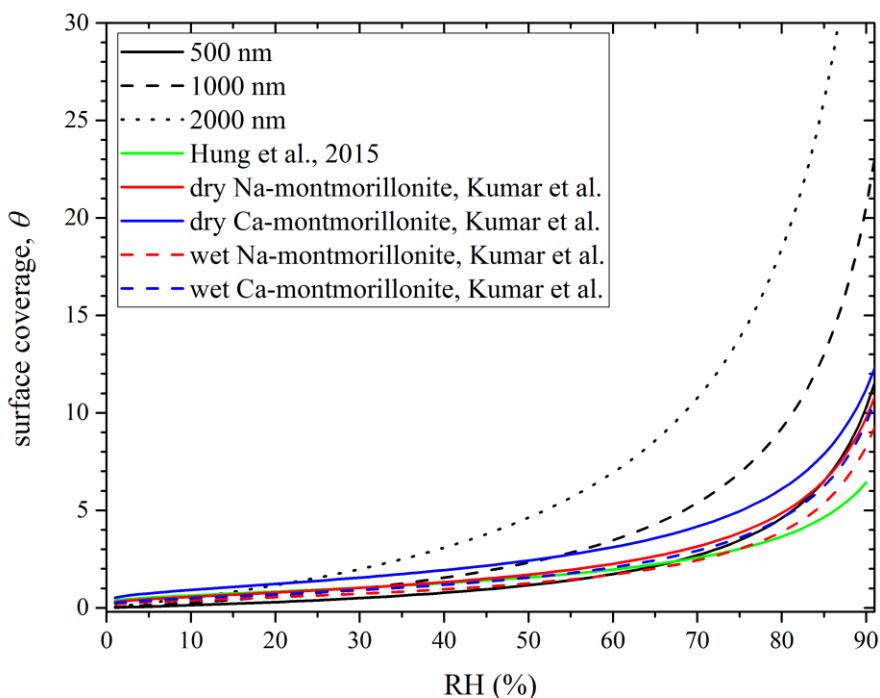
1432 al.<sup>383</sup> carried out the measurement at 222 K and the other two studies <sup>249,268</sup> were conducted at  
1433 room temperature. Considering earlier measurements which are plotted in Figure 22, one could  
1434 conclude that most of the available studies <sup>249,268,379-381,383</sup> in which samples were supported on  
1435 substrates reported similar water adsorption for SWy-2 montmorillonite, although different  
1436 experimental techniques were used to quantify the amount of adsorbed water.

1437  
1438 Optical extinction of wet-generated Clay Mineral Society montmorillonite particles at 532 nm was  
1439 measured at room temperature and at different RH by Attwood and Greenslade <sup>253</sup> to study their  
1440 hygroscopic growth, using Cavity Ring-Down spectroscopy. Their reported hygroscopic growth  
1441 factors are 1.03 at 50% RH, 1.18% at 68% RH, and 1.4 at 90%, respectively.<sup>253</sup> As discussed in  
1442 Sections 4.3 and 4.4, their reported hygroscopic growth factors are <1 for illite and kaolinite,<sup>253</sup>  
1443 likely due to restructure of clay particles at elevated RH. Restructure of montmorillonite particles  
1444 may also occur during humidification. In addition, since montmorillonite particles are non-  
1445 spherical, it is non-trivial to convert change in optical properties at different RH to the amount of  
1446 adsorbed water by the particles. Therefore, the result reported by Attwood and Greenslade <sup>253</sup> for  
1447 montmorillonite is not included in comparison. Using the same experimental method, in a  
1448 following study Attwood and Greenslade <sup>384</sup> found that internal mixing with montmorillonite  
1449 would decrease the deliquescence RH of both ammonia sulfate and sodium chloride.

1450  
1451 Using H-TDMA and CCNc, Herich et al.<sup>49</sup> studied the hygroscopicity and CCN activity of  
1452 montmorillonite particles provided Aldrich and Clay Mineral Society. Aerosol particles were  
1453 produced by both dry- and wet-generation.<sup>49</sup> Wet generation was found to increase the CCN  
1454 activity of montmorillonite particles, compared to dry generation.<sup>49</sup> The single hygroscopicity  
1455 parameter,  $\kappa$ , was determined to be ~0.003 for dry-generated montmorillonite particles and close  
1456 to 0.02 for wet-generated particles.<sup>49</sup> The CCN activation of dry-generated Na-montmorillonite

1457 provided by Clay Mineral Society was investigated by Garimella et al.,<sup>259</sup> with  $\kappa$  reported to be  
1458 0.0088.

1459  
1460 Kumar et al.<sup>262,263</sup> investigated the CCN activity of dry and wet-generated Na- and Ca-  
1461 montmorillonite aerosol particles, and suggested that the FHH adsorption activation theory could  
1462 better describe the CCN activation of montmorillonite aerosol particles. Reported  $A_{FHH}$  and  $B_{FHH}$   
1463 are  $1.23 \pm 0.31$  and  $1.08 \pm 0.03$  for dry-generated Na-montmorillonite,<sup>262</sup>  $2.06 \pm 0.72$  and  $1.23 \pm 0.04$   
1464 for dry-generated Ca-montmorillonite,<sup>262</sup> 0.87 and 1.00 for wet-generated Na-montmorillonite,<sup>263</sup>  
1465 and 1.09 and 1.04 for wet-generated Ca-montmorillonite,<sup>263</sup> respectively.



1466  
1467 **Figure 24.** Comparison of surface coverages of adsorbed water on montmorillonite measured by Hung et  
1468 al.<sup>270</sup> (solid green curve) with those extrapolated from CCN activity measurements. Surface coverages of  
1469 adsorbed water are also calculated using an average  $\kappa$  of 0.005<sup>49,259</sup> and assumed dry particle diameters of  
1470 500 (solid black curve), 1000 (dashed black curve), and 2000 nm (dotted black curve), respectively. In  
1471 addition,  $\theta$  are calculated using  $A_{FHH}$  and  $B_{FHH}$  values reported by Kumar et al.<sup>262,263</sup> Red curves: calculated  
1472 using  $A_{FHH}$  and  $B_{FHH}$  parameters for dry- (solid) and wet-generated (dashed) Na-montmorillonite; blue

1473 curves: calculated using  $A_{FHH}$  and  $B_{FHH}$  parameters for dry- (solid) and wet-generated (dashed) Ca-  
1474 montmorillonite.

1475  
1476 Recently Hung et al.<sup>270</sup> measured water adsorption on kaolinite K10 powders (provided by Sigma  
1477 Aldrich) at 28 °C and at different RH, using a PSA. For comparison, the measurements<sup>49,259,262,263</sup>  
1478 in which the CCN activity of aerosol particles were investigated are extrapolated to sub-saturation  
1479 conditions and plotted in Figure 24 together with the surface coverage of adsorbed water directly  
1480 measured Hung et al.<sup>270</sup> As shown in Figure 24, reasonably good agreement is found, though large  
1481 errors can occur in these extrapolations, as discussed in Section 3.2.

1482  
1483 However, differences can be found when comparing studies plotted in Figures 22-23, to those  
1484 shown in Figure 24. For example, Schuttlefield et al.<sup>249</sup> suggested that at around 70% RH,  
1485 approximately 50-60 and 200 monolayers of adsorbed water were formed on SWy-2 and SAz-1  
1486 kaolinite particles, compared to approximately 10 or less monolayers at the same RH for studies  
1487 shown in Figure 24. It should be noted that the surface coverage is calculated by dividing the total  
1488 amount of adsorbed water by the BET surface area of particles under investigation. The reasons  
1489 for such relatively large discrepancies are complicated and unclear at this stage. For example, the  
1490 difference between using particles supported on substrates and aerosol particles cannot explain the  
1491 discrepancies alone, because Hung et al.<sup>270</sup> also studied particles deposited on a substrate but  
1492 reported similar results to those using aerosol particles.<sup>49,259,262,263</sup> This can not be explained by  
1493 clay swelling effects alone which may play a role in several studies, for example, by Frinak et  
1494 al.,<sup>383</sup> Schuttlefield et al.,<sup>249</sup> and Hatch et al.<sup>268</sup> This is because the calculated surface coverages of  
1495 adsorbed water from the CCN activity measurement of wet-generated particles by Kumar et al.<sup>263</sup>  
1496 are not very different from those for dry-generated particles,<sup>262</sup> as shown in Figure 24. In addition,  
1497 such discrepancies cannot be only due to the usage of different types of montmorillonite particles,

1498 because studies <sup>49,259,262,263,270</sup> included in Figure 24 used montmorillonite from various sources but  
 1499 still showed reasonably good agreement. Careful and systematical measurements in future can help  
 1500 resolve these discrepancies and better understand the interaction of montmorillonite with water  
 1501 vapor.

## 1502 4.6 Quartz

1503 Table 10 provides a summary of previous studies in which water adsorption, hygroscopicity, and  
 1504 CCN activity of SiO<sub>2</sub>, TiO<sub>2</sub>, Al<sub>2</sub>O<sub>3</sub>, and Fe<sub>2</sub>O<sub>3</sub> were determined. Section 4.6 discusses previous  
 1505 studies on SiO<sub>2</sub>, while those for TiO<sub>2</sub>, Al<sub>2</sub>O<sub>3</sub>, and Fe<sub>2</sub>O<sub>3</sub> are reviewed in Section 4.7.

1506  
 1507 **Table 10.** Water adsorption, hygroscopicity, and CCN activity of fresh SiO<sub>2</sub>, TiO<sub>2</sub>, Al<sub>2</sub>O<sub>3</sub>, and Fe<sub>2</sub>O<sub>3</sub>:  
 1508 summary of previous studies.

mineral	References	techniques
SiO <sub>2</sub>	Goodman et al., 2001 <sup>250</sup>	Transmission FTIR
	Schuttlefield et al., 2007 <sup>273</sup>	ATR-FTIR and QCM
	Ma et al., 2010 <sup>269</sup>	DRIFTS
	Keskinen et al., 2011 <sup>320</sup>	H-TDMA (wet generation)
	Kumar et al., 2011 <sup>262</sup>	CCNc (dry generation)
TiO <sub>2</sub>	Dalirian et al., 2015 <sup>385</sup>	CCNc (wet generation)
	Goodman et al., 2001 <sup>250</sup>	Transmission FTIR
	Ketteler et al., 2007 <sup>241</sup>	AP-XPS
Al <sub>2</sub> O <sub>3</sub>	Ma et al., 2010 <sup>269</sup>	DRIFTS
	Goodman et al., 2001 <sup>250</sup>	Transmission FTIR
	Al-Abadleh and Grassian, 2003 <sup>240</sup>	Transmission FTIR
	Schuttlefield et al., 2007 <sup>249</sup>	ATR-FTIR and QCM
	Ma et al., 2012 <sup>212</sup>	PSA
Fe <sub>2</sub> O <sub>3</sub>	Goodman et al., 2001 <sup>250</sup>	Transmission FTIR



1509

---

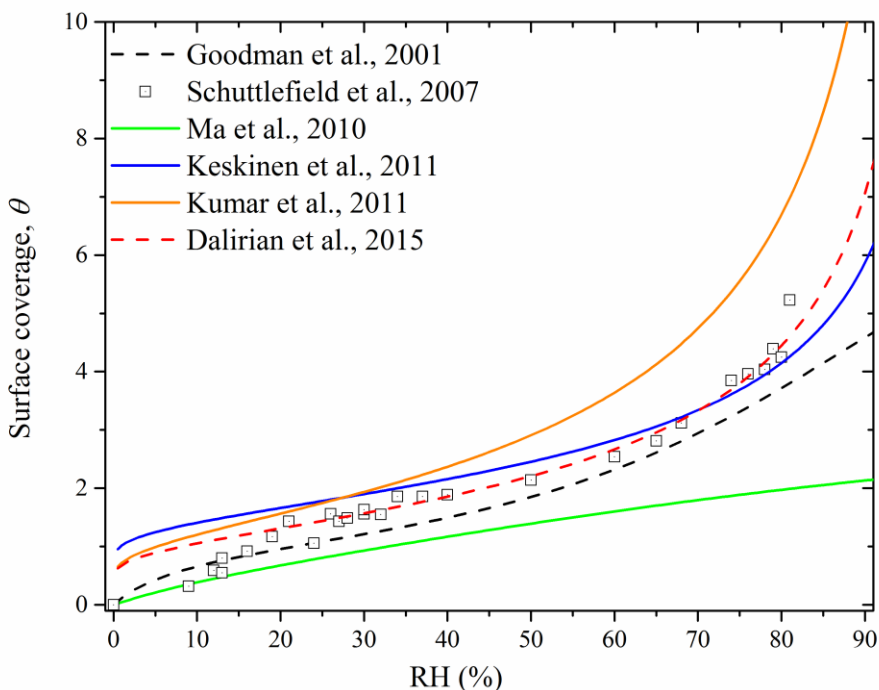
1510 Water adsorbed on SiO<sub>2</sub> particles was measured using transmission FTIR, and its surface coverage  
1511 at different RH was fitted by a modified three-parameter BET equation with  $n$  equal to 10 and  $c$   
1512 equal to 13.1.<sup>250</sup> Schuttlefield et al.<sup>273</sup> investigated water adsorption on SiO<sub>2</sub> particles by coupling  
1513 ATR-FTIR with QCM in tandem. In another study, DRIFTS was used by Ma et al.<sup>269</sup> to investigate  
1514 the interaction of water vapor with SiO<sub>2</sub> surface at different RH, and the result was also fitted with  
1515 a modified three-parameter BET equation with  $n$  equal to 3.8 and  $c$  equal to 4.8.

1516

1517 H-TDMA was used to study the hygroscopic growth of spherical SiO<sub>2</sub> aerosol particles of 8-10  
1518 nm,<sup>320</sup> and it is suggested that the water adsorption on SiO<sub>2</sub> particles can be described by the FHH  
1519 adsorption isotherm, with  $A_{\text{FHH}}$  and  $B_{\text{FHH}}$  equal to 4.82 and 2.16. It is also suggested that compact  
1520 agglomerate particles which contain a few primary spherical particles could adsorb ~1.5 times  
1521 more water at the same RH, compared to small spherical particles.<sup>320</sup> This may probably result  
1522 from the capillary effects of these small cavities between primary small particles in the  
1523 agglomerate.<sup>320</sup>

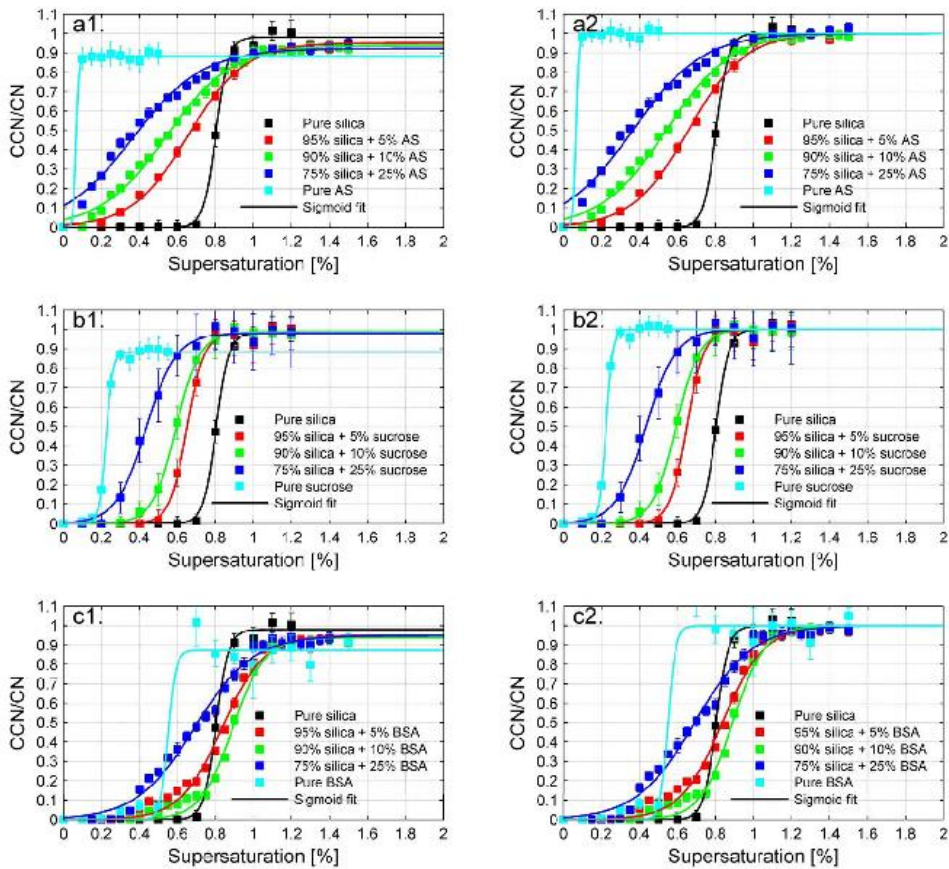
1524

1525 Kumar et al.<sup>262</sup> investigated the CCN activity of SiO<sub>2</sub> aerosol particles under super-saturation  
1526 conditions. Their measurements were interpreted using the FHH adsorption activation theory,  
1527 with  $A_{\text{FHH}}$  and  $B_{\text{FHH}}$  equal to 2.96 and 1.36, respectively.<sup>262</sup> The CCN activity of SiO<sub>2</sub> aerosol  
1528 particles were also investigated by Dalirian et al.,<sup>385</sup> and they suggested that the activation of SiO<sub>2</sub>  
1529 particles can be described by the FHH activation theory with  $A_{\text{FHH}}$  and  $B_{\text{FHH}}$  equal to 2.50 and 1.62,  
1530 respectively.



1531  
 1532 **Figure 25.** Comparison of surface coverage of adsorbed water on SiO<sub>2</sub> particles reported by Goodman et  
 1533 al.<sup>250</sup> (black dashed curve), Schuttlefield et al.<sup>273</sup> (squares), Ma et al.<sup>269</sup> (green solid curve), Keskinen et  
 1534 al.<sup>320</sup> (blue solid curve), Kumar et al.<sup>262</sup> (orange solid curve) and Dalirian et al.<sup>385</sup> (red dashed curve).

1535  
 1536 Water adsorption on SiO<sub>2</sub> particles, as measured by previous studies under sub-saturation  
 1537 conditions<sup>250,269,273,320</sup> or calculated using the two FHH parameters derived from CCN activation  
 1538 measurements under super-saturation conditions,<sup>262,385</sup> is plotted in Figure 25 for comparison. In  
 1539 general good agreement is found, though different experimental techniques and different SiO<sub>2</sub>  
 1540 samples were used. Significant discrepancies also exist. For example, the surface coverages of  
 1541 adsorbed water reported by Ma et al.<sup>269</sup> are always lower than those reported by other studies, and  
 1542 the discrepancy becomes more evident for RH >50%. In addition, for RH >50%, the difference  
 1543 between the calculated surface coverages of adsorbed water using the two FHH parameters  
 1544 reported by Kumar et al.<sup>262</sup> and those reported by Goodman et al.,<sup>250</sup> Schuttlefield et al.,<sup>273</sup>  
 1545 Keskinen et al.<sup>320</sup> and Dalirian et al.<sup>385</sup> appears to increase with RH.



1547  
 1548 **Figure 26.** CCN activation curves for 150 nm pure SiO<sub>2</sub> particles and SiO<sub>2</sub> particles mixed with (a1-a2)  
 1549 ammonia sulfate (AS), (b1-b2) sucrose, and (c1-c2) bovine serum albumin. The left three panels show the  
 1550 un-normalized data and the right three panels show the normalized data. Reprinted with permission from  
 1551 ref 385. Copyright 2015 Copernicus Publications.

1552  
 1553 Coating of SiO<sub>2</sub> particles with more hygroscopic materials can increase their CCN activities.  
 1554 Dalirian et al.<sup>385</sup> generated SiO<sub>2</sub> particles mixed with different amounts of ammonia sulfate (AS),  
 1555 sucrose, and bovine serum albumin (BSA). As shown in Figure 26, mixing SiO<sub>2</sub> with compounds  
 1556 with higher CCN activities (compared to SiO<sub>2</sub>) can decrease the critical super-saturation ratios and  
 1557 increase their CCN activity, when compared to pure SiO<sub>2</sub> particles.<sup>385</sup> The extent of decrease in  
 1558 critical super-saturation ratios depends on the mass fraction of SiO<sub>2</sub>, i.e. the less SiO<sub>2</sub> the mixed  
 1559 particles contain, the more CCN active these particles are. In addition, different materials have  
 1560 different effects even when their mass fractions are the same. For the three compounds investigated

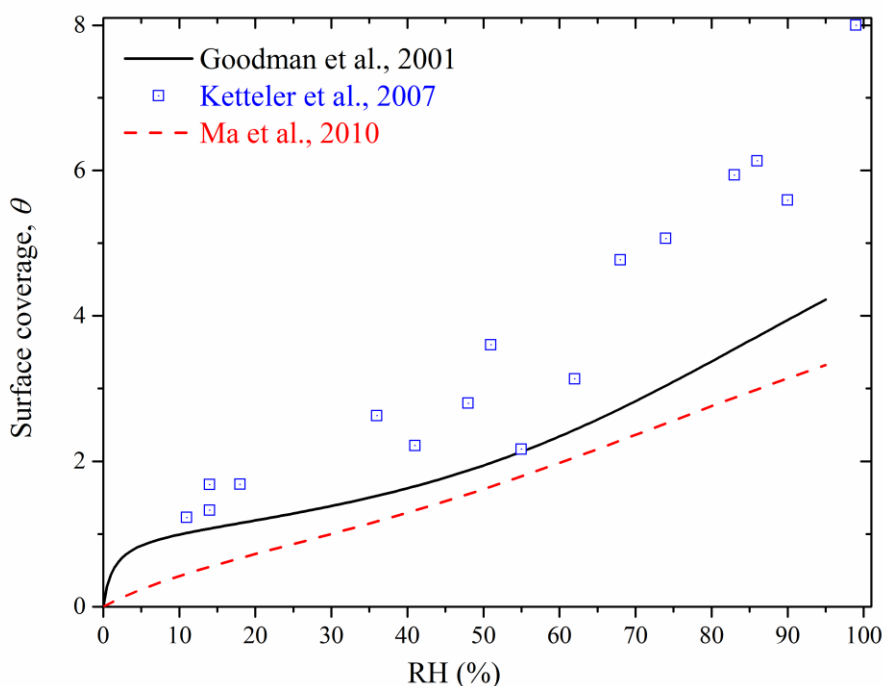
1561 by Dalirian et al.,<sup>385</sup> ammonia sulfate has the most significant effect because it is most CCN activity  
1562 with a  $\kappa$  value of 0.61, while BSA has a smaller effect because its  $\kappa$  value is  $\sim 0.13$  (and the  $\kappa$  value  
1563 is 0.084 for sucrose).<sup>385</sup>

#### 1564 **4.7 Metal oxides (TiO<sub>2</sub>, Al<sub>2</sub>O<sub>3</sub>, and Fe<sub>2</sub>O<sub>3</sub>)**

1565 Previous studies which have investigated water adsorption on fresh and/or reacted TiO<sub>2</sub>, Al<sub>2</sub>O<sub>3</sub>,  
1566 and Fe<sub>2</sub>O<sub>3</sub> particles are summarized in Table 10.

##### 1567 **4.7.1 TiO<sub>2</sub>**

1568 Goodman et al.<sup>250</sup> investigated water adsorption on P25 TiO<sub>2</sub> particles (BET surface area: 50 m<sup>2</sup> g<sup>-1</sup>)  
1569 at different RH using transmission FTIR. It was found that<sup>250</sup> the surface coverage of adsorbed  
1570 water can be fitted by the modified three-parameter BET equation, i.e. Eq. (5), with  $n$  equal to 8  
1571 and  $c$  equal to 74.8. Ma et al.<sup>269</sup> used DRIFTS to study the water adsorption on P25 TiO<sub>2</sub> particles,  
1572 and suggested that surface coverage of adsorbed water can be fitted with the modified three-  
1573 parameter BET equation with  $n$  equal to 6.2 and  $c$  equal to 5.5. The results reported by these two  
1574 studies are plotted in Figure 27, suggesting that the surface coverage of adsorbed water measured  
1575 by Goodman et al.<sup>250</sup> is slightly higher than that determined by Ma et al.<sup>269</sup>



1576

1577 **Figure 27.** Surface coverage of adsorbed water on TiO<sub>2</sub> particles reported by previous studies. Solid curve:  
 1578 Goodman et al.;<sup>250</sup> squares: Ketteler et al.;<sup>241</sup> dashed curve: Ma et al.<sup>269</sup>

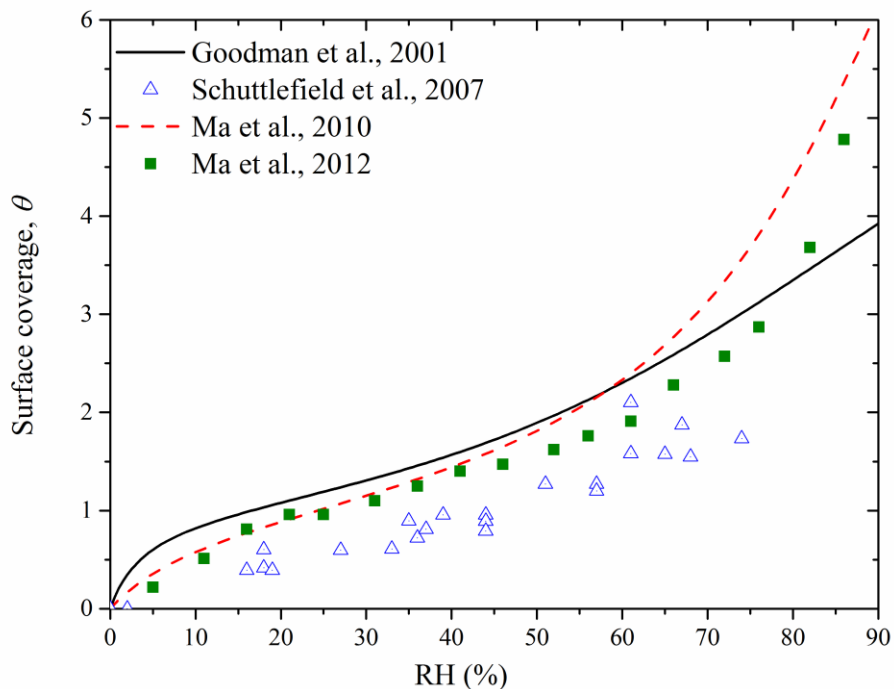
1579

1580 In addition, AP-XPS was also used to study water adsorption on the rutile single crystal  
 1581 surface(110).<sup>241</sup> The AP-XPS measurement suggested that 2 and 3 monolayers of adsorbed water  
 1582 are found at 12% and 25%,<sup>241</sup> and the surface coverage is higher than those reported Goodman et  
 1583 al.<sup>250</sup> and Ma et al.<sup>269</sup> However, it may not be directly comparable because Ketteler et al.<sup>241</sup> used  
 1584 single crystals while P25 TiO<sub>2</sub> particles were used by the other two studies.<sup>250,269</sup> Many previous  
 1585 studies have investigated water adsorption on rutile and anatase singles crystals, as summarized  
 1586 by Chen et al.<sup>155</sup> Since those studies are not of direct atmospheric relevance, they are not further  
 1587 discussed.

#### 1588 4.7.2 Al<sub>2</sub>O<sub>3</sub>

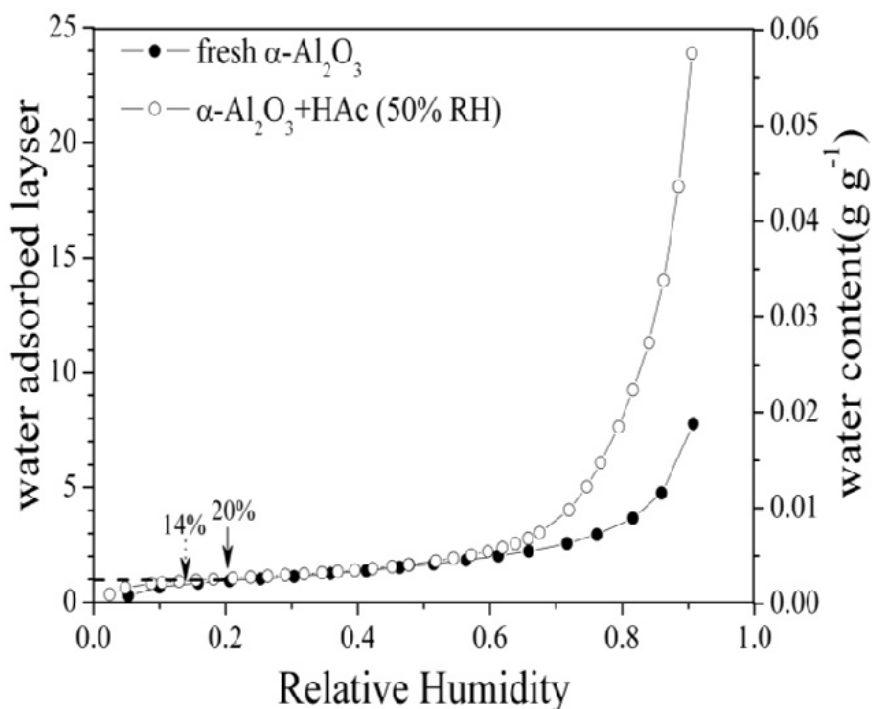
1589 Transmission FTIR was used to study water adsorption on α-Al<sub>2</sub>O<sub>3</sub> particles,<sup>250</sup> and it was  
 1590 suggested that the surface coverage of adsorbed water can be fitted with the modified three-

1591 parameter BET equation with  $n$  equal to 8 and  $c$  equal to 25.2. Transmission FTIR was also used  
 1592 to investigate water adsorption on  $\alpha$ -Al<sub>2</sub>O<sub>3</sub> single crystals;<sup>240</sup> this work is of less atmospheric  
 1593 relevance and thus not further discussed. Water adsorption on  $\alpha$ -Al<sub>2</sub>O<sub>3</sub> particles was further  
 1594 investigated by Schuttlefield et al.<sup>249</sup> using ATR-FTIR and QCM, and the amount of adsorbed  
 1595 water at different RH was reported. Ma et al.<sup>269</sup> used DRIFTS to measure the amount of water  
 1596 adsorbed on  $\alpha$ -Al<sub>2</sub>O<sub>3</sub> particles, and suggested that its surface coverage can be described by a  
 1597 modified three-parameter BET equation, with  $n$  equal to 15.4 and  $c$  equal to 9.66. In addition, PSA  
 1598 was used by Ma et al.<sup>212</sup> to measure water adsorbed on  $\alpha$ -Al<sub>2</sub>O<sub>3</sub>, and it was shown that one  
 1599 monolayer adsorbed water is formed at ~20% RH.



1600  
 1601 **Figure 28.** Comparison of surface coverage of adsorbed water on  $\alpha$ -Al<sub>2</sub>O<sub>3</sub> at different RH, as reported in  
 1602 previous studies. Solid curve: Goodman et al.;<sup>250</sup> dashed curve: Ma et al.;<sup>269</sup> squares: Ma et al.;<sup>212</sup> triangles:  
 1603 chuttlefield et al.<sup>249</sup>  
 1604  
 1605 Surface coverages of adsorbed water on  $\alpha$ -Al<sub>2</sub>O<sub>3</sub>, as measured by these four different studies, are  
 1606 displayed together in Figure 28 as a function of RH. As evident in Figure 28, in general different

1607 studies show good agreement, though different methods have been used to quantify the amount of  
1608 water adsorbed on the particle surface. A close inspection also reveals that for  $RH > 80\%$ , the  
1609 discrepancy between Goodman et al.<sup>250</sup> and Ma et al.<sup>212,269</sup> may increase. This may suggest that  
1610 experimental uncertainties increase with RH.



1611  
1612 **Figure 29.** Amounts of water adsorbed on  $\alpha\text{-Al}_2\text{O}_3$  particles before and after heterogeneous reaction with  
1613 gaseous acetic acid. Reprinted with permission from ref 212. Copyright 2012 the PCCP Owner Societies.

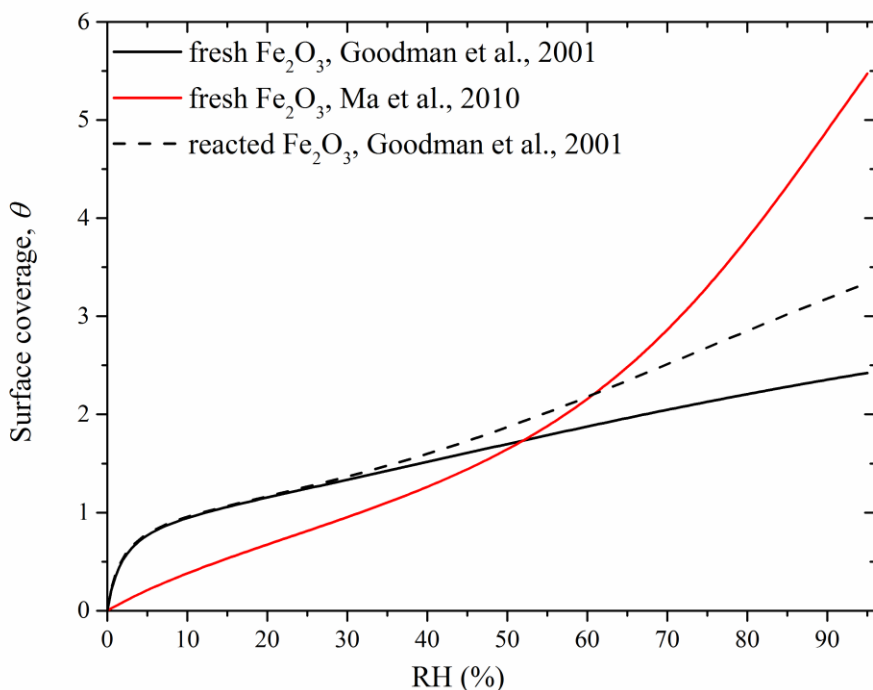
1614  
1615 Heterogeneous reactions can change the hygroscopicity of  $\alpha\text{-Al}_2\text{O}_3$ . For example, Ma et al.<sup>212</sup>  
1616 measured the amount of water adsorbed on  $\alpha\text{-Al}_2\text{O}_3$  before and after reaction with acetic acid. As  
1617 shown in Figure 29, it was found that the RH required to form one monolayer of adsorbed water  
1618 decreased from  $\sim 20\%$  to  $14\%$  after the reaction with acetic acid.<sup>212</sup> In addition, at  $90\%$  RH the  
1619 amount of water adsorbed on the surface increased from  $1.7\%$  (by mass) for fresh particles to  $5.2\%$   
1620 (by mass) for reacted particles.<sup>212</sup> The study by Ma et al.<sup>212</sup> suggests that heterogeneous reaction

1621 with acetic acid increases the hygroscopicity of  $\alpha$ -Al<sub>2</sub>O<sub>3</sub> particles. In contract, another study by  
1622 Rubasinghege et al.<sup>386</sup> found that exposure to formic acid could largely reduce the amount of water  
1623 adsorbed by  $\gamma$ -Al<sub>2</sub>O<sub>3</sub>.

#### 1624 **4.7.3 Fe<sub>2</sub>O<sub>3</sub>**

1625 Water adsorption on Fe<sub>2</sub>O<sub>3</sub> was investigated by transmission FTIR<sup>250</sup> and DRIFTS<sup>269</sup> respectively.  
1626 Both studies suggest that the surface coverage of adsorbed water can be described by a modified  
1627 three-parameter BET equation, with  $n$  and  $c$  equal to 4 and 51.1 reported by Goodman et al.<sup>250</sup> and  
1628 11.3 and 4.68 derived by Ma et al.<sup>269</sup> As shown in Figure 30, the surface coverage of adsorbed  
1629 water measured by Goodman et al.<sup>250</sup> is higher for RH < ~55% and lower for RH > ~55% than that  
1630 measured by Ma et al.<sup>269</sup> In addition, the discrepancy between the two studies seems to increase  
1631 with RH for RH > ~55%.





1632

1633 **Figure 30.** Surface coverages of adsorbed water on Fe<sub>2</sub>O<sub>3</sub>. Solid black curve: fresh particles measured by  
 1634 Goodman et al.;<sup>250</sup> dashed black curve: reacted particles measured by Goodman et al.;<sup>250</sup> solid red curve:  
 1635 fresh particles measured by Ma et al.<sup>269</sup>

1636

1637 In addition, Goodman et al.<sup>250</sup> found that the exposure to HNO<sub>3</sub> significantly increased the amount  
 1638 of water adsorbed by Fe<sub>2</sub>O<sub>3</sub> particles, with *n* and *c* equal 6 and 55.3 for aged Fe<sub>2</sub>O<sub>3</sub>, compared to  
 1639 4 and 51.1, respectively, for fresh Fe<sub>2</sub>O<sub>3</sub>.

#### 1640 **4.8 Authentic complex dust mixture**

1641 Water adsorption properties, hygroscopicity, and CCN activity of a variety of authentic dust  
 1642 samples have been investigated in the last two decades, and Table 11 provides a quick overview  
 1643 of these studies. Arizona Test Dust is also an authentic dust sample; however, it has been separately  
 1644 discussed in Section 4.2 because it has been extensively studied and is often used as a dust standard.  
 1645 A direct comparison between different studies is difficult, because dust particles, even if they have

1646 the same name (for examples, Saharan dust), may be collected from different locations and thus  
 1647 their compositions may show large variations.

1648

1649 **Table 11.** Water adsorption, hygroscopicity, and CCN activity of authentic dust particles: summary of  
 1650 previous studies.

reference	techniques	dust
Seisel et al., 2004 <sup>298</sup>	Knudsen cell	Saharan dust
Seisel et al., 2005 <sup>299</sup>	Knudsen cell	Saharan dust
Koehler et al., 2007 <sup>387</sup>	H-TDMA and CCNc	Owens (dry) Lake dust
Koehler et al., 2009 <sup>46</sup>	H-TDMA and CCNc	Canary Islands dust, Cairo dust
Herich et al., 2009 <sup>49</sup>	H-TDMA and CCNc	Saharan dust, Chinese dust
Navea et al., 2010 <sup>246</sup>	ATR-FTIR and QCM	Saharan dust, China loess
Yamashita et al., 2011 <sup>376</sup>	CCNc	Asian mineral dust
Kumar et al., 2011 <sup>262</sup>	CCNc	Niger dust, and five different East Asian dust
Kumar et al., 2011 <sup>263</sup>	CCNc	Niger dust, and five different East Asian dust
Ma et al., 2012 <sup>182</sup>	DRIFTS	Asian dust

1651

1652 Using a Knudsen cell reactor coupled to a mass spectrometer, Seisel et al.<sup>298,299</sup> measured the  
 1653 uptake of water vapor by Saharan dust particles over 203-298 K, and the initial uptake coefficient  
 1654 was determined to be  $(6.3 \pm 0.7) \times 10^{-2}$ , independent of temperature. Yamashita et al.<sup>376</sup> studied the  
 1655 CCN activity of dry-generated Asian mineral dust particles, and reported an average  $\kappa$  of 0.014.  
 1656 Ma et al.<sup>182</sup> collected Asian dust particles in Beijing during a dust storm event, and measured the  
 1657 water adsorption by these dust particles at different RH before and after heterogeneous reaction  
 1658 with SO<sub>2</sub>. They<sup>182</sup> found that ~8 monolayers of adsorbed water were found at 90% RH, and that  
 1659 the reaction with SO<sub>2</sub> did not significantly change the hygroscopicity of Asian dust particles they  
 1660 collected.

1661

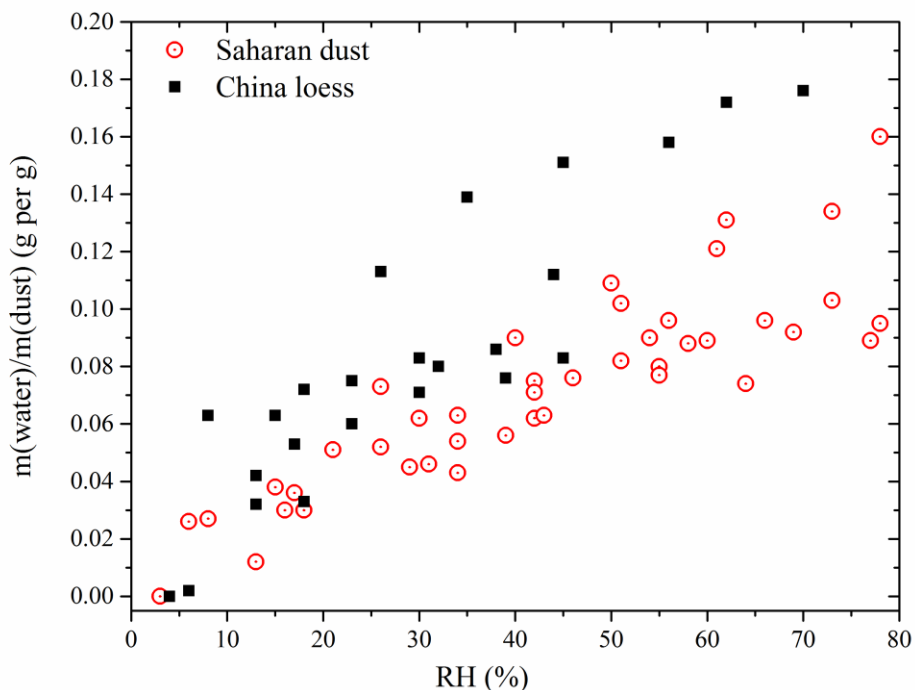
1662 Koehler et al.<sup>387</sup> measured the hygroscopicity and CCN activity of dust particles collected from  
1663 Owens Lake region (California, USA), using H-TDMA and CCNc. They<sup>387</sup> found that 35% of the  
1664 dry-generated particles are very hygroscopic with an average  $\kappa$  of 0.69 and the other 65% are much  
1665 less hygroscopic with an average  $\kappa$  of  $\sim 0.05$ . Koehler et al.<sup>46</sup> also investigated the hygroscopicity  
1666 and CCN activity of two North African dust samples: one from the Canary Islands and the other  
1667 one from outside Cairo. It is suggested that the CCN activity of these dust particles can be  
1668 represented using the single hygroscopicity parameter of  $0.01 < \kappa < 0.08$ .<sup>46</sup> In addition, wet-  
1669 generated Canary Islands dust and Cairo dust were found to be much more hygroscopic, with  $\kappa$   
1670 equal to 0.26 and 0.7,<sup>46</sup> suggesting that wet-generation may artificially enhance the hygroscopicity  
1671 and CCN activity of dust particles.

1672

1673 Using H-TDMA and CCNc, Herich et al.<sup>49</sup> investigated the hygroscopicity and CCN activity of  
1674 Saharan dust and Chinese dust. Dust aerosol particles were produced by both dry- and wet-  
1675 generation, and it was found that wet generation could significantly increase the CCN activity of  
1676 dust particles.<sup>49</sup> The single hygroscopicity parameter,  $\kappa$ , was found to be 0.023 for dry-generated  
1677 Saharan dust and 0.007 for dry-generated Chinese dust.<sup>49</sup> In addition, Herich et al.<sup>49</sup> found that  $\kappa$   
1678 derived from H-TDMA measurement may be smaller than those derived from CCNc measurement;  
1679 nevertheless, the difference may be within the experimental uncertainties.

1680

1681 QCM was used to study water adsorption on Saharan dust and China Loess at room temperature  
1682 and at different RH.<sup>246</sup> The results are displayed in Figure 31, suggesting that both Saharan dust  
1683 and China loess can adsorb substantial amount of water.<sup>246</sup> In addition, it appears that the two  
1684 samples show somewhat similar water uptake capacities on a per mass basis, although their  
1685 chemical compositions based on the XPS, SEM-EDX, and ATR-FTIR analyses show large  
1686 differences.<sup>246</sup>



1687  
 1688 **Figure 31.** The amounts of water adsorbed by Saharan dust (red circles) and China loess (black squares) at  
 1689 room temperature and at different RH, as measured by Navea et al.<sup>246</sup>

1690  
 1691 Kumar et al.<sup>262</sup> investigated the CCN activity of six different types of dust particles, one collected  
 1692 from Niger (Sahel) and the other five collected from different locations in East Asian deserts. It  
 1693 was suggested that the FHH adsorption activation theory could better describe the CCN activation  
 1694 of these dry-generated dust aerosol particles,<sup>262</sup> compared to the  $\kappa$ -Köhler activation theory. The  
 1695 measured CCN activity of all the dust particles can be represented by one set of FHH parameters  
 1696 with  $A_{FHH}$  equal to  $\sim 2.25 \pm 0.75$  and  $B_{FHH}$  equal to  $\sim 1.20 \pm 0.10$ .<sup>262</sup> Kumar et al.<sup>263</sup> also measured the  
 1697 CCN activity of wet-generated aerosol particles for these six types of dust, and found that  $\kappa$  for  
 1698 these wet-generated dust aerosol particles varies in the range of 0.14-0.44.<sup>263</sup> It was also suggested  
 1699 that wet-generation can lead to enhancement of the measured CCN activity of dust particles,  
 1700 compared to dry generation.<sup>262,263</sup>

## 1701 **4.9 Theoretical studies on water adsorption on mineral dust surface**

1702 There have been several theoretical studies focused on adsorption of gas phase water on mineral  
1703 surfaces. These studies include but are not limited to calcite,<sup>388-390</sup> kaolinite,<sup>391-395</sup>  
1704 montmorillonite,<sup>377,396,397</sup> quartz,<sup>398,399</sup> titanium dioxide,<sup>400-402</sup> and FeOOH.<sup>275,403,404</sup> In this review  
1705 we do not provide a comprehensive review of these studies, but instead we highlight a few these.  
1706 In particular, we highlight several theoretical studies which have significantly improved our  
1707 understanding of water adsorption on mineral dust particles of atmospheric relevance at a  
1708 fundamental level. This discussion is limited to four representative components contained by  
1709 mineral dust aerosol particles in the troposphere. These components are representative of carbonate  
1710 minerals (calcite), clay minerals (kaolinite and montmorillonite), and oxide minerals (quartz). A  
1711 recent review paper<sup>155</sup> summarized some theoretical work for water adsorption on TiO<sub>2</sub>(110)  
1712 surface. In general, it appears that it is non-trivial for theoretical studies to quantitatively predict  
1713 the amount of water adsorbed by mineral surfaces as a function of RH. However, insights into  
1714 fundamental processes involved in water-mineral interactions can be gained from these theoretical  
1715 studies. Recently Gerber et al.<sup>405</sup> provided several excellent examples to illustrate how theoretical  
1716 studies could help us understand atmospherically relevant chemical reactions at various  
1717 interfaces/surfaces.

### 1718 **4.9.1 Calcium carbonate**

1719 Using molecular dynamics simulations, de Leeuw and Parker<sup>388</sup> investigated the effect of water  
1720 adsorption on the surface structures and energetics for several different planar calcite surfaces.  
1721 They found that physisorption of water is energetically favourable for all the planar surfaces,  
1722 among which the (1014) surface is most stable.<sup>388</sup> Kerist and Parker<sup>406</sup> calculated the free energy  
1723 of water adsorption on the (1014) calcite surface using molecular dynamics simulations. Their  
1724 simulations<sup>406</sup> suggested that the free energy of water adsorption is smaller than the enthalpy,  
1725 indicating that there is a large change in entropy associated with water adsorption on the surface.

1726 Additionally, ab-initio calculations by Kerisit et al.<sup>389</sup> were used to predict the surface phase  
1727 diagram for the (1014) calcite surface, and they<sup>389</sup> suggested that nonstoichiometric surfaces can  
1728 be important in determining the chemistry of calcite at high RH.

1729

1730 Rahaman et al.<sup>390</sup> developed a molecular dynamics scheme to study the dynamics of water  
1731 adsorption on the (1014) calcite surface at different RH. They<sup>390</sup> found that the timescale for the  
1732 surface to become in equilibrium with the environment is of several nanoseconds, and predicted  
1733 that water adsorption on the surface would follow a BET-like isotherm. They<sup>390</sup> also suggested  
1734 that mobility of adsorbed water is enhanced at higher RH, and that at lower RH adsorbed water is  
1735 more tightly bound to the surface.

#### 1736 **4.9.2 Kaolinite**

1737 Previous theoretical studies on water adsorption on kaolinite, for example, by Hu and  
1738 Michaelides,<sup>407-409</sup> mostly focused on the Al-terminated(001) and Si-terminated(001) surfaces.  
1739 Croteau et al.<sup>392-395</sup> used grand canonical Monte Carlo simulations to investigate adsorption and  
1740 structure of water on kaolinite surfaces. They<sup>392</sup> found that at 235 K, the Si-surface is hydrophobic  
1741 and does not display potential to adsorb water when RH is less than 100%, and adsorption on the  
1742 Al-surface exhibits first-order characteristics. More importantly, they<sup>392</sup> suggested that adsorption  
1743 on edges, dominated by strong water-surface interactions, is much more continuous and  
1744 contributes significantly to water uptake by kaolinite.

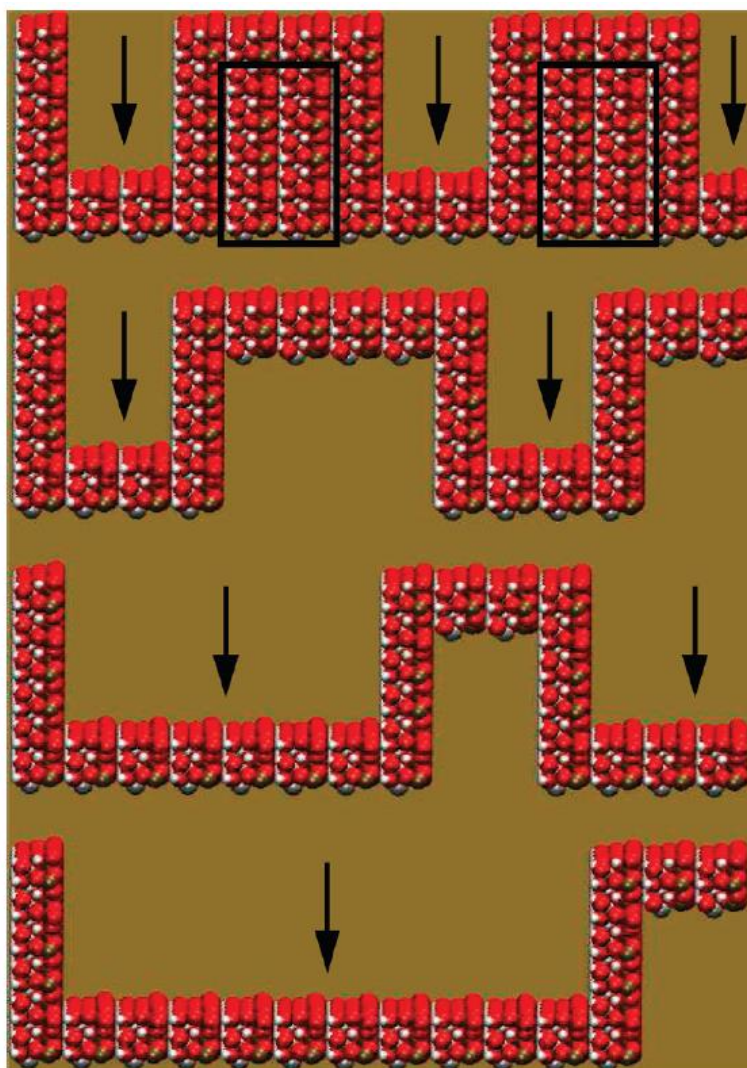
1745

1746 In a following study, Croteau et al.<sup>393</sup> further investigated water adsorbed on four different surfaces  
1747 (the Al-terminated surface, the Si-terminated surface, and two edge-like surfaces) of kaolinite at  
1748 different RH and at two different temperatures (235 and 298 K), using Monte Carlo simulations.  
1749 Several conclusions have been drawn from their simulations:<sup>393</sup> i) the Si-terminated surface does  
1750 not uptake significant amount of water, and the Al-terminated surface and the two edge-like

1751 surfaces can adsorb monolayers of water for RH below 100%; ii) the edge-like surfaces have the  
1752 largest affinity for water; iii) water adsorption on the edge-like surfaces grows continuously until  
1753 one monolayer is reached, while on the Al-surface the formation of one monolayer adsorbed water  
1754 appears as a sharp transition (this also indicates that collective behavior occurs among water  
1755 molecules on the Al-surface but not on the edges) and practically there is no submonolayer  
1756 adsorption. This suggests that mechanisms of water adsorption on the Al-surface and the edge-  
1757 like surfaces are distinctively different.<sup>393</sup>

1758

1759 The two previous studies carried out by Croteau et al.<sup>392,393</sup> used atomistically smooth kaolinite  
1760 surfaces in these simulations, and their predicted surface coverages of adsorbed water are much  
1761 lower than those experimentally measured by Schuttlefield et al.<sup>249</sup> In an effort to explain the  
1762 experimental results, Croteau et al.<sup>395</sup> further performed water adsorption simulations at 296 K on  
1763 kaolinite surfaces which contain trenchlike structures. The structures of different trenches  
1764 considered by Croteau et al.<sup>395</sup> are shown in Figure 32.

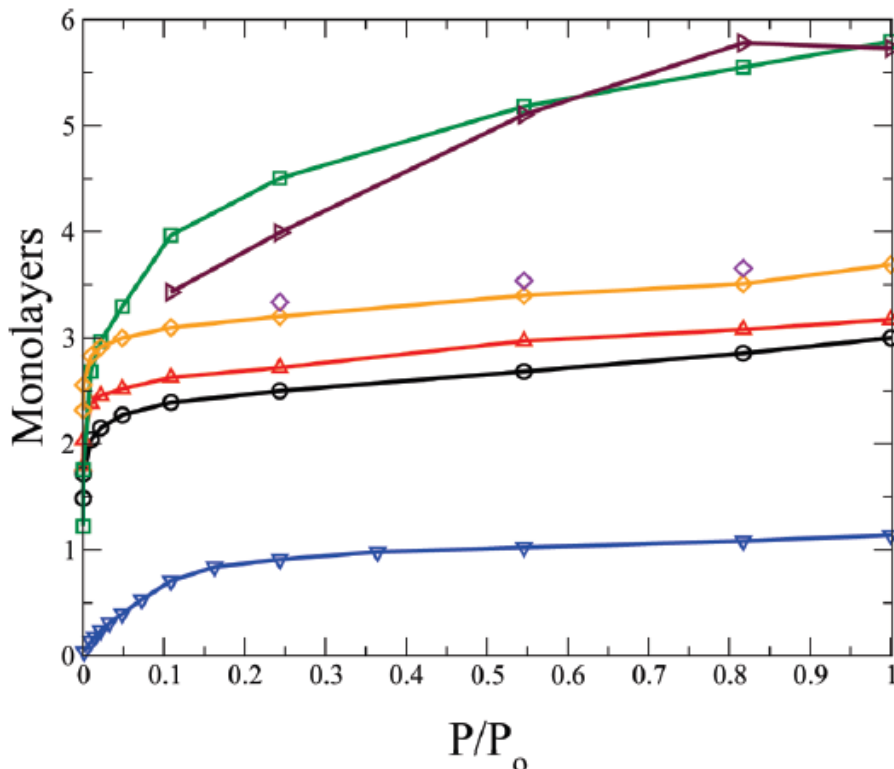


1765  
 1766 **Figure 32.** The structures of different trenches on kaolinite surfaces considered by Croteau et al.<sup>395</sup> in their  
 1767 simulations. O, H, Al, and Si atoms are in red, white, gray, and brown. From top to bottom, the trenches  
 1768 are referred as 1, 2, 3, and 4, with trench widths of 14.78, 14.78, 44.34, and 73.91 Å, respectively. Simulations  
 1769 were carried out for trench 1 without (1A) and with (1B) intertrench spacing filled (atoms inside the black  
 1770 rectangle). Black arrows indicate where the trenches are. Reprinted from permission from ref 395.  
 1771 Copyright 2010 American Chemical Society.

1772  
 1773 Simulated water adsorption on kaolinite surfaces with different trenches at 298 K are shown in  
 1774 Figure 33 as a function of RH. Compared to that for an atomistically smooth edge-like surface, it  
 1775 was found that the amount of adsorbed water is largely increased for surfaces with all the different



1776 trenches.<sup>395</sup> The study by Croteau et al.<sup>395</sup> suggests that surface trenches (and very likely other  
1777 surface defects) may have strong affinity for water and thus can adsorb multilayers of water. The  
1778 amounts of adsorbed water on kaolinite predicted by Croteau et al.<sup>395</sup> as a function of RH are on  
1779 the same order of magnitude as those measured by Hung et al.,<sup>270</sup> but appear to be significantly  
1780 smaller than those measured by Schuttlefield et al.<sup>249</sup> and Hatch et al.<sup>348</sup>



1781  
1782 **Figure 33.** Simulated surface coverages of adsorbed water on an atomistically smooth edge kaolinite  
1783 surface (blue triangles) and kaolinite surfaces containing different types of trenches as a function of RH  
1784 ( $P/P_0$ , defined as the ratio of partial pressure of water vapor to the saturated vapor pressure of water) at 298  
1785 K. Blue triangles: atomistically smooth edge-like surface; red triangles: trenches 1A; orange diamonds:  
1786 trenches 1B; black circles: trenches 2; green squares: trenches 3; maroon triangles: trenches 4. Trench  
1787 structures are given in Figure 32. Reprinted from permission from ref 395. Copyright 2010 American  
1788 Chemical Society.

### 1789 **4.9.3 Montmorillonite**

1790 Hensen et al.<sup>396</sup> combined molecular dynamics and Monte Carlo simulations to investigate water  
1791 adsorption by Li-, Na-, and K-montmorillonite. It is found that water adsorption by these  
1792 montmorillonite occurs via two mechanism:<sup>396</sup> 1) at low RH, water adsorption is driven by  
1793 hydration of interlayer counterions, and the extent of water adsorption increases with cation-H<sub>2</sub>O  
1794 hydration energy ( $\text{Li}^+ > \text{Na}^+ > \text{K}^+$ ); 2) at high RH, water molecules are adsorbed near mineral  
1795 surface, coordinating to the structural OH groups. This enables the formation of an extensive  
1796 hydrogen bonding network and therefore leads to a sharp increase of adsorbed water with RH.<sup>396</sup>

1797  
1798 In a following theoretical study, Hensen and Smit<sup>377</sup> was able to quantitatively predict the amount  
1799 of water adsorbed by Na-montmorillonite as a function of RH. In addition, their simulations<sup>377</sup>  
1800 suggested that montmorillonite swelling occurs by migration of counterions (which are initially  
1801 strongly bound to clay surface) to positions in the clay interlayers where these ions can be fully  
1802 hydrated.

### 1803 **4.9.4 Quartz**

1804 Several review articles<sup>410,411</sup> and books<sup>412,413</sup> have summarized theoretical studies on the  
1805 interaction of water with silica surfaces, especially for liquid water-quartz interactions. Interested  
1806 readers are referred to these publications for more information. Density functional theory based  
1807 molecular dynamics simulations were used by Sulpiz et al.<sup>414</sup> to understand the molecular behavior  
1808 of quartz-water interface. They<sup>414</sup> suggested that two types of silanol groups exist at the quartz  
1809 surface: i) out-of-plane silanols with a pKa of 5.6, forming strong and short H-bonds with  
1810 interfacial water molecules, giving rise to highly correlated hydrogen-bonding network and thus  
1811 exhibiting a band at  $\sim 3200 \text{ cm}^{-1}$  in the sum frequency generation (SFG) spectroscopy.<sup>415-417</sup> For  
1812 simplicity, these water molecules are also referred to as the “ice-like” water because of their  
1813 similarity in structure to water molecules in bulk ice;<sup>418</sup> ii) in-plane silanols with a pKa of 8.5,

1814 forming weak hydrogen bonds with interfacial water molecules and showing a broad band at ~3400  
1815  $\text{cm}^{-1}$  in the SFG spectrum.<sup>415-417</sup> Intensity in this region corresponds with OH stretch intensities of  
1816 bulk liquid water, and therefore for simplicity these water molecules are sometimes referred to as  
1817 “liquid-like” water.<sup>418</sup>

1818  
1819 Recently Murdachaew et al.<sup>399</sup> used initio molecular dynamics to study the adsorption of HCl on  
1820 the hydroxylated  $\alpha$ -quartz (0001) surface, and observed that adsorbed HCl is rapidly dissociated  
1821 and ionized on wetted surface at temperatures between 250 and 300 K. Ionization of adsorbed HCl  
1822 seems to be enhanced by lattice mismatch between the silica and water layer.<sup>399</sup> The dissociation  
1823 and ionization of HCl on  $\text{SiO}_2$  surface has several important implications for atmospheric  
1824 chemistry. For example, it lowers the pH for silica surface and leads to the charging and  
1825 disordering of adsorbed water.<sup>399</sup> These changes could significantly impact chemical processes on  
1826 silica surfaces.<sup>399</sup>

#### 1827 **4.10 Chemical aging modifies the interaction of water vapor with mineral dust** 1828 **particles: results from field measurements**

1829 As summarized in previous sections, numerous laboratory studies have suggested that atmospheric  
1830 heterogeneous reactions could substantially increase the water adsorption ability, hygroscopicity,  
1831 and CCN activity of mineral dust particles. Very frequently tropospheric dust aerosol particles  
1832 have been observed to be internally mixed with nitrate, sulfate, chloride, and organic  
1833 compounds.<sup>158,159,162,202,206,419-425</sup> <sup>158,159,162,202,206,419-425</sup> More importantly, the effect of atmospheric  
1834 aging processes has also been supported by increasing evidence from field measurements. Instead  
1835 of providing an exhaustive literature survey, here we highlight some important findings from field  
1836 measurements to provide evidence if atmospheric chemical transformation could influence the  
1837 interaction of mineral dust particles with water vapor. Tables 12 summarizes the major findings of  
1838 field studies which are discussed in the section. A recent review paper by Li et al.<sup>426</sup> summarized

- 1839 single particle studies on the changes in chemical compositions, morphology, and hygroscopicity  
1840 of aerosol particles (including mineral dust) collected in East Asia.

1841 **Table 12.** Field measurements of water adsorption, hygrsoscopicity, and CCN activity of mineral dust aerosol particles: summary of major findings  
 1842 from previous studied included in this review.

reference	Location	major findings
Perry et al., 2004 <sup>427</sup>	Trinidad Head, California, USA	Elemental (Al, Si, and Fe) mass distributions all shifted toward smaller sizes as RH was reduced, indicating that mineral dust particles transported from Asia to the west coast of the United States is somewhat more hygroscopic upon its arrival.
Laskin et al., 2005 <sup>245</sup>	Shoresh, Israel	In agreement with laboratory studies, it was shown that solid nonspherical calcium carbonate particles were converted to spherical liquid droplets which contain Ca(NO <sub>3</sub> ) <sub>2</sub> , due to heterogeneous reactions with HNO <sub>3</sub> .
Matsuki et al., 2005 <sup>159</sup>	Beijing, China	Some Ca-rich dust particle are spherical under humid conditions, due to the formation of nitrate and sulfate on these particles.
Massling et al. 2007 <sup>428</sup>	off the coasts of Japan, Korea, and China	For all continentally influenced air masses, 1 μm particles can be classified as two groups according to their hygroscopic growth factors at 90% RH: one with growth factors of around 1.0 (representative of dust particles) and the other one with a growth factors of ~2 (representative of sea spray particles).
Shi et al., 2008 <sup>429</sup>	southwestern Japan	Nitrate free dust particle, even though they may contain sulfate, did not change their morphology when RH was increased from 15% to 90%; however, dust particles containing nitrate became aqueous droplets even at 15% RH.
Crumeyroille et al., 2008 <sup>430</sup>	Banizoumbou, Niger	Cloud processing during a mesoscale convective system may enhance the formation of soluble materials associated with dust particles and therefore enhance their CCN activity.
Tobo et al., 2009, <sup>431</sup> Tobo et al., 2010 <sup>432</sup>	Kanazawa, Japan	Some Ca-rich particles contain substantial amount of chloride, and they existed in an amorphous state and were nearly spherical even under high vacuum.

---

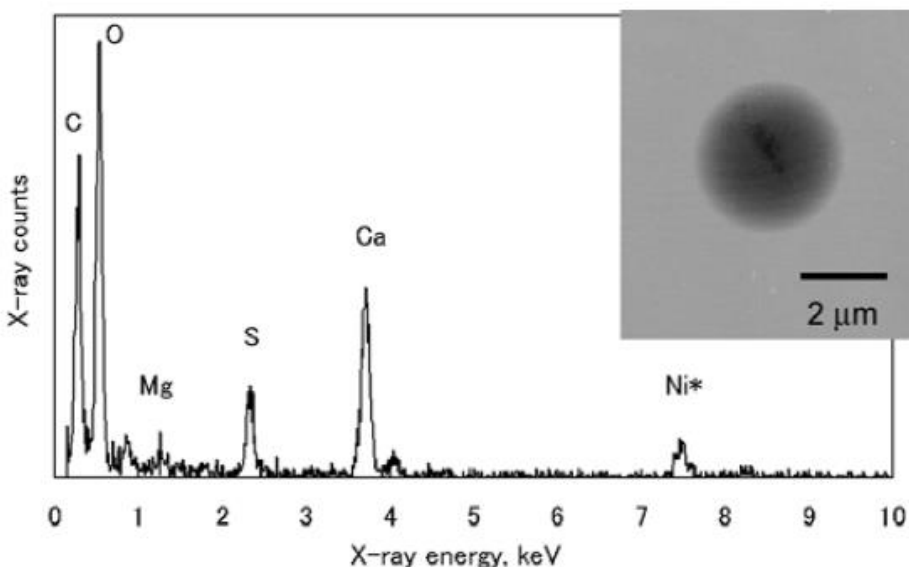
Kim and Park, 2012 <sup>433</sup>	Gwangju, Korea	Dust aerosol particles transported to Korea exhibited enhanced hygroscopicity, compared to fresh aluminum silicate and calcium carbonate.
Begue et al., 2015 <sup>267</sup>	Cabauw, Netherlands	CCN activities of Saharan dust aerosol particles transported to Netherlands were significantly increased due to heterogeneous reactions with anthropogenic pollutants.
Denjean et al., 2015 <sup>434</sup>	Fajardo, Puerto Rico	Supermicron African dust particles, after being transported across the Atlantic in summertime, were largely unprocessed and did not show significant change in hygroscopic properties.

---

1843

1844

1845 Laskin et al.<sup>245</sup> collected mineral dust particles at Shoresh, Israel, and analyzed the morphology  
1846 and composition of individual dust particles using scanning electron microscopy with energy  
1847 dispersive analysis of X-ray (SEM-EDX). For the first time, they <sup>245</sup> provided field evidence that  
1848 due to heterogeneous reactions with HNO<sub>3</sub>, solid nonspherical calcium carbonate particles were  
1849 converted to spherical liquid droplets which contain Ca(NO<sub>3</sub>)<sub>2</sub>. This important finding has been  
1850 supported by a number of following studies. For example, Matsuki et al.<sup>159</sup> collected Asian dust  
1851 particles (>1 μm) in Beijing and analysed them using electron microscopy. As shown in Figure 34,  
1852 Matsuki et al.<sup>159</sup> found that some Ca-rich dust particle are spherical under humid conditions, due  
1853 to the formation of nitrate and sulfate on these particles.



1854  
1855 **Figure 34.** Electron micrograph and X-ray spectrum of a typical Ca-rich spherical particle collected in the  
1856 boundary layer in Beijing. The signal of Ni in the X-ray spectrum was caused by the Ni-containing grids  
1857 used to support the films on which particles were collected. Reprinted with permission from ref 159.  
1858 Copyright 2005 John Wiley & Sons, Inc.

1859  
1860 Asian dust particles (>1 μm) were also collected in Southwestern Japan after long-range transport  
1861 and analyzed with environmental scanning electron microscopy.<sup>429</sup> It was found that nitrate free

1862 dust particle, even though they may contain sulfate, did not change their morphology when RH  
1863 was increased from 15% to 90%;<sup>429</sup> in contrast, dust particles containing nitrate became aqueous  
1864 droplets even at 15% RH.<sup>429</sup> This suggested that the formation of nitrate coating could substantially  
1865 increase the hygroscopicity of dust particles, whereas the formation of sulfate did not.<sup>429</sup> This  
1866 observation can be explained by the fact that  $\text{Ca}(\text{NO}_3)_2$  is more hygroscopic than  $\text{CaSO}_4$ .<sup>217,357</sup>

1867  
1868 Tobo et al.<sup>431,432</sup> collected Asian dust particles around Japan Islands and analyzed them by SEM-  
1869 EDX. They<sup>432</sup> found that substantial amount of chloride was found on Ca-rich particles, and these  
1870 particles existed in an amorphous state and were nearly spherical even under high vacuum.  
1871 Consequently, Tobo et al.<sup>432</sup> proposed that in remote marine troposphere where the concentrations  
1872 of reactive nitrogen species are typically very low, heterogeneous reactions with HCl can also  
1873 significantly change the composition and thus hygroscopicity of dust particles.

1874  
1875 In another study, Asian dust particles were collected in Trinidad Head (California, USA) after  
1876 long-range transport during three significant dust episodes.<sup>427</sup> Two impactors were used in parallel,  
1877 one maintained at ambient RH and the other one maintained at a lower RH of 55%.<sup>427</sup> Elemental  
1878 analysis of collected samples using synchrotron X-ray fluorescence suggested that the elemental  
1879 (Al, Si, and Fe) mass distributions all shifted toward smaller sizes as the RH was reduced.<sup>427</sup> This  
1880 may indicate that mineral dust particles transported from Asia to the west coast of the United States  
1881 is somewhat more hygroscopic upon its arrival, and it was tentatively attributed to the formation  
1882 of sulfate coatings on dust particles.<sup>427</sup>

1883  
1884 Most of studies which investigated the hygroscopicity of ambient dust particles require collection  
1885 of dust particles followed by offline analysis. In an airborne field campaign in West African,  
1886 aerosol properties in a layer between 1300 and 3000 m were measured during the passage of a



1887 mesoscale convective system (MCS).<sup>430</sup> After passage of the MCS, a significant increase in CCN  
1888 fraction was observed together with higher contribution of sulfate, nitrate, and chloride to the total  
1889 aerosol mass.<sup>430</sup> A mesoscale model was used to interpret the results, and it was concluded that  
1890 cloud processing during the MCS could enhance the formation of soluble materials associated with  
1891 dust particles and therefore enhance their CCN activity.<sup>430</sup> In another study, Kim and Park<sup>433</sup>  
1892 measured the hygroscopicity of Asian dust aerosol particles using a system similar to H-TDMA.  
1893 They<sup>433</sup> found that dust aerosol particles transported to Korea exhibited enhanced hygroscopicity  
1894 compared to fresh aluminum silicate and calcium carbonate, due to heterogeneous reactions and  
1895 cloud processing. More recently, it is suggested that the CCN activity of Saharan dust aerosol  
1896 particles transported to Netherlands were significantly increased due to heterogeneous reactions  
1897 with anthropogenic pollutants.<sup>267</sup>

1898

1899 However, not all the field measurements conclude that after long-range transport in the troposphere,  
1900 the hygroscopicity of mineral dust aerosol particles will be significantly enhanced. Massling et  
1901 al.<sup>428</sup> measured the hygroscopic growth of 1  $\mu\text{m}$  (dry diameter) particles off the coasts of Japan,  
1902 Korea, and China in spring 2001 during the ACE-Asia study. It is found that for all continentally  
1903 influenced air masses, 1  $\mu\text{m}$  particles can be classified as two groups according to their hygroscopic  
1904 growth factors at 90% RH: one with growth factors of around 1.0 and the other one with a growth  
1905 factors of  $\sim 2$ .<sup>19,428 435,436</sup> The first one was suggested to be representative of dust particles, and the  
1906 second one appears to be similar to sea spray particles.<sup>437</sup> This study may indicate that the change  
1907 in hygroscopicity of Asian dust particles after long-range transport can be very small, though lack  
1908 of particle composition measurements makes it difficult to draw more convincing conclusions. A  
1909 recent field campaign in Fajardo, Puerto Rico found that supermicron African dust particles, after  
1910 being transported across the Atlantic in summertime, did not show significant change in  
1911 hygroscopic properties.<sup>434</sup> Measurements of chemical composition suggest that most of mineral

1912 dust was chemically unprocessed and externally mixed, and only a minor portion of mineral dust  
1913 was internally mixed with sulfate and/or chloride.<sup>434</sup> In addition, Kaaden et al.<sup>438</sup> measured the  
1914 hygroscopic growth of aerosol particles at Tinfou, Morocco, and found that particles larger than  
1915 720 nm were completely hydrophobic. The hygroscopic growth of aerosol particles at Cape Verde  
1916 was investigated by Schladitz et al.,<sup>439</sup> who found that the  $\kappa$  value was almost 0 for particles with  
1917 volume equivalent diameters of >250 nm. Both studies<sup>438,439</sup> seem to suggest that Saharan dust  
1918 particles they detected are largely hydrophobic; nevertheless, both measurements are very close to  
1919 source regions and therefore it is highly likely that those dust particles have not aged much in the  
1920 atmosphere and may not have been exposed very much to acidic gases.

1921  
1922 Discrepancies reported by the aforementioned field measurements of hygroscopicity of mineral  
1923 dust particles may be due to their different exposure histories (and thus the effective aging extents)  
1924 and their variations in mineralogy. Several single particle studies<sup>159,245,429,432,440</sup> seem to indicate  
1925 that the major components of hygroscopic aged dust particles could be carbonates (e.g., calcite and  
1926 dolomite), which can undergo rapid reactions with acidic trace gases, leading to the formation of  
1927 very hygroscopic salts, such as  $\text{Ca}(\text{NO}_3)_2$  and  $\text{CaCl}_2$ . The only solid conclusion which can be  
1928 drawn up to now is that some dust particles can be converted to aqueous droplets after long-range  
1929 transport, but it is still unclear to which extent the hygroscopicity distribution of mineral dust  
1930 aerosol particles will change during their residence time in the troposphere. In addition, there will  
1931 be a very strong dependence on the mineralogy as noted above.

## 1932 **4.11 Summary**

### 1933 **4.11.1 Fresh dust particles**

1934 Table 13 summarizes CCN activity, as represented by  $\kappa$ , of  $\text{CaCO}_3$ , ATD, illite, kaolinite,  
1935 montmorillonite, and African and Asian dust particles reported in previous studies. Only studies  
1936 using dry-generated aerosol particles are included, because wet-generation may enhance the CCN

1937 activity of dust particles.<sup>49,256,259,262,263</sup> In order for simple and direct comparison, CCN activity  
 1938 measurements interpreted using the FHH adsorption activation theory are not included, but they  
 1939 have been discussed in previous subsections. Garimella et al.<sup>259</sup> provided an intercomparison of  
 1940 measured critical super-saturations as a function of particles diameter for several types of dry-  
 1941 generated mineral dust particles. H-TDMA measurements have also been used to derive  $\kappa$ ;  
 1942 however, these measurements can be significantly influenced by the non-sphericity of dust  
 1943 particles. Therefore, Table 13 does not include H-TDMA measurements.

1944

1945 **Table 13.** Summary of single hygroscopicity parameter ( $\kappa$ ) of CaCO<sub>3</sub>, ATD, illite, kaolinite,  
 1946 montmorillonite, and African and Asian dust particles reported in previous studies. Only studies in which  
 1947 the CCN activity of dry-generated mineral aerosol particles were measured are included.

mineral	reported $\kappa$	reference
CaCO <sub>3</sub>	0.0008-0.0018	Sullivan et al., 2010 <sup>256</sup>
	0.0019±0.0007	Zhao et al., 2010 <sup>264</sup>
	0.0013-0.0033	Tang et al., 2015 <sup>357</sup>
ATD	~0.025	Koehler et al., 2009 <sup>46</sup>
	~0.003	Herich et al., 2009 <sup>49</sup>
	0.002	Sullivan et al., 2010 <sup>261</sup>
	0.0042	Sullivan et al., 2010 <sup>375</sup>
	0.017	Yamashita et al., 2011 <sup>376</sup>
	0.0041	Garimella et al., 2014 <sup>259</sup>
illite	0.002-0.003	Herich et al., 2009 <sup>49</sup>
	0.0072	Garimella et al., 2014 <sup>259</sup>
kaolinite	~0.001	Herich et al., 2009 <sup>49</sup>
montmorillonite	~0.003	Herich et al., 2009 <sup>49</sup>
	0.0088	Garimella et al., 2014 <sup>259</sup>
North African dust	0.01-0.08	Koehler et al., 2009 <sup>46</sup>

Saharan dust	0.023	Herich et al., 2009 <sup>49</sup>
Chinese dust	0.007	Herich et al., 2009 <sup>49</sup>
Asian dust	0.014	Yamashita et al., 2011 <sup>376</sup>

1948

1949  $\kappa$  values given in Table 13 reveal that there is fairly good agreement between previous studies. It  
 1950 appears that the CCN activity of CaCO<sub>3</sub>, ATD, illite, kaolinite, and montmorillonite particles is  
 1951 very low and can be described with a  $\kappa$  value of less than 0.01. Authentic dust samples collected  
 1952 in Africa and Asia show somehow slightly higher  $\kappa$  value, probably because those samples contain  
 1953 more soluble components which increase their CCN activity.

1954

1955 In this section, we have compared measurements carried out under sub-saturation conditions using  
 1956 particles supported on substrates and those using aerosol particles performed under sub- and super-  
 1957 saturations conditions. Despite experimental and theoretical issues which can make such  
 1958 comparisons difficult (as discussed in Sections 2-3), reasonably good agreement has been found  
 1959 for CaCO<sub>3</sub>, SiO<sub>2</sub>, TiO<sub>2</sub>, Al<sub>2</sub>O<sub>3</sub>, and Fe<sub>2</sub>O<sub>3</sub>. On the other hand, as discussed in Sections 4.2-4.5,  
 1960 large discrepancies exist between studies using aerosol particles and those using particles  
 1961 supported on substrates for ATD, illite, kaolinite, and montmorillonite, and surface coverages of  
 1962 adsorbed water interpreted from measurements using aerosol particles are much lower. Even  
 1963 among studies which used very similar sample preparation methods and experimental techniques,  
 1964 significant disagreement are also observed for some clay minerals, with illite as an example shown  
 1965 in Figure 18b.

1966

1967 In experiments in which particles were supported on substrates, normally a slurry of dust particles  
 1968 in a solvent (e.g., water, methanol, or ethanol) was deposited on the supporting substrates to form  
 1969 a film. We speculate that though this type of sample preparation methods may not lead to

1970 substantial change in physicochemical properties for relative simple minerals such as  $\text{Al}_2\text{O}_3$  and  
1971  $\text{SiO}_2$ , it has the potential to cause some artifacts for clays and authentic dust samples. The effects  
1972 of different sample preparation methods needs to be carefully and systematically examined in  
1973 future studies.

1974

1975 The interactions of mineral dust particles with water vapor at temperatures above the onset of ice  
1976 nucleation can influence their heterogeneous reactivity, hygroscopic growth, and CCN activity;  
1977 therefore, a better understanding of these interactions is very important. Efforts are required to  
1978 reduce the existing large discrepancies among different studies. In a well-coordinated  
1979 collaboration, same mineral dust samples can be distributed to different groups which may use a  
1980 variety of experimental techniques to study their interactions with water vapor, and reported results  
1981 can be directly compared in order to find out the advantages and limitations of different experiment  
1982 techniques. Very recently a similar campaign has been successfully carried out to investigate the  
1983 ice nucleation activity of illite particles,<sup>441</sup> and similar actions will also definitely be beneficial for  
1984 investigation of water adsorption, hygroscopicity, and CCN activity of mineral dust particles.

1985

1986 Compared to the  $\kappa$ -Köhler theory, the FHH theory is less used to interpret the hygroscopic growth  
1987 and CCN activity of mineral dust particles. The two FHH parameters ( $A_{\text{FHH}}$  and  $B_{\text{FHH}}$ ) reported for  
1988 mineral dust particles, are compiled in Table 14. Direct comparison of hygroscopicity or CCN  
1989 activity from the two FHH parameters is difficult, and interested readers can calculate the surface  
1990 coverage of adsorbed water as a function of RH, using Eqs. (10) or (20).

1991 **Table 14.** Summary of  $A_{FHH}$  and  $B_{FHH}$  parameteres of mineral dust particles reported in the literature.

mineral	sample preparation method	$A_{FHH}$	$B_{FHH}$	reference
CaCO <sub>3</sub>	dry-generated aerosol particles	3.00±0.04	1.30±0.03	Kumar et al., 2011 <sup>262</sup>
	wet-generated aerosol particles	1.74	1.22	Kumar et al., 2011 <sup>263</sup>
ATD	dry-generated aerosol particles	2.96±0.03	1.28±0.03	Kumar et al., 2011 <sup>262</sup>
illite	dry-generated aerosol particles	1.02±0.38	1.12±0.04	Kumar et al., 2011 <sup>262</sup>
	wet-generated aerosol particles	3.00	1.27	Kumar et al., 2011 <sup>263</sup>
	particles supported on substrates	75±17	1.77±0.11	Hatch et al., 2014 <sup>348</sup>
kaolinite	particles supported on substrates	1.70	2.25	Hung et al., 2015 <sup>270</sup>
montmorillonite	dry-generated aerosol particles <sup>a</sup>	2.06±0.72	1.23±0.04	Kumar et al., 2011 <sup>262</sup>
	dry-generated aerosol particles <sup>b</sup>	1.23±0.31	1.08±0.03	Kumar et al., 2011 <sup>262</sup>
	wet-generated aerosol particles <sup>a</sup>	1.09	1.04	Kumar et al., 2011 <sup>263</sup>
	wet-generated aerosol particles <sup>b</sup>	0.87	1.00	Kumar et al., 2011 <sup>263</sup>
	particles supported on substrates	98±22	1.79±0.11	Hatch et al., 2014 <sup>348</sup>
	particles supported on substrates	1.25	1.33	Hung et al., 2015 <sup>270</sup>
SiO <sub>2</sub>	dry-generated aerosol particles	2.95±0.05	1.36±0.03	Kumar et al., 2011 <sup>262</sup>

1992

1993 <sup>a</sup>: Ca-montmorillonite; <sup>b</sup>: Na-montmorillonite

1994 It is noteworthy that most of the previous measurements have only been performed at around room  
1995 temperature, near 295 K. However, the relevant temperatures in the troposphere range  
1996 approximately from 200 to 300 K, and mineral dust particles mainly exist in the free troposphere  
1997 where the temperature is much lower than room temperature. Therefore, the effects of temperature  
1998 on the water adsorption, hygroscopicity, and CCN activity of mineral dust particles, which have  
1999 been seldom examined, deserve further investigation.

#### 2000 **4.11.2 Aged dust particles**

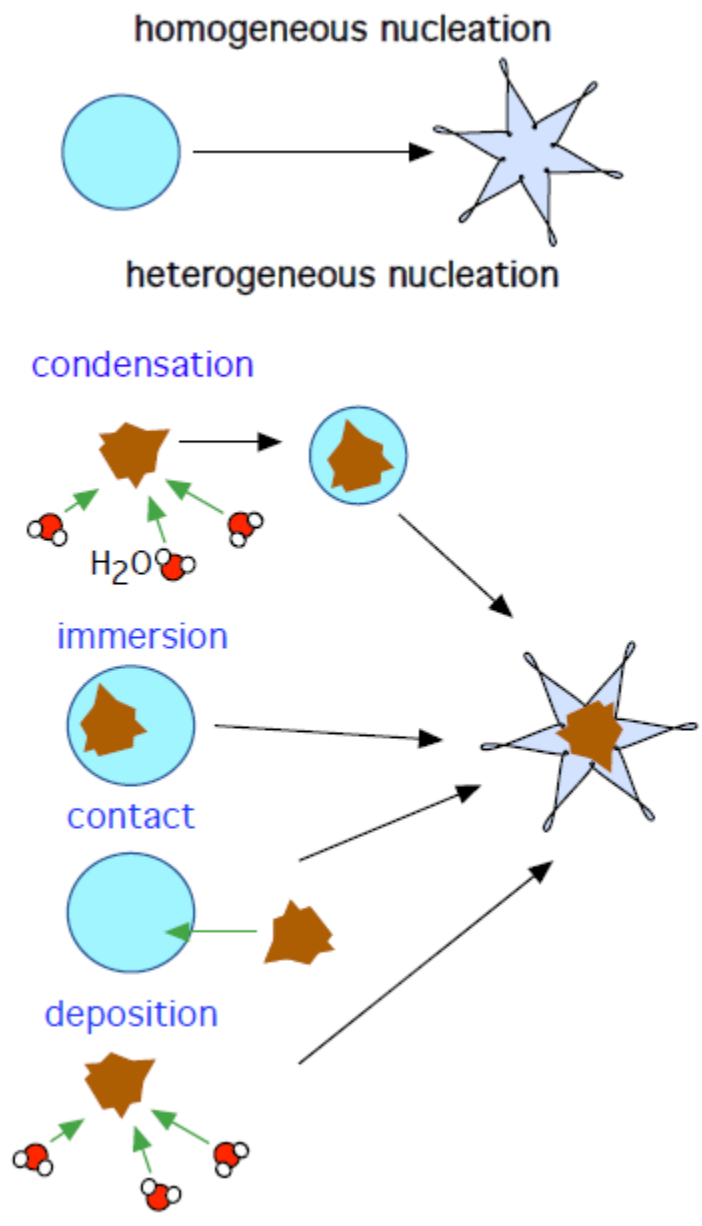
2001 Due to numerous studies over the last 1-2 decades, it is widely recognized that heterogeneous  
2002 reactions, mostly through the formation of more soluble materials (although sometimes insoluble  
2003 compounds can also be formed), can lead to significant enhancement of water adsorption,  
2004 hygroscopicity, and CCN activity of mineral dust particles. Nevertheless, most of previous studies  
2005 are either rather qualitative or their direct atmospheric relevance is lacking. Further research, which  
2006 are carried out at atmospherically relevant conditions to quantitatively understand the effects of  
2007 atmospheric chemical transformation, will be very helpful.

2008  
2009 Most of previous studies on the atmospheric aging effects focuses on  $\text{CaCO}_3$ , probably the most  
2010 reactive mineral contained by tropospheric dust aerosol particles. It is recommended that future  
2011 studies should also examine the effect of aging processes for more abundant clay minerals and  
2012 authentic dust samples which have more direct relevance for tropospheric dust aerosol particles.

### 2013 **5 Effects of chemical aging on ice nucleation activity of mineral dust particles**

2014 The formation of ice crystals in clouds is of particular scientific interest, because more than 50%  
2015 of the global precipitation is initiated via the ice phase.<sup>442</sup> Ice formation may occur in clouds  
2016 through both homogeneous and heterogeneous ice nucleation. Different ice nucleation  
2017 mechanisms are depicted in Figure 35.<sup>443</sup> Homogeneous ice nucleation requires the temperature to  
2018 be lower than  $-36\text{ }^\circ\text{C}$ ,<sup>167,444</sup> while heterogeneous ice nucleation can occur at higher

2019 temperature.<sup>167,445,446</sup> Heterogeneous ice nucleation can be classified into four modes:<sup>167</sup> 1)  
2020 deposition nucleation, which occurs on particles in the absence of the formation of liquid water  
2021 (below water saturation); 2 and 3) condensation freezing and immersion freezing: ice formation  
2022 occurs either during the simultaneous action of IN as CCN (condensation freezing) or during the  
2023 subsequent lifting and cooling of cloud droplets containing insoluble particles (immersion  
2024 freezing), 4) contact freezing, which occurs via collisions of particles with supercooled cloud  
2025 droplets.



2026  
2027

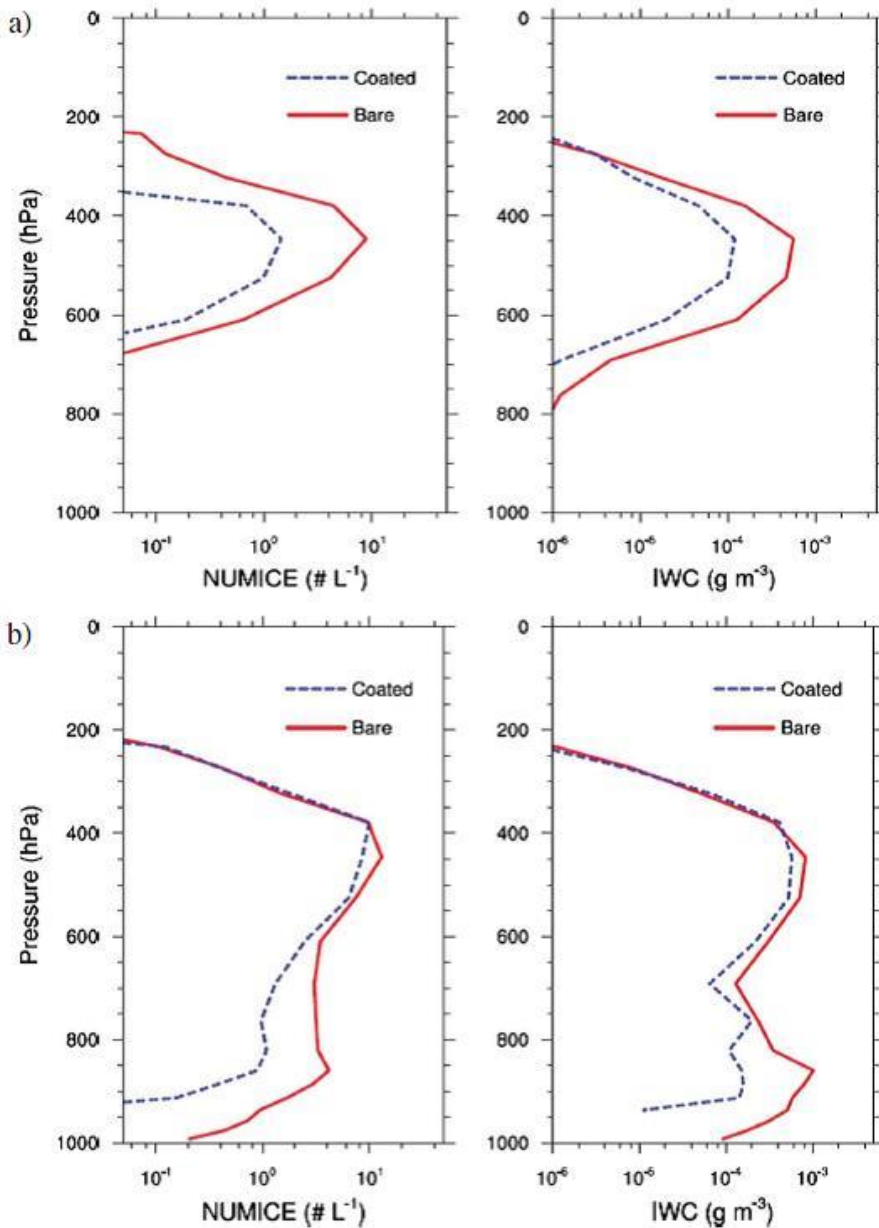


2028 **Figure 35.** Illustration of homogeneous nucleation and heterogeneous nucleation mechanisms.  
2029 Heterogeneous nucleation can occur via deposition nucleation, condensation freezing, immersion freezing,  
2030 and contact freezing. Reprinted with permission from ref 443 by Freedman. Copyright 2011 American  
2031 Chemical Society.

2032  
2033 Mineral dust particles may be the most abundant IN in the troposphere,<sup>58,74,75</sup> and the ice nucleation  
2034 activity of fresh mineral dust particles (and also other types of aerosol particles) has been recently  
2035 discussed in several excellent review papers.<sup>140,167,237,238,447,448</sup> In the last several years, numerous  
2036 laboratory studies have suggested that atmospheric aging processes can substantially change the  
2037 ice nucleation activity of mineral dust particles, as will be discussed here. Hoose and Möhler<sup>238</sup>  
2038 briefly summarized the effect of atmospheric chemical reactions on the IN activity of mineral dust  
2039 particles and below we expand on this discussion.

2040  
2041 The impacts of change in IN activity due to atmospheric aging processes have been supported by  
2042 several modeling studies. For example, using parameterizations based on their laboratory  
2043 measurements, Kulkarni et al.<sup>449</sup> simulated the influence of particle coatings on the ice crystal  
2044 number concentration and the ice water content in clouds over the Southern Great Plain (SGP) site  
2045 near Lamont, Oklahoma, USA. As shown in Figure 36a, under water sub-saturation conditions  
2046 where only deposition nucleation is possible, the modeled monthly mean ice crystal number for  
2047 the coated case (aged dust particles) was about one order of magnitude lower than the uncoated  
2048 case (fresh dust particles).<sup>449</sup> Under water super-saturation conditions (Figure 36b), both the  
2049 simulated ice crystal number and ice water content are higher in the uncoated case than in the  
2050 coated case;<sup>449</sup> the difference between them in regions with pressure <600 hPa is significantly  
2051 smaller,<sup>449</sup> and this is partly due to that the difference between the IN activity of uncoated and  
2052 coated dust particles (illite in this case) is smaller at lower temperatures.<sup>449</sup> Girard et al.<sup>450</sup> used the

2053 Global Multiscale Environmental Model to assess the potential influence of acid coatings on cloud  
2054 and radiation processes in the Arctic during January and February 2007. Their modeling results<sup>450</sup>  
2055 suggest that acid coating on dust particles may have significant impacts on cloud microphysics  
2056 and radiation over the Central Arctic. More specifically, modification in the cloud microstructures,  
2057 due to acid coating, could change the radiation at the top of the atmosphere by 0 and  $-6 \text{ W m}^{-2}$  over  
2058 the region which is covered by the Arctic air masses.<sup>450</sup>



2059

2060 **Figure 36.** Modeled monthly mean profiles of the ice crystal number concentration (NUMICE) and ice  
2061 water content (IWC) over the SGP site in (a) deposition ice nucleation mode and (b)  
2062 condensation/immersion freezing mode. Reprinted with permission from ref 449. Copyright 2014 John  
2063 Wiley & Sons, Inc.

2064  
2065 In this section, we have taken a comprehensive approach to review laboratory studies on the  
2066 potential effects of atmospheric aging processes on the IN activity of mineral dust particles. This  
2067 section is divided into several subsections, according to the types of coatings formed on dust  
2068 particles and/or the trace gases used to react with dust particles to form these coatings.

### 2069 **5.1 Sulfate coating and exposure to SO<sub>2</sub>**

2070 Table 15 summarizes previous laboratory studies which investigated the effects of sulfate coating  
2071 and reaction with SO<sub>2</sub> on the IN activity of mineral dust particles. Previous studies were mainly  
2072 focused the influence of H<sub>2</sub>SO<sub>4</sub> and (NH<sub>4</sub>)<sub>2</sub>SO<sub>4</sub> coating on the IN activity of mineral dust particles,  
2073 and only one study<sup>451</sup> explored the impact due to the heterogeneous reaction with SO<sub>2</sub>.

2074

2075 **Table 15.** Summary of laboratory studies on the effects of chemical aging processes on the IN activity of mineral dust particles: sulfate coatings and  
 2076 reaction with SO<sub>2</sub>

coating or trace gases used to form coating	mineral dust	ice nucleation mode	references	major finding
H <sub>2</sub> SO <sub>4</sub>	aluminum oxide, alumina-silicate, iron oxide	deposition	Archuleta et al. <sup>452</sup>	H <sub>2</sub> SO <sub>4</sub> coating largely reduced the IN activity of alumina-silicate particles, had no significant impact for aluminium oxide particles, and may increase the IN activity of iron oxides.
	ATD	deposition	Knopf and Koop <sup>453</sup>	No significant difference in IN activity was observed between fresh and H <sub>2</sub> SO <sub>4</sub> -coated ATD particles in the deposition nucleation mode.
	ATD, illite	deposition, immersion, condensation	Cziczo et al. <sup>219</sup>	H <sub>2</sub> SO <sub>4</sub> coating reduced the IN activity of ATD and illite particles, and the extent of reduction depended on the coating thickness.
	kaolinite	deposition	Eastwood et al. <sup>454</sup>	H <sub>2</sub> SO <sub>4</sub> coating reduced the IN activity of kaolinite particles in the deposition nucleation mode.
	illite, kaolinite, montmorillonite, quartz	deposition	Chernoff and Bertram <sup>455</sup>	H <sub>2</sub> SO <sub>4</sub> coating substantially reduced the IN activity of illite, kaolinite, montmorillonite, and quartz particles.

ATD	immersion	Niedermeier et al. <sup>456</sup>	H <sub>2</sub> SO <sub>4</sub> coatings could substantially reduce the IN activity of ATD particles in the immersion freezing mode.
ATD	deposition, immersion, condensation	Sullivan et al. <sup>261</sup>	H <sub>2</sub> SO <sub>4</sub> coatings always reduced the IN activity of ATD particles, and the extent of decrease was much larger in the deposition nucleation mode than in the immersion/condensation freezing modes.
ATD	immersion	Niedermeier et al. <sup>221</sup>	Exposure of H <sub>2</sub> SO <sub>4</sub> -coated ATD particles to water vapor resulted in further decrease in the IN activity.
kaolinite	deposition, immersion, condensation	Tobo et al. <sup>440</sup>	H <sub>2</sub> SO <sub>4</sub> coating reduced the IN activity of kaolinite particles in both deposition nucleation and immersion/condensation freezing modes.
kaolinite	deposition, immersion	Wex et al. <sup>457</sup>	For immersion freezing, H <sub>2</sub> SO <sub>4</sub> coating (with a thickness of a few nm or less) largely reduced the IN activity of Fluka kaolinite but did not lead to a significant change for CMS kaolinite. In the deposition nucleation mode, for both types of kaolinite particles, H <sub>2</sub> SO <sub>4</sub> coating led to a decrease in IN activity at RH <95% but an increase in IN activity for RH >95%.

	ATD, illite, deposition, montmorillonite, immersion, K-feldspar, condensation quartz	Kulkarni et al. <sup>449</sup>	H <sub>2</sub> SO <sub>4</sub> coating reduced the IN activity of all the dust particles in the deposition nucleation modes, but its effects were not observable in the immersion/condensation freezing modes.
	kaolinite, deposition montmorillonite	Sihvonen et al. <sup>458</sup>	Treatments of kaolinite and montmorillonite with H <sub>2</sub> SO <sub>4</sub> led to compositional and structural changes of the surfaces, causing reduction in IN activity in the deposition nucleation modes.
	feldspar, ATD, immersion illite, kaolinite	Augustin-Bauditz et al. <sup>459</sup>	H <sub>2</sub> SO <sub>4</sub> coating could reduce the IN activity (in the immersion freezing mode) of all the dust particles under investigation, and the largest effect was observed for feldspar.
(NH <sub>4</sub> ) <sub>2</sub> SO <sub>4</sub>	ATD, illite deposition, immersion, condensation	Cziczko et al. <sup>219</sup>	(NH <sub>4</sub> ) <sub>2</sub> SO <sub>4</sub> coatings could reduce the IN activity of ATD and illite particles, and the extent of reduction depended on the coating thickness.
	kaolinite deposition	Eastwood et al. <sup>454</sup>	(NH <sub>4</sub> ) <sub>2</sub> SO <sub>4</sub> coating reduced the IN activity of kaolinite particles in the deposition nucleation mode, though the effects appeared to be less significant compared to H <sub>2</sub> SO <sub>4</sub> .
	ATD immersion	Niedermeier et al. <sup>456</sup>	(NH <sub>4</sub> ) <sub>2</sub> SO <sub>4</sub> coatings could substantially reduce the IN activity of ATD particles in the immersion freezing mode. Compared to H <sub>2</sub> SO <sub>4</sub> , the effects of (NH <sub>4</sub> ) <sub>2</sub> SO <sub>4</sub> were more significant.

	ATD	deposition, immersion, condensation	Sullivan et al. <sup>261</sup>	In the immersion/condensation freezing modes, exposure of H <sub>2</sub> SO <sub>4</sub> -coated ATD particles to NH <sub>3</sub> would further suppress the IN activity.
	ATD	immersion	Niedermeier et al. <sup>221</sup>	Exposure of ATD particles to H <sub>2</sub> SO <sub>4</sub> followed by NH <sub>3</sub> led to a significant reduction in IN activity, compared to fresh particles.
NH <sub>4</sub> HSO <sub>4</sub>	illite, kaolinite, montmorillonite, quartz	deposition	Chernoff and Bertram <sup>455</sup>	NH <sub>4</sub> HSO <sub>4</sub> coatings substantially reduced the IN activity of illite, kaolinite, montmorillonite, and quartz particles, and the effects varied with temperature.
SO <sub>2</sub>	montmorillonite	deposition	Salam et al. <sup>451</sup>	After exposure to pure SO <sub>2</sub> for 2.5 h or 45 ppmv SO <sub>2</sub> for 70 h at ~0% RH, no significant change in IN activity in the deposition nucleation mode was observed for montmorillonite.

2078 **5.1.1 Sulfate coating**

2079 Archuleta et al.<sup>452</sup> measured the ice nucleation activity of fresh and H<sub>2</sub>SO<sub>4</sub>-coated submicron  
2080 aluminium oxides, alumina-silicate, and iron oxide particles under deposition nucleation mode  
2081 conditions between -60 and -45 °C, and found that H<sub>2</sub>SO<sub>4</sub> coating influenced the IN activity of  
2082 different minerals in different ways. For example, although the coating had no significant impact  
2083 for aluminium oxide particles, it largely reduced the IN activity of alumina-silicate particles.<sup>452</sup>  
2084 For iron oxides, H<sub>2</sub>SO<sub>4</sub> coatings statistically reduced the required RHi (relative humidity with  
2085 respect to ice) to freeze for iron oxides;<sup>452</sup> in other words, the H<sub>2</sub>SO<sub>4</sub> coating may increase the IN  
2086 activity of iron oxides.

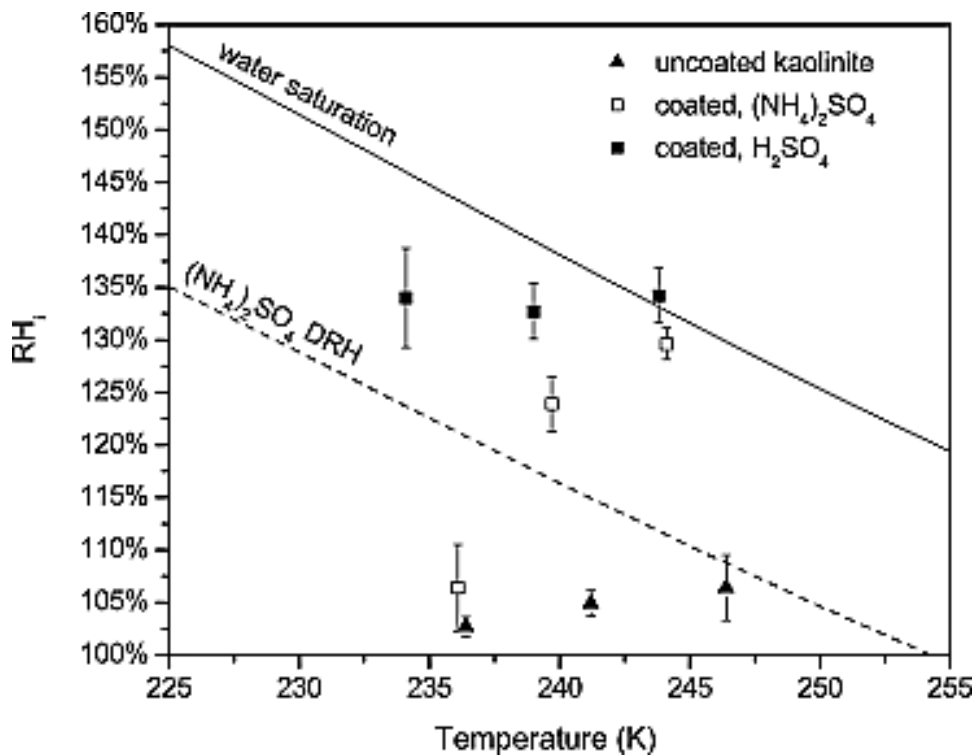
2087

2088 IN activity of fresh and coated ATD and illite aerosol particles were investigated in deposition  
2089 nucleation, immersion freezing, and condensation freezing modes by Cziczo et al.,<sup>219</sup> using the  
2090 Aerosol Interactions and Dynamics in the Atmosphere (AIDA) chamber in Karlsruhe, Germany.  
2091 It was found <sup>219</sup> that coating with H<sub>2</sub>SO<sub>4</sub> or (NH<sub>4</sub>)<sub>2</sub>SO<sub>4</sub> would largely reduce the IN activity of  
2092 ATD particles, and that the super-saturations required by freezing coated ATD particles often  
2093 approached those for homogeneous freezing of aqueous H<sub>2</sub>SO<sub>4</sub> and (NH<sub>4</sub>)<sub>2</sub>SO<sub>4</sub> solution alone.  
2094 Inhibition of ice nucleation by H<sub>2</sub>SO<sub>4</sub> and (NH<sub>4</sub>)<sub>2</sub>SO<sub>4</sub> coatings was also observed for illite particles,  
2095 though the effect was smaller compared to ATD particles.<sup>219</sup> In addition, they <sup>219</sup> observed that  
2096 dust particles coated with less material were activated earlier than those coated with more material,  
2097 suggesting that the amount of coating determines to which extent the IN activity of dust particles  
2098 is reduced. Another study by Niedermeier et al.<sup>456</sup> suggested that H<sub>2</sub>SO<sub>4</sub> and (NH<sub>4</sub>)<sub>2</sub>SO<sub>4</sub> both could  
2099 significantly reduce the IN activity of ATD particles in the immersion freezing mode (233.15-  
2100 239.15 K), and the effect of (NH<sub>4</sub>)<sub>2</sub>SO<sub>4</sub> coating is more significant than H<sub>2</sub>SO<sub>4</sub>. In contrast, an  
2101 earlier study by Knopf and Koop <sup>453</sup> did not observe significant difference in the ice nucleation  
2102 ability between fresh and H<sub>2</sub>SO<sub>4</sub>-coated ATD particles in the deposition nucleation mode.



2103

2104 Eastwood et al.<sup>454</sup> investigated the deposition nucleation properties (represented by ice nucleation  
2105 onset conditions, defined as the RH<sub>i</sub> and temperature at which the first ice nucleation event was  
2106 observed) of fresh and coated kaolinite particles over 233-246 K. As shown in Figure 37, it was  
2107 found that H<sub>2</sub>SO<sub>4</sub> coatings drastically reduced the ice nucleating ability of kaolinite particles,  
2108 increasing the RH<sub>i</sub> required for ice nucleation by approximately 30% across the entire temperature  
2109 range they investigated.<sup>454</sup> On the other hand, the decrease of ice nucleation activity due to  
2110 (NH<sub>4</sub>)<sub>2</sub>SO<sub>4</sub> coating was much smaller at 245 K compared to that at 236 K.<sup>454</sup> Tobo et al.<sup>440</sup> also  
2111 suggested that H<sub>2</sub>SO<sub>4</sub> coating reduced the IN activity of kaolinite aerosol particles for both  
2112 deposition nucleation and immersion/condensation freezing modes for temperature between -34  
2113 to -26 °C.



2114

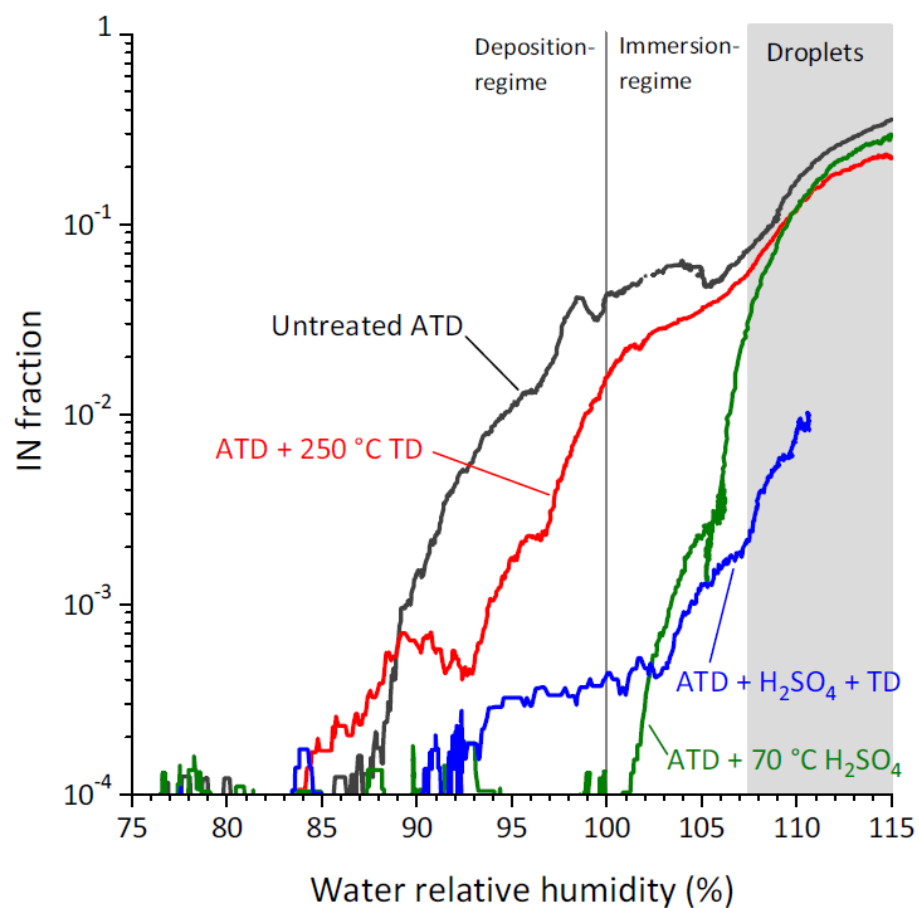
2115 **Figure 37.** Summary of ice nucleation onset conditions for uncoated, H<sub>2</sub>SO<sub>4</sub>-, and (NH<sub>4</sub>)<sub>2</sub>SO<sub>4</sub>-coated  
2116 kaolinite particles. The error bars represent 95% confidence intervals based on at least six measurements  
2117 per data point. Reprinted with permission from ref 454. Copyright 2009 John Wiley & Sons, Inc.

2118

2119 The effects of  $\text{H}_2\text{SO}_4$  and  $\text{NH}_4\text{HSO}_4$  coatings on the IN activity of several mineral dust particles  
2120 in the deposition nucleation mode from 234-247 K were examined by Chernoff and Bertram.<sup>455</sup>  
2121 They<sup>455</sup> found that  $\text{H}_2\text{SO}_4$  coatings increased the onset  $\text{RH}_i$  (and thus reduced the IN activity) by  
2122 ~30% for kaolinite and illite and ~20% for montmorillonite and quartz. Additionally, it was found  
2123 by Chernoff and Bertram<sup>455</sup> that  $\text{NH}_4\text{HSO}_4$  coatings also impair the IN activity of kaolinite  
2124 particles, increasing the onset  $\text{RH}_i$  by 18-26%, depending on the temperature under which the ice  
2125 nucleation occurred.

2126

2127 Sullivan et al.<sup>261</sup> investigated the change in ice nucleation properties of 300 nm ATD particles (in  
2128 both deposition nucleation and immersion/condensation freezing modes) after being exposure to  
2129  $\text{H}_2\text{SO}_4$  alone or  $\text{H}_2\text{SO}_4$  followed by  $\text{NH}_3$ , and some representative results are shown in Figure 38.  
2130 Several conclusions have been drawn by this study:<sup>261</sup> i) heating of ATD particles in a thermal  
2131 denuder up to 200 °C did not lead to significant change in their IN activity; ii)  $\text{H}_2\text{SO}_4$  coating  
2132 always reduced the IN activity of ATD, compared to fresh particles, and the extent of decrease is  
2133 much larger in the deposition nucleation mode than the immersion/condensation freezing modes;  
2134 iii) heating the  $\text{H}_2\text{SO}_4$ -coated ATD particles further decreased IN activity in the  
2135 immersion/condensation freezing mode, probably because heating may accelerate the reaction of  
2136 coated  $\text{H}_2\text{SO}_4$  with ATD particle surface; and iv) in the immersion/condensation freezing modes,  
2137 subsequent exposure of  $\text{H}_2\text{SO}_4$ -coated ATD particles to  $\text{NH}_3$  would further suppress the IN activity.



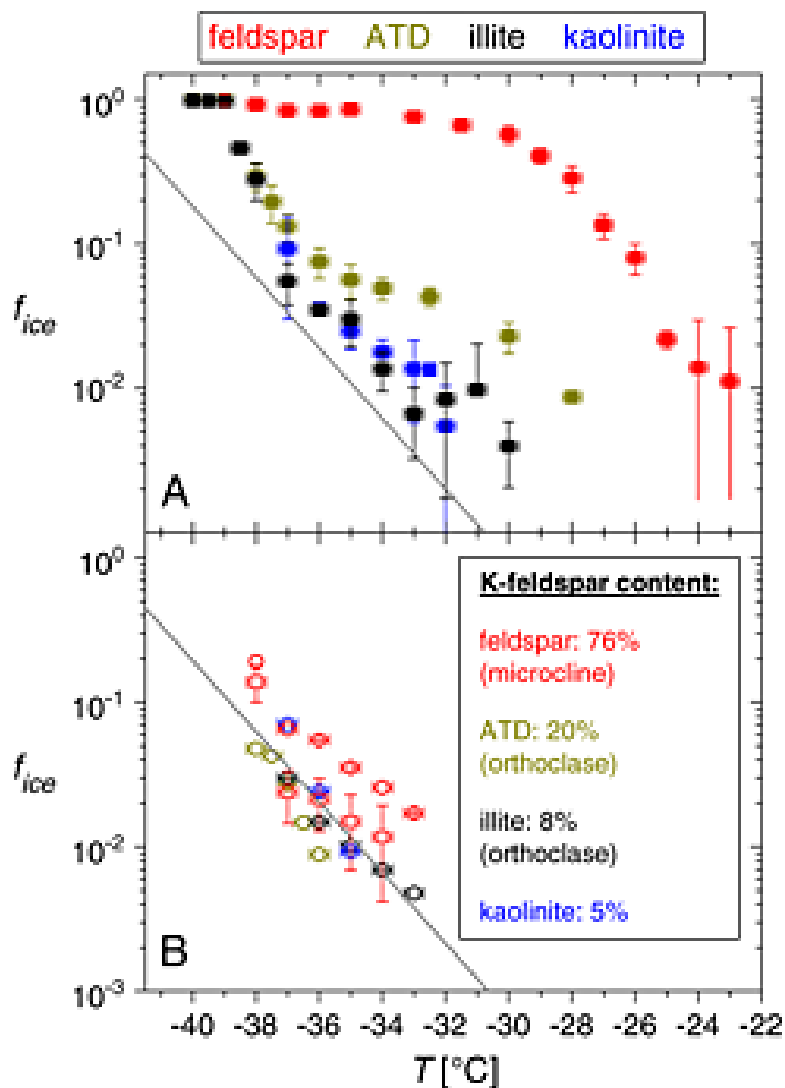
2138  
 2139 **Figure 38.** Measured fractions of 300 nm fresh and aged ATD particles which were activated to ice crystals  
 2140 at -30 °C as a function of RH. Black curve: untreated ATD; red curve: ATD heated in the thermodenuder  
 2141 (TD) at 250 °C; green curve: ATD coated with sulphuric acid; blue curve: ATD coated with sulfuric acid  
 2142 and then heated in the TD at 250 °C. In the region (RH >107%) covered by the grey box, measurements  
 2143 were not reliable because droplets could survive in the evaporation region (of the ice nuclei counter) and  
 2144 therefore could not be distinguished from ice crystals. Reprinted with permission from ref 261. Copyright  
 2145 2010 Copernicus Publications.

2146  
 2147 Using an Aerosol Mass Spectrometer and an Aerosol Time of Flight Mass Spectrometer, Reitz et  
 2148 al.<sup>220</sup> simultaneously measured the composition of H<sub>2</sub>SO<sub>4</sub>-coated ATD particles (the IN activity of  
 2149 which were studied by Sullivan et al.<sup>261</sup>), and found that condensation of H<sub>2</sub>SO<sub>4</sub> vapor onto ATD  
 2150 particles not only resulted in the formation of a H<sub>2</sub>SO<sub>4</sub> coating on the particle surface but also led

2151 to reactions which produced metal (including Na, K, Mg, Al, and etc.) sulfate, ammonium metal  
2152 sulfate, and ammonia sulfate on the surface. These surface modifications may be responsible for  
2153 that observed decrease in IN activity of ATD particles.<sup>220</sup> In the same campaign as Sullivan et al.<sup>261</sup>  
2154 and Reitz et al.,<sup>220</sup> Niedermeier et al.<sup>221</sup> found that additional exposure of H<sub>2</sub>SO<sub>4</sub>-coated ATD  
2155 particles to water vapor could further strongly reduce their IN activity, and this may be caused by  
2156 that the presence of water could accelerate the chemical reaction of H<sub>2</sub>SO<sub>4</sub> coating with particle  
2157 surface, leading to further depletion of ice nucleation active sites on the surface.

2158  
2159 Using the Leipzig Aerosol Cloud Interaction Simulator, Augustin-Bauditz et al.<sup>459</sup> measured the  
2160 IN activity of fresh (with mobility diameters of 300 nm) and H<sub>2</sub>SO<sub>4</sub>-coated dust particles in the  
2161 immersion freezing mode. As shown in Figure 39, H<sub>2</sub>SO<sub>4</sub> coating could reduce the IN activity of  
2162 all the dust particles (including feldspar, ATD, illite, and kaolinite) from around -38 °C to -32 °C,  
2163 and the largest suppression in IN activity was observed for feldspar particles.<sup>459</sup>

2164



2165  
 2166 **Figure 39.** Measured ice nucleation fractions of (a) uncoated particles and (b) particles coated with sulfuric  
 2167 acid (circles: coating at 70 °C; squares: coating at 80 °C). Reprinted with permission from ref 459. Copyright  
 2168 2014 John Wiley & Sons, Inc.  
 2169  
 2170 Sihvonen et al.<sup>458</sup> found that the treatment with H<sub>2</sub>SO<sub>4</sub> could cause reduction in IN activity for  
 2171 kaolinite and illite particles in the deposition nucleation mode. They<sup>458</sup> also used X-ray diffraction,  
 2172 TEM, and inductively coupled plasma-atomic emission spectroscopy to measure the physical and  
 2173 chemical changes of dust particle treated with H<sub>2</sub>SO<sub>4</sub>. Formation of new products and structural  
 2174 change of the surface were observed, both probably explaining the suppression of IN activities

2175 after treatment with H<sub>2</sub>SO<sub>4</sub>.<sup>458</sup> This study<sup>458</sup> shows the importance of post-analysis of modified  
2176 dust particles to better understand the impact of chemical processing on IN activity.

2177

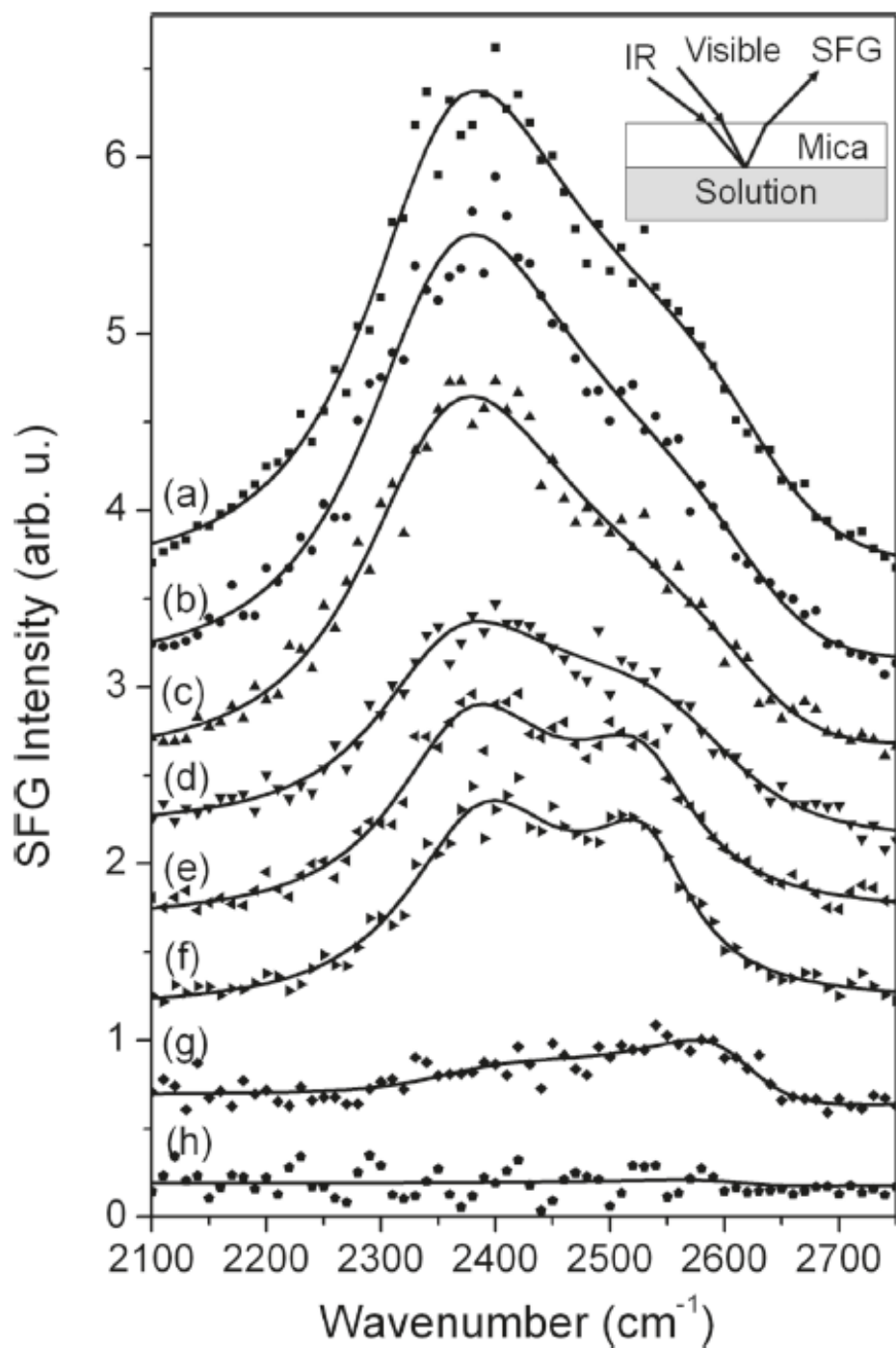
2178 Kulkarni et al.<sup>449</sup> studied the IN activity of 200 nm fresh and H<sub>2</sub>SO<sub>4</sub>-coated ATD, illite,  
2179 montmorillonite, K-feldspar, and quartz particles as a function of temperature (-35 to -25 °C) and  
2180 RH (75-110%). It was found<sup>449</sup> that H<sub>2</sub>SO<sub>4</sub> coating led to reduction in IN activity of all five  
2181 different types of dust particles in the deposition nucleation mode; nevertheless, its effect under  
2182 water-super-saturation conditions (i.e. in immersion/condensation freezing modes) was not  
2183 observable for any type of dust particles.<sup>449</sup> X-ray diffraction measurements showed that coating  
2184 dust particles with H<sub>2</sub>SO<sub>4</sub> changed the surface crystalline nature and resulted in surface structural  
2185 disorders.<sup>449</sup> Therefore, it was further concluded that the suppression of IN activity of dust particles  
2186 in the deposition freezing mode due to H<sub>2</sub>SO<sub>4</sub> coating was caused by the lack of structured order  
2187 of the surface after treatment with H<sub>2</sub>SO<sub>4</sub>.<sup>449</sup>

2188

2189 The effect of H<sub>2</sub>SO<sub>4</sub> (with a thickness of a few nm or less) on the IN activity of two different types  
2190 of kaolinite particles was investigated by Wex et al.<sup>457</sup> in the deposition nucleation and immersion  
2191 freezing mode. For immersion freezing, while H<sub>2</sub>SO<sub>4</sub> substantially reduced the IN activity of Fluka  
2192 kaolinite particles, it did not lead to significant change to Clay Mineral Society kaolinite.<sup>457</sup> The  
2193 following explanation was provided:<sup>457</sup> Fluka kaolinite contained K-feldspar which is very IN  
2194 active<sup>141</sup> but the other type of kaolinite did not, and H<sub>2</sub>SO<sub>4</sub> coating could efficiently react with K-  
2195 feldspar and thus largely reduce its IN activity. Under water sub-saturation conditions, H<sub>2</sub>SO<sub>4</sub>  
2196 coating suppressed the ice nucleation of kaolinite particles for RH <95% while a significant  
2197 increase in ice nucleation activity was observed for RH >95%.<sup>457</sup> For RH in the range of 95-100 %,   
2198 H<sub>2</sub>SO<sub>4</sub> coating kaolinite particles may become aqueous droplets with solid inclusion, and therefore  
2199 immersion freezing actually dominated over deposition freezing.<sup>457</sup>

2200

2201 Though many studies have shown that sulfate coating could significantly modify the IN activity  
2202 of mineral dust particles, fundamental understanding of deactivation mechanisms on the molecular  
2203 level is lacking. Yang et al.<sup>460</sup> explored why sulfuric acid coatings influence the IN activity of  
2204 mineral dust particles. They<sup>460</sup> probed the structure of water at the interface between mica (used  
2205 as a surrogate as dust particles) and aqueous D<sub>2</sub>SO<sub>4</sub> solutions of different concentrations using sum  
2206 frequency generation vibrational spectroscopy. In this study<sup>460</sup> deuterated water and sulfuric acid  
2207 were used to avoid the overlap with the IR absorption peak of mica at 3620 cm<sup>-1</sup>.<sup>461</sup> The spectra of  
2208 interfacial D<sub>2</sub>O molecules show two peaks at around 2375 and 2550 cm<sup>-1</sup>. These two peaks are  
2209 sometimes called the “ice-like” and the “liquid-like” peaks, because their peak positions are similar  
2210 to those of bulk ice and liquid water, respectively.<sup>286,462</sup> It is usually believed that the interfacial  
2211 water molecules observed by SFG are more ordered than those in the bulk because SFG is largely  
2212 depressed in a disordered medium.<sup>463</sup> As shown in Figure 40, Yang et al.<sup>460</sup> found that when the  
2213 concentration of D<sub>2</sub>SO<sub>4</sub> in the aqueous solution increased from 0 to 5 M, the two peaks at 2375  
2214 and 2550 cm<sup>-1</sup> both gradually disappeared.



2215  
 2216 **Figure 40.** SFG spectra of D<sub>2</sub>O/mica interfaces with D<sub>2</sub>SO<sub>4</sub> concentrations of (a) 0, (b)  $5 \times 10^{-6}$ , (c)  $5 \times 10^{-5}$ ,  
 2217 (d)  $5 \times 10^{-4}$ , (e) 0.005, (f) 0.05, (g) 0.5, and (h) 5 M. The inset shows the schematic layout of the  
 2218 spectroscopic setup. Reprinted with permission from ref 460. Copyright 2011 American Chemical Society.  
 2219



2220 The observation shown in Figure 40 is interpreted as the reduction of ordered water structures at  
2221 the interface with increasing D<sub>2</sub>SO<sub>4</sub> concentrations.<sup>460</sup> It was further suggested by Yang et al.<sup>460</sup>  
2222 that IN activity is correlated with the presence of structured water at the interface. The reduction  
2223 in ordered water structure was due to the combination of several factors,<sup>460</sup> including i) reduced  
2224 mica surface potential at low pH, ii) adsorption of sulfate on mica surface, iii) decrease of free  
2225 water molecules at higher H<sub>2</sub>SO<sub>4</sub> in the aqueous solution. Though it has provided fundamental  
2226 insights into the structure of the mineral-aqueous solution interface, the study by Yang et al.<sup>460</sup> was  
2227 carried at room temperature instead of those at which ice nucleation may occur.

2228  
2229 Very recently second harmonic generation spectroscopy has been used to monitor the mineral-  
2230 water interface during the occurrence of immersion freezing in an in-situ and online manner.<sup>464</sup>  
2231 Local ordering of water on the mica (which provides a good ice nucleating surface) was observed  
2232 by SFG during cooling down to the freezing point,<sup>464</sup> in contrast, no significant change in water  
2233 structure at sapphire (which is a poor ice nucleator) surface was observed during cooling.<sup>464</sup> This  
2234 is supported by a recent molecular dynamics simulation study,<sup>465</sup> suggesting that layering and  
2235 ordering of interfacial liquid water are critical to heterogeneous nucleation of ice. This novel  
2236 application developed by Abdelmonem et al.<sup>464</sup> has a great potential to help understand how  
2237 heterogeneous ice nucleation occurs in general and more specifically how chemical aging alters  
2238 the IN activity at the molecular level.

### 2239 **5.1.2 Exposure to SO<sub>2</sub>**

2240 To our knowledge only one previous study<sup>451</sup> explored the effect of SO<sub>2</sub> exposure on the IN  
2241 activity of mineral dust particles. No significant change in deposition ice nucleation efficiency was  
2242 observed for montmorillonite particles after being exposed to pure SO<sub>2</sub> for 2.5 h or 45 ppmv SO<sub>2</sub>  
2243 for 70 h at room temperature and ~0% RH.<sup>451</sup>

2244 **5.2 Organic coatings**

2245 Several previous studies have investigated how organic coatings can alter the IN activities of  
2246 mineral dust particles, and an overview of these studies is provided in Table 16.

2247

2248

2249 **Table 16.** Summary of laboratory studies on the effects of chemical aging processes on the IN activity of mineral dust particles: organic coatings,  
 2250 and reactions with HNO<sub>3</sub>, NH<sub>3</sub>, and O<sub>3</sub>.

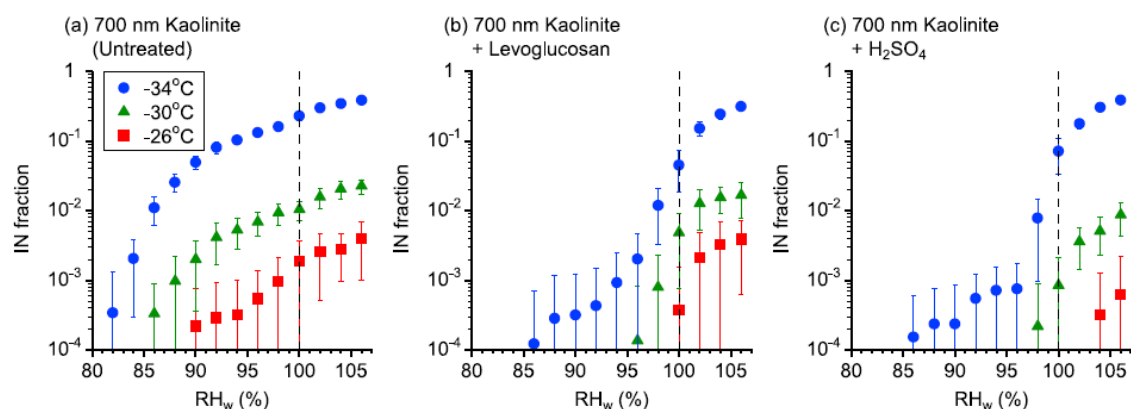
coating or trace gases used to form coating	mineral dust	ice nucleation mode	references	major finding
organic coating	ATD, kaolinite	deposition, immersion, condensation	Möhler et al. <sup>466</sup>	Organic coating formed by ozonolysis of $\alpha$ -pinene could substantially reduced the IN activity of ATD and illite particles, and the extent of decrease depended on the coating thickness.
	ATD	immersion	Niedermeier et al. <sup>456</sup>	ATD particles coated with succinic acid had lower IN activity in the immersion freezing mode, compared to fresh ATD particles
	kaolinite	deposition, immersion, condensation	Tobo et al., <sup>440</sup>	Levoglusocan coating significantly reduced the IN activity of kaolinite particles in the deposition nucleation mode, while its impact was not observable in the immersion/condensation freezing modes.
	kaolinite	deposition, immersion	Wex et al., <sup>457</sup>	In the immersion freezing mode, neither succinic acid or levoglusocan changed the IN activity of kaolinite particles. In the deposition nucleation mode, both organic coatings suppressed the IN activity of kaolinite particles for RH below 95%, while a significant increase in IN activity was observed for RH >95%.

HNO <sub>3</sub>	ATD	deposition, immersion, condensation	Sullivan et al. <sup>375</sup>	In the immersion/condensation freezing modes, exposure to HNO <sub>3</sub> (g) has no significant impact on IN activity. For RH <97%, heterogeneous reaction with HNO <sub>3</sub> (g) significantly reduced the IN activity of ATD particles; while around the RH of 97-100 % no significant difference in IN activity was observed between fresh and aged particles
	kaolinite and montmorillonite	deposition	Sihvonen et al. <sup>458</sup>	In the deposition nucleation mode, treatment with HNO <sub>3</sub> reduced the IN activity of kaolinite but did not significantly affect the ice nucleation properties of montmorillonite.
	ATD, illite, K- feldspar, and quartz	deposition, immersion, condensation	Kulkarni et al. <sup>467</sup>	In deposition nucleation mode, aged dust particles, except quartz, showed reduced IN activity compared to fresh particles. In the immersion/condensation freezing modes, fresh and aged dust particles exhibited equivalent IN activity.
NH <sub>3</sub>	montmorillonite	deposition	Salam et al. <sup>468</sup>	Exposure to pure and 25 ppmv NH <sub>3</sub> could enhance the IN activity of montmorillonite particles in the deposition nucleation mode.
	montmorillonite	deposition	Salam et al. <sup>451</sup>	Exposure to ~100 pptv NH <sub>3</sub> for 70 h increased the ice nucleation efficiency of montmorillonite by a factor of ~2.

O <sub>3</sub>	montmorillonite	deposition	Salam et al. <sup>451</sup>	Exposure of montmorillonite to 200 ppbv O <sub>3</sub> for 70 h at room temperature and at 0% RH did not significantly change the IN activity in the deposition nucleation mode.
	ATD kaolinite	and deposition, immersion	Kanji et al., <sup>469</sup>	The change in IN activity after exposure to O <sub>3</sub> was found to be complex, depending on O <sub>3</sub> concentrations, ice nucleation modes, and minerals.

2251

2252 The ice nucleation activity (in deposition and immersion/condensation freezing modes) of ATD  
 2253 and kaolinite aerosol particles with and without secondary organic matter (SOM) coating formed  
 2254 by the ozonolysis of  $\alpha$ -pinene was investigated using the AIDA chamber at 205-210 K.<sup>466</sup> It was  
 2255 found that the SOM coating could substantially suppress the IN activity of both ATD and illite  
 2256 particles, and the suppression extent depended on the thickness of the coating.<sup>466</sup> Almost all the  
 2257 fresh ATD and illite particles with diameters of 0.1-1.0  $\mu\text{m}$  were efficient deposition mode IN at  
 2258  $\text{RH}_i$  between 105 and 120%.<sup>466</sup> However, if coated with 17 wt% SOM, only ~20% of ATD  
 2259 particles were activated to ice crystals at  $\text{RH}_i$  between 115 and 130%;<sup>466</sup> and only 10% of illite  
 2260 particles were ice-active at  $\text{RH}_i$  between 160 and 170%, if coated with 41 wt% SOM.<sup>466</sup> In another  
 2261 study by Niedermeier et al.,<sup>456</sup> ATD particles coated with succinic acid were found to have lower  
 2262 IN activity in the immersion freezing mode (233.15-239.15 K), compared to fresh ATD particles.



2263  
 2264 **Figure 41.** Fractions of 700 nm kaolinite particles which were activated to ice particles at -34 (circles), -  
 2265 30 (triangles), and -26 °C (squares) as a function of RH. (a) fresh kaolinite particles, (b) kaolinite particles  
 2266 treated with levoglucosan at 93 °C, and (c) kaolinite particles treated with H<sub>2</sub>SO<sub>4</sub> at 70 °C. Dashed lines  
 2267 indicate liquid water saturated conditions. Error bars indicate the standard deviation from multiple  
 2268 measurements. Reprinted with permission from ref 440. Copyright 2014 John Wiley & Sons, Inc.

2269  
 2270 Tobo et al.<sup>440</sup> investigated the effects of levoglucosan coating on the IN activity of kaolinite  
 2271 particles. As shown in Figure 41, they<sup>440</sup> found that for temperature ranging from -34 to -26 °C,

2272 levoglucosan coating significantly reduced the IN activity of kaolinite particles for the deposition  
2273 nucleation mode while its impact was not observable for immersion/condensation freezing modes.  
2274 Wex et al.<sup>457</sup> systematically examined how succinic acid and levoglucosan coatings with a  
2275 thickness of a few nm or less could change the IN activity of kaolinite particles in deposition  
2276 nucleation and immersion freezing modes. In the immersion freezing mode, neither organic  
2277 compounds changed the IN activity of kaolinite particles.<sup>457</sup> Under water sub-saturation conditions,  
2278 the effect of organic coatings were more complicated:<sup>457</sup> i) for RH below 95%, both organic  
2279 coatings were found to suppress the ice nucleation of kaolinite particles; ii) on the other hand, a  
2280 significant increase in ice nucleation activity was observed for RH >95%, probably because in this  
2281 RH range mainly immersion freezing instead of deposition nucleation took place (i.e. coated  
2282 kaolinite particles at RH >95% may become aqueous particles with solid inclusion).

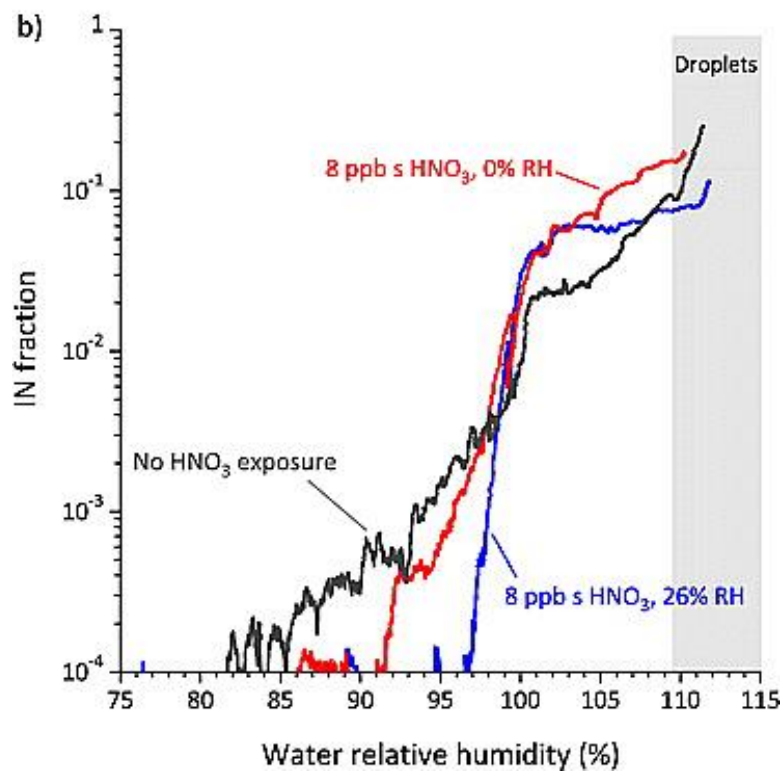
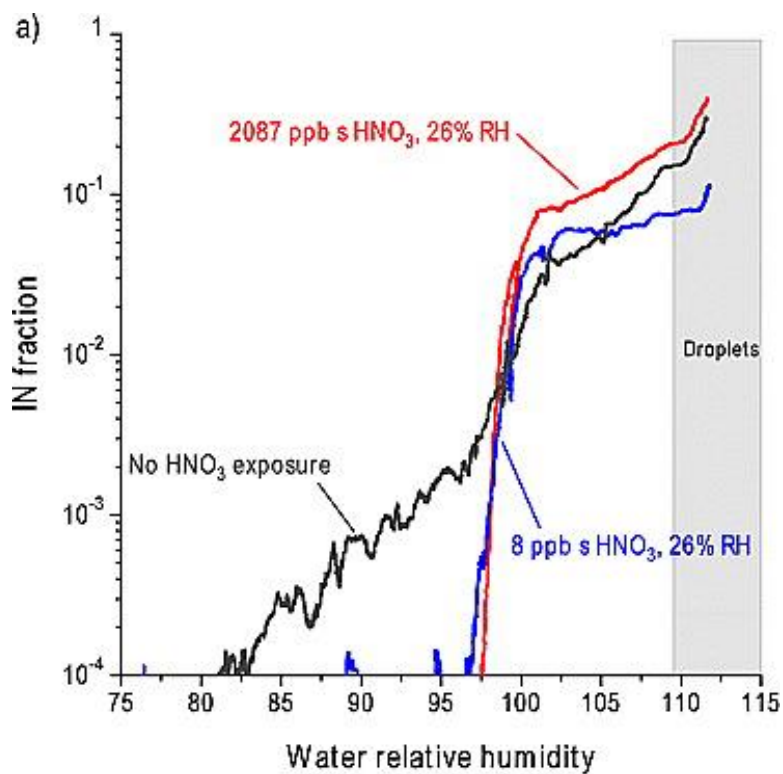
### 2283 **5.3 Exposure to HNO<sub>3</sub>**

2284 Nitrate has been frequently observed to internally mixed with mineral dust particles in the  
2285 troposphere by field measurements<sup>158-160,202,429</sup> due to the heterogeneous reactions with  
2286 HNO<sub>3</sub>,<sup>199,227,365,470-473</sup> N<sub>2</sub>O<sub>5</sub>,<sup>131-134,136,139</sup> NO<sub>2</sub>,<sup>474-478</sup> and NO<sub>3</sub> radicals.<sup>177,479</sup> Nevertheless, only a  
2287 few studies<sup>375,458,467</sup> have investigated whether and how nitrate coatings could alter the IN activity  
2288 of mineral dust particles, as summarized in Table 16.

2289  
2290 The effects of HNO<sub>3</sub> exposure on the IN activity of ATD aerosol particles were investigated by  
2291 Sullivan et al.,<sup>375</sup> who reacted 200 nm ATD particles with HNO<sub>3</sub>(g) in an aerosol flow tube at room  
2292 temperature and at different RH and then measured their ice nucleation properties at -30 °C as a  
2293 function of RH. As shown in Figure 42, for RH <97% under which deposition nucleation occurred,  
2294 heterogeneous reaction with HNO<sub>3</sub>(g) significantly reduced the IN activity of ATD particles;<sup>375</sup>  
2295 however, for RH >100% where immersion/condensation freezing dominated, the effect of exposure  
2296 to HNO<sub>3</sub>(g) was insignificant.<sup>375</sup> In addition, around the RH of 97-100 % no significant difference

2297 in IN activity was observed between fresh and coated particles.<sup>375</sup> At 97-100 % RH deposition  
2298 nucleation dominated for fresh particles; however, at this RH range aged particles may become  
2299 aqueous particles (due to the formation of nitrate coating) and thus immersion/condensation  
2300 freezing can become the main ice nucleation mechanism. The change in ice nucleation modes  
2301 could cause fresh and aged particles to be activated under similar conditions, though their  
2302 compositions differ.





2303  
 2304 **Figure 42.** Fractions of 200 nm fresh and HNO<sub>3</sub>-exposed ATD aerosol particles that were activated to ice  
 2305 crystals at -30 °C as a function of RH. (a) black curve: no HNO<sub>3</sub> exposure; blue curve: HNO<sub>3</sub> exposure of  
 2306 8 ppbv·s at 26% RH; red curve: HNO<sub>3</sub> exposure of 2087 ppbv·s at 26% RH. (b) Black curve: no HNO<sub>3</sub>

2307 exposure; blue curve: HNO<sub>3</sub> exposure of 8 ppbv·s at 26% RH; red curve: HNO<sub>3</sub> exposure of 8 ppbv·s at 0%  
2308 RH. In the region covered by the grey box, droplets may interfere with IN measurements and therefore  
2309 these measurement may not be reliable. Reprinted with permission from ref 375. Copyright 2010 John  
2310 Wiley & Sons, Inc.

2311  
2312 In addition, exposure to HNO<sub>3</sub> at 26% RH, compared to that at 0%, will more significantly reduce  
2313 the deposition nucleation activity of ATD particles for RH<97%,<sup>375</sup> as shown in Figure 42. This  
2314 may be explained by the fact that heterogeneous reaction of HNO<sub>3</sub> with ATD particles is  
2315 accelerated and thus more particulate nitrate is formed at higher RH.<sup>213</sup>

2316  
2317 Sihvonen et al.<sup>458</sup> showed that in the deposition nucleation mode, while treatment with HNO<sub>3</sub>  
2318 decreased the IN activity of kaolinite, it did not significantly affect the ice nucleation properties of  
2319 montmorillonite. In another study, Kulkarni et al.<sup>467</sup> investigated the ice nucleation activity of ATD,  
2320 illite, K-feldspar, and quartz as a function of temperature and RH before and after reaction with  
2321 HNO<sub>3</sub>. They<sup>467</sup> found that at subsaturated conditions (i.e. in deposition nucleation mode), aged  
2322 dust particles, except quartz, showed reduced IN activity compared to fresh particles. In contract,  
2323 at super-saturation conditions (i.e. in immersion/condensation freezing modes), fresh and aged  
2324 dust particles exhibited equivalent IN activity.<sup>467</sup>

#### 2325 **5.4 Exposure to NH<sub>3</sub>**

2326 As summarized in Table 16, the impacts of heterogeneous reaction with NH<sub>3</sub> have been  
2327 investigated by two previous studies.<sup>451,468</sup> Salam et al.<sup>468</sup> studied the ice nucleation activity of  
2328 NH<sub>3</sub>-exposed montmorillonite particles under the deposition nucleation mode and provided the  
2329 first experimental evidence that exposure to NH<sub>3</sub> could enhance the IN activity of mineral dust  
2330 particles. They<sup>468</sup> suggested that ice nucleation activity of montmorillonite particles increased  
2331 with exposure time to NH<sub>3</sub>. It was further observed by Salam et al.<sup>468</sup> that compared to fresh

2332 montmorillonite particles, the activation temperature (defined as the highest temperature at  
2333 which >1% particles were activated to ice crystals) at RH of 100% and 90% was 15 °C higher for  
2334 particles exposed to pure NH<sub>3</sub>, and was 5 °C higher for particles exposed to 25 ppmv NH<sub>3</sub>. In a  
2335 following study, Salam et al.<sup>451</sup> further measured the deposition ice nucleation activity of  
2336 montmorillonite particles after exposed to NH<sub>3</sub> of ~100 pptv (a typical atmospheric concentration)  
2337 for 70 h, and found that this exposure increased the ice nucleation efficiency of montmorillonite  
2338 by a factor of around two.

### 2339 **5.5 Exposure to O<sub>3</sub>**

2340 The influence of heterogeneous reaction with O<sub>3</sub> on the IN activity of mineral dust particles have  
2341 also been explored,<sup>451,469</sup> as shown in Table 16. Salam et al.<sup>451</sup> exposed montmorillonite particles  
2342 to 200 ppbv O<sub>3</sub> for 70 h at room temperature and ~0% RH. No clear change in deposition  
2343 nucleation efficiency was observed after exposure, compared to fresh particles.<sup>451</sup> Kanji et al.<sup>469</sup>  
2344 systematically investigated the IN activity of ATD and kaolinite aerosol particles in deposition and  
2345 immersion modes (between 233 and 263 K) before and after exposure to 0.4-4.3 ppmv O<sub>3</sub> at room  
2346 temperature and 0% RH in a stainless steel aerosol chamber. Complex response of IN activity to  
2347 O<sub>3</sub> exposure was reported.<sup>469</sup> 1) after exposure to 430 ppbv O<sub>3</sub> for ~130 min, kaolinite particles  
2348 showed enhanced ice nucleation activity in both deposition and immersion modes over the  
2349 temperature range (233-263 K) they studied, whereas the change of IN activity was insignificant  
2350 for ATD particles in either deposition or immersion nucleation modes; 2) compared to fresh  
2351 particles, kaolinite particles exposed to 1.4 ppmv O<sub>3</sub> for ~130 min showed a lower ice nucleation  
2352 activity over 232-240 K in the deposition mode, and only slight suppression of IN activity was  
2353 observed for the immersion over 233-263 K; 3) additionally, ATD particles exposed to 4.3 ppmv  
2354 O<sub>3</sub> for ~130 min, compared to unexposed particles, showed significantly lower IN activity in both  
2355 deposition and immersion modes over 233-263 K.

2356 **5.6 Summary**

2357 Increasing numbers of laboratory studies have shown that chemical aging processes can  
2358 substantially change the IN activity of mineral dust particles. Furthermore, several modeling  
2359 studies have suggested that these changes can have important impacts on cloud microphysics,  
2360 radiation, and thus the climate. In the last two decades significant progress has been made in this  
2361 field, and a comprehensive and systematic picture is emerging. Nevertheless, our understanding in  
2362 the effects of atmospheric aging processes on the IN activity of mineral dust particles is still not  
2363 comprehensive or quantitative.

2364

2365 The same coating formed on dust particles may influence on the IN activity for different minerals  
2366 and different ice nucleation modes in different ways. In addition, it is not unusual that inconsistent  
2367 results have been reported by different studies for the same coating on the same type of dust in the  
2368 same ice nucleation mode. For example, most studies suggest that sulfuric acid coating typically  
2369 reduces the IN activity, while the effect of HNO<sub>3</sub> coating is largely unclear. This may be partly  
2370 due to the fact that it is still nontrivial or even challenging to measure the IN activity of aerosol  
2371 particles. What makes it more complicated is that the formation of coating could change the mode  
2372 in which dust particles are activated to ice crystals (e.g., from deposition nucleation to  
2373 condensation/immersion freezing, due to the increase in CCN activity of aged dust particles).<sup>375</sup>  
2374 Several studies have revealed that the extent of IN activity changes depends on the thickness of  
2375 coatings;<sup>219,375,466</sup> however, a quantitative understanding of effects of chemical aging processes on  
2376 IN activity of mineral dust particles is still lacking.

2377

2378 Furthermore, it is still not clear at the molecular level why and how chemical processes with acids  
2379 usually turn to reduce the IN activity of mineral dust particles. It may be largely due to the fact  
2380 that we still do not understand why some minerals are more ice nucleation active than others and

2381 the nature of ice nucleation active sites on the surface.<sup>443,480</sup> Five factors have been empirically  
2382 proposed to promote heterogeneous ice nucleation.<sup>167</sup> 1) It is typically assumed that the number of  
2383 ice nucleation active sites is proportional to the particle surface area.<sup>238,481-484</sup> 2) Heterogeneous  
2384 ice nucleation is preferentially initiated by surfaces of insoluble materials. 3) The ability of a  
2385 surface to form hydrogen bonds usually promotes water adsorption and ice nucleation. 4) Surfaces  
2386 which have similar crystallographic structures to that of ice will promote ice nucleation. 5)  
2387 Morphological, chemical, and electrical heterogeneities on the surface can also promote ice  
2388 nucleation. Several hypotheses have been suggested to explain why exposure to acid gases (e.g.,  
2389 H<sub>2</sub>SO<sub>4</sub> and HNO<sub>3</sub>) may suppress the IN activity of mineral dust particles. Laboratory studies  
2390 <sup>220,261,458</sup> have shown that reaction products which are more soluble (and thus less IN active) can  
2391 lead to the loss of or cover the active sites. Chemical aging processes can also lead to structural  
2392 changes of surfaces, alter their crystalline nature, and cause structural disorders,<sup>443,449,458</sup> therefore  
2393 reducing their ice nucleation activity. The patterns in which surfaces interact with water can also  
2394 be changed due to chemical processes, resulting in changes in heterogeneous ice formation.<sup>460</sup> In  
2395 addition, a few recent studies <sup>457,459</sup> also suggest that the loss/deactivation of feldspar (which is  
2396 very IN active) heterogeneities may be responsible for the decrease in IN activity of clay minerals.

## 2397 **6 Concluding remarks and recommendations for future studies**

2398 Interactions of mineral dust particles with water vapor influence their heterogeneous reactivity  
2399 towards reactive trace gases, their hygroscopicity and hence their ability to directly scatter and  
2400 absorb solar and terrestrial radiation, and their activity to serve as CCN and IN and therefore their  
2401 roles in indirect radiative forcing. Additionally, atmospheric heterogeneous and multiphase  
2402 reactions will change their chemical compositions after mineral dust particles are lifted into the  
2403 troposphere, as a result modifying the interactions of mineral dust particles with water vapor. A  
2404 complete and in-depth understanding of the interactions of fresh and aged dust particles with water

2405 vapor will help us assess the roles of mineral dust aerosols in many aspects of atmosphere  
2406 chemistry and climate change.

2407

2408 In this article we provide a comprehensive review of water adsorption, hygroscopicity, and CCN  
2409 activity of fresh and aged mineral dust particles, and the effects of chemical aging on the IN activity  
2410 of mineral dust particles. As shown in this review, previous studies have largely improved our  
2411 understanding of the interactions of mineral dust particles with water vapor. Brief summaries are  
2412 provided in Section 4.11 for water adsorption, hygroscopicity, and CCN activities of fresh and  
2413 aged mineral dust particles and in Section 5.6 for the IN activity of aged mineral dust particles.  
2414 However, there still remain many open questions which can only be satisfactorily answered  
2415 through a close collaboration among laboratory studies, field measurements, modeling work, and  
2416 theoretical analysis. Several future directions are recommended here in order to address these  
2417 challenges:

2418

2419 (1) Large discrepancies still exist for water adsorption and hygroscopicity of fresh mineral dust  
2420 particles reported by different studies, especially for clay minerals. Reasons for these discrepancies  
2421 are largely unclear. Further measurements are recommended to solve these discrepancies, and  
2422 well-coordinated collaborations in which same dust samples are distributed to different groups and  
2423 experimental results are intercompared will be very helpful. Most experimental data are only  
2424 presented in graphical forms, yet numerical tabulation of the data can enhance their accessibility  
2425 and usability.

2426

2427 (2) Previous studies which measured water adsorption and hygroscopicity of fresh mineral dust  
2428 particles were mainly carried out at RH lower than 80%. It is recommended that future  
2429 measurements should be extended to RH above 90% or even 99%. Nevertheless, it is non-trivial

2430 to do these measurements at RH very close to 100%. In addition, most previous studies have been  
2431 performed at or near room temperature, but temperature varies from ~200 to ~300 K in the  
2432 troposphere, and profound effects of temperature on the hygroscopicity have been reported for  
2433 some materials of atmospheric relevance.<sup>485-487</sup> Therefore, the effects of temperature on the water  
2434 adsorption and hygroscopicity of mineral dust particles need to be systematically investigated by  
2435 future studies.

2436

2437 (3) Large numbers of previous laboratory studies have suggested that chemical aging could  
2438 substantially increase the water adsorption ability, hygroscopicity, and CCN activity of mineral  
2439 dust particles. However, most of these studies focused on CaCO<sub>3</sub>, and the effect of chemical aging  
2440 should also been examined for more abundant minerals and real dust samples. It is also  
2441 recommended that future laboratory work should be carried out at atmospherically relevant  
2442 conditions (e.g., concentrations of reactive trace gases, reaction time, and RH etc.). Studies of this  
2443 type can help to answer how rapidly water adsorption, hygroscopicity, and CCN activity of mineral  
2444 dust particles will be changed during their residence in the atmosphere.

2445

2446 (4) The interactions of mineral dust particles with water vapor influences, and is influenced by,  
2447 interactions with reactive trace gases. Such complex interactions are likely to involve mass transfer  
2448 <sup>306,488-492</sup> and chemical reactions in and between all three different phases (gas, liquid, and solid)  
2449 in nonlinear manners.<sup>172,173,493-499</sup> Multiphase models have been developed in order to integrate  
2450 these processes and have been applied to study chemical reactions and phase transition of organic  
2451 particles.<sup>499-502</sup> If developed for and applied to mineral dust chemistry, they can be very helpful for  
2452 a better understanding of the complex interactions between mineral dust particles, water, and  
2453 reactive trace gases.

2454

2455 (5) Many field measurements have shown that coated dust particles in the troposphere have  
2456 different phase transition properties when compared to uncoated dust particles. However, most of  
2457 these studies are of a qualitative nature. It will be useful for future field measurements to  
2458 quantitatively and simultaneously determine 1) the amount and type of coating formed on ambient  
2459 mineral dust particles, and 2) the change of water adsorption, hygroscopicity, or CCN activity of  
2460 these coated mineral dust particles. Measurements of this type, though very challenging, will  
2461 largely improve our understanding of the effects of chemical aging processes in the atmosphere.

2462

2463 (6) The impacts of heterogeneous reactions on trace gases and compositions of mineral dust  
2464 particles have been assessed by many regional and global models in the last 2-3 decades. However,  
2465 their effects on the hygroscopicity and CCN activity of mineral dust particles have seldom been  
2466 investigated by modeling studies. Modeling analyses will give a better understanding, on a much  
2467 larger spatial and temporal scale, of the atmospheric relevance of change in hygroscopicity and  
2468 CCN activity of mineral dust particles due to chemical aging processes.

2469

2470 (7) Compared to the effects of atmospheric aging processes on hygroscopicity and CCN activity,  
2471 the impact on IN activity has been much less widely investigated. While sulfate coatings have  
2472 received some attention, much less has been paid to the effects of nitrate and organic species on  
2473 the IN activity of mineral dust particles. In order for a more comprehensive understanding, further  
2474 studies are needed on the effect of different coatings, especially nitrate and organic, on the IN  
2475 activity of mineral dust particles. It is also highly desirable to carry out aging experiments at  
2476 atmospheric relevant conditions, and to control the amount of coatings and/or exposure conditions  
2477 in more quantitative and atmospherically relevant ways. One of the current limitations on our  
2478 ability to understand how chemical aging changes the IN activity of mineral dust particles is to  
2479 correctly mimic atmospheric processing of aerosol particles in the laboratory. For example, it is



2480 critical that surface coating composition and thickness realistically mimic what is present in the  
2481 atmosphere. Since coatings, in particular, appear to effectively deactivate effective mineral dust  
2482 ice nuclei,<sup>74,219</sup> future studies will need to consider how to properly compare laboratory particles  
2483 to atmospheric measurements.

2484

2485 (8) Mechanisms that change IN activity of dust particles due to atmospheric aging processes are  
2486 largely unknown on a molecular level, and a collaborative effort from experts in aerosol/cloud  
2487 chemistry microphysics, surface science and surface chemistry, and theoretical chemistry will be  
2488 very beneficial.

2489

2490 (9) Field measurements are required to understand if and to which extent the IN activity of mineral  
2491 dust particles in the troposphere is influenced by a variety of aging processes during transport.  
2492 Modeling studies are encouraged to include more laboratory-derived and realistic  
2493 parameterizations for the effects of aging processes on IN activity in their simulations, in order to  
2494 better evaluate the effects of atmospheric aging processes on IN activity, cloud microphysics, and  
2495 climate impacts.

2496

## 2497 **Author information**

### 2498 **Corresponding author**

2499 \*Phone: (319)335-1392. Fax: (319)353-1115. E-mail: vicki-grassian@uiowa.edu.

### 2500 **Notes**

2501 The authors declare no competing financial interest.

## 2502 **Biographies**

2503 Mingjin Tang is currently a postdoctoral fellow in Professor Grassian's group, Department of  
2504 Chemistry, University of Iowa, USA. Before arriving in the USA in the beginning of 2015, he  
2505 received his BSc (in 2005) and MSc (in 2008) from Peking University (China) under the  
2506 supervision of Professor Tong Zhu, and then received his PhD (in 2011) in Max Planck Institute  
2507 for Chemistry and Johannes Gutenberg-Universität Mainz (Germany), advised by Drs. John N  
2508 Crowley, Ulrich Pöschl, and Thorsten Hoffmann. After a short postdoc in Max Planck Institute for  
2509 Chemistry, he joined Dr. Markus Kalberer's group at Department of Chemistry, University of  
2510 Cambridge (UK) as a postdoctoral fellow. His research interest focuses on the fundamental  
2511 physical chemistry of atmospheric aerosol particles and how physicochemical changes of aerosol  
2512 particles influence air quality, clouds, and climate. He would like to thank Professor Tong Zhu for  
2513 bringing him into atmospheric heterogeneous and multiphase chemistry studies as a young  
2514 scientist in Peking University.

2515

2516 Daniel J. Cziczo is currently the Victor P. Starr Professor of Atmospheric Chemistry in the  
2517 Department of Earth, Atmospheric and Planetary Sciences and Civil and Environmental  
2518 Engineering at the Massachusetts Institute of Technology, USA. His research revolves around the  
2519 interrelationship of particulate matter and cloud formation. His group utilizes laboratory and field  
2520 studies to elucidate how small particles interact with water vapor to form droplets and ice crystals  
2521 which are important players in the Earth's climate system. Experiments include using small cloud  
2522 chambers in the laboratory to mimic atmospheric conditions that lead to cloud formation and  
2523 observing clouds in situ from remote mountaintop sites or through the use of research aircraft.

2524

2525 As of January 2016, Vicki H. Grassian is a Distinguished Professor at the University of California  
2526 San Diego (UCSD) with appointments in Chemistry and Biochemistry, Nanoengineering and

2527 Scripps Institution of Oceanography. She is also Distinguished Chair of Physical Chemistry and  
2528 currently serves as co-director at the Center for Aerosol Impacts on Climate and the Environment  
2529 centered at UCSD. Prior to her move to UCSD, she was the F. Wendell Miller Professor in  
2530 Chemistry at the University of Iowa. Her research area focuses on environmental molecular  
2531 surface science, heterogeneous and multiphase chemistry of atmospheric aerosol particles, the  
2532 impact of atmospheric aerosol on air quality and climate, and environmental and health aspects of  
2533 nanoscience and nanotechnology.

### 2534 **Acknowledgement**

2535 The preparation of this review paper was initiated when M. J. T was working in University of  
2536 Cambridge (UK) as a postdoctoral fellow under the supervision of Dr. M Kalberer. M. J. T. would  
2537 like to thank Dr. Kalberer for his support and useful discussion, and the Isaac Newton Trust  
2538 (Trinity College, University of Cambridge, UK) for sponsoring him with a research scholarship.  
2539 V. H. G acknowledges that this work was supported by the NSF under grant CHE-1305723. Any  
2540 opinions, findings, and conclusions or recommendations expressed in this material are those of the  
2541 authors and do not necessarily reflect the views of National Science Foundation. D. J. C.  
2542 acknowledges funding from NASA (Grant NNX13AO15G) and the Victor P. Starr Career  
2543 Development Chair for funding that made this work possible.

2544

### 2545 **References**

- 2546 (1) Seinfeld, J. H.; Pandis, S. N. *Atmospheric Chemistry and Physics: From air pollution to*  
2547 *climate change*; Wiley Interscience: New York, 2006.
- 2548 (2) Finlayson-Pitts, B. J.; Pitts, J. N. *Chemistry of the Upper and Lower Atmosphere: Theory,*  
2549 *Experiments, and Applications*; Academic Press: San Diego, 2000.
- 2550 (3) Stevens, B.; Feingold, G. Untangling aerosol effects on clouds and precipitation in a  
2551 buffered system. *Nature* **2009**, *461*, 607-613.
- 2552 (4) Carslaw, K. S.; Lee, L. A.; Reddington, C. L.; Pringle, K. J.; Rap, A.; Forster, P. M.;  
2553 Mann, G. W.; Spracklen, D. V.; Woodhouse, M. T.; Regayre, L. A. *et al.* Large  
2554 contribution of natural aerosols to uncertainty in indirect forcing. *Nature* **2013**, *503*, 67-  
2555 71.

- 2556 (5) IPCC *Climate Change 2013: The Physical Science Basis*; Cambridge University Press:  
2557 Cambridge, UK, 2013.
- 2558 (6) Laurent, B.; Marticorena, B.; Bergametti, G.; Léon, J. F.; Mahowald, N. M. Modeling  
2559 mineral dust emissions from the Sahara desert using new surface properties and soil  
2560 database. *J. Geophys. Res.-Atmos* **2008**, *113*, D14218, doi:  
2561 14210.11029/12007JD009484.
- 2562 (7) Laurent, B.; Marticorena, B.; Bergametti, G.; Mei, F. Modeling mineral dust emissions  
2563 from Chinese and Mongolian deserts. *Glob. Planet. Change* **2006**, *52*, 121-141.
- 2564 (8) Textor, C.; Schulz, M.; Guibert, S.; Kinne, S.; Balkanski, Y.; Bauer, S.; Berntsen, T.;  
2565 Berglen, T.; Boucher, O.; Chin, M. *et al.* Analysis and quantification of the diversities of  
2566 aerosol life cycles within AeroCom. *Atmos. Chem. Phys.* **2006**, *6*, 1777-1813.
- 2567 (9) Huneeus, N.; Schulz, M.; Balkanski, Y.; Griesfeller, J.; Prospero, J.; Kinne, S.; Bauer, S.;  
2568 Boucher, O.; Chin, M.; Dentener, F. *et al.* Global dust model intercomparison in  
2569 AeroCom phase I. *Atmos. Chem. Phys.* **2011**, *11*, 7781-7816.
- 2570 (10) Ginoux, P.; Prospero, J. M.; Gill, T. E.; Hsu, N. C.; Zhao, M. Global-scale attribution of  
2571 anthropogenic and natural dust sources and their emission rates based on MODIS Deep  
2572 Blue aerosol products. *Rev. Geophys.* **2012**, *50*, RG3005, doi:  
2573 3010.1029/2012RG000388.
- 2574 (11) Forster, P.; Ramaswamy, V.; Artaxo, P.; Berntsen, T.; Betts, R.; Fahey, D. W.; Haywood,  
2575 J.; Lean, J.; Lowe, D. C.; Myhre, G. *et al.* In *Climate Change 2007: The Physical Science  
2576 Basis. Contribution of Working Group I to the Fourth Assessment Report of the  
2577 Intergovernmental Panel on Climate Change*; Solomon, S., Qin, D., Manning, M., Chen,  
2578 Z., Marquis, M., Averyt, K. B., Tignor, M., Miller, H. L., Eds.; Cambridge University  
2579 Press: Cambridge, United Kingdom, 2007.
- 2580 (12) Prospero, J. M. Long-range transport of mineral dust in the global atmosphere: Impact of  
2581 African dust on the environment of the southeastern United States. *Proc. Natl. Acad. Sci.  
2582 U. S. A.* **1999**, *96*, 3396-3403.
- 2583 (13) Uno, I.; Eguchi, K.; Yumimoto, K.; Takemura, T.; Shimizu, A.; Uematsu, M.; Liu, Z.;  
2584 Wang, Z.; Hara, Y.; Sugimoto, N. Asian dust transported one full circuit around the  
2585 globe. *Nature Geosci.* **2009**, *2*, 557-560.
- 2586 (14) Schepanski, K.; Tegen, I.; Macke, A. Saharan dust transport and deposition towards the  
2587 tropical northern Atlantic. *Atmos. Chem. Phys.* **2009**, *9*, 1173-1189.
- 2588 (15) Hande, L. B.; Engler, C.; Hoose, C.; Tegen, I. Seasonal variability of Saharan desert dust  
2589 and ice nucleating particles over Europe. *Atmos. Chem. Phys.* **2015**, *15*, 4389-4397.
- 2590 (16) Fairlie, T. D.; Jacob, D. J.; Dibb, J. E.; Alexander, B.; Avery, M. A.; van Donkelaar, A.;  
2591 Zhang, L. Impact of mineral dust on nitrate, sulfate, and ozone in transpacific Asian  
2592 pollution plumes. *Atmos. Chem. Phys.* **2010**, *10*, 3999-4012.
- 2593 (17) Fairlie, T. D.; Jacob, D. J.; Park, R. J. The impact of transpacific transport of mineral dust  
2594 in the United States. *Atmos. Environ.* **2007**, *41*, 1251-1266.
- 2595 (18) Prospero, J. M.; Mayol-Bracero, O. L. Understanding the Transport and Impact of  
2596 African Dust on the Caribbean Basin. *Bull. Amer. Meteorol. Soc.* **2013**, *94*, 1329-1337.
- 2597 (19) Quinn, P. K.; Collins, D. B.; Grassian, V. H.; Prather, K. A.; Bates, T. S. Chemistry and  
2598 Related Properties of Freshly Emitted Sea Spray Aerosol. *Chem. Rev.* **2015**, *115*, 4383-  
2599 4399.
- 2600 (20) Prospero, J. M.; Lamb, P. J. African droughts and dust transport to the Caribbean:  
2601 Climate change implications. *Science* **2003**, *302*, 1024-1027.
- 2602 (21) Mahowald, N. M.; Kloster, S.; Engelstaedter, S.; Moore, J. K.; Mukhopadhyay, S.;  
2603 McConnell, J. R.; Albani, S.; Doney, S. C.; Bhattacharya, A.; Curran, M. A. J. *et al.*

- 2604 Observed 20th century desert dust variability: impact on climate and biogeochemistry.  
 2605 *Atmos. Chem. Phys.* **2010**, *10*, 10875-10893.
- 2606 (22) Tegen, I.; Lacis, A. A.; Fung, I. The influence on climate forcing of mineral aerosols  
 2607 from disturbed soils. *Nature* **1996**, *380*, 419-422.
- 2608 (23) Tegen, I.; Harrison, S. P.; Kohfeld, K.; Prentice, I. C.; Coe, M.; Heimann, M. Impact of  
 2609 vegetation and preferential source areas on global dust aerosol: Results from a model  
 2610 study. *J. Geophys. Res.-Atmos.* **2002**, *107*, 4576, DOI: 4510.1029/2001JD000963.
- 2611 (24) Tegen, I.; Werner, M.; Harrison, S. P.; Kohfeld, K. E. Relative importance of climate and  
 2612 land use in determining present and future global soil dust emission. *Geophys. Res. Lett.*  
 2613 **2004**, *31*, L05105, doi: 05110.01029/02003GL019216.
- 2614 (25) Muhs, D. R. The geologic records of dust in the Quaternary. *Aeolian Res.* **2013**, *9*, 3-48.
- 2615 (26) Muhs, D.; Prospero, J.; Baddock, M.; Gill, T. In *Mineral Dust*; Knippertz, P., Stuut, J.-B.  
 2616 W., Eds.; Springer: Netherlands, 2014.
- 2617 (27) Mahowald, N. Aerosol Indirect Effect on Biogeochemical Cycles and Climate. *Science*  
 2618 **2011**, *334*, 794-796.
- 2619 (28) Choobari, O. A.; Zawar-Reza, P.; Sturman, A. The global distribution of mineral dust and  
 2620 its impacts on the climate system: A review. *Atmos. Res.* **2014**, *138*, 152-165.
- 2621 (29) Li, X.; Maring, H.; Savoie, D.; Voss, K.; Prospero, J. M. Dominance of mineral dust in  
 2622 aerosol light-scattering in the North Atlantic trade winds. *Nature* **1996**, *380*, 416-419.
- 2623 (30) Balkanski, Y.; Schulz, M.; Claquin, T.; Guibert, S. Reevaluation of Mineral aerosol  
 2624 radiative forcings suggests a better agreement with satellite and AERONET data. *Atmos.*  
 2625 *Chem. Phys.* **2007**, *7*, 81-95.
- 2626 (31) Sokolik, I. N.; Toon, O. B. Direct radiative forcing by anthropogenic airborne mineral  
 2627 aerosols. *Nature* **1996**, *381*, 681-683.
- 2628 (32) Linke, C.; Möhler, O.; Veres, A.; Mohácsi, Á.; Bozóki, Z.; Szabó, G.; Schnaiter, M.  
 2629 Optical properties and mineralogical composition of different Saharan mineral dust  
 2630 samples: a laboratory study. *Atmos. Chem. Phys.* **2006**, *6*, 3315-3323.
- 2631 (33) Sokolik, I. N.; Winker, D. M.; Bergametti, G.; Gillette, D. A.; Carmichael, G.; Kaufman,  
 2632 Y. J.; Gomes, L.; Schuetz, L.; Penner, J. E. Introduction to special section: Outstanding  
 2633 problems in quantifying the radiative impacts of mineral dust. *J. Geophys. Res.-Atmos.*  
 2634 **2001**, *106*, 18015-18027.
- 2635 (34) Huang, X.; Song, Y.; Zhao, C.; Cai, X.; Zhang, H.; Zhu, T. Direct Radiative Effect by  
 2636 Multicomponent Aerosol over China. *J. Climate* **2015**, *28*, 3472-3495.
- 2637 (35) Wu, Z. J.; Cheng, Y. F.; Hu, M.; Wehner, B.; Sugimoto, N.; Wiedensohler, A. Dust  
 2638 events in Beijing, China (2004–2006): comparison of ground-based measurements with  
 2639 columnar integrated observations. *Atmos. Chem. Phys.* **2009**, *9*, 6915-6932.
- 2640 (36) Di Biagio, C.; Boucher, H.; Caqueneau, S.; Chevaillier, S.; Cuesta, J.; Formenti, P.  
 2641 Variability of the infrared complex refractive index of African mineral dust: experimental  
 2642 estimation and implications for radiative transfer and satellite remote sensing. *Atmos.*  
 2643 *Chem. Phys.* **2014**, *14*, 11093-11116.
- 2644 (37) McConnell, C. L.; Formenti, P.; Highwood, E. J.; Harrison, M. A. J. Using aircraft  
 2645 measurements to determine the refractive index of Saharan dust during the DODO  
 2646 Experiments. *Atmos. Chem. Phys.* **2010**, *10*, 3081-3098.
- 2647 (38) Lemaitre, C.; Flamant, C.; Cuesta, J.; Raut, J. C.; Chazette, P.; Formenti, P.; Pelon, J.  
 2648 Radiative heating rates profiles associated with a springtime case of Bodele and Sudan  
 2649 dust transport over West Africa. *Atmos. Chem. Phys.* **2010**, *10*, 8131-8150.
- 2650 (39) Tanre, D.; Haywood, J.; Pelon, J.; Leon, J. F.; Chatenet, B.; Formenti, P.; Francis, P.;  
 2651 Goloub, P.; Highwood, E. J.; Myhre, G. Measurement and modeling of the Saharan dust

- 2652 radiative impact: Overview of the Saharan Dust Experiment (SHADE). *J. Geophys. Res.-*  
 2653 *Atmos.* **2003**, *108*, 8574, doi: 8510.1029/2002jd003273.
- 2654 (40) Highwood, E.; Ryder, C. In *Mineral Dust*; Knippertz, P., Stuut, J.-B. W., Eds.; Springer:  
 2655 Netherlands, 2014.
- 2656 (41) Kim, K. W.; He, Z.; Kim, Y. J. Physicochemical characteristics and radiative properties  
 2657 of Asian dust particles observed at Kwangju, Korea, during the 2001 ACE-Asia intensive  
 2658 observation period. *J. Geophys. Res.-Atmos* **2004**, *109*, D19S02, doi:  
 2659 10.1029/2003JD003693.
- 2660 (42) Jung, J.; Kim, Y. J.; Lee, K. Y.; Cayetano, M. G.; Batmunkh, T.; Koo, J. H.; Kim, J.  
 2661 Spectral optical properties of long-range transport Asian dust and pollution aerosols over  
 2662 Northeast Asia in 2007 and 2008. *Atmos. Chem. Phys.* **2010**, *10*, 5391-5408.
- 2663 (43) Miller, R.; Knippertz, P.; Pérez García-Pando, C.; Perlwitz, J.; Tegen, I. In *Mineral Dust*;  
 2664 Knippertz, P., Stuut, J.-B. W., Eds.; Springer: Netherlands, 2014.
- 2665 (44) Schladitz, A.; Müller, T.; Nordmann, S.; Tesche, M.; Groß, S.; Freudenthaler, V.;  
 2666 Gasteiger, J.; Wiedensohler, A. In situ aerosol characterization at Cape Verde Part 2:  
 2667 Parametrization of relative humidity- and wavelength-dependent aerosol optical  
 2668 properties. *Tellus B* **2011**, *63*.
- 2669 (45) Jeong, G. R.; Sokolik, I. N. Effect of mineral dust aerosols on the photolysis rates in the  
 2670 clean and polluted marine environments. *J. Geophys. Res.-Atmos.* **2007**, *112*, D21308,  
 2671 doi: 21310.21029/22007jd008442.
- 2672 (46) Koehler, K. A.; Kreidenweis, S. M.; DeMott, P. J.; Petters, M. D.; Prenni, A. J.; Carrico,  
 2673 C. M. Hygroscopicity and cloud droplet activation of mineral dust aerosol. *Geophys. Res.*  
 2674 *Lett.* **2009**, *36*, L08805, doi: 08810.01029/02009gl037348.
- 2675 (47) Kumar, P.; Sokolik, I. N.; Nenes, A. Parameterization of cloud droplet formation for  
 2676 global and regional models: including adsorption activation from insoluble CCN. *Atmos.*  
 2677 *Chem. Phys.* **2009**, *9*, 2517-2532.
- 2678 (48) Twohy, C. H.; Kreidenweis, S. M.; Eidhammer, T.; Browell, E. V.; Heymsfield, A. J.;  
 2679 Bansemer, A. R.; Anderson, B. E.; Chen, G.; Ismail, S.; DeMott, P. J. *et al.* Saharan dust  
 2680 particles nucleate droplets in eastern Atlantic clouds. *Geophys. Res. Lett.* **2009**, *36*,  
 2681 L01807, doi: 01810.01029/02008gl035846.
- 2682 (49) Herich, H.; Tritscher, T.; Wiacek, A.; Gysel, M.; Weingartner, E.; Lohmann, U.;  
 2683 Baltensperger, U.; Cziczo, D. J. Water uptake of clay and desert dust aerosol particles at  
 2684 sub- and supersaturated water vapor conditions. *Phys. Chem. Chem. Phys.* **2009**, *11*,  
 2685 7804-7809.
- 2686 (50) Manktelow, P. T.; Carslaw, K. S.; Mann, G. W.; Spracklen, D. V. The impact of dust on  
 2687 sulfate aerosol, CN and CCN during an East Asian dust storm. *Atmos. Chem. Phys.* **2010**,  
 2688 *10*, 365-382.
- 2689 (51) Karydis, V. A.; Kumar, P.; Barahona, D.; Sokolik, I. N.; Nenes, A. On the effect of dust  
 2690 particles on global cloud condensation nuclei and cloud droplet number. *J. Geophys.*  
 2691 *Res.-Atmos.* **2011**, *116*, D23204, doi: 23210.21029/22011jd016283.
- 2692 (52) Kumar, P.; Nenes, A.; Sokolik, I. N. Importance of adsorption for CCN activity and  
 2693 hygroscopic properties of mineral dust aerosol. *Geophys. Res. Lett.* **2009**, *36*, L24804,  
 2694 doi: 24810.21029/22009gl040827.
- 2695 (53) Solomos, S.; Kallos, G.; Kushta, J.; Astitha, M.; Tremback, C.; Nenes, A.; Levin, Z. An  
 2696 integrated modelling study on the effects of mineral dust and sea salt particles on clouds  
 2697 and precipitation. *Atmos. Chem. Phys.* **2011**, *11*, 873-892.
- 2698 (54) Nenes, A.; Murray, B.; Bougiatioti, A. In *Mineral Dust*; Knippertz, P., Stuut, J.-B. W.,  
 2699 Eds.; Springer: Netherlands, 2014.

- 2700 (55) Zhang, H.; McFarquhar, G. M.; Cotton, W. R.; Deng, Y. Direct and indirect impacts of  
2701 Saharan dust acting as cloud condensation nuclei on tropical cyclone eyewall  
2702 development. *Geophys. Res. Lett.* **2009**, *36*, L06802, doi: 06810.01029/02009GL037276.
- 2703 (56) DeMott, P. J.; Sassen, K.; Poellot, M. R.; Baumgardner, D.; Rogers, D. C.; Brooks, S. D.;  
2704 Prenni, A. J.; Kreidenweis, S. M. African dust aerosols as atmospheric ice nuclei.  
2705 *Geophys. Res. Lett.* **2003**, *30*, 1732, doi: 1710.1029/2003gl017410.
- 2706 (57) Klein, H.; Nickovic, S.; Haunold, W.; Bundke, U.; Nillius, B.; Ebert, M.; Weinbruch, S.;  
2707 Schuetz, L.; Levin, Z.; Barrie, L. A. *et al.* Saharan dust and ice nuclei over Central  
2708 Europe. *Atmos. Chem. Phys.* **2010**, *10*, 10211-10221.
- 2709 (58) Creamean, J. M.; Suski, K. J.; Rosenfeld, D.; Cazorla, A.; DeMott, P. J.; Sullivan, R. C.;  
2710 White, A. B.; Ralph, F. M.; Minnis, P.; Comstock, J. M. *et al.* Dust and Biological  
2711 Aerosols from the Sahara and Asia Influence Precipitation in the Western U.S. *Science*  
2712 **2013**, *339*, 1572-1578.
- 2713 (59) Hoose, C.; Lohmann, U.; Erdin, R.; Tegen, I. The global influence of dust mineralogical  
2714 composition on heterogeneous ice nucleation in mixed-phase clouds. *Environ. Res. Lett.*  
2715 **2008**, *3*, 025003.
- 2716 (60) Field, P. R.; Mohler, O.; Connolly, P.; Kramer, M.; Cotton, R.; Heymsfield, A. J.;  
2717 Saathoff, H.; Schnaiter, M. Some ice nucleation characteristics of Asian and Saharan  
2718 desert dust. *Atmos. Chem. Phys.* **2006**, *6*, 2991-3006.
- 2719 (61) DeMott, P. J.; Cziczo, D. J.; Prenni, A. J.; Murphy, D. M.; Kreidenweis, S. M.; Thomson,  
2720 D. S.; Borys, R.; Rogers, D. C. Measurements of the concentration and composition of  
2721 nuclei for cirrus formation. *Proc. Natl. Acad. Sci. U. S. A.* **2003**, *100*, 14655-14660.
- 2722 (62) DeMott, P. J.; Prenni, A. J.; Liu, X.; Kreidenweis, S. M.; Petters, M. D.; Twohy, C. H.;  
2723 Richardson, M. S.; Eidhammer, T.; Rogers, D. C. Predicting global atmospheric ice  
2724 nuclei distributions and their impacts on climate. *Proc. Natl. Acad. Sci. U. S. A.* **2010**,  
2725 *107*, 11217-11222.
- 2726 (63) Zimmermann, F.; Weinbruch, S.; Schutz, L.; Hofmann, H.; Ebert, M.; Kandler, K.;  
2727 Worringer, A. Ice nucleation properties of the most abundant mineral dust phases. *J.*  
2728 *Geophys. Res.-Atmos.* **2008**, *113*, D23204, doi: 23210.21029/22008jd010655.
- 2729 (64) Stith, J. L.; Ramanathan, V.; Cooper, W. A.; Roberts, G. C.; DeMott, P. J.; Carmichael,  
2730 G.; Hatch, C. D.; Adhikary, B.; Twohy, C. H.; Rogers, D. C. *et al.* An overview of  
2731 aircraft observations from the Pacific Dust Experiment campaign. *J. Geophys. Res.-*  
2732 *Atmos.* **2009**, *114*, D05207, doi: 05210.01029/02008jd010924.
- 2733 (65) Ryder, C. L.; McQuaid, J. B.; Flamant, C.; Rosenberg, P. D.; Washington, R.; Brindley,  
2734 H. E.; Highwood, E. J.; Marsham, J. H.; Parker, D. J.; Todd, M. C. *et al.* Advances in  
2735 understanding mineral dust and boundary layer processes over the Sahara from Fennec  
2736 aircraft observations. *Atmos. Chem. Phys.* **2015**, *15*, 8479-8520.
- 2737 (66) Burrows, S. M.; Hoose, C.; Pöschl, U.; Lawrence, M. G. Ice nuclei in marine air:  
2738 biogenic particles or dust? *Atmos. Chem. Phys.* **2013**, *13*, 245-267.
- 2739 (67) Pratt, K. A.; DeMott, P. J.; French, J. R.; Wang, Z.; Westphal, D. L.; Heymsfield, A. J.;  
2740 Twohy, C. H.; Prenni, A. J.; Prather, K. A. In situ detection of biological particles in  
2741 cloud ice-crystals. *Nature Geoscience* **2009**, *2*, 397-400.
- 2742 (68) Baustian, K. J.; Cziczo, D. J.; Wise, M. E.; Pratt, K. A.; Kulkarni, G.; Hallar, A. G.;  
2743 Tolbert, M. A. Importance of aerosol composition, mixing state, and morphology for  
2744 heterogeneous ice nucleation: A combined field and laboratory approach. *J. Geophys.*  
2745 *Res.-Atmos.* **2012**, *117*, D06217, doi: 06210.01029/02011jd016784.
- 2746 (69) Cziczo, D. J.; Froyd, K. D. Sampling the composition of cirrus ice residuals. *Atmos. Res.*  
2747 **2014**, *142*, 15-31.

- 2748 (70) Ebert, M.; Worrigen, A.; Benker, N.; Mertes, S.; Weingartner, E.; Weinbruch, S.  
 2749 Chemical composition and mixing-state of ice residuals sampled within mixed phase  
 2750 clouds. *Atmos. Chem. Phys.* **2011**, *11*, 2805-2816.
- 2751 (71) Kamphus, M.; Ettner-Mahl, M.; Klimach, T.; Drewnick, F.; Keller, L.; Cziczo, D. J.;  
 2752 Mertes, S.; Borrmann, S.; Curtius, J. Chemical composition of ambient aerosol, ice  
 2753 residues and cloud droplet residues in mixed-phase clouds: single particle analysis during  
 2754 the Cloud and Aerosol Characterization Experiment (CLACE 6). *Atmos. Chem. Phys.*  
 2755 **2010**, *10*, 8077-8095.
- 2756 (72) DeMott, P. J.; Prenni, A. J.; McMeeking, G. R.; Sullivan, R. C.; Petters, M. D.; Tobo, Y.;  
 2757 Niemand, M.; Möhler, O.; Snider, J. R.; Wang, Z. *et al.* Integrating laboratory and field  
 2758 data to quantify the immersion freezing ice nucleation activity of mineral dust particles.  
 2759 *Atmos. Chem. Phys.* **2015**, *15*, 393-409.
- 2760 (73) Prenni, A. J.; Petters, M. D.; Kreidenweis, S. M.; Heald, C. L.; Martin, S. T.; Artaxo, P.;  
 2761 Garland, R. M.; Wollny, A. G.; Poschl, U. Relative roles of biogenic emissions and  
 2762 Saharan dust as ice nuclei in the Amazon basin. *Nat. Geosci.* **2009**, *2*, 401-404.
- 2763 (74) Cziczo, D. J.; Froyd, K. D.; Hoose, C.; Jensen, E. J.; Diao, M.; Zondlo, M. A.; Smith, J.  
 2764 B.; Twohy, C. H.; Murphy, D. M. Clarifying the Dominant Sources and Mechanisms of  
 2765 Cirrus Cloud Formation. *Science* **2013**, *340*, 1320-1324.
- 2766 (75) Hoose, C.; Kristjansson, J. E.; Burrows, S. M. How important is biological ice nucleation  
 2767 in clouds on a global scale? *Environ. Res. Lett.* **2010**, *5*, 024009.
- 2768 (76) Lohmann, U.; Feichter, J. Global indirect aerosol effects: a review. *Atmos. Chem. Phys.*  
 2769 **2005**, *5*, 715-737.
- 2770 (77) Baker, M. B. Cloud microphysics and climate. *Science* **1997**, *276*, 1072-1078.
- 2771 (78) Gettelman, A.; Liu, X.; Barahona, D.; Lohmann, U.; Chen, C. Climate impacts of ice  
 2772 nucleation. *J. Geophys. Res.-Atmos.* **2012**, *117*.
- 2773 (79) Wiacek, A.; Peter, T. On the availability of uncoated mineral dust ice nuclei in cold cloud  
 2774 regions. *Geophys. Res. Lett.* **2009**, *36*.
- 2775 (80) Rosenfeld, D.; Lohmann, U.; Raga, G. B.; O'Dowd, C. D.; Kulmala, M.; Fuzzi, S.;  
 2776 Reissell, A.; Andreae, M. O. Flood or drought: How do aerosols affect precipitation?  
 2777 *Science* **2008**, *321*, 1309-1313.
- 2778 (81) Yin, Y.; Wurzler, S.; Levin, Z.; Reisin, T. G. Interactions of mineral dust particles and  
 2779 clouds: Effects on precipitation and cloud optical properties. *J. Geophys. Res.-Atmos.*  
 2780 **2002**, *107*, 4724, doi: 4710.1029/2001jd001544.
- 2781 (82) Ramanathan, V.; Crutzen, P. J.; Kiehl, J. T.; Rosenfeld, D. Atmosphere - Aerosols,  
 2782 climate, and the hydrological cycle. *Science* **2001**, *294*, 2119-2124.
- 2783 (83) Rosenfeld, D.; Rudich, Y.; Lahav, R. Desert dust suppressing precipitation: A possible  
 2784 desertification feedback loop. *Proc. Natl. Acad. Sci. U. S. A.* **2001**, *98*, 5975-5980.
- 2785 (84) Shi, Z. B.; Krom, M. D.; Jickells, T. D.; Bonneville, S.; Carslaw, K. S.; Mihalopoulos,  
 2786 N.; Baker, A. R.; Benning, L. G. Impacts on iron solubility in the mineral dust by  
 2787 processes in the source region and the atmosphere: A review. *Aeolian Res.* **2012**, *5*, 21-  
 2788 42.
- 2789 (85) Boyd, P. W.; Ellwood, M. J. The biogeochemical cycle of iron in the ocean. *Nature*  
 2790 *Geosci* **2010**, *3*, 675-682.
- 2791 (86) Boyd, P. W.; Jickells, T.; Law, C. S.; Blain, S.; Boyle, E. A.; Buesseler, K. O.; Coale, K.  
 2792 H.; Cullen, J. J.; de Baar, H. J. W.; Follows, M. *et al.* Mesoscale Iron Enrichment  
 2793 Experiments 1993-2005: Synthesis and Future Directions. *Science* **2007**, *315*, 612-617.
- 2794 (87) Moore, J. K.; Braucher, O. Sedimentary and mineral dust sources of dissolved iron to the  
 2795 world ocean. *Biogeosciences* **2008**, *5*, 631-656.



- 2796 (88) Nenes, A.; Krom, M. D.; Mihalopoulos, N.; Van Cappellen, P.; Shi, Z.; Bougiatioti, A.;  
2797 Zampas, P.; Herut, B. Atmospheric acidification of mineral aerosols: a source of  
2798 bioavailable phosphorus for the oceans. *Atmos. Chem. Phys.* **2011**, *11*, 6265-6272.
- 2799 (89) Okin, G. S.; Baker, A. R.; Tegen, I.; Mahowald, N. M.; Dentener, F. J.; Duce, R. A.;  
2800 Galloway, J. N.; Hunter, K.; Kanakidou, M.; Kubilay, N. *et al.* Impacts of atmospheric  
2801 nutrient deposition on marine productivity: Roles of nitrogen, phosphorus, and iron.  
2802 *Glob. Biogeochem. Cycle* **2011**, *25*, GB2022, doi: 2010.1029/2010GB003858.
- 2803 (90) Okin, G. S.; Mahowald, N.; Chadwick, O. A.; Artaxo, P. Impact of desert dust on the  
2804 biogeochemistry of phosphorus in terrestrial ecosystems. *Glob. Biogeochem. Cycle* **2004**,  
2805 *18*, GB2005, doi: 2010.1029/2003GB002145.
- 2806 (91) Mahowald, N.; Jickells, T. D.; Baker, A. R.; Artaxo, P.; Benitez-Nelson, C. R.;  
2807 Bergametti, G.; Bond, T. C.; Chen, Y.; Cohen, D. D.; Herut, B. *et al.* Global distribution  
2808 of atmospheric phosphorus sources, concentrations and deposition rates, and  
2809 anthropogenic impacts. *Glob. Biogeochem. Cycle* **2008**, *22*, GB4026, doi:  
2810 4010.1029/2008GB003240.
- 2811 (92) Jordi, A.; Basterretxea, G.; Tovar-Sánchez, A.; Alastuey, A.; Querol, X. Copper aerosols  
2812 inhibit phytoplankton growth in the Mediterranean Sea. *Proc. Natl. Acad. Sci. U.S.A.*  
2813 **2012**, *109*, 21246-21249.
- 2814 (93) Paytan, A.; Mackey, K. R. M.; Chen, Y.; Lima, I. D.; Doney, S. C.; Mahowald, N.;  
2815 Labiosa, R.; Post, A. F. Toxicity of atmospheric aerosols on marine phytoplankton. *Proc.*  
2816 *Natl. Acad. Sci. U.S.A.* **2009**, *106*, 4601-4605.
- 2817 (94) Mahowald, N. M.; Baker, A. R.; Bergametti, G.; Brooks, N.; Duce, R. A.; Jickells, T. D.;  
2818 Kubilay, N.; Prospero, J. M.; Tegen, I. Atmospheric global dust cycle and iron inputs to  
2819 the ocean. *Glob. Biogeochem. Cycle* **2005**, *19*, GB4025, doi:4010.1029/2004GB002402.
- 2820 (95) Schulz, M.; Prospero, J. M.; Baker, A. R.; Dentener, F.; Ickes, L.; Liss, P. S.; Mahowald,  
2821 N. M.; Nickovic, S.; García-Pando, C. P.; Rodríguez, S. *et al.* Atmospheric Transport and  
2822 Deposition of Mineral Dust to the Ocean: Implications for Research Needs. *Environ. Sci.*  
2823 *Technol.* **2012**, *46*, 10390-10404.
- 2824 (96) Meskhidze, N.; Chameides, W. L.; Nenes, A. Dust and pollution: A recipe for enhanced  
2825 ocean fertilization? *J. Geophys. Res.-Atmos.* **2005**, *110*, D03301, doi:  
2826 03310.01029/02004jd005082.
- 2827 (97) Paytan, A.; McLaughlin, K. The Oceanic Phosphorus Cycle. *Chem. Rev.* **2007**, *107*, 563-  
2828 576.
- 2829 (98) Bristow, C. S.; Hudson-Edwards, K. A.; Chappell, A. Fertilizing the Amazon and  
2830 equatorial Atlantic with West African dust. *Geophys. Res. Lett.* **2010**, *37*, L14807, doi:  
2831 14810.11029/12010GL043486.
- 2832 (99) Yu, H.; Chin, M.; Yuan, T.; Bian, H.; Remer, L. A.; Prospero, J. M.; Omar, A.; Winker,  
2833 D.; Yang, Y.; Zhang, Y. *et al.* The Fertilizing Role of African Dust in the Amazon  
2834 Rainforest: A First Multiyear Assessment Based on CALIPSO Lidar Observations.  
2835 *Geophys. Res. Lett.* **2015**, *42*, GL063040, doi: 063010.061002/062015GL063040.
- 2836 (100) Mahowald, N.; Ward, D. S.; Kloster, S.; Flanner, M. G.; Heald, C. L.; Heavens, N. G.;  
2837 Hess, P. G.; Lamarque, J.-F.; Chuang, P. Y. Aerosol Impacts on Climate and  
2838 Biogeochemistry. *Annu. Rev. Environ. Resour.* **2011**, *36*, 45-74.
- 2839 (101) Jickells, T. D.; An, Z. S.; Andersen, K. K.; Baker, A. R.; Bergametti, G.; Brooks, N.;  
2840 Cao, J. J.; Boyd, P. W.; Duce, R. A.; Hunter, K. A. *et al.* Global iron connections  
2841 between desert dust, ocean biogeochemistry, and climate. *Science* **2005**, *308*, 67-71.
- 2842 (102) Garrison, V. H.; Shinn, E. A.; Foreman, W. T.; Griffin, D. W.; Holmes, C. W.; Kellogg,  
2843 C. A.; Majewski, M. S.; Richardson, L. L.; Ritchie, K. B.; Smith, G. W. African and  
2844 Asian Dust: From Desert Soils to Coral Reefs. *BioScience* **2003**, *53*, 469-480.

- 2845 (103) Jickells, T.; Boyd, P.; Hunter, K. In *Mineral Dust*; Knippertz, P., Stuut, J.-B. W., Eds.;  
2846 Springer: Netherlands, 2014.
- 2847 (104) Zhu, T.; Shang, J.; Zhao, D. F. The roles of heterogeneous chemical processes in the  
2848 formation of an air pollution complex and gray haze. *Sci. China-Chem.* **2011**, *54*, 145-  
2849 153.
- 2850 (105) Lelieveld, J.; Evans, J. S.; Fnais, M.; Giannadaki, D.; Pozzer, A. The contribution of  
2851 outdoor air pollution sources to premature mortality on a global scale. *Nature* **2015**, *525*,  
2852 367-371.
- 2853 (106) Morman, S.; Plumlee, G. In *Mineral Dust*; Knippertz, P., Stuut, J.-B. W., Eds.; Springer:  
2854 Netherlands, 2014.
- 2855 (107) Mahowald, N. M.; Ballantine, J. A.; Feddema, J.; Ramankutty, N. Global trends in  
2856 visibility: implications for dust sources. *Atmos. Chem. Phys.* **2007**, *7*, 3309-3339.
- 2857 (108) Giannadaki, D.; Pozzer, A.; Lelieveld, J. Modeled global effects of airborne desert dust  
2858 on air quality and premature mortality. *Atmos. Chem. Phys.* **2014**, *14*, 957-968.
- 2859 (109) De Longueville, F.; Hountondji, Y.-C.; Henry, S.; Ozer, P. What do we know about  
2860 effects of desert dust on air quality and human health in West Africa compared to other  
2861 regions? *Sci. Total Environ.* **2010**, *409*, 1-8.
- 2862 (110) de Longueville, F.; Ozer, P.; Doumbia, S.; Henry, S. Desert dust impacts on human  
2863 health: an alarming worldwide reality and a need for studies in West Africa. *Int. J.*  
2864 *Biometeorol.* **2013**, *57*, 1-19.
- 2865 (111) Perez, L.; Tobias, A.; Querol, X.; Künzli, N.; Pey, J.; Alastuey, A.; Viana, M.; Valero,  
2866 N.; González-Cabré, M.; Sunyer, J. Coarse Particles From Saharan Dust and Daily  
2867 Mortality. *Epidemiology* **2008**, *19*, 800-807.
- 2868 (112) Karanasiou, A.; Moreno, N.; Moreno, T.; Viana, M.; de Leeuw, F.; Querol, X. Health  
2869 effects from Sahara dust episodes in Europe: Literature review and research gaps.  
2870 *Environ. Int.* **2012**, *47*, 107-114.
- 2871 (113) Meng, Z.; Lu, B. Dust events as a risk factor for daily hospitalization for respiratory and  
2872 cardiovascular diseases in Minqin, China. *Atmos. Environ.* **2007**, *41*, 7048-7058.
- 2873 (114) Kwon, H.-J.; Cho, S.-H.; Chun, Y.; Lagarde, F.; Pershagen, G. Effects of the Asian Dust  
2874 Events on Daily Mortality in Seoul, Korea. *Environ. Res.* **2002**, *90*, 1-5.
- 2875 (115) Fubini, B.; Otero Arean, C. Chemical aspects of the toxicity of inhaled mineral dusts.  
2876 *Chem. Soc. Rev.* **1999**, *28*, 373-381.
- 2877 (116) Thalib, L.; Al-Taiar, A. Dust storms and the risk of asthma admissions to hospitals in  
2878 Kuwait. *Sci. Total Environ.* **2012**, *433*, 347-351.
- 2879 (117) Yang, C.-Y.; Chen, Y.-S.; Chiu, H.-F.; Goggins, W. B. Effects of Asian dust storm events  
2880 on daily stroke admissions in Taipei, Taiwan. *Environ. Res.* **2005**, *99*, 79-84.
- 2881 (118) Tobías, A.; Pérez, L.; Díaz, J.; Linares, C.; Pey, J.; Alastruey, A.; Querol, X. Short-term  
2882 effects of particulate matter on total mortality during Saharan dust outbreaks: A case-  
2883 crossover analysis in Madrid (Spain). *Sci. Total Environ.* **2011**, *412-413*, 386-389.
- 2884 (119) Chen, Y.-S.; Sheen, P.-C.; Chen, E.-R.; Liu, Y.-K.; Wu, T.-N.; Yang, C.-Y. Effects of  
2885 Asian dust storm events on daily mortality in Taipei, Taiwan. *Environ. Res.* **2004**, *95*,  
2886 151-155.
- 2887 (120) Alessandrini, E. R.; Stafoggia, M.; Faustini, A.; Gobbi, G. P.; Forastiere, F. Saharan dust  
2888 and the association between particulate matter and daily hospitalisations in Rome, Italy.  
2889 *Occup. Environ. Med.* **2013**, *70*, 432-434.
- 2890 (121) Claquin, T.; Schulz, M.; Balkanski, Y. J. Modeling the mineralogy of atmospheric dust  
2891 sources. *J. Geophys. Res.-Atmos.* **1999**, *104*, 22243-22256.

- 2892 (122) Nickovic, S.; Vukovic, A.; Vujadinovic, M.; Djurdjevic, V.; Pejanovic, G. Technical  
 2893 Note: High-resolution mineralogical database of dust-productive soils for atmospheric  
 2894 dust modeling. *Atmos. Chem. Phys.* **2012**, *12*, 845-855.
- 2895 (123) Journet, E.; Balkanski, Y.; Harrison, S. P. A new data set of soil mineralogy for dust-  
 2896 cycle modeling. *Atmos. Chem. Phys.* **2014**, *14*, 3801-3816.
- 2897 (124) Formenti, P.; Schutz, L.; Balkanski, Y.; Desboeufs, K.; Ebert, M.; Kandler, K.; Petzold,  
 2898 A.; Scheuvens, D.; Weinbruch, S.; Zhang, D. Recent progress in understanding physical  
 2899 and chemical properties of African and Asian mineral dust. *Atmos. Chem. Phys.* **2011**, *11*,  
 2900 8231-8256.
- 2901 (125) Klaver, A.; Formenti, P.; Caquineau, S.; Chevaillier, S.; Ausset, P.; Calzolari, G.;  
 2902 Osborne, S.; Johnson, B.; Harrison, M.; Dubovik, O. Physico-chemical and optical  
 2903 properties of Sahelian and Saharan mineral dust: in situ measurements during the  
 2904 GERBILS campaign. *Q. J. R. Meteorol. Soc.* **2011**, *137*, 1193-1210.
- 2905 (126) Fitzgerald, E.; Ault, A. P.; Zauscher, M. D.; Mayol-Bracero, O. L.; Prather, K. A.  
 2906 Comparison of the mixing state of long-range transported Asian and African mineral  
 2907 dust. *Atmos. Environ.* **2015**, *115*, 19-25.
- 2908 (127) Scheuvens, D.; Schütz, L.; Kandler, K.; Ebert, M.; Weinbruch, S. Bulk composition of  
 2909 northern African dust and its source sediments - A compilation. *Earth-Sci. Rev.* **2013**,  
 2910 *116*, 170-194.
- 2911 (128) Scheuvens, D.; Kandler, K. In *Mineral Dust*; Knippertz, P., Stuut, J.-B. W., Eds.;  
 2912 Springer: Netherlands, 2014.
- 2913 (129) Perchwitz, J. P.; Pérez García-Pando, C.; Miller, R. L. Predicting the mineral composition  
 2914 of dust aerosols – Part 1: Representing key processes. *Atmos. Chem. Phys.* **2015**, *15*,  
 2915 11593-11627.
- 2916 (130) Perchwitz, J. P.; Pérez García-Pando, C.; Miller, R. L. Predicting the mineral composition  
 2917 of dust aerosols – Part 2: Model evaluation and identification of key processes with  
 2918 observations. *Atmos. Chem. Phys.* **2015**, *15*, 11629-11652.
- 2919 (131) Seisel, S.; Borensen, C.; Vogt, R.; Zellner, R. Kinetics and mechanism of the uptake of  
 2920 N<sub>2</sub>O<sub>5</sub> on mineral dust at 298 K. *Atmos. Chem. Phys.* **2005**, *5*, 3423-3432.
- 2921 (132) Karagulian, F.; Santschi, C.; Rossi, M. J. The heterogeneous chemical kinetics of N<sub>2</sub>O<sub>5</sub>  
 2922 on CaCO<sub>3</sub> and other atmospheric mineral dust surrogates. *Atmos. Chem. Phys.* **2006**, *6*,  
 2923 1373-1388.
- 2924 (133) Mogili, P. K.; Kleiber, P. D.; Young, M. A.; Grassian, V. H. N<sub>2</sub>O<sub>5</sub> hydrolysis on the  
 2925 components of mineral dust and sea salt aerosol: Comparison study in an environmental  
 2926 aerosol reaction chamber. *Atmos. Environ.* **2006**, *40*, 7401-7408.
- 2927 (134) Wagner, C.; Hanisch, F.; Holmes, N.; de Coninck, H.; Schuster, G.; Crowley, J. N. The  
 2928 interaction of N<sub>2</sub>O<sub>5</sub> with mineral dust: aerosol flow tube and Knudsen reactor studies.  
 2929 *Atmos. Chem. Phys.* **2008**, *8*, 91-109.
- 2930 (135) Wagner, C.; Schuster, G.; Crowley, J. N. An aerosol flow tube study of the interaction of  
 2931 N<sub>2</sub>O<sub>5</sub> with calcite, Arizona dust and quartz. *Atmos. Environ.* **2009**, *43*, 5001-5008.
- 2932 (136) Tang, M. J.; Thieser, J.; Schuster, G.; Crowley, J. N. Kinetics and mechanism of the  
 2933 heterogeneous reaction of N<sub>2</sub>O<sub>5</sub> with mineral dust particles. *Phys. Chem. Chem. Phys.*  
 2934 **2012**, *14*, 8551-8561.
- 2935 (137) Tang, M. J.; Schuster, G.; Crowley, J. N. Heterogeneous reaction of N<sub>2</sub>O<sub>5</sub> with illite and  
 2936 Arizona test dust particles. *Atmos. Chem. Phys.* **2014**, *14*, 245-254.
- 2937 (138) Tang, M. J.; Telford, P. J.; Pope, F. D.; Rkiouak, L.; Abraham, N. L.; Archibald, A. T.;  
 2938 Braesicke, P.; Pyle, J. A.; McGregor, J.; Watson, I. M. *et al.* Heterogeneous reaction of  
 2939 N<sub>2</sub>O<sub>5</sub> with airborne TiO<sub>2</sub> particles and its implication for stratospheric particle injection.  
 2940 *Atmos. Chem. Phys.* **2014**, *14*, 6035-6048.

- 2941 (139) Tang, M. J.; Camp, J. C. J.; Rkiouak, L.; McGregor, J.; Watson, I. M.; Cox, R. A.;  
 2942 Kalberer, M.; Ward, A. D.; Pope, F. D. Heterogeneous Interaction of SiO<sub>2</sub> with N<sub>2</sub>O<sub>5</sub>:  
 2943 Aerosol Flow Tube and Single Particle Optical Levitation-Raman Spectroscopy Studies.  
 2944 *J. Phys. Chem. A* **2014**, *118*, 8817-8827.
- 2945 (140) Murray, B. J.; O'Sullivan, D.; Atkinson, J. D.; Webb, M. E. Ice nucleation by particles  
 2946 immersed in supercooled cloud droplets. *Chem. Soc. Rev.* **2012**, *41*, 6519-6554.
- 2947 (141) Atkinson, J. D.; Murray, B. J.; Woodhouse, M. T.; Whale, T. F.; Baustian, K. J.; Carslaw,  
 2948 K. S.; Dobbie, S.; O'Sullivan, D.; Malkin, T. L. The importance of feldspar for ice  
 2949 nucleation by mineral dust in mixed-phase clouds. *Nature* **2013**, *498*, 355-358.
- 2950 (142) Journet, E.; Desboeufs, K. V.; Caquineau, S.; Colin, J.-L. Mineralogy as a critical factor  
 2951 of dust iron solubility. *Geophys. Res. Lett.* **2008**, *35*, L07805, doi:  
 2952 07810.01029/02007GL031589.
- 2953 (143) Cwiertny, D. M.; Baltrusaitis, J.; Hunter, G. J.; Laskin, A.; Scherer, M. M.; Grassian, V.  
 2954 H. Characterization and acid-mobilization study of iron-containing mineral dust source  
 2955 materials. *J. Geophys. Res.-Atmos.* **2008**, *113*, D05202, doi:  
 2956 05210.01029/02007JD009332.
- 2957 (144) Fu, H. B.; Cwiertny, D. M.; Carmichael, G. R.; Scherer, M. M.; Grassian, V. H.  
 2958 Photoreductive dissolution of Fe-containing mineral dust particles in acidic media. *J.*  
 2959 *Geophys. Res.-Atmos.* **2010**, *115*, D11304, doi: 11310.11029/12009JD012702.
- 2960 (145) Formenti, P.; Caquineau, S.; Desboeufs, K.; Klaver, A.; Chevaillier, S.; Journet, E.;  
 2961 Rajot, J. L. Mapping the physico-chemical properties of mineral dust in western Africa:  
 2962 mineralogical composition. *Atmos. Chem. Phys.* **2014**, *14*, 10663-10686.
- 2963 (146) Jeong, G. Y. Bulk and single-particle mineralogy of Asian dust and a comparison with its  
 2964 source soils. *J. Geophys. Res.-Atmos.* **2008**, *113*, D02208, doi:  
 2965 02210.01029/02007jd008606.
- 2966 (147) Avila, A.; QueraltMitjans, I.; Alarcon, M. Mineralogical composition of African dust  
 2967 delivered by red rains over northeastern Spain. *J. Geophys. Res.-Atmos.* **1997**, *102*,  
 2968 21977-21996.
- 2969 (148) Caquineau, S.; Gaudichet, A.; Gomes, L.; Legrand, M. Mineralogy of Saharan dust  
 2970 transported over northwestern tropical Atlantic Ocean in relation to source regions. *J.*  
 2971 *Geophys. Res.-Atmos.* **2002**, *107*, 4251, doi: 4210.1029/2000jd000247.
- 2972 (149) Kandler, K.; Schutz, L.; Deutscher, C.; Ebert, M.; Hofmann, H.; Jackel, S.; Jaenicke, R.;  
 2973 Knippertz, P.; Lieke, K.; Massling, A. *et al.* Size distribution, mass concentration,  
 2974 chemical and mineralogical composition and derived optical parameters of the boundary  
 2975 layer aerosol at Tinfou, Morocco, during SAMUM 2006. *Tellus Ser. B-Chem. Phys.*  
 2976 *Meteorol.* **2009**, *61*, 32-50.
- 2977 (150) Scanza, R. A.; Mahowald, N.; Ghan, S.; Zender, C. S.; Kok, J. F.; Liu, X.; Zhang, Y.;  
 2978 Albani, S. Modeling dust as component minerals in the Community Atmosphere Model:  
 2979 development of framework and impact on radiative forcing. *Atmos. Chem. Phys.* **2015**,  
 2980 *15*, 537-561.
- 2981 (151) Hanisch, F.; Crowley, J. N. Ozone decomposition on Saharan dust: an experimental  
 2982 investigation. *Atmos. Chem. Phys.* **2003**, *3*, 119-130.
- 2983 (152) Adedokun, J. A.; Emofurieta, W. O.; Adedeji, O. A. Physical, mineralogical and  
 2984 chemical properties of harmattan dust at Ile-Ife, Nigeria. *Theor. Appl. Climatol.* **1989**, *40*,  
 2985 161-169.
- 2986 (153) Hsu, S.-C.; Liu, S. C.; Huang, Y.-T.; Chou, C. C. K.; Lung, S. C. C.; Liu, T.-H.; Tu, J.-  
 2987 Y.; Tsai, F. Long-range southeastward transport of Asian biomass pollution: Signature  
 2988 detected by aerosol potassium in Northern Taiwan. *J. Geophys. Res.-Atmos* **2009**, *114*,  
 2989 D14301, doi: 14310.11029/12009JD011725.

- 2990 (154) George, C.; D'Anna, B.; Herrmann, H.; Weller, C.; Vaida, V.; Donaldson, D. J.; Bartels-  
 2991 Rausch, T.; Ammann, M. In *Atmospheric and Aerosol Chemistry*; McNeill, V. F., Ariya,  
 2992 P. A., Eds.; Springer Berlin Heidelberg, 2014; Vol. 339.
- 2993 (155) Chen, H. H.; Nanayakkara, C. E.; Grassian, V. H. Titanium Dioxide Photocatalysis in  
 2994 Atmospheric Chemistry. *Chem. Rev.* **2012**, *112*, 5919-5948.
- 2995 (156) George, C.; Ammann, M.; D'Anna, B.; Donaldson, D. J.; Nizkorodov, S. A.  
 2996 Heterogeneous Photochemistry in the Atmosphere. *Chem. Rev.* **2015**, *115*, 4218-4258.
- 2997 (157) Harris, E.; Sinha, B.; van Pinxteren, D.; Tilgner, A.; Fomba, K. W.; Schneider, J.; Roth,  
 2998 A.; Gnauk, T.; Fahlbusch, B.; Mertes, S. *et al.* Enhanced Role of Transition Metal Ion  
 2999 Catalysis During In-Cloud Oxidation of SO<sub>2</sub>. *Science* **2013**, *340*, 727-730.
- 3000 (158) Sullivan, R. C.; Guazzotti, S. A.; Sodeman, D. A.; Prather, K. A. Direct observations of  
 3001 the atmospheric processing of Asian mineral dust. *Atmos. Chem. Phys.* **2007**, *7*, 1213-  
 3002 1236.
- 3003 (159) Matsuki, A.; Iwasaka, Y.; Shi, G. Y.; Zhang, D. Z.; Trochkin, D.; Yamada, M.; Kim, Y.  
 3004 S.; Chen, B.; Nagatani, T.; Miyazawa, T. *et al.* Morphological and chemical modification  
 3005 of mineral dust: Observational insight into the heterogeneous uptake of acidic gases.  
 3006 *Geophys. Res. Lett.* **2005**, *32*, L22806, doi: 22810.21029/22005gl024176.
- 3007 (160) Mori, I.; Nishikawa, M.; Tanimura, T.; Quan, H. Change in size distribution and  
 3008 chemical composition of kosa (Asian dust) aerosol during long-range transport. *Atmos.*  
 3009 *Environ.* **2003**, *37*, 4253-4263.
- 3010 (161) Usher, C. R.; Michel, A. E.; Grassian, V. H. Reactions on mineral dust. *Chem. Rev.* **2003**,  
 3011 *103*, 4883-4939.
- 3012 (162) Matsuki, A.; Schwarzenboeck, A.; Venzac, H.; Laj, P.; Crumeyrolle, S.; Gomes, L. Cloud  
 3013 processing of mineral dust: direct comparison of cloud residual and clear sky particles  
 3014 during AMMA aircraft campaign in summer 2006. *Atmos. Chem. Phys.* **2010**, *10*, 1057-  
 3015 1069.
- 3016 (163) Pope, F. D.; Braesicke, P.; Grainger, R. G.; Kalberer, M.; Watson, I. M.; Davidson, P. J.;  
 3017 Cox, R. A. Stratospheric aerosol particles and solar-radiation management. *Nature Clim.*  
 3018 *Change* **2012**, *2*, 713-719.
- 3019 (164) Ferraro, A. J.; Highwood, E. J.; Charlton-Perez, A. J. Stratospheric heating by potential  
 3020 geoengineering aerosols. *Geophys. Res. Lett.* **2011**, *38*, L24706, doi:  
 3021 24710.21029/22011gl049761.
- 3022 (165) Weisenstein, D. K.; Keith, D. W. Solar geoengineering using solid aerosol in the  
 3023 stratosphere. *Atmos. Chem. Phys. Discuss.* **2015**, *15*, 11799-11851.
- 3024 (166) Crutzen, P. J. Albedo enhancement by stratospheric sulfur injections: A contribution to  
 3025 resolve a policy dilemma? *Clim. Change* **2006**, *77*, 211-219.
- 3026 (167) Pruppacher, H. R.; Klett, J. D. *Microphysics of Clouds and Precipitation* Kluwer  
 3027 Academic Publishers: Dordrecht, Netherlands 1994.
- 3028 (168) Dusek, U.; Frank, G. P.; Hildebrandt, L.; Curtius, J.; Schneider, J.; Walter, S.; Chand, D.;  
 3029 Drewnick, F.; Hings, S.; Jung, D. *et al.* Size Matters More Than Chemistry for Cloud-  
 3030 Nucleating Ability of Aerosol Particles. *Science* **2006**, *312*, 1375-1378.
- 3031 (169) Petters, M. D.; Kreidenweis, S. M. A single parameter representation of hygroscopic  
 3032 growth and cloud condensation nucleus activity. *Atmos. Chem. Phys.* **2007**, *7*, 1961-1971.
- 3033 (170) McFiggans, G.; Artaxo, P.; Baltensperger, U.; Coe, H.; Facchini, M. C.; Feingold, G.;  
 3034 Fuzzi, S.; Gysel, M.; Laaksonen, A.; Lohmann, U. *et al.* The effect of physical and  
 3035 chemical aerosol properties on warm cloud droplet activation. *Atmos. Chem. Phys.* **2006**,  
 3036 *6*, 2593-2649.
- 3037 (171) Cwiertny, D. M.; Young, M. A.; Grassian, V. H. Chemistry and photochemistry of  
 3038 mineral dust aerosol. *Annu. Rev. Phys. Chem.* **2008**, *59*, 27-51.

- 3039 (172) Crowley, J. N.; Ammann, M.; Cox, R. A.; Hynes, R. G.; Jenkin, M. E.; Mellouki, A.;  
3040 Rossi, M. J.; Troe, J.; Wallington, T. J. Evaluated kinetic and photochemical data for  
3041 atmospheric chemistry: Volume V - heterogeneous reactions on solid substrates. *Atmos.*  
3042 *Chem. Phys.* **2010**, *10*, 9059-9223.
- 3043 (173) Kolb, C. E.; Cox, R. A.; Abbatt, J. P. D.; Ammann, M.; Davis, E. J.; Donaldson, D. J.;  
3044 Garrett, B. C.; George, C.; Griffiths, P. T.; Hanson, D. R. *et al.* An overview of current  
3045 issues in the uptake of atmospheric trace gases by aerosols and clouds. *Atmos. Chem.*  
3046 *Phys.* **2010**, *10*, 10561-10605.
- 3047 (174) Tong, S. R.; Wu, L. Y.; Ge, M. F.; Wang, W. G.; Pu, Z. F. Heterogeneous chemistry of  
3048 monocarboxylic acids on  $\alpha$ -Al<sub>2</sub>O<sub>3</sub> at different relative humidities. *Atmos. Chem. Phys.*  
3049 **2010**, *10*, 7561-7574.
- 3050 (175) Wu, L. Y.; Tong, S. R.; Wang, W. G.; Ge, M. F. Effects of temperature on the  
3051 heterogeneous oxidation of sulfur dioxide by ozone on calcium carbonate. *Atmos. Chem.*  
3052 *Phys.* **2011**, *11*, 6593-6605.
- 3053 (176) Tang, M. J.; Li, M. Q.; Zhu, T. Heterogeneous reactions of gaseous methanesulfonic acid  
3054 with calcium carbonate and kaolinite particles. *Sci. China-Chem.* **2010**, *53*, 2657-2662.
- 3055 (177) Tang, M. J.; Thieser, J.; Schuster, G.; Crowley, J. N. Uptake of NO<sub>3</sub> and N<sub>2</sub>O<sub>5</sub> to Saharan  
3056 dust, ambient urban aerosol and soot: a relative rate study. *Atmos. Chem. Phys.* **2010**, *10*,  
3057 2965-2974.
- 3058 (178) Fu, H. B.; Wang, X.; Wu, H. B.; Yin, Y.; Chen, J. M. Heterogeneous uptake and  
3059 oxidation of SO<sub>2</sub> on iron oxides. *J. Phys. Chem. C* **2007**, *111*, 6077-6085.
- 3060 (179) Kong, L. D.; Zhao, X.; Sun, Z. Y.; Yang, Y. W.; Fu, H. B.; Zhang, S. C.; Cheng, T. T.;  
3061 Yang, X.; Wang, L.; Chen, J. M. The effects of nitrate on the heterogeneous uptake of  
3062 sulfur dioxide on hematite. *Atmos. Chem. Phys.* **2014**, *14*, 9451-9467.
- 3063 (180) Zhao, X.; Kong, L. D.; Sun, Z. Y.; Ding, X. X.; Cheng, T. T.; Yang, X.; Chen, J. M.  
3064 Interactions between Heterogeneous Uptake and Adsorption of Sulfur Dioxide and  
3065 Acetaldehyde on Hematite. *J. Phys. Chem. A* **2015**, *119*, 4001-4008.
- 3066 (181) He, H.; Wang, Y.; Ma, Q.; Ma, J.; Chu, B.; Ji, D.; Tang, G.; Liu, C.; Zhang, H.; Hao, J.  
3067 Mineral dust and NO<sub>x</sub> promote the conversion of SO<sub>2</sub> to sulfate in heavy pollution days.  
3068 *Sci. Rep.* **2014**, *4*, 4172, doi: 4110.1038/srep04172.
- 3069 (182) Ma, Q.; Liu, Y.; Liu, C.; Ma, J.; He, H. A case study of Asian dust storm particles:  
3070 Chemical composition, reactivity to SO<sub>2</sub> and hygroscopic properties. *J. Environ. Sci.*  
3071 **2012**, *24*, 62-71.
- 3072 (183) Wu, L.-Y.; Tong, S.-R.; Zhou, L.; Wang, W.-G.; Ge, M.-F. Synergistic Effects between  
3073 SO<sub>2</sub> and HCOOH on  $\alpha$ -Fe<sub>2</sub>O<sub>3</sub>. *J. Phys. Chem. A* **2013**, *117*, 3972-3979.
- 3074 (184) Zhou, L.; Wang, W. G.; Gai, Y. B.; Ge, M. F. Knudsen cell and smog chamber study of  
3075 the heterogeneous uptake of sulfur dioxide on Chinese mineral dust. *J. Environ. Sci.*  
3076 **2014**, *26*, 2423-2433.
- 3077 (185) Zhao, Y.; Chen, Z. M.; Shen, X. L.; Huang, D. Heterogeneous reactions of gaseous  
3078 hydrogen peroxide on pristine and acidic gas-processed calcium carbonate particles:  
3079 Effects of relative humidity and surface coverage of coating. *Atmos. Environ.* **2013**, *67*,  
3080 63-72.
- 3081 (186) Zhao, Y.; Chen, Z. M.; Shen, X. L.; Zhang, X. A. Kinetics and Mechanisms of  
3082 Heterogeneous Reaction of Gaseous Hydrogen Peroxide on Mineral Oxide Particles.  
3083 *Environ. Sci. Technol.* **2011**, *45*, 3317-3324.
- 3084 (187) Arimoto, R.; Kim, Y. J.; Kim, Y. P.; Quinn, P. K.; Bates, T. S.; Anderson, T. L.; Gong,  
3085 S.; Uno, I.; Chin, M.; Huebert, B. J. *et al.* Characterization of Asian Dust during ACE-  
3086 Asia. *Glob. Planet. Change* **2006**, *52*, 23-56.

- 3087 (188) Deguillaume, L.; Leriche, M.; Desboeufs, K.; Mailhot, G.; George, C.; Chaumerliac, N.  
3088 Transition metals in atmospheric liquid phases: Sources, reactivity, and sensitive  
3089 parameters. *Chem. Rev.* **2005**, *105*, 3388-3431.
- 3090 (189) Jacob, D. J. Heterogeneous chemistry and tropospheric ozone. *Atmos. Environ.* **2000**, *34*,  
3091 2131-2159.
- 3092 (190) Hoose, C.; Lohmann, U.; Bennartz, R.; Croft, B.; Lesins, G. Global simulations of  
3093 aerosol processing in clouds. *Atmos. Chem. Phys.* **2008**, *8*, 6939-6963.
- 3094 (191) Desboeufs, K.; Journet, E.; Rajot, J. L.; Chevaillier, S.; Triquet, S.; Formenti, P.; Zakou,  
3095 A. Chemistry of rain events in West Africa: evidence of dust and biogenic influence in  
3096 convective systems. *Atmos. Chem. Phys.* **2010**, *10*, 9283-9293.
- 3097 (192) Dentener, F. J.; Carmichael, G. R.; Zhang, Y.; Lelieveld, J.; Crutzen, P. J. Role of  
3098 mineral aerosol as a reactive surface in the global troposphere. *J. Geophys. Res.-Atmos.*  
3099 **1996**, *101*, 22869-22889.
- 3100 (193) de Reus, M.; Fischer, H.; Sander, R.; Gros, V.; Kormann, R.; Salisbury, G.; Van  
3101 Dingenen, R.; Williams, J.; Zollner, M.; Lelieveld, J. Observations and model  
3102 calculations of trace gas scavenging in a dense Saharan dust plume during MINATROC.  
3103 *Atmos. Chem. Phys.* **2005**, *5*, 1787-1803.
- 3104 (194) Bauer, S. E.; Balkanski, Y.; Schulz, M.; Hauglustaine, D. A.; Dentener, F. Global  
3105 modeling of heterogeneous chemistry on mineral aerosol surfaces: Influence on  
3106 tropospheric ozone chemistry and comparison to observations. *J. Geophys. Res.-Atmos.*  
3107 **2004**, *109*, D02304, doi: 02310.01029/02003JD003868.
- 3108 (195) Matthews, P. S. J.; Baeza-Romero, M. T.; Whalley, L. K.; Heard, D. E. Uptake of HO<sub>2</sub>  
3109 radicals onto Arizona test dust particles using an aerosol flow tube. *Atmos. Chem. Phys.*  
3110 **2014**, *14*, 7397-7408.
- 3111 (196) Romanias, M. N.; El Zein, A.; Bedjanian, Y. Heterogeneous Interaction of H<sub>2</sub>O<sub>2</sub> with  
3112 TiO<sub>2</sub> Surface under Dark and UV Light Irradiation Conditions. *J. Phys. Chem. A* **2012**,  
3113 *116*, 8191-8200.
- 3114 (197) El Zein, A.; Romanias, M. N.; Bedjanian, Y. Heterogeneous Interaction of H<sub>2</sub>O<sub>2</sub> with  
3115 Arizona Test Dust. *J. Phys. Chem. A* **2014**, *118*, 441-448.
- 3116 (198) Sullivan, R. C.; Guazzotti, S. A.; Sodeman, D. A.; Tang, Y. H.; Carmichael, G. R.;  
3117 Prather, K. A. Mineral dust is a sink for chlorine in the marine boundary layer. *Atmos.*  
3118 *Environ.* **2007**, *41*, 7166-7179.
- 3119 (199) Goodman, A. L.; Underwood, G. M.; Grassian, V. H. A laboratory study of the  
3120 heterogeneous reaction of nitric acid on calcium carbonate particles. *J. Geophys. Res.-*  
3121 *Atmos.* **2000**, *105*, 29053-29064.
- 3122 (200) Prince, A. P.; Kleiber, P. D.; Grassian, V. H.; Young, M. A. Reactive uptake of acetic  
3123 acid on calcite and nitric acid reacted calcite aerosol in an environmental reaction  
3124 chamber. *Phys. Chem. Chem. Phys.* **2008**, *10*, 142-152.
- 3125 (201) Li, H. J.; Zhu, T.; Zhao, D. F.; Zhang, Z. F.; Chen, Z. M. Kinetics and mechanisms of  
3126 heterogeneous reaction of NO<sub>2</sub> on CaCO<sub>3</sub> surfaces under dry and wet conditions. *Atmos.*  
3127 *Chem. Phys.* **2010**, *10*, 463-474.
- 3128 (202) Li, W. J.; Shao, L. Y. Observation of nitrate coatings on atmospheric mineral dust  
3129 particles. *Atmos. Chem. Phys.* **2009**, *9*, 1863-1871.
- 3130 (203) Li, W. J.; Shao, L. Y. Transmission electron microscopy study of aerosol particles from  
3131 the brown hazes in northern China. *J. Geophys. Res.-Atmos.* **2009**, *114*, D09302, doi:  
3132 09310.01029/02008jd011285.
- 3133 (204) Huang, X.; Song, Y.; Zhao, C.; Li, M.; Zhu, T.; Zhang, Q.; Zhang, X. Pathways of sulfate  
3134 enhancement by natural and anthropogenic mineral aerosols in China. *J. Geophys. Res.-*  
3135 *Atmos* **2014**, *119*, 14165-14179.

- 3136 (205) Tang, Y. H.; Carmichael, G. R.; Seinfeld, J. H.; Dabdub, D.; Weber, R. J.; Huebert, B.;  
3137 Clarke, A. D.; Guazzotti, S. A.; Sodeman, D. A.; Prather, K. A. *et al.* Three-dimensional  
3138 simulations of inorganic aerosol distributions in east Asia during spring 2001. *J.*  
3139 *Geophys. Res.-Atmos.* **2004**, *109*, D19s23, doi: 10.1029/2003jd004201.
- 3140 (206) Hand, V. L.; Capes, G.; Vaughan, D. J.; Formenti, P.; Haywood, J. M.; Coe, H. Evidence  
3141 of internal mixing of African dust and biomass burning particles by individual particle  
3142 analysis using electron beam techniques. *J. Geophys. Res.-Atmos.* **2010**, *115*, D13301,  
3143 doi: 13310.11029/12009jd012938.
- 3144 (207) Formenti, P.; Elbert, W.; Maenhaut, W.; Haywood, J.; Andreae, M. O. Chemical  
3145 composition of mineral dust aerosol during the Saharan Dust Experiment (SHADE)  
3146 airborne campaign in the Cape Verde region, September 2000. *J. Geophys. Res.-Atmos.*  
3147 **2003**, *108*, 8576, doi: 8510.1029/2002jd002648.
- 3148 (208) Sullivan, R. C.; Prather, K. A. Investigations of the diurnal cycle and mixing state of  
3149 oxalic acid in individual particles in Asian aerosol outflow. *Environ. Sci. Technol.* **2007**,  
3150 *41*, 8062-8069.
- 3151 (209) Trochkin, D.; Iwasaka, Y.; Matsuki, A.; Yamada, M.; Kim, Y. S.; Nagatani, T.; Zhang,  
3152 D.; Shi, G. Y.; Shen, Z. Mineral aerosol particles collected in Dunhuang, China, and their  
3153 comparison with chemically modified particles collected over Japan. *J. Geophys. Res.-*  
3154 *Atmos* **2003**, *108*.
- 3155 (210) Matsuki, A.; Iwasaka, Y.; Shi, G. Y.; Chen, H. B.; Osada, K.; Zhang, D.; Kido, M.;  
3156 Inomata, Y.; Kim, Y. S.; Trochkin, D. *et al.* Heterogeneous Sulfate Formation on Dust  
3157 Surface and Its Dependence on Mineralogy: Balloon-Borne Observations from Balloon-  
3158 Borne Measurements in The Surface Atmosphere of Beijing, China. *Water Air Soil*  
3159 *Pollut: Focus* **2005**, *5*, 101-132.
- 3160 (211) Al-Abadleh, H. A.; Krueger, B. J.; Ross, J. L.; Grassian, V. H. Phase transitions in  
3161 calcium nitrate thin films. *Chem. Commun.* **2003**, 2796-2797.
- 3162 (212) Ma, Q. X.; Liu, Y. C.; Liu, C.; He, H. Heterogeneous reaction of acetic acid on MgO,  $\alpha$ -  
3163 Al<sub>2</sub>O<sub>3</sub>, and CaCO<sub>3</sub> and the effect on the hygroscopic behavior of these particles. *Phys.*  
3164 *Chem. Chem. Phys.* **2012**, *14*, 8403-8409.
- 3165 (213) Vlasenko, A.; Sjogren, S.; Weingartner, E.; Stemmler, K.; Gaggeler, H. W.; Ammann, M.  
3166 Effect of humidity on nitric acid uptake to mineral dust aerosol particles. *Atmos. Chem.*  
3167 *Phys.* **2006**, *6*, 2147-2160.
- 3168 (214) Krueger, B. J.; Grassian, V. H.; Laskin, A.; Cowin, J. P. The transformation of solid  
3169 atmospheric particles into liquid droplets through heterogeneous chemistry: Laboratory  
3170 insights into the processing of calcium containing mineral dust aerosol in the troposphere.  
3171 *Geophys. Res. Lett.* **2003**, *30*, 1148, doi: 1110.1029/2002gl016563.
- 3172 (215) Liu, Y. J.; Zhu, T.; Zhao, D. F.; Zhang, Z. F. Investigation of the hygroscopic properties  
3173 of Ca(NO<sub>3</sub>)<sub>2</sub> and internally mixed Ca(NO<sub>3</sub>)<sub>2</sub>/CaCO<sub>3</sub> particles by micro-Raman  
3174 spectrometry. *Atmos. Chem. Phys.* **2008**, *8*, 7205-7215.
- 3175 (216) Hatch, C. D.; Gierlus, K. M.; Schuttlefield, J. D.; Grassian, V. H. Water adsorption and  
3176 cloud condensation nuclei activity of calcite and calcite coated with model humic and  
3177 fulvic acids. *Atmos. Environ.* **2008**, *42*, 5672-5684.
- 3178 (217) Sullivan, R. C.; Moore, M. J. K.; Petters, M. D.; Kreidenweis, S. M.; Roberts, G. C.;  
3179 Prather, K. A. Effect of chemical mixing state on the hygroscopicity and cloud nucleation  
3180 properties of calcium mineral dust particles. *Atmos. Chem. Phys.* **2009**, *9*, 3303-3316.
- 3181 (218) Gierlus, K. M.; Laskina, O.; Abernathy, T. L.; Grassian, V. H. Laboratory study of the  
3182 effect of oxalic acid on the cloud condensation nuclei activity of mineral dust aerosol.  
3183 *Atmos. Environ.* **2012**, *46*, 125-130.



- 3184 (219) Cziczo, D. J.; Froyd, K. D.; Gallavardin, S. J.; Moehler, O.; Benz, S.; Saathoff, H.;  
3185 Murphy, D. M. Deactivation of ice nuclei due to atmospherically relevant surface  
3186 coatings. *Environ. Res. Lett.* **2009**, *4*, 044013.
- 3187 (220) Reitz, P.; Spindler, C.; Mentel, T. F.; Poulain, L.; Wex, H.; Mildenerger, K.;  
3188 Niedermeier, D.; Hartmann, S.; Clauss, T.; Stratmann, F. *et al.* Surface modification of  
3189 mineral dust particles by sulphuric acid processing: implications for ice nucleation  
3190 abilities. *Atmos. Chem. Phys.* **2011**, *11*, 7839-7858.
- 3191 (221) Niedermeier, D.; Hartmann, S.; Clauss, T.; Wex, H.; Kiselev, A.; Sullivan, R. C.;  
3192 DeMott, P. J.; Petters, M. D.; Reitz, P.; Schneider, J. *et al.* Experimental study of the role  
3193 of physicochemical surface processing on the IN ability of mineral dust particles. *Atmos.*  
3194 *Chem. Phys.* **2011**, *11*, 11131-11144.
- 3195 (222) Laskina, O.; Young, M. A.; Kleiber, P. D.; Grassian, V. H. Infrared extinction  
3196 spectroscopy and micro-Raman spectroscopy of select components of mineral dust mixed  
3197 with organic compounds. *J. Geophys. Res.-Atmos.* **2013**, *118*, 6593-6606.
- 3198 (223) Abdelkader, M.; Metzger, S.; Mamouri, R. E.; Astitha, M.; Barrie, L.; Levin, Z.;  
3199 Lelieveld, J. Dust-air pollution dynamics over the eastern Mediterranean. *Atmos. Chem.*  
3200 *Phys.* **2015**, *15*, 9173-9189.
- 3201 (224) Fan, S. M.; Horowitz, L. W.; Levy, H.; Moxim, W. J. Impact of air pollution on wet  
3202 deposition of mineral dust aerosols. *Geophys. Res. Lett.* **2004**, *31*, 4.
- 3203 (225) Meskhidze, N.; Chameides, W. L.; Nenes, A.; Chen, G. Iron mobilization in mineral dust:  
3204 Can anthropogenic SO<sub>2</sub> emissions affect ocean productivity? *Geophys. Res. Lett.* **2003**,  
3205 *30*, 2085, doi: 2010.1029/2003GL018035.
- 3206 (226) Pradhan, M.; Kalberer, M.; Griffiths, P. T.; Braban, C. F.; Pope, F. D.; Cox, R. A.;  
3207 Lambert, R. M. Uptake of Gaseous Hydrogen Peroxide by Submicrometer Titanium  
3208 Dioxide Aerosol as a Function of Relative Humidity. *Environ. Sci. Technol.* **2010**, *44*,  
3209 1360-1365.
- 3210 (227) Liu, Y.; Gibson, E. R.; Cain, J. P.; Wang, H.; Grassian, V. H.; Laskin, A. Kinetics of  
3211 heterogeneous reaction of CaCO<sub>3</sub> particles with gaseous HNO<sub>3</sub> over a wide range of  
3212 humidity. *J. Phys. Chem. A* **2008**, *112*, 1561-1571.
- 3213 (228) Nicolas, M.; Ndour, M.; Ka, O.; D'anna, B.; George, C. Photochemistry of atmospheric  
3214 dust: ozone decomposition on illuminated titanium dioxide. *Environ. Sci. Technol.* **2009**,  
3215 *43*, 7347-7442.
- 3216 (229) Rubasinghe, G.; Grassian, V. H. Role(s) of adsorbed water in the surface chemistry of  
3217 environmental interfaces. *Chem. Commun.* **2013**, *49*, 3071-3094.
- 3218 (230) Ewing, G. E. Ambient Thin Film Water on Insulator Surfaces. *Chem. Rev.* **2006**, *106*,  
3219 1511-1526.
- 3220 (231) Henderson, M. A. Structural Sensitivity in the Dissociation of Water on TiO<sub>2</sub> Single-  
3221 Crystal Surfaces. *Langmuir* **1996**, *12*, 5093-5098.
- 3222 (232) Schaub, R.; Thosttrup, P.; Lopez, N.; Lægsgaard, E.; Stensgaard, I.; Nørskov, J. K.;  
3223 Besenbacher, F. Oxygen Vacancies as Active Sites for Water Dissociation on Rutile  
3224 TiO<sub>2</sub>(110). *Phys. Rev. Lett.* **2001**, *87*, 266104.
- 3225 (233) Beaglehole, D.; Radlinska, E. Z.; Ninham, B. W.; Christenson, H. K. Inadequacy of  
3226 Lifshitz theory for thin liquid films. *Phys. Rev. Lett.* **1991**, *66*, 2084-2087.
- 3227 (234) Miranda, P. B.; Xu, L.; Shen, Y. R.; Salmeron, M. Icelike Water Monolayer Adsorbed on  
3228 Mica at Room Temperature. *Phys. Rev. Lett.* **1998**, *81*, 5876-5879.
- 3229 (235) Zhang, Z.; Bondarchuk, O.; Kay, B. D.; White, J. M.; Dohnálek, Z. Imaging Water  
3230 Dissociation on TiO<sub>2</sub>(110): Evidence for Inequivalent Geminate OH Groups. *J. Phys.*  
3231 *Chem. B* **2006**, *110*, 21840-21845.

- 3232 (236) Smith, R. S.; Li, Z.; Chen, L.; Dohnálek, Z.; Kay, B. D. Adsorption, Desorption, and  
3233 Displacement Kinetics of H<sub>2</sub>O and CO<sub>2</sub> on TiO<sub>2</sub>(110). *J. Phys. Chem. B* **2014**, *118*,  
3234 8054-8061.
- 3235 (237) Cantrell, W.; Heymsfield, A. Production of ice in tropospheric clouds - A review. *Bull.*  
3236 *Amer. Meteorol. Soc.* **2005**, *86*, 795-807.
- 3237 (238) Hoose, C.; Moehler, O. Heterogeneous ice nucleation on atmospheric aerosols: a review  
3238 of results from laboratory experiments. *Atmos. Chem. Phys.* **2012**, *12*, 9817-9854.
- 3239 (239) Ladino, L. A.; Stetzer, O.; Lohmann, U. Contact freezing: a review of experimental  
3240 studies. *Atmos. Chem. Phys.* **2013**, *13*, 9745-9769.
- 3241 (240) Al-Abadleh, H. A.; Grassian, V. H. FT-IR study of water adsorption on aluminum oxide  
3242 surfaces. *Langmuir* **2003**, *19*, 341-347.
- 3243 (241) Ketteler, G.; Yamamoto, S.; Bluhm, H.; Andersson, K.; Starr, D. E.; Ogletree, D. F.;  
3244 Ogasawara, H.; Nilsson, A.; Salmeron, M. The Nature of Water Nucleation Sites on  
3245 TiO<sub>2</sub>(110) Surfaces Revealed by Ambient Pressure X-ray Photoelectron Spectroscopy. *J.*  
3246 *Phys. Chem. C* **2007**, *111*, 8278-8282.
- 3247 (242) Yamamoto, S.; Kendelewicz, T.; Newberg, J. T.; Ketteler, G.; Starr, D. E.; Mysak, E. R.;  
3248 Andersson, K. J.; Ogasawara, H.; Bluhm, H.; Salmeron, M. *et al.* Water Adsorption on  $\alpha$ -  
3249 Fe<sub>2</sub>O<sub>3</sub>(0001) at near Ambient Conditions. *J. Phys. Chem. C* **2010**, *114*, 2256-2266.
- 3250 (243) Murphy, D. M.; Thomson, D. S.; Mahoney, T. M. J. In situ measurements of organics,  
3251 meteoritic material, mercury, and other elements in aerosols at 5 to 19 kilometers.  
3252 *Science* **1998**, *282*, 1664-1669.
- 3253 (244) Cziczo, D. J.; Murphy, D. M.; Hudson, P. K.; Thomson, D. S. Single particle  
3254 measurements of the chemical composition of cirrus ice residue during CRYSTAL-  
3255 FACE. *J. Geophys. Res.-Atmos.* **2004**, *109*, D04201, doi: 04210.01029/02003jd004032.
- 3256 (245) Laskin, A.; Iedema, M. J.; Ichkovich, A.; Graber, E. R.; Taraniuk, I.; Rudich, Y. Direct  
3257 observation of completely processed calcium carbonate dust particles. *Faraday Discuss.*  
3258 **2005**, *130*, 453-468.
- 3259 (246) Navea, J. G.; Chen, H. H.; Huang, M.; Carmichael, G. R.; Grassian, V. H. A comparative  
3260 evaluation of water uptake on several mineral dust sources. *Environ. Chem.* **2010**, *7*, 162-  
3261 170.
- 3262 (247) Gustafsson, R. J.; Orlov, A.; Badger, C. L.; Griffiths, P. T.; Cox, R. A.; Lambert, R. M. A  
3263 comprehensive evaluation of water uptake on atmospherically relevant mineral surfaces:  
3264 DRIFT spectroscopy, thermogravimetric analysis and aerosol growth measurements.  
3265 *Atmos. Chem. Phys.* **2005**, *5*, 3415-3421.
- 3266 (248) Ma, Q. X.; Liu, Y. C.; He, H. The Utilization of Physisorption Analyzer for Studying the  
3267 Hygroscopic Properties of Atmospheric Relevant Particles. *J. Phys. Chem. A* **2010**, *114*,  
3268 4232-4237.
- 3269 (249) Schuttlefield, J. D.; Cox, D.; Grassian, V. H. An investigation of water uptake on clays  
3270 minerals using ATR-FTIR spectroscopy coupled with quartz crystal microbalance  
3271 measurements. *J. Geophys. Res.-Atmos.* **2007**, *112*, D21303, doi:  
3272 21310.21029/22007JJD008973.
- 3273 (250) Goodman, A. L.; Bernard, E. T.; Grassian, V. H. Spectroscopic study of nitric acid and  
3274 water adsorption on oxide particles: Enhanced nitric acid uptake kinetics in the presence  
3275 of adsorbed water. *J. Phys. Chem. A* **2001**, *105*, 6443-6457.
- 3276 (251) Pope, F. D.; Dennis-Smith, B. J.; Griffiths, P. T.; Clegg, S. L.; Cox, R. A. Studies of  
3277 Single Aerosol Particles Containing Malonic Acid, Glutaric Acid, and Their Mixtures  
3278 with Sodium Chloride. I. Hygroscopic Growth. *J. Phys. Chem. A* **2010**, *114*, 5335-5341.

- 3279 (252) Tong, H. J.; Reid, J. P.; Bones, D. L.; Luo, B. P.; Krieger, U. K. Measurements of the  
3280 timescales for the mass transfer of water in glassy aerosol at low relative humidity and  
3281 ambient temperature. *Atmos. Chem. Phys.* **2011**, *11*, 4739-4754.
- 3282 (253) Attwood, A. R.; Greenslade, M. E. Optical Properties and Associated Hygroscopicity of  
3283 Clay Aerosols. *Aerosol Sci. Technol.* **2011**, *45*, 1350-1359.
- 3284 (254) Li-Jones, X.; Maring, H. B.; Prospero, J. M. Effect of relative humidity on light scattering  
3285 by mineral dust aerosol as measured in the marine boundary layer over the tropical  
3286 Atlantic Ocean. *J. Geophys. Res.-Atmos* **1998**, *103*, 31113-31121.
- 3287 (255) Utry, N.; Ajtai, T.; Pintér, M.; Tombácz, E.; Illés, E.; Bozóki, Z.; Szabó, G. Mass-specific  
3288 optical absorption coefficients and imaginary part of the complex refractive indices of  
3289 mineral dust components measured by a multi-wavelength photoacoustic spectrometer.  
3290 *Atmos. Meas. Tech.* **2015**, *8*, 401-410.
- 3291 (256) Sullivan, R. C.; Moore, M. J. K.; Petters, M. D.; Kreidenweis, S. M.; Qafoku, O.; Laskin,  
3292 A.; Roberts, G. C.; Prather, K. A. Impact of Particle Generation Method on the Apparent  
3293 Hygroscopicity of Insoluble Mineral Particles. *Aerosol Sci. Technol.* **2010**, *44*, 830-846.
- 3294 (257) Gibson, E. R.; Gierlus, K. M.; Hudson, P. K.; Grassian, V. H. Generation of internally  
3295 mixed insoluble and soluble aerosol particles to investigate the impact of atmospheric  
3296 aging and heterogeneous processing on the CCN activity of mineral dust aerosol. *Aerosol*  
3297 *Sci. Technol.* **2007**, *41*, 914-924.
- 3298 (258) Sullivan, R. C.; Moore, M. J. K.; Petters, M. D.; Kreidenweis, S. M.; Roberts, G. C.;  
3299 Prather, K. A. Timescale for hygroscopic conversion of calcite mineral particles through  
3300 heterogeneous reaction with nitric acid. *Phys. Chem. Chem. Phys.* **2009**, *11*, 7826-7837.
- 3301 (259) Garimella, S.; Huang, Y. W.; Seewald, J. S.; Cziczo, D. J. Cloud condensation nucleus  
3302 activity comparison of dry- and wet-generated mineral dust aerosol: the significance of  
3303 soluble material. *Atmos. Chem. Phys.* **2014**, *14*, 6003-6019.
- 3304 (260) Vlasenko, A.; Sjogren, S.; Weingartner, E.; Gaggeler, H. W.; Ammann, M. Generation of  
3305 submicron Arizona test dust aerosol: Chemical and hygroscopic properties. *Aerosol Sci.*  
3306 *Technol.* **2005**, *39*, 452-460.
- 3307 (261) Sullivan, R. C.; Petters, M. D.; DeMott, P. J.; Kreidenweis, S. M.; Wex, H.; Niedermeier,  
3308 D.; Hartmann, S.; Clauss, T.; Stratmann, F.; Reitz, P. *et al.* Irreversible loss of ice  
3309 nucleation active sites in mineral dust particles caused by sulphuric acid condensation.  
3310 *Atmos. Chem. Phys.* **2010**, *10*, 11471-11487.
- 3311 (262) Kumar, P.; Sokolik, I. N.; Nenes, A. Measurements of cloud condensation nuclei activity  
3312 and droplet activation kinetics of fresh unprocessed regional dust samples and minerals.  
3313 *Atmos. Chem. Phys.* **2011**, *11*, 3527-3541.
- 3314 (263) Kumar, P.; Sokolik, I. N.; Nenes, A. Cloud condensation nuclei activity and droplet  
3315 activation kinetics of wet processed regional dust samples and minerals. *Atmos. Chem.*  
3316 *Phys.* **2011**, *11*, 8661-8676.
- 3317 (264) Zhao, D. F.; Buchholz, A.; Mentel, T. F.; Müller, K. P.; Borchardt, J.; Kiendler-Scharr,  
3318 A.; Spindler, C.; Tillmann, R.; Trimborn, A.; Zhu, T. *et al.* Novel method of generation  
3319 of Ca(HCO<sub>3</sub>)<sub>2</sub> and CaCO<sub>3</sub> aerosols and first determination of hygroscopic and cloud  
3320 condensation nuclei activation properties. *Atmos. Chem. Phys.* **2010**, *10*, 8601-8616.
- 3321 (265) Wurzler, S.; Reisin, T. G.; Levin, Z. Modification of mineral dust particles by cloud  
3322 processing and subsequent effects on drop size distributions. *J. Geophys. Res.-Atmos*  
3323 **2000**, *105*, 4501-4512.
- 3324 (266) Smoydzin, L.; Teller, A.; Tost, H.; Fnais, M.; Lelieveld, J. Impact of mineral dust on  
3325 cloud formation in a Saharan outflow region. *Atmos. Chem. Phys.* **2012**, *12*, 11383-  
3326 11393.

- 3327 (267) Begue, N.; Tulet, P.; Pelon, J.; Aouizerats, B.; Berger, A.; Schwarzenboeck, A. Aerosol  
 3328 processing and CCN formation of an intense Saharan dust plume during the EUCAARI  
 3329 2008 campaign. *Atmos. Chem. Phys.* **2015**, *15*, 3497-3516.
- 3330 (268) Hatch, C. D.; Wiese, J. S.; Crane, C. C.; Harris, K. J.; Kloss, H. G.; Baltrusaitis, J. Water  
 3331 Adsorption on Clay Minerals As a Function of Relative Humidity: Application of BET  
 3332 and Freundlich Adsorption Models. *Langmuir* **2011**, *28*, 1790-1803.
- 3333 (269) Ma, Q. X.; He, H.; Liu, Y. C. In situ DRIFTS study of hygroscopic behavior of mineral  
 3334 aerosol. *J. Environ. Sci.* **2010**, *22*, 555-560.
- 3335 (270) Hung, H. M.; Wang, K. C.; Chen, J. P. Adsorption of nitrogen and water vapor by  
 3336 insoluble particles and the implication on cloud condensation nuclei activity. *J. Aerosol.*  
 3337 *Sci.* **2015**, *86*, 24-31.
- 3338 (271) Arenas, K. J. L.; Schill, S. R.; Malla, A.; Hudson, P. K. Deliquescence Phase Transition  
 3339 Measurements by Quartz Crystal Microbalance Frequency Shifts. *J. Phys. Chem. A* **2012**,  
 3340 *116*, 7658-7667.
- 3341 (272) Lu, C. S.; Lewis, O. Investigation of film - thickness determination by oscillating quartz  
 3342 resonators with large mass load. *J. Appl. Phys.* **1972**, *43*, 4385-4390.
- 3343 (273) Schuttlefield, J.; Al-Hosney, H.; Zachariah, A.; Grassian, V. H. Attenuated total  
 3344 reflection Fourier transform infrared spectroscopy to investigate water uptake and phase  
 3345 transitions in atmospherically relevant particles. *Appl. Spectrosc.* **2007**, *61*, 283-292.
- 3346 (274) Wijenayaka, L. A.; Rubasinghege, G.; Baltrusaitis, J.; Grassian, V. H. Surface Chemistry  
 3347 of alpha-FeOOH Nanorods and Microrods with Gas-Phase Nitric Acid and Water Vapor:  
 3348 Insights into the Role of Particle Size, Surface Structure, and Surface Hydroxyl Groups in  
 3349 the Adsorption and Reactivity of alpha-FeOOH with Atmospheric Gases. *J. Phys. Chem.*  
 3350 *C* **2012**, *116*, 12566-12577.
- 3351 (275) Song, X. W.; Boily, J. F. Water Vapor Adsorption on Goethite. *Environ. Sci. Technol.*  
 3352 **2013**, *47*, 7171-7177.
- 3353 (276) Wendt, S.; Schaub, R.; Matthiesen, J.; Vestergaard, E. K.; Wahlström, E.; Rasmussen, M.  
 3354 D.; Thostrup, P.; Molina, L. M.; Lægsgaard, E.; Stensgaard, I. *et al.* Oxygen vacancies on  
 3355 TiO<sub>2</sub>(1 1 0) and their interaction with H<sub>2</sub>O and O<sub>2</sub>: A combined high-resolution STM  
 3356 and DFT study. *Surf. Sci.* **2005**, *598*, 226-245.
- 3357 (277) Wendt, S.; Matthiesen, J.; Schaub, R.; Vestergaard, E. K.; Lægsgaard, E.; Besenbacher,  
 3358 F.; Hammer, B. Formation and Splitting of Paired Hydroxyl Groups on Reduced  
 3359 TiO<sub>2</sub>(110). *Phys. Rev. Lett.* **2006**, *96*, 066107.
- 3360 (278) He, Y.; Tilocca, A.; Dulub, O.; Selloni, A.; Diebold, U. Local ordering and electronic  
 3361 signatures of submonolayer water on anatase TiO<sub>2</sub>(101). *Nat Mater* **2009**, *8*, 585-589.
- 3362 (279) Krueger, B. J.; Grassian, V. H.; Iedema, M. J.; Cowin, J. P.; Laskin, A. Probing  
 3363 heterogeneous chemistry of individual atmospheric particles using scanning electron  
 3364 microscopy and energy-dispersive X-ray analysis. *Anal. Chem.* **2003**, *75*, 5170-5179.
- 3365 (280) Salmeron, M.; Schlogl, R. Ambient pressure photoelectron spectroscopy: A new tool for  
 3366 surface science and nanotechnology. *Surf. Sci. Rep.* **2008**, *63*, 169-199.
- 3367 (281) Lampimäki, M.; Schreiber, S.; Zelenay, V.; Křepelová, A.; Birrer, M.; Axnanda, S.; Mao,  
 3368 B.; Liu, Z.; Bluhm, H.; Ammann, M. Exploring the Environmental Photochemistry on the  
 3369 TiO<sub>2</sub>(110) Surface in Situ by Near Ambient Pressure X-ray Photoelectron Spectroscopy.  
 3370 *J. Phys. Chem. C* **2015**, *119*, 7076-7085.
- 3371 (282) Lampimaki, M.; Zelenay, V.; Krepelova, A.; Liu, Z.; Chang, R.; Bluhm, H.; Ammann,  
 3372 M. Ozone-Induced Band Bending on Metal-Oxide Surfaces Studied under Environmental  
 3373 Conditions. *ChemPhysChem* **2013**, *14*, 2419 – 2425.
- 3374 (283) Rosseler, O.; Sleiman, M.; Montesinos, V. N.; Shavorskiy, A.; Keller, V.; Keller, N.;  
 3375 Litter, M. I.; Bluhm, H.; Salmeron, M.; Destailats, H. Chemistry of NO<sub>x</sub> on TiO<sub>2</sub>

- 3376 Surfaces Studied by Ambient Pressure XPS: Products, Effect of UV Irradiation, Water,  
3377 and Coadsorbed K<sup>+</sup>. *J. Phys. Chem. Lett.* **2013**, *4*, 536-541.
- 3378 (284) Starr, D. E.; Liu, Z.; Havecker, M.; Knop-Gericke, A.; Bluhm, H. Investigation of  
3379 solid/vapor interfaces using ambient pressure X-ray photoelectron spectroscopy. *Chem.*  
3380 *Soc. Rev.* **2013**, *42*, 5833-5857.
- 3381 (285) Perry, A.; Neipert, C.; Space, B.; Moore, P. B. Theoretical modeling of interface specific  
3382 vibrational spectroscopy: Methods and applications to aqueous interfaces. *Chem. Rev.*  
3383 **2006**, *106*, 1234-1258.
- 3384 (286) Shen, Y. R.; Ostroverkhov, V. Sum-frequency vibrational spectroscopy on water  
3385 interfaces: Polar orientation of water molecules at interfaces. *Chem. Rev.* **2006**, *106*,  
3386 1140-1154.
- 3387 (287) Ebben, C. J.; Ault, A. P.; Ruppel, M. J.; Ryder, O. S.; Bertram, T. H.; Grassian, V. H.;  
3388 Prather, K. A.; Geiger, F. M. Size-Resolved Sea Spray Aerosol Particles Studied by  
3389 Vibrational Sum Frequency Generation. *J. Phys. Chem. A* **2013**, *117*, 6589-6601.
- 3390 (288) Jubb, A. M.; Hua, W.; Allen, H. C. Environmental Chemistry at Vapor/Water Interfaces:  
3391 Insights from Vibrational Sum Frequency Generation Spectroscopy. *Annu. Rev. Phys.*  
3392 *Chem.* **2012**, *63*, 107-130.
- 3393 (289) Ma, G.; Liu, D. F.; Allen, H. C. Piperidine adsorption on hydrated alpha-alumina (0001)  
3394 surface studied by vibrational sum frequency generation spectroscopy. *Langmuir* **2004**,  
3395 *20*, 11620-11629.
- 3396 (290) Liu, D. F.; Ma, G.; Xu, M.; Allen, H. C. Adsorption of ethylene glycol vapor on  $\alpha$ -  
3397 Al<sub>2</sub>O<sub>3</sub>(0001) and amorphous SiO<sub>2</sub> surfaces: Observation of molecular orientation and  
3398 surface hydroxyl groups as sorption sites. *Environ. Sci. Technol.* **2005**, *39*, 206-212.
- 3399 (291) Baltrusaitis, J.; Grassian, V. H. Calcite (1014) surface in humid environments. *Surf. Sci.*  
3400 **2009**, *603*, L99-L104.
- 3401 (292) Stipp, S. L. S.; Konnerup-Madsen, J.; Franzreb, K.; Kulik, A.; Mathieu, H. J.  
3402 Spontaneous movement of ions through calcite at standard temperature and pressure.  
3403 *Nature* **1998**, *396*, 356-359.
- 3404 (293) Carpick, R. W.; Salmeron, M. Scratching the Surface: Fundamental Investigations of  
3405 Tribology with Atomic Force Microscopy. *Chem. Rev.* **1997**, *97*, 1163-1194.
- 3406 (294) Xu, L.; Lio, A.; Hu, J.; Ogletree, D. F.; Salmeron, M. Wetting and Capillary Phenomena  
3407 of Water on Mica. *J. Phys. Chem. B* **1998**, *102*, 540-548.
- 3408 (295) Caloz, F.; Fenter, F. F.; Tabor, K. D.; Rossi, M. J. Paper I: Design and construction of a  
3409 Knudsen-cell reactor for the study of heterogeneous reactions over the temperature range  
3410 130-750 K: Performances and limitations. *Rev. Sci. Instrum.* **1997**, *68*, 3172-3179.
- 3411 (296) Underwood, G. M.; Miller, T. M.; Grassian, V. H. Transmission FT-IR and Knudsen cell  
3412 study of the heterogeneous reactivity of gaseous nitrogen dioxide on mineral oxide  
3413 particles. *J. Phys. Chem. A* **1999**, *103*, 6184-6190.
- 3414 (297) Liu, Y.; Ma, J.; Liu, C.; He, H. Heterogeneous uptake of carbonyl sulfide onto kaolinite  
3415 within a temperature range of 220–330 K. *J. Geophys. Res.-Atmos* **2010**, *115*, D24311,  
3416 doi: 24310.21029/22010JD014778.
- 3417 (298) Seisel, S.; Lian, Y.; Keil, T.; Trukhin, M. E.; Zellner, R. Kinetics of the interaction of  
3418 water vapour with mineral dust and soot surfaces at T=298 K. *Phys. Chem. Chem. Phys.*  
3419 **2004**, *6*, 1926-1932.
- 3420 (299) Seisel, S.; Pashkova, A.; Lian, Y.; Zellner, R. Water uptake on mineral dust and soot: A  
3421 fundamental view of the hydrophilicity of atmospheric particles? *Faraday Discuss.* **2005**,  
3422 *130*, 437-451.
- 3423 (300) Nathanson, G. M.; Davidovits, P.; Worsnop, D. R.; Kolb, C. E. Dynamics and kinetics at  
3424 the gas-liquid interface. *J. Phys. Chem.* **1996**, *100*, 13007-13020.

- 3425 (301) Kong, X.; Thomson, E. S.; Papagiannakopoulos, P.; Johansson, S. M.; Pettersson, J. B. C.  
3426 Water Accommodation on Ice and Organic Surfaces: Insights from Environmental  
3427 Molecular Beam Experiments. *J. Phys. Chem. B* **2014**, *118*, 13378-13386.
- 3428 (302) Nathanson, G. M. Molecular beam studies of gas-liquid interfaces. *Annu. Rev. Phys.*  
3429 *Chem.* **2004**, *55*, 231-255.
- 3430 (303) Burden, D. K.; Johnson, A. M.; Nathanson, G. M. HCl Uptake through Films of  
3431 Pentanoic Acid and Pentanoic Acid/Hexanol Mixtures at the Surface of Sulfuric Acid. *J.*  
3432 *Phys. Chem. A* **2009**, *113*, 14131-14140.
- 3433 (304) Kong, X.; Papagiannakopoulos, P.; Thomson, E. S.; Marković, N.; Pettersson, J. B. C.  
3434 Water Accommodation and Desorption Kinetics on Ice. *J. Phys. Chem. A* **2014**, *118*,  
3435 3973-3979.
- 3436 (305) Thomson, E. S.; Kong, X.; Papagiannakopoulos, P.; Pettersson, J. B. C. Deposition-mode  
3437 ice nucleation reexamined at temperatures below 200 K. *Atmos. Chem. Phys.* **2015**, *15*,  
3438 1621-1632.
- 3439 (306) Krieger, U. K.; Marcolli, C.; Reid, J. P. Exploring the complexity of aerosol particle  
3440 properties and processes using single particle techniques. *Chem. Soc. Rev.* **2012**, *41*,  
3441 6631-6662.
- 3442 (307) Peng, C.; Chan, C. K. The water cycles of water-soluble organic salts of atmospheric  
3443 importance. *Atmos. Environ.* **2001**, *35*, 1183-1192.
- 3444 (308) Reid, J. P.; Sayer, R. M. Heterogeneous atmospheric aerosol chemistry: laboratory  
3445 studies of chemistry on water droplets. *Chem. Soc. Rev.* **2003**, *32*, 70-79.
- 3446 (309) King, M. D.; Thompson, K. C.; Ward, A. D. Laser Tweezers Raman Study of Optically  
3447 Trapped Aerosol Droplets of Seawater and Oleic Acid Reacting with Ozone:  
3448 Implications for Cloud-Droplet Properties. *J. Am. Chem. Soc.* **2004**, *126*, 16710-16711.
- 3449 (310) Hunt, O. R.; Ward, A. D.; King, M. D. Heterogeneous oxidation of nitrite anion by gas-  
3450 phase ozone in an aqueous droplet levitated by laser tweezers (optical trap): is there any  
3451 evidence for enhanced surface reaction? *Phys. Chem. Chem. Phys.* **2015**, *17*, 2734-2741.
- 3452 (311) Rkiouak, L.; Tang, M. J.; Camp, J. C. J.; McGregor, J.; Watson, I. M.; Cox, R. A.;  
3453 Kalberer, M.; Ward, A. D.; Pope, F. D. Optical trapping and Raman Spectroscopy of  
3454 solid aerosol particles. *Phys. Chem. Chem. Phys.* **2014**, *16*, 11426-11434.
- 3455 (312) Miles, R. E. H.; Walker, J. S.; Burnham, D. R.; Reid, J. P. Retrieval of the complex  
3456 refractive index of aerosol droplets from optical tweezers measurements. *Phys. Chem.*  
3457 *Chem. Phys.* **2012**, *14*, 3037-3047.
- 3458 (313) Power, R. M.; Burnham, D. R.; Reid, J. P. Toward optical-tweezers-based force  
3459 microscopy for airborne microparticles. *Appl. Optics* **2014**, *53*, 8522-8534.
- 3460 (314) Lee, A. K. Y.; Ling, T. Y.; Chan, C. K. Understanding hygroscopic growth and phase  
3461 transformation of aerosols using single particle Raman spectroscopy in an electrodynamic  
3462 balance. *Faraday Discuss.* **2008**, *137*, 245-263.
- 3463 (315) Choi, M. Y.; Chan, C. K. Investigation of Efflorescence of Inorganic Aerosols Using  
3464 Fluorescence Spectroscopy. *J. Phys. Chem. A* **2005**, *109*, 1042-1048.
- 3465 (316) Swietlicki, E.; Hansson, H. C.; Hameri, K.; Svenningsson, B.; Massling, A.; McFiggans,  
3466 G.; McMurry, P. H.; Petaja, T.; Tunved, P.; Gysel, M. *et al.* Hygroscopic properties of  
3467 submicrometer atmospheric aerosol particles measured with H-TDMA instruments in  
3468 various environments - a review. *Tellus Ser. B-Chem. Phys. Meteorol.* **2008**, *60*, 432-469.
- 3469 (317) Weingartner, E.; Gysel, M.; Baltensperger, U. Hygroscopicity of Aerosol Particles at  
3470 Low Temperatures. 1. New Low-Temperature H-TDMA Instrument: Setup and First  
3471 Applications. *Environ. Sci. Technol.* **2002**, *36*, 55-62.

- 3472 (318) Duplissy, J.; Gysel, M.; Sjogren, S.; Meyer, N.; Good, N.; Kammermann, L.; Michaud,  
3473 V.; Weigel, R.; Martins dos Santos, S.; Gruening, C. *et al.* Intercomparison study of six  
3474 HTDMAs: results and recommendations. *Atmos. Meas. Tech.* **2009**, *2*, 363-378.
- 3475 (319) Wex, H.; Petters, M. D.; Carrico, C. M.; Hallbauer, E.; Massling, A.; McMeeking, G. R.;  
3476 Poulain, L.; Wu, Z.; Kreidenweis, S. M.; Stratmann, F. Towards closing the gap between  
3477 hygroscopic growth and activation for secondary organic aerosol: Part 1 – Evidence from  
3478 measurements. *Atmos. Chem. Phys.* **2009**, *9*, 3987-3997.
- 3479 (320) Keskinen, H.; Romakkaniemi, S.; Jaatinen, A.; Miettinen, P.; Saukko, E.; Jorma, J.;  
3480 Mäkelä, J. M.; Virtanen, A.; Smith, J. N.; Laaksonen, A. On-Line Characterization of  
3481 Morphology and Water Adsorption on Fumed Silica Nanoparticles. *Aerosol Sci. Technol.*  
3482 **2011**, *45*, 1441-1447.
- 3483 (321) Ardon-Dryer, K.; Garimella, S.; Huang, Y. W.; Christopoulos, C.; Cziczo, D. J.  
3484 Evaluation of DMA Size Selection of Dry Dispersed Mineral Dust Particles. *Aerosol Sci.*  
3485 *Technol.* **2015**, *49*, 828-841.
- 3486 (322) Veghte, D. P.; Freedman, M. A. The Necessity of Microscopy to Characterize the Optical  
3487 Properties of Size-Selected, Nonspherical Aerosol Particles. *Anal. Chem.* **2012**, *84*, 9101-  
3488 9108.
- 3489 (323) Garland, R. M.; Ravishankara, A. R.; Lovejoy, E. R.; Tolbert, M. A.; Baynard, T.  
3490 Parameterization for the relative humidity dependence of light extinction: Organic-  
3491 ammonium sulfate aerosol. *J. Geophys. Res.-Atmos.* **2007**, *112*, D19303, doi:  
3492 19310.11029/12006JD008179.
- 3493 (324) Langridge, J. M.; Richardson, M. S.; Lack, D.; Law, D.; Murphy, D. M. Aircraft  
3494 Instrument for Comprehensive Characterization of Aerosol Optical Properties, Part I:  
3495 Wavelength-Dependent Optical Extinction and Its Relative Humidity Dependence  
3496 Measured Using Cavity Ringdown Spectroscopy. *Aerosol Sci. Technol.* **2011**, *45*, 1305-  
3497 1318.
- 3498 (325) Washenfelder, R. A.; Flores, J. M.; Brock, C. A.; Brown, S. S.; Rudich, Y. Broadband  
3499 measurements of aerosol extinction in the ultraviolet spectral region. *Atmos. Meas. Tech.*  
3500 **2013**, *6*, 861-877.
- 3501 (326) Baynard, T.; Garland, R. M.; Ravishankara, A. R.; Tolbert, M. A.; Lovejoy, E. R. Key  
3502 factors influencing the relative humidity dependence of aerosol light scattering. *Geophys.*  
3503 *Res. Lett.* **2006**, *33*, L06813, doi: 06810.01029/02005GL024898.
- 3504 (327) Meland, B.; Kleiber, P. D.; Grassian, V. H.; Young, M. A. Visible light scattering study  
3505 at 470, 550, and 660 nm of components of mineral dust aerosol: Hematite and goethite. *J.*  
3506 *Quant. Spectrosc. Radiat. Transf.* **2011**, *112*, 1108-1118.
- 3507 (328) Malm, W. C.; Day, D. E.; Kreidenweis, S. M. Light Scattering Characteristics of  
3508 Aerosols as a Function of Relative Humidity: Part I—A Comparison of Measured  
3509 Scattering and Aerosol Concentrations Using the Theoretical Models. *J. Air Waste*  
3510 *Manage. Assoc.* **2000**, *50*, 686-700.
- 3511 (329) Lack, D. A.; Lovejoy, E. R.; Baynard, T.; Pettersson, A.; Ravishankara, A. R. Aerosol  
3512 absorption measurement using photoacoustic spectroscopy: Sensitivity, calibration, and  
3513 uncertainty developments. *Aerosol Sci. Technol.* **2006**, *40*, 697-708.
- 3514 (330) Roberts, G. C.; Nenes, A. A continuous-flow streamwise thermal-gradient CCN chamber  
3515 for atmospheric measurements. *Aerosol Sci. Technol.* **2005**, *39*, 206-221.
- 3516 (331) Lance, S.; Medina, J.; Smith, J. N.; Nenes, A. Mapping the operation of the DMT  
3517 Continuous Flow CCN counter. *Aerosol Sci. Technol.* **2006**, *40*, 242-254.
- 3518 (332) Good, N.; Coe, H.; McFiggans, G. Instrumentational operation and analytical  
3519 methodology for the reconciliation of aerosol water uptake under sub- and supersaturated  
3520 conditions. *Atmos. Meas. Tech.* **2010**, *3*, 1241-1254.

- 3521 (333) Lathem, T. L.; Nenes, A. Water Vapor Depletion in the DMT Continuous-Flow CCN  
3522 Chamber: Effects on Supersaturation and Droplet Growth. *Aerosol Sci. Technol.* **2011**,  
3523 *45*, 604-615.
- 3524 (334) Ehara, K.; Hagwood, C.; Coakley, K. J. Novel method to classify aerosol particles  
3525 according to their mass-to-charge ratio—Aerosol particle mass analyser. *J. Aerosol. Sci.*  
3526 **1996**, *27*, 217-234.
- 3527 (335) Park, K.; Cao, F.; Kittelson, D. B.; McMurry, P. H. Relationship between Particle Mass  
3528 and Mobility for Diesel Exhaust Particles. *Environ. Sci. Technol.* **2003**, *37*, 577-583.
- 3529 (336) Khalizov, A. F.; Zhang, R. Y.; Zhang, D.; Xue, H. X.; Pagels, J.; McMurry, P. H.  
3530 Formation of highly hygroscopic soot aerosols upon internal mixing with sulfuric acid  
3531 vapor. *J. Geophys. Res.-Atmos.* **2009**, *114*, D05208, doi: 05210.01029/02008JD010595.
- 3532 (337) Abegglen, M.; Durdina, L.; Brem, B. T.; Wang, J.; Rindlisbacher, T.; Corbin, J. C.;  
3533 Lohmann, U.; Sierau, B. Effective density and mass–mobility exponents of particulate  
3534 matter in aircraft turbine exhaust: Dependence on engine thrust and particle size. *J.*  
3535 *Aerosol. Sci.* **2015**, *88*, 135-147.
- 3536 (338) Amaral, S. S.; de Carvalho, J. A.; Costa, M. A. M.; Pinheiro, C. An Overview of  
3537 Particulate Matter Measurement Instruments. *Atmosphere* **2015**, *6*, 1327-1345.
- 3538 (339) Pope, F. D. Pollen grains are efficient cloud condensation nuclei. *Environ. Res. Lett.*  
3539 **2010**, *5*, 044015.
- 3540 (340) Atkins, P. W. *Physical Chemistry (Sixth Edition)*; Oxford University Press: Oxford, UK,  
3541 1998.
- 3542 (341) Lowell, S.; Shields, J. E.; Thomas, M. A.; Thommes, M. *Characterization of Porous*  
3543 *Solids and Powders: Surface Area, Pore Size and Density*; Springer: Netherlands, 2010.
- 3544 (342) Crittenden, B.; Thomas, W. J. *Adsorption Technology & Design*; Butterworth-  
3545 Heinemann: Oxford, UK, 1998.
- 3546 (343) Langmuir, I. The constitution and fundamental properties of solids and liquids. Part I.  
3547 Solids. *J. Am. Chem. Soc.* **1916**, *38*, 2221-2295.
- 3548 (344) Brunauer, S.; Emmett, P. H.; Teller, E. Adsorption of Gases in Multimolecular Layers. *J.*  
3549 *Am. Chem. Soc.* **1938**, *60*, 309-319.
- 3550 (345) Joyner, L. G.; Weinberger, E. B.; Montgomery, C. W. Surface Area Measurements of  
3551 Activated Carbons, Silica Gel and other Adsorbents. *J. Am. Chem. Soc.* **1945**, *67*, 2182-  
3552 2188.
- 3553 (346) Sips, R. On the Structure of a Catalyst Surface. *J. Chem. Phys.* **1948**, *16*, 490-495.
- 3554 (347) Skopp, J. Derivation of the Freundlich Adsorption Isotherm from Kinetics. *J. Chem.*  
3555 *Educ.* **2009**, *86*, 1341.
- 3556 (348) Hatch, C. D.; Greenaway, A. L.; Christie, M. J.; Baltrusaitis, J. Water adsorption  
3557 constrained Frenkel–Halsey–Hill adsorption activation theory: Montmorillonite and illite.  
3558 *Atmos. Environ.* **2014**, *87*, 26-33.
- 3559 (349) Sorjamaa, R.; Laaksonen, A. The effect of H<sub>2</sub>O adsorption on cloud drop activation of  
3560 insoluble particles: a theoretical framework. *Atmos. Chem. Phys.* **2007**, *7*, 6175-6180.
- 3561 (350) Kohler, H. The nucleus in and the growth of hygroscopic droplets. *Trans. Faraday Soc.*  
3562 **1936**, *32*, 1152-1161.
- 3563 (351) Farmer, D. K.; Cappa, C. D.; Kreidenweis, S. M. Atmospheric Processes and Their  
3564 Controlling Influence on Cloud Condensation Nuclei Activity. *Chem. Rev.* **2015**, *115*,  
3565 4199-4217.
- 3566 (352) Henson, B. F. An adsorption model of insoluble particle activation: Application to black  
3567 carbon. *J. Geophys. Res.-Atmos* **2007**, *112*, D24S16, doi: 10.1029/2007JD008549.



- 3568 (353) DeCarlo, P. F.; Slowik, J. G.; Worsnop, D. R.; Davidovits, P.; Jimenez, J. L. Particle  
3569 morphology and density characterization by combined mobility and aerodynamic  
3570 diameter measurements. Part 1: Theory. *Aerosol Sci. Technol.* **2004**, *38*, 1185-1205.
- 3571 (354) Al-Hosney, H. A.; Grassian, V. H. Water, sulfur dioxide and nitric acid adsorption on  
3572 calcium carbonate: A transmission and ATR-FTIR study. *Phys. Chem. Chem. Phys.*  
3573 **2005**, *7*, 1266-1276.
- 3574 (355) Gibson, E. R.; Hudson, P. K.; Grassian, V. H. Aerosol chemistry and climate: Laboratory  
3575 studies of the carbonate component of mineral dust and its reaction products. *Geophys.*  
3576 *Res. Lett.* **2006**, *33*, L13811, doi: 13810.11029/12006GL026386.
- 3577 (356) Schuttlefield, J. D. *Laboratory studies of reactions of atmospheric gases with components*  
3578 *of mineral dust aerosol and research in chemical education, PhD Dissertation*; The  
3579 University of Iowa, Iowa City, USA, 2008.
- 3580 (357) Tang, M. J.; Whitehead, J.; Davidson, N. M.; Pope, F. D.; Alfarra, M. R.; McFiggans, G.;  
3581 Kalberer, M. Cloud condensation nucleation activities of calcium carbonate and its  
3582 atmospheric ageing products. *Phys. Chem. Chem. Phys.* **2015**, *17*, 32194-32203.
- 3583 (358) Neagle, W.; Rochester, C. H. Infrared study of the adsorption of water and ammonia on  
3584 calcium carbonate. *J. Chem. Soc., Faraday Trans.* **1990**, *86*, 181-183.
- 3585 (359) Bohr, J.; Wogelius, R. A.; Morris, P. M.; Stipp, S. L. S. Thickness and structure of the  
3586 water film deposited from vapour on calcite surfaces. *Geochim. Cosmochim. Acta* **2010**,  
3587 *74*, 5985-5999.
- 3588 (360) Stipp, S. L. S.; Eggleston, C. M.; Nielsen, B. S. Calcite Surface-Structure Observed at  
3589 Microtopographic and Molecular Scales with Atomic-Force Microscopy (Afm).  
3590 *Geochim. Cosmochim. Acta* **1994**, *58*, 3023-3033.
- 3591 (361) Stipp, S. L. S. Toward a conceptual model of the calcite surface: Hydration, hydrolysis,  
3592 and surface potential. *Geochim. Cosmochim. Acta* **1999**, *63*, 3121-3131.
- 3593 (362) Hausner, D. B.; Reeder, R. J.; Strongin, D. R. Humidity-induced restructuring of the  
3594 calcite surface and the effect of divalent heavy metals. *J. Colloid Interface Sci.* **2007**,  
3595 *305*, 101-110.
- 3596 (363) Al-Abadleh, H. A.; Grassian, V. H. Phase transitions in magnesium nitrate thin films: A  
3597 transmission FT-IR study of the deliquescence and efflorescence of nitric acid reacted  
3598 magnesium oxide interfaces. *J. Phys. Chem. B* **2003**, *107*, 10829-10839.
- 3599 (364) Tang, I. N.; Fung, K. H. Hydration and Raman scattering studies of levitated  
3600 microparticles: Ba(NO<sub>3</sub>)<sub>2</sub>, Sr(NO<sub>3</sub>)<sub>2</sub>, and Ca(NO<sub>3</sub>)<sub>2</sub>. *J. Chem. Phys.* **1997**, *106*, 1653-  
3601 1660.
- 3602 (365) Seisel, S.; Borensen, C.; Vogt, R.; Zellner, R. The heterogeneous reaction of HNO<sub>3</sub> on  
3603 mineral dust and gamma-alumina surfaces: a combined Knudsen cell and DRIFTS study.  
3604 *Phys. Chem. Chem. Phys.* **2004**, *6*, 5498-5508.
- 3605 (366) Kelly, J. T.; Wexler, A. S. Thermodynamics of carbonates and hydrates related to  
3606 heterogeneous reactions involving mineral aerosol. *J. Geophys. Res.-Atmos* **2005**, *110*,  
3607 D11201, doi: 11210.11029/12004jd005583.
- 3608 (367) Kelly, J. T.; Chuang, C. C.; Wexler, A. S. Influence of dust composition on cloud droplet  
3609 formation. *Atmos. Environ.* **2007**, *41*, 2904-2916.
- 3610 (368) Huey, L. G.; Dunlea, E. J.; Lovejoy, E. R.; Hanson, D. R.; Norton, R. B.; Fehsenfeld, F.  
3611 C.; Howard, C. J. Fast time response measurements of HNO<sub>3</sub> in air with a chemical  
3612 ionization mass spectrometer. *J. Geophys. Res.-Atmos.* **1998**, *103*, 3355-3360.
- 3613 (369) Hanke, M.; Umann, B.; Uecker, J.; Arnold, F.; Bunz, H. Atmospheric measurements of  
3614 gas-phase HNO<sub>3</sub> and SO<sub>2</sub> using chemical ionization mass spectrometry during the  
3615 MINATROC field campaign 2000 on Monte Cimone. *Atmos. Chem. Phys.* **2003**, *3*, 417-  
3616 436.

- 3617 (370) Bey, I.; Jacob, D. J.; Logan, J. A.; Yantosca, R. M. Asian chemical outflow to the Pacific  
3618 in spring: Origins, pathways, and budgets. *J. Geophys. Res.-Atmos* **2001**, *106*, 23097-  
3619 23113.
- 3620 (371) Brown, S. S.; Stark, H.; Ryerson, T. B.; Williams, E. J.; Nicks, D. K.; Trainer, M.;  
3621 Fehsenfeld, F. C.; Ravishankara, A. R. Nitrogen oxides in the nocturnal boundary layer:  
3622 Simultaneous in situ measurements of NO<sub>3</sub>, N<sub>2</sub>O<sub>5</sub>, NO<sub>2</sub>, NO, and O<sub>3</sub>. *J. Geophys. Res.-*  
3623 *Atmos* **2003**, *108*, 4299.
- 3624 (372) Osthoff, H. D.; Roberts, J. M.; Ravishankara, A. R.; Williams, E. J.; Lerner, B. M.;  
3625 Sommariva, R.; Bates, T. S.; Coffman, D.; Quinn, P. K.; Dibb, J. E. *et al.* High levels of  
3626 nitryl chloride in the polluted subtropical marine boundary layer. *Nature Geosci.* **2008**, *1*,  
3627 324-328.
- 3628 (373) Thornton, J. A.; Kercher, J. P.; Riedel, T. P.; Wagner, N. L.; Cozic, J.; Holloway, J., S.;  
3629 Dube, W. P.; Wolfe, G. M.; Quinn, P. K.; Middlebrook, A. M. *et al.* A large atomic  
3630 chlorine source inferred from mid-continental reactive nitrogen chemistry. *Nature* **2010**,  
3631 *464*, 271-174.
- 3632 (374) Crowley, J. N.; Thieser, J.; Tang, M. J.; Schuster, G.; Bozem, H.; Beygi, Z. H.; Fischer,  
3633 H.; Diesch, J. M.; Drewnick, F.; Borrmann, S. *et al.* Variable lifetimes and loss  
3634 mechanisms for NO<sub>3</sub> and N<sub>2</sub>O<sub>5</sub> during the DOMINO campaign: contrasts between  
3635 marine, urban and continental air. *Atmos. Chem. Phys.* **2011**, *11*, 10853-10870.
- 3636 (375) Sullivan, R. C.; Minambres, L.; DeMott, P. J.; Prenni, A. J.; Carrico, C. M.; Levin, E. J.  
3637 T.; Kreidenweis, S. M. Chemical processing does not always impair heterogeneous ice  
3638 nucleation of mineral dust particles. *Geophys. Res. Lett.* **2010**, *37*, L24805, doi:  
3639 24810.21029/22010GL045540.
- 3640 (376) Yamashita, K.; Murakami, M.; Hashimoto, A.; Tajiri, T. CCN Ability of Asian Mineral  
3641 Dust Particles and Their Effects on Cloud Droplet Formation. *J. Meteorol. Soc. Jpn.*  
3642 **2011**, *89*, 581-587.
- 3643 (377) Hensen, E. J. M.; Smit, B. Why clays swell. *J. Phys. Chem. B* **2002**, *106*, 12664-12667.
- 3644 (378) Keskinen, H.; Kortelainen, A. M.; Jaatinen, A.; Yli-Pirila, P.; Joutsensaari, J.;  
3645 Romakkaniemi, S.; Hao, L. Q.; Torvela, T.; Miettinen, P.; Virtanen, A. *et al.* Increased  
3646 hygroscopicity of Arizona Test Dust seeds by secondary organic aerosol coating from  
3647 alpha-pinene ozonolysis. *Boreal Environ. Res.* **2014**, *19*, 182-190.
- 3648 (379) Hall, P. L.; Astill, D. M. Adsorption of water by homoionic exchange forms of Wyoming  
3649 montmorillonite (SWY-1). *Clays Clay Miner.* **1989**, *37*, 355-363.
- 3650 (380) Cases, J. M.; Berend, I.; Besson, G.; Francois, M.; Uriot, J. P.; Thomas, F.; Poirier, J. E.  
3651 Mechanism of adsorption and desorption of water vapor by homoionic montmorillonite.  
3652 1. The sodium-exchanged form. *Langmuir* **1992**, *8*, 2730-2739.
- 3653 (381) Xu, W. Z.; Johnston, C. T.; Parker, P.; Agnew, S. F. Infrared study of water sorption on  
3654 Na-, Li-, Ca-, and Mg-exchanged (SWy-1 and SAz-1) montmorillonite. *Clays Clay*  
3655 *Miner.* **2000**, *48*, 120-131.
- 3656 (382) Zent, A. P.; Howard, D. J.; Quinn, R. C. H<sub>2</sub>O adsorption on smectites: Application to the  
3657 diurnal variation of H<sub>2</sub>O in the Martian atmosphere. *J. Geophys. Res.-Planets* **2001**, *106*,  
3658 14667-14674.
- 3659 (383) Frinak, E. K.; Mashburn, C. D.; Tolbert, M. A.; Toon, O. B. Infrared characterization of  
3660 water uptake by low-temperature Na-montmorillonite: Implications for Earth and Mars.  
3661 *J. Geophys. Res.-Atmos.* **2005**, *110*, D09308, doi: 09310.01029/02004JD005647.
- 3662 (384) Attwood, A. R.; Greenslade, M. E. Deliquescence Behavior of Internally Mixed Clay and  
3663 Salt Aerosols by Optical Extinction Measurements. *J. Phys. Chem. A* **2012**, *116*, 4518-  
3664 4527.

- 3665 (385) Dalirian, M.; Keskinen, H.; Ahlm, L.; Ylisirniö, A.; Romakkaniemi, S.; Laaksonen, A.;  
3666 Virtanen, A.; Riipinen, I. CCN activation of fumed silica aerosols mixed with soluble  
3667 pollutants. *Atmos. Chem. Phys.* **2015**, *15*, 3815-3829.
- 3668 (386) Rubasinghege, G.; Ogden, S.; Baltrusaitis, J.; Grassian, V. H. Heterogeneous Uptake and  
3669 Adsorption of Gas-Phase Formic Acid on Oxide and Clay Particle Surfaces: The Roles of  
3670 Surface Hydroxyl Groups and Adsorbed Water in Formic Acid Adsorption and the  
3671 Impact of Formic Acid Adsorption on Water Uptake. *J. Phys. Chem. A* **2013**, *117*, 11316-  
3672 11327.
- 3673 (387) Koehler, K. A.; Kreidenweis, S. M.; DeMott, P. J.; Prenni, A. J.; Petters, M. D. Potential  
3674 impact of Owens (dry) Lake dust on warm and cold cloud formation. *J. Geophys. Res.-*  
3675 *Atmos.* **2007**, *112*, D12210, doi: 12210.11029/12007jd008413.
- 3676 (388) deLeeuw, N. H.; Parker, S. C. Atomistic simulation of the effect of molecular adsorption  
3677 of water on the surface structure and energies of calcite surfaces. *J. Chem. Soc.-Faraday*  
3678 *Trans.* **1997**, *93*, 467-475.
- 3679 (389) Kerisit, S.; Marmier, A.; Parker, S. C. Ab initio surface phase diagram of the {10(1)over-  
3680 bar4} calcite surface. *J. Phys. Chem. B* **2005**, *109*, 18211-18213.
- 3681 (390) Rahaman, A.; Grassian, V. H.; Margulis, C. J. Dynamics of water adsorption onto a  
3682 calcite surface as a function of relative humidity. *J. Phys. Chem. C* **2008**, *112*, 2109-  
3683 2115.
- 3684 (391) Tunega, D.; Gerzabek, M. H.; Lischka, H. Ab initio molecular dynamics study of a  
3685 monomolecular water layer on octahedral and tetrahedral kaolinite surfaces. *J. Phys.*  
3686 *Chem. B* **2004**, *108*, 5930-5936.
- 3687 (392) Croteau, T.; Bertram, A. K.; Patey, G. N. Adsorption and Structure of Water on Kaolinite  
3688 Surfaces: Possible Insight into Ice Nucleation from Grand Canonical Monte Carlo  
3689 Calculations. *J. Phys. Chem. A* **2008**, *112*, 10708-10712.
- 3690 (393) Croteau, T.; Bertram, A. K.; Patey, G. N. Simulation of Water Adsorption on Kaolinite  
3691 under Atmospheric Conditions. *J. Phys. Chem. A* **2009**, *113*, 7826-7833.
- 3692 (394) Croteau, T.; Bertram, A. K.; Patey, G. N. Observations of High-Density Ferroelectric  
3693 Ordered Water in Kaolinite Trenches using Monte Carlo Simulations. *J. Phys. Chem. A*  
3694 **2010**, *114*, 8396-8405.
- 3695 (395) Croteau, T.; Bertram, A. K.; Patey, G. N. Water adsorption on kaolinite surfaces  
3696 containing trenches. *J. Phys. Chem. A* **2010**, *114*, 2171-2178.
- 3697 (396) Hensen, E. J. M.; Tambach, T. J.; Blik, A.; Smit, B. Adsorption isotherms of water in  
3698 Li-, Na-, and K-montmorillonite by molecular simulation. *J. Chem. Phys.* **2001**, *115*,  
3699 3322-3329.
- 3700 (397) Tambach, T. J.; Hensen, E. J. M.; Smit, B. Molecular simulations of swelling clay  
3701 minerals. *J. Phys. Chem. B* **2004**, *108*, 7586-7596.
- 3702 (398) Argyris, D.; Tummala, N. R.; Striolo, A.; Cole, D. R. Molecular structure and dynamics  
3703 in thin water films at the silica and graphite surfaces. *J. Phys. Chem. C* **2008**, *112*, 13587-  
3704 13599.
- 3705 (399) Murdachaew, G.; Gageot, M.-P.; Halonen, L.; Gerber, R. B. Dissociation of HCl into  
3706 Ions on Wet Hydroxylated (0001)  $\alpha$ -Quartz. *J. Phys. Chem. Lett.* **2013**, *4*, 3500-3507.
- 3707 (400) Lindan, P. J. D.; Harrison, N. M.; Gillan, M. J. Mixed dissociative and molecular  
3708 adsorption of water on the rutile (110) surface. *Phys. Rev. Lett.* **1998**, *80*, 762-765.
- 3709 (401) Jug, K.; Nair, N. N.; Bredow, T. Molecular dynamics investigation of water adsorption  
3710 on rutile surfaces. *Surf. Sci.* **2005**, *590*, 9-20.
- 3711 (402) Harris, L. A.; Quong, A. A. Molecular chemisorption as the theoretically preferred  
3712 pathway for water adsorption on ideal rutile TiO<sub>2</sub>(110). *Phys. Rev. Lett.* **2004**, *93*,  
3713 086105.

- 3714 (403) Rustad, J. R.; Boily, J. F. Density functional calculation of the infrared spectrum of  
3715 surface hydroxyl groups on goethite ( $\alpha$ -FeOOH). *Am. Mineral.* **2010**, *95*, 414-417.
- 3716 (404) Song, X. W.; Boily, J. F. Water vapor interactions with FeOOH particle surfaces. *Chem.*  
3717 *Phys. Lett.* **2013**, *560*, 1-9.
- 3718 (405) Gerber, R. B.; Varner, M. E.; Hammerich, A. D.; Riikonen, S.; Murdachaew, G.;  
3719 Shemesh, D.; Finlayson-Pitts, B. J. Computational Studies of Atmospherically-Relevant  
3720 Chemical Reactions in Water Clusters and on Liquid Water and Ice Surfaces. *Accounts*  
3721 *Chem. Res.* **2015**, *48*, 399-406.
- 3722 (406) Kerisit, S.; Parker, S. C. Free energy of adsorption of water and metal ions on the {1014}  
3723 calcite surface. *J. Am. Chem. Soc.* **2004**, *126*, 10152-10161.
- 3724 (407) Hu, X. L.; Michaelides, A. Water on the hydroxylated (001) surface of kaolinite: From  
3725 monomer adsorption to a flat 2D wetting layer. *Surf. Sci.* **2008**, *602*, 960-974.
- 3726 (408) Hu, X. L.; Michaelides, A. Ice formation on kaolinite: Lattice match or amphoterism?  
3727 *Surf. Sci.* **2007**, *601*, 5378-5381.
- 3728 (409) Hu, X. L.; Michaelides, A. The kaolinite (001) polar basal plane. *Surf. Sci.* **2010**, *604*,  
3729 111-117.
- 3730 (410) Yang, J.; Wang, E. G. Reaction of water on silica surfaces. *Curr. Opin. Solid State Mater.*  
3731 *Sci.* **2006**, *10*, 33-39.
- 3732 (411) Rimola, A.; Costa, D.; Sodupe, M.; Lambert, J. F.; Ugliengo, P. Silica Surface Features  
3733 and Their Role in the Adsorption of Biomolecules: Computational Modeling and  
3734 Experiments. *Chem. Rev.* **2013**, *113*, 4216-4313.
- 3735 (412) Legrand, A. P. *The Surface Properties of Silicas*; Wiley: Chichester, U.K., 1998.
- 3736 (413) Papirer, E. *Adsorption on Silica Surfaces*; CRC Press: Boca Raton, USA, 2000.
- 3737 (414) Sulpizi, M.; Gageot, M. P.; Sprik, M. The Silica-Water Interface: How the Silanols  
3738 Determine the Surface Acidity and Modulate the Water Properties. *J. Chem. Theory*  
3739 *Comput.* **2012**, *8*, 1037-1047.
- 3740 (415) Du, Q.; Freysz, E.; Shen, Y. R. Vibrational spectra of water molecules at quartz/water  
3741 interfaces. *Phys. Rev. Lett.* **1994**, *72*, 238-241.
- 3742 (416) Ostroverkhov, V.; Waychunas, G. A.; Shen, Y. R. Vibrational spectra of water at  
3743 water/ $\alpha$ -quartz (0001) interface. *Chem. Phys. Lett.* **2004**, *386*, 144-148.
- 3744 (417) Ostroverkhov, V.; Waychunas, G. A.; Shen, Y. R. New information on water interfacial  
3745 structure revealed by phase-sensitive surface spectroscopy. *Phys. Rev. Lett.* **2005**, *94*,  
3746 046102.
- 3747 (418) Richmond, G. L. Molecular bonding and interactions at aqueous surfaces as probed by  
3748 vibrational sum frequency spectroscopy. *Chem. Rev.* **2002**, *102*, 2693-2724.
- 3749 (419) Falkovich, A. H.; Ganor, E.; Levin, Z.; Formenti, P.; Rudich, Y. Chemical and  
3750 mineralogical analysis of individual mineral dust particles. *J. Geophys. Res.-Atmos* **2001**,  
3751 *106*, 18029-18036.
- 3752 (420) Falkovich, A. H.; Schkolnik, G.; Ganor, E.; Rudich, Y. Adsorption of organic compounds  
3753 pertinent to urban environments onto mineral dust particles. *J. Geophys. Res.-Atmos.*  
3754 **2004**, *109*, D02208, doi: 10.1029/2003JD003919.
- 3755 (421) Maxwell-Meier, K.; Weber, R.; Song, C.; Orsini, D.; Ma, Y.; Carmichael, G. R.; Streets,  
3756 D. G. Inorganic composition of fine particles in mixed mineral dust-pollution plumes  
3757 observed from airborne measurements during ACE-Asia. *J. Geophys. Res.-Atmos.* **2004**,  
3758 *109*, D19s07, doi: 10.1029/2003jd004464.
- 3759 (422) Ro, C. U.; Hwang, H.; Chun, Y.; Van Grieken, R. Single-particle characterization of four  
3760 "Asian Dust" samples collected in Korea, using low-Z particle electron probe X-ray  
3761 microanalysis. *Environ. Sci. Technol.* **2005**, *39*, 1409-1419.

- 3762 (423) Shi, Z. B.; Shao, L. T.; Jones, T. P.; Lu, S. L. Microscopy and mineralogy of airborne  
3763 particles collected during severe dust storm episodes in Beijing, China. *J. Geophys. Res.-*  
3764 *Atmos.* **2005**, *110*, D01303, doi: 01310.01029/02004jd005073.
- 3765 (424) Geng, H.; Park, Y.; Hwang, H.; Kang, S.; Ro, C. U. Elevated nitrogen-containing  
3766 particles observed in Asian dust aerosol samples collected at the marine boundary layer  
3767 of the Bohai Sea and the Yellow Sea. *Atmos. Chem. Phys.* **2009**, *9*, 6933-6947.
- 3768 (425) Li, W. J.; Shao, L. Y.; Shi, Z. B.; Chen, J. M.; Yang, L. X.; Yuan, Q.; Yan, C.; Zhang, X.  
3769 Y.; Wang, Y. Q.; Sun, J. Y. *et al.* Mixing state and hygroscopicity of dust and haze  
3770 particles before leaving Asian continent. *J. Geophys. Res.-Atmos* **2014**, *119*, 1044-1059.
- 3771 (426) Li, W.; Shao, L.; Zhang, D.; Ro, C.-U.; Hu, M.; Bi, X.; Geng, H.; Matsuki, A.; Niu, H.;  
3772 Chen, J. A review of single aerosol particle studies in the atmosphere of East Asia:  
3773 morphology, mixing state, source, and heterogeneous reactions. *J. Clean. Prod.* **2015**,  
3774 *112*, 1330-1349.
- 3775 (427) Perry, K. D.; Cliff, S. S.; Jimenez-Cruz, M. P. Evidence for hygroscopic mineral dust  
3776 particles from the Intercontinental Transport and Chemical Transformation Experiment.  
3777 *J. Geophys. Res.-Atmos* **2004**, *109*, D23S28, doi: 10.1029/2004JD004979.
- 3778 (428) Massling, A.; Leinert, S.; Wiedensohler, A.; Covert, D. Hygroscopic growth of sub-  
3779 micrometer and one-micrometer aerosol particles measured during ACE-Asia. *Atmos.*  
3780 *Chem. Phys.* **2007**, *7*, 3249-3259.
- 3781 (429) Shi, Z.; Zhang, D.; Hayashi, M.; Ogata, H.; Ji, H.; Fujie, W. Influences of sulfate and  
3782 nitrate on the hygroscopic behaviour of coarse dust particles. *Atmos. Environ.* **2008**, *42*,  
3783 822-827.
- 3784 (430) Crumeyrolle, S.; Gomes, L.; Tulet, P.; Matsuki, A.; Schwarzenboeck, A.; Crahan, K.  
3785 Increase of the aerosol hygroscopicity by cloud processing in a mesoscale convective  
3786 system: a case study from the AMMA campaign. *Atmos. Chem. Phys.* **2008**, *8*, 6907-  
3787 6924.
- 3788 (431) Tobo, Y.; Zhang, D. Z.; Nakata, N.; Yamada, M.; Ogata, H.; Hara, K.; Iwasaka, Y.  
3789 Hygroscopic mineral dust particles as influenced by chlorine chemistry in the marine  
3790 atmosphere. *Geophys. Res. Lett.* **2009**, *36*, L05817, doi: 05810.01029/02008gl036883.
- 3791 (432) Tobo, Y.; Zhang, D.; Matsuki, A.; Iwasaka, Y. Asian dust particles converted into  
3792 aqueous droplets under remote marine atmospheric conditions. *Proc. Natl. Acad. Sci. U.*  
3793 *S. A.* **2010**, *107*, 17905-17910.
- 3794 (433) Kim, J. S.; Park, K. Atmospheric Aging of Asian Dust Particles During Long Range  
3795 Transport. *Aerosol Sci. Technol.* **2012**, *46*, 913-924.
- 3796 (434) Denjean, C.; Caquineau, S.; Desboeufs, K.; Laurent, B.; Maille, M.; Quiñones Rosado,  
3797 M.; Vallejo, P.; Mayol-Bracero, O. L.; Formenti, P. Long-range transport across the  
3798 Atlantic in summertime does not enhance the hygroscopicity of African mineral dust.  
3799 *Geophys. Res. Lett.* **2015**, *42*, 7835-7843.
- 3800 (435) Bates, T. S.; Quinn, P. K.; Frossard, A. A.; Russell, L. M.; Hakala, J.; Petaja, T.;  
3801 Kulmala, M.; Covert, D. S.; Cappa, C. D.; Li, S. M. *et al.* Measurements of ocean derived  
3802 aerosol off the coast of California. *J. Geophys. Res.-Atmos.* **2012**, *117*, D00V15, doi:  
3803 10.1029/2012jd017588.
- 3804 (436) Fuentes, E.; Coe, H.; Green, D.; McFiggans, G. On the impacts of phytoplankton-derived  
3805 organic matter on the properties of the primary marine aerosol - Part 2: Composition,  
3806 hygroscopicity and cloud condensation activity. *Atmos. Chem. Phys.* **2011**, *11*, 2585-  
3807 2602.
- 3808 (437) Laskina, O.; Morris, H. S.; Grandquist, J. R.; Qin, Z.; Stone, E. A.; Tivanski, A. V.;  
3809 Grassian, V. H. Size Matters in the Water Uptake and Hygroscopic Growth of

- 3810 Atmospherically Relevant Multicomponent Aerosol Particles. *J. Phys. Chem. A* **2015**,  
3811 *119*, 4489-4497.
- 3812 (438) Kaaden, N.; Massling, A.; Schladitz, A.; Müller, T.; Kandler, K.; Schützl, L.; Weinzierl,  
3813 B.; Petzold, A.; Tesche, M.; Leinert, S. *et al.* State of mixing, shape factor, number size  
3814 distribution, and hygroscopic growth of the Saharan anthropogenic and mineral dust  
3815 aerosol at Tinfou, Morocco. *Tellus B* **2009**, *61*, 51-63.
- 3816 (439) Schladitz, A.; Müller, Thomas; Nowak, A.; Kandler, K.; Lieke, K.; Massling, A.;  
3817 Wiedensohler, A. In situ aerosol characterization at Cape Verde. Part 1: particle number  
3818 size distributions, hygroscopic growth and state of mixing of the marine and Saharan dust  
3819 aerosol. *Tellus B* **2011**, *63*, 531-548.
- 3820 (440) Tobo, Y.; DeMott, P. J.; Raddatz, M.; Niedermeier, D.; Hartmann, S.; Kreidenweis, S.  
3821 M.; Stratmann, F.; Wex, H. Impacts of chemical reactivity on ice nucleation of kaolinite  
3822 particles: A case study of levoglucosan and sulfuric acid. *Geophys. Res. Lett.* **2012**, *39*,  
3823 L19803, doi: 19810.11029/12012gl053007.
- 3824 (441) Hiranuma, N.; Augustin-Bauditz, S.; Bingemer, H.; Budke, C.; Curtius, J.; Danielczok,  
3825 A.; Diehl, K.; Dreischmeier, K.; Ebert, M.; Frank, F. *et al.* A comprehensive laboratory  
3826 study on the immersion freezing behavior of illite NX particles: a comparison of 17 ice  
3827 nucleation measurement techniques. *Atmos. Chem. Phys.* **2015**, *15*, 2489-2518.
- 3828 (442) Lau, K. M.; Wu, H. T. Warm rain processes over tropical oceans and climate  
3829 implications. *Geophys. Res. Lett.* **2003**, *30*, 2290, doi: 2210.1029/2003gl018567.
- 3830 (443) Freedman, M. A. Potential Sites for Ice Nucleation on Aluminosilicate Clay Minerals and  
3831 Related Materials. *J. Phys. Chem. Lett.* **2015**, *6*, 3850-3858.
- 3832 (444) DeMott, P. J.; Möhler, O.; Stetzer, O.; Vali, G.; Levin, Z.; Petters, M. D.; Murakami, M.;  
3833 Leisner, T.; Bundke, U.; Klein, H. *et al.* Resurgence in Ice Nuclei Measurement  
3834 Research. *Bull. Amer. Meteorol. Soc.* **2011**, *92*, 1623-1635.
- 3835 (445) Vali, G. Nucleation terminology. *Bull. Amer. Meteorol. Soc.* **1985**, *66*, 1426-1427.
- 3836 (446) Vali, G.; DeMott, P. J.; Möhler, O.; Whale, T. F. Technical Note: A proposal for ice  
3837 nucleation terminology. *Atmos. Chem. Phys.* **2015**, *15*, 10263-10270.
- 3838 (447) Martin, S. T. Phase transitions of aqueous atmospheric particles. *Chem. Rev.* **2000**, *100*,  
3839 3403-3453.
- 3840 (448) Szyrmer, W.; Zawadzki, I. Biogenic and Anthropogenic Sources of Ice-Forming Nuclei:  
3841 A Review. *Bull. Amer. Meteorol. Soc.* **1997**, *78*, 209-228.
- 3842 (449) Kulkarni, G.; Sanders, C.; Zhang, K.; Liu, X.; Zhao, C. Ice nucleation of bare and  
3843 sulfuric acid-coated mineral dust particles and implication for cloud properties. *J.*  
3844 *Geophys. Res.-Atmos* **2014**, *119*, 9993-10011.
- 3845 (450) Girard, E.; Dueymes, G.; Du, P.; Bertram, A. K. Assessment of the effects of acid-coated  
3846 ice nuclei on the Arctic cloud microstructure, atmospheric dehydration, radiation and  
3847 temperature during winter. *Int. J. Climatol.* **2013**, *33*, 599-614.
- 3848 (451) Salam, A.; Lesins, G.; Lohmann, U. Laboratory study of heterogeneous ice nucleation in  
3849 deposition mode of montmorillonite mineral dust particles aged with ammonia, sulfur  
3850 dioxide, and ozone at polluted atmospheric concentrations. *Air Qual. Atmos. Health*  
3851 **2008**, *1*, 135-142.
- 3852 (452) Archuleta, C. M.; DeMott, P. J.; Kreidenweis, S. M. Ice nucleation by surrogates for  
3853 atmospheric mineral dust and mineral dust/sulfate particles at cirrus temperatures. *Atmos.*  
3854 *Chem. Phys.* **2005**, *5*, 2617-2634.
- 3855 (453) Knopf, D. A.; Koop, T. Heterogeneous nucleation of ice on surrogates of mineral dust. *J.*  
3856 *Geophys. Res.-Atmos.* **2006**, *111*, D12201, doi: 12210.11029/12005jd006894.
- 3857 (454) Eastwood, M. L.; Cremel, S.; Wheeler, M.; Murray, B. J.; Girard, E.; Bertram, A. K.  
3858 Effects of sulfuric acid and ammonium sulfate coatings on the ice nucleation properties

- 3859 of kaolinite particles. *Geophys. Res. Lett.* **2009**, *36*, L02811, doi:  
3860 02810.01029/02008gl035997.
- 3861 (455) Chernoff, D. I.; Bertram, A. K. Effects of sulfate coatings on the ice nucleation properties  
3862 of a biological ice nucleus and several types of minerals. *J. Geophys. Res.-Atmos.* **2010**,  
3863 *115*, D20205, doi: 20210.21029/22010JD014254.
- 3864 (456) Niedermeier, D.; Hartmann, S.; Shaw, R. A.; Covert, D.; Mentel, T. F.; Schneider, J.;  
3865 Poulain, L.; Reitz, P.; Spindler, C.; Clauss, T. *et al.* Heterogeneous freezing of droplets  
3866 with immersed mineral dust particles – measurements and parameterization. *Atmos.*  
3867 *Chem. Phys.* **2010**, *10*, 3601-3614.
- 3868 (457) Wex, H.; DeMott, P. J.; Tobo, Y.; Hartmann, S.; Rösch, M.; Clauss, T.; Tomsche, L.;  
3869 Niedermeier, D.; Stratmann, F. Kaolinite particles as ice nuclei: learning from the use of  
3870 different kaolinite samples and different coatings. *Atmos. Chem. Phys.* **2014**, *14*, 5529-  
3871 5546.
- 3872 (458) Sihvonen, S. K.; Schill, G. P.; Lykтей, N. A.; Veghte, D. P.; Tolbert, M. A.; Freedman,  
3873 M. A. Chemical and Physical Transformations of Aluminosilicate Clay Minerals Due to  
3874 Acid Treatment and Consequences for Heterogeneous Ice Nucleation. *J. Phys. Chem. A*  
3875 **2014**, *118*, 8787-8796.
- 3876 (459) Augustin-Bauditz, S.; Wex, H.; Kanter, S.; Ebert, M.; Niedermeier, D.; Stolz, F.; Prager,  
3877 A.; Stratmann, F. The immersion mode ice nucleation behavior of mineral dusts: A  
3878 comparison of different pure and surface modified dusts. *Geophys. Res. Lett.* **2014**, *41*,  
3879 7375-7382.
- 3880 (460) Yang, Z.; Bertram, A. K.; Chou, K. C. Why Do Sulfuric Acid Coatings Influence the Ice  
3881 Nucleation Properties of Mineral Dust Particles in the Atmosphere? *J. Phys. Chem. Lett.*  
3882 **2011**, *2*, 1232-1236.
- 3883 (461) Serratos, J. M.; Bradley, W. F. Infra-Red Absorption of OH Bonds in Micas. *Nature*  
3884 **1958**, *181*, 111-111.
- 3885 (462) Du, Q.; Freysz, E.; Shen, Y. R. Surface Vibrational Spectroscopic Studies of Hydrogen  
3886 Bonding and Hydrophobicity. *Science* **1994**, *264*, 826-828.
- 3887 (463) Sovago, M.; Campen, R. K.; Wurfel, G. W. H.; Müller, M.; Bakker, H. J.; Bonn, M.  
3888 Vibrational Response of Hydrogen-Bonded Interfacial Water is Dominated by  
3889 Intramolecular Coupling. *Phys. Rev. Lett.* **2008**, *100*, 173901.
- 3890 (464) Abdelmonem, A.; Lützenkirchen, J.; Leisner, T. Probing ice-nucleation processes on the  
3891 molecular level using second harmonic generation spectroscopy. *Atmos. Meas. Tech.*  
3892 **2015**, *8*, 3519-3526.
- 3893 (465) Lupi, L.; Molinero, V. Does Hydrophilicity of Carbon Particles Improve Their Ice  
3894 Nucleation Ability? *J. Phys. Chem. A* **2014**, *118*, 7330-7337.
- 3895 (466) Möhler, O.; Benz, S.; Saathoff, H.; Schnaiter, M.; Wagner, R.; Schneider, J.; Walter, S.;  
3896 Ebert, V.; Wagner, S. The effect of organic coating on the heterogeneous ice nucleation  
3897 efficiency of mineral dust aerosols. *Environ. Res. Lett.* **2008**, *3*, 025007.
- 3898 (467) Kulkarni, G.; Zhang, K.; Zhao, C.; Nandasiri, M.; Shutthanandan, V.; Liu, X.; Fast, J.;  
3899 Berg, L. Ice formation on nitric acid coated dust particles: Laboratory and modeling  
3900 studies. *J. Geophys. Res.-Atmos* **2015**, *120*, 7682-7698.
- 3901 (468) Salam, A.; Lohmann, U.; Lesins, G. Ice nucleation of ammonia gas exposed  
3902 montmorillonite mineral dust particles. *Atmos. Chem. Phys.* **2007**, *7*, 3923-3931.
- 3903 (469) Kanji, Z. A.; Welti, A.; Chou, C.; Stetzer, O.; Lohmann, U. Laboratory studies of  
3904 immersion and deposition mode ice nucleation of ozone aged mineral dust particles.  
3905 *Atmos. Chem. Phys.* **2013**, *13*, 9097-9118.
- 3906 (470) Fenter, F. F.; Caloz, F.; Rossi, M. J. Experimental-Evidence for the Efficient Dry  
3907 Deposition of Nitric-Acid on Calcite. *Atmos. Environ.* **1995**, *29*, 3365-3372.

- 3908 (471) Hanisch, F.; Crowley, J. N. Heterogeneous reactivity of gaseous nitric acid on Al<sub>2</sub>O<sub>3</sub>,  
3909 CaCO<sub>3</sub>, and atmospheric dust samples: A Knudsen cell study. *J. Phys. Chem. A* **2001**,  
3910 *105*, 3096-3106.
- 3911 (472) Mashburn, C. D.; Frinak, E. K.; Tolbert, M. A. Heterogeneous uptake of nitric acid on  
3912 Na-montmorillonite clay as a function of relative humidity. *J. Geophys. Res.-Atmos.*  
3913 **2006**, *111*, D15213, doi: 15210.11029/12005JD006525.
- 3914 (473) Vlasenko, A.; Huthwelker, T.; Gaggeler, H. W.; Ammann, M. Kinetics of the  
3915 heterogeneous reaction of nitric acid with mineral dust particles: an aerosol flow tube  
3916 study. *Phys. Chem. Chem. Phys.* **2009**, *11*, 7921-7930.
- 3917 (474) Underwood, G. M.; Li, P.; Al-Abadleh, H.; Grassian, V. H. A Knudsen cell study of the  
3918 heterogeneous reactivity of nitric acid on oxide and mineral dust particles. *J. Phys. Chem.*  
3919 *A* **2001**, *105*, 6609-6620.
- 3920 (475) Gustafsson, R. J.; Orlov, A.; Griffiths, P. T.; Cox, R. A.; Lambert, R. M. Reduction of  
3921 NO<sub>2</sub> to nitrous acid on illuminated titanium dioxide aerosol surfaces: implications for  
3922 photocatalysis and atmospheric chemistry. *Chem. Commun.* **2006**, 3936-3938.
- 3923 (476) Angelini, M. M.; Garrard, R. J.; Rosen, S. J.; Hinrichs, R. Z. Heterogeneous reactions of  
3924 gaseous HNO<sub>3</sub> and NO<sub>2</sub> on the clay minerals kaolinite and pyrophyllite. *J. Phys. Chem. A*  
3925 **2007**, *111*, 3326-3335.
- 3926 (477) Ndour, M.; D'Anna, B.; George, C.; Ka, O.; Balkanski, Y.; Kleffmann, J.; Stemmler, K.;  
3927 Ammann, M. Photoenhanced uptake of NO<sub>2</sub> on mineral dust: Laboratory experiments  
3928 and model simulations. *Geophys. Res. Lett.* **2008**, *35*, L05812, doi:  
3929 05810.01029/02007gl032006.
- 3930 (478) Ndour, M.; Nicolas, M.; D'Anna, B.; Ka, O.; George, C. Photoreactivity of NO<sub>2</sub> on  
3931 mineral dusts originating from different locations of the Sahara desert. *Phys. Chem.*  
3932 *Chem. Phys.* **2009**, *11*, 1312-1319.
- 3933 (479) Karagulian, F.; Rossi, M. J. The heterogeneous chemical kinetics of NO<sub>3</sub> on atmospheric  
3934 mineral dust surrogates. *Phys. Chem. Chem. Phys.* **2005**, *7*, 3150-3162.
- 3935 (480) Zolles, T.; Burkart, J.; Häusler, T.; Pummer, B.; Hitzengerger, R.; Grothe, H.  
3936 Identification of Ice Nucleation Active Sites on Feldspar Dust Particles. *J. Phys. Chem. A*  
3937 **2015**, *119*, 2692-2700.
- 3938 (481) Steinke, I.; Hoose, C.; Möhler, O.; Connolly, P.; Leisner, T. A new temperature- and  
3939 humidity-dependent surface site density approach for deposition ice nucleation. *Atmos.*  
3940 *Chem. Phys.* **2015**, *15*, 3703-3717.
- 3941 (482) Connolly, P. J.; Moehler, O.; Field, P. R.; Saathoff, H.; Burgess, R.; Choulaton, T.;  
3942 Gallagher, M. Studies of heterogeneous freezing by three different desert dust samples.  
3943 *Atmos. Chem. Phys.* **2009**, *9*, 2805-2824.
- 3944 (483) Niemand, M.; Möhler, O.; Vogel, B.; Vogel, H.; Hoose, C.; Connolly, P.; Klein, H.;  
3945 Bingemer, H.; DeMott, P.; Skrotzki, J. *et al.* A Particle-Surface-Area-Based  
3946 Parameterization of Immersion Freezing on Desert Dust Particles. *J. Atmos. Sci.* **2012**,  
3947 *69*, 3077-3092.
- 3948 (484) Phillips, V. T. J.; DeMott, P. J.; Andronache, C. An empirical parameterization of  
3949 heterogeneous ice nucleation for multiple chemical species of aerosol. *J. Atmos. Sci.*  
3950 **2008**, *65*, 2757-2783.
- 3951 (485) Gysel, M.; Weingartner, E.; Baltensperger, U. Hygroscopicity of Aerosol Particles at  
3952 Low Temperatures. 2. Theoretical and Experimental Hygroscopic Properties of  
3953 Laboratory Generated Aerosols. *Environ. Sci. Technol.* **2002**, *36*, 63-68.
- 3954 (486) Zeng, G.; Kelley, J.; Kish, J. D.; Liu, Y. Temperature-Dependent Deliquescent and  
3955 Efflorescent Properties of Methanesulfonate Sodium Studied by ATR-FTIR  
3956 Spectroscopy. *J. Phys. Chem. A* **2014**, *118*, 583-591.



- 3957 (487) Christensen, S. I.; Petters, M. D. The Role of Temperature in Cloud Droplet Activation.  
3958 *J. Phys. Chem. A* **2012**, *116*, 9706-9717.
- 3959 (488) Tang, M. J.; Cox, R. A.; Kalberer, M. Compilation and evaluation of gas phase diffusion  
3960 coefficients of reactive trace gases in the atmosphere: volume 1. Inorganic compounds.  
3961 *Atmos. Chem. Phys.* **2014**, *14*, 9233-9247.
- 3962 (489) Tang, M. J.; Shiraiwa, M.; Pöschl, U.; Cox, R. A.; Kalberer, M. Compilation and  
3963 evaluation of gas phase diffusion coefficients of reactive trace gases in the atmosphere:  
3964 Volume 2. Diffusivities of organic compounds, pressure-normalised mean free paths, and  
3965 average Knudsen numbers for gas uptake calculations. *Atmos. Chem. Phys.* **2015**, *15*,  
3966 5585-5598.
- 3967 (490) Shiraiwa, M.; Ammann, M.; Koop, T.; Poschl, U. Gas uptake and chemical aging of  
3968 semisolid organic aerosol particles. *Proc. Natl. Acad. Sci. U. S. A.* **2011**, *108*, 11003-  
3969 11008.
- 3970 (491) Zobrist, B.; Soonsin, V.; Luo, B. P.; Krieger, U. K.; Marcolli, C.; Peter, T.; Koop, T.  
3971 Ultra-slow water diffusion in aqueous sucrose glasses. *Phys. Chem. Chem. Phys.* **2011**,  
3972 *13*, 3514-3526.
- 3973 (492) Vaden, T. D.; Imre, D.; Beranek, J.; Shrivastava, M.; Zelenyuk, A. Evaporation kinetics  
3974 and phase of laboratory and ambient secondary organic aerosol. *Proc. Natl. Acad. Sci. U.*  
3975 *S. A.* **2011**, *108*, 2190-2195.
- 3976 (493) Davidovits, P.; Hu, J. H.; Worsnop, D. R.; Zahniser, M. S.; Kolb, C. E. Entry of gas  
3977 molecules into liquids. *Faraday Discuss.* **1995**, *100*, 65-81.
- 3978 (494) Pöschl, U. Atmospheric aerosols: Composition, transformation, climate and health  
3979 effects. *Angew. Chem.-Int. Edit.* **2005**, *44*, 7520-7540.
- 3980 (495) Davidovits, P.; Kolb, C. E.; Williams, L. R.; Jayne, J. T.; Worsnop, D. R. Update 1 of:  
3981 Mass Accommodation and Chemical Reactions at Gas-Liquid Interfaces. *Chem. Rev.*  
3982 **2011**, *111*, PR76-PR109.
- 3983 (496) Pöschl, U. Gas-particle interactions of tropospheric aerosols: Kinetic and thermodynamic  
3984 perspectives of multiphase chemical reactions, amorphous organic substances, and the  
3985 activation of cloud condensation nuclei. *Atmos. Res.* **2011**, *101*, 562-573.
- 3986 (497) Ammann, M.; Cox, R. A.; Crowley, J. N.; Jenkin, M. E.; Mellouki, A.; Rossi, M. J.;  
3987 Troe, J.; Wallington, T. J. Evaluated kinetic and photochemical data for atmospheric  
3988 chemistry: Volume VI - heterogeneous reactions with liquid substrates. *Atmos. Chem.*  
3989 *Phys.* **2013**, *12*, 8045-8228.
- 3990 (498) Sander, S. P.; Abbatt, J. P. D.; Barker, J. R.; Burkholder, J. B.; Friedl, R. R.; Golden, D.  
3991 M.; Huie, R. E.; Kolb, C. E.; Kurylo, M. J.; Moortgat, G. K. *et al.* "Chemical Kinetics  
3992 and Photochemical Data for Use in Atmospheric Studies, Evaluation No. 17, JPL  
3993 Publication 10-6," Jet Propulsion Lab., 2011.
- 3994 (499) Pöschl, U.; Shiraiwa, M. Multiphase Chemistry at the Atmosphere-Biosphere Interface  
3995 Influencing Climate and Public Health in the Anthropocene. *Chem. Rev.* **2015**, *115*,  
3996 4440-4475.
- 3997 (500) Pöschl, U.; Rudich, Y.; Ammann, M. Kinetic model framework for aerosol and cloud  
3998 surface chemistry and gas-phase interaction-Part 1: General equation, parameters, and  
3999 terminology. *Atmos. Chem. Phys.* **2007**, *7*, 5989-6023.
- 4000 (501) Shiraiwa, M.; Pfrang, C.; Koop, T.; Poschl, U. Kinetic multi-layer model of gas-particle  
4001 interactions in aerosols and clouds (KM-GAP): linking condensation, evaporation and  
4002 chemical reactions of organics, oxidants and water. *Atmos. Chem. Phys.* **2012**, *12*, 2777-  
4003 2794.
- 4004 (502) Berkemeier, T.; Huisman, A. J.; Ammann, M.; Shiraiwa, M.; Koop, T.; Pöschl, U.  
4005 Kinetic regimes and limiting cases of gas uptake and heterogeneous reactions in

4006 atmospheric aerosols and clouds: a general classification scheme. *Atmos. Chem. Phys.*  
4007 **2013**, *13*, 6663-6686.  
4008